MODELING OF GAS ADSORPTION USING
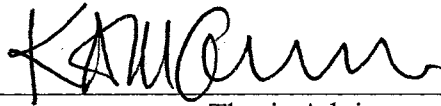
TWO-DIMENSIONAL EQUATIONS

OF STATE

By

ZHEJUN PAN

Bachelor of Science
Zhejiang University
Hangzhou, People's Republic of China
1996

Master of Science
Zhejiang University
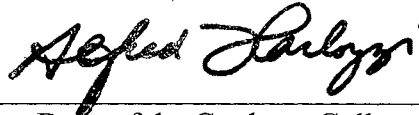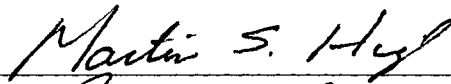Hangzhou, People's Republic of China
1999

Submitted to the Faculty of the
Graduate College of the
Oklahoma State University
in partial fulfillment of
the requirements for
the Degree of
DOCTOR OF PHILOSOPHY
May, 2004

MODELING OF GAS ADSORPTION USING

TWO-DIMENSIONAL EQUATIONS

OF STATE

Thesis Approved:

_____
Thesis Adviser

_____

_____

_____

_____
Dean of the Graduate College

PREFACE

Coalbed methane (CBM) is an important additional supply for meeting the increasing demand for natural gas. Moreover, the enhanced CBM recovery technology offers realistic opportunities for carbon dioxide (CO_2) sequestration.

Accurate modeling of the adsorption behavior of CBM gases (CO_2, methane, and nitrogen) is essential in CBM operations and in CO_2 sequestration. Further, knowledge of the competitive adsorption of mixed coalbed gases is required to elucidate mechanisms for the enhanced recovery and CO_2 sequestration processes. Among the various theories that can be used for describing high-pressure adsorption, the two-dimensional (2-D) equations of state (EOSs) are particularly attractive.

In this study, new temperature relations were developed for the two-dimensional (2-D) equation of state (EOS) parameters to facilitate precise representations and accurate predictions of high-pressure, supercritical pure-gas adsorption encountered in coalbed methane (CBM) recovery and carbon dioxide (CO_2) sequestration. One-fluid mixing rules and the Wong-Sandler excess Gibbs free energy mixing rules were applied to extend the 2-D EOSs to mixture adsorption modeling. In addition, an iteration function method (IFM) for mixture adsorption equilibrium calculations was developed for 2-D EOSs, and the robustness of the IFM algorithm was evaluated for CBM-type systems.

Systematically-selected adsorption measurements were conducted to supplement existing data on carbon matrices. The measurements were conducted for pure methane, nitrogen, CO_2, and their mixtures on an activated carbon and on selected coals at

temperatures of 319 K and 328 K and pressures to 13.8 MPa. These data were used to support the model development efforts.

The new temperature relations for the 2-D EOS parameters appear effective in modeling pure-gas adsorption on carbon matrices at supercritical and near-critical regions. The 2-D Peng-Robinson (PR) EOS with the new temperature relations can represent adsorption on activated carbon and coals within their expected experimental uncertainties. Further, the new temperature relations, which are generalized in terms of adsorbate properties and accessible adsorbent characterizations, can represent the adsorption data on activated carbon within 3% average absolute deviation (AAD) and predict the adsorption isotherms on activated carbon within an AAD of 9% or within three times the expected experimental uncertainties. Similarly, the 2-D EOS parameters are effective in modeling pure-gas adsorption on wet coals with an AAD of 5%, when the coal moisture content is above its equilibrium value.

The 2-D EOSs are capable of predicting binary and ternary gas adsorption within twice the experimental uncertainties, on average. Further, the total and individual component adsorption can be represented to within the expected experimental uncertainties with the use of binary interaction parameters. The 2-D PR EOS with the Wong-Sandler mixing rules provide a marginally better quality of fit, which suggests the possibility of nonrandom mixing in the adsorbed phase.

The present results involving many CBM adsorption systems indicate that the new IFM algorithm for the 2-D EOSs is effective in performing equilibrium mixture adsorption calculations based on feed compositions.

iv

ACKNOWLEDGEMENTS

TABLE OF CONTENTS

LIST OF TABLES

viii

LIST OF FIGURES

NOMENCLATURE

A   Helmholtz free energy; surface area per unit mass of adsorbent; area obtained from chromatographic analysis

A_0 Benedict-Webb-Rubin (BWR) equation of state (EOS) parameter

a   attractive term parameter in three-dimensional (3-D) EOS; molar area; BWR EOS model parameter

a_2 attractive term parameter in two-dimensional (2-D) EOS

b   co-volume parameter in 3-D EOS; BWR EOS parameter

b_2 co-volume parameter in 2-D EOS

B   Langmuir adsorption model parameter

B_0 BWR EOS parameter

C   maximum adsorption capacity in Ono-Kondo model; BET adsorption isotherm model parameter

C_{ij} binary interaction parameter for 2-D EOS; binary interaction parameter for Wong-Sandler mixing rules

C_0 BWR EOS parameter

c   BWR EOS parameter

E   characteristic energy in pore volume filling theory

F   number of degrees of freedom

$\hat{f}_i^a$ fugacity of component i in an adsorbed-phase mixture

$\hat{f}_i^g$ fugacity of component i in a gas-phase mixture

G   Gibbs free energy

$\overline{G}$ partial molar Gibbs free energy

K   equilibrium constant

k	2-D EOS parameter; Boltzmann constant
k_d	desorption rate constant
L	maximum adsorption capacity in the Langmuir and BET models; slit width
M	total number of lattice cells; molecular weight
M_s	total mass of adsorbent in a closed adsorption system
m	number of layers in the lattice model; 2-D EOS constant; mass in gravimetric adsorption measurement
N_a	Avogadro number
NC	number of components
NPTS	number of data points
n	moles of fluid(s) in the bulk gas phase or adsorbed phase
n_{inj}	amount of gas injected from the pump section into the cell section
n_{sol}	number of moles of gas dissolved in water
P	pressure
P_o	saturation pressure
Q	configurational partition function in statistical thermodynamics
R	universal gas constant
R_a	rate of adsorption
R_d	rate of desorption
S	entropy; objective function
T	temperature
T_o	normal boiling point of the adsorbate (or triple point for CO_2)
U	model constant for the generalized EOS
V	volume
V_{ads}	adsorbed-phase volume
V_s	micropore saturation volume in the theory of volume filling of micropores

V_{void} void volume

W model constant for the generalized EOS

x_{ads} fractional coverage of a pure component in the monolayer lattice model

x_i mole fraction of component i in an adsorbed-phase mixture

$x_{i,b}$ fraction of gas molecules i occupying cells in a layer of the lattice model

$x_{i,t}$ fractional coverage of component i in t^{th} layer of the lattice model

x_t fractional coverage of pure component in t^{th} layer of the lattice model

y_i mole fraction of component i in the gas phase

z distance from a molecule to the surface

Z compressibility factor

Z_a compressibility factor as defined in the 2-D EOSs

z_i feed gas mole fraction

Greek Symbols

α 2-D EOS parameter; BWR EOS parameter; Non-Random Two-Liquid (NRTL) model parameter

β 2-D EOS parameter; coefficient of similarity in pore volume filling model

δ thermal expansion coefficient of the adsorbed phase

ε^* well depth of the Lennard-Jones 12-6 potential

ε_{ij} fluid-fluid interaction energy parameter in the OK model

ε_{is} fluid-solid interaction energy parameter in the OK model

Φ adsorbate-adsorbent potential; potential energy

Φ_D dispersion energy

Φ_R close-range repulsion energy

Φ_{Ind} induction energy (interaction between electric field and an induced dipole)

$\Phi_{F\mu}$ interaction between an electric field (F) and a permanent dipole (μ)

$\Phi_{\dot{F}Q}$ interaction between a field gradient ($\dot{F}$) and a quadrupole (with quadrupole moment Q)

$\hat{\phi}_i^a$ fugacity coefficient of component i in an adsorbed-phase mixture

γ BWR EOS model parameter

Γ Gibbs excess adsorption per unit mass of adsorbent in the lattice model

Ψ_{ij} correlation coefficient in the lattice model representing the deviations of a non-random mixture from its random limit

Ψ_z fluid-solid potential at distance z to the surface

μ_i chemical potential for component i

π number of phases; spreading pressure

ρ density

ρ_{ads} adsorbed-phase density

ρ_{mc} adsorbed-phase density corresponding to the maximum adsorption capacity

ρ_{atom} density of atoms or molecules on the surface

σ surface density; diameter of a molecule; the expected experimental uncertainty;

θ fractional coverage; fractional component Gibbs adsorption

ϑ specific area of the molecule on the surface

τ NRTL model parameter

ω amount of gas adsorbed per unit mass of adsorbent

Subscripts

ads   the adsorbed amount within the equilibrium cell; adsorbed phase

b   bulk phase or gas phase

f   fluid

He   properties obtained with the use of helium gas

i,j,k,l component i,j,k,l; data point i,j,

m   gas mixture; maximum

unads   the un-adsorbed amount within the equilibrium cell

o   reference state

s   solid phase; solid

t   layer in multilayer adsorption modeling

Superscripts

Abs   absolute adsorption

c   calculated value

E   excess property

e   experimental data

Gibbs   Gibbs excess adsorption

g   gas phase

IG   ideal gas

IGM   ideal gas mixture

L   liquid phase

t   total amount

V   vapor phase

*   value at infinitesimally low pressure

CHAPTER 1

INTRODUCTION

1.1 Industrial Context and Scientific Significance

Natural gas provides an alternative to oil or coal as an energy resource. According to the United States Department of Energy, in the year 2000, the United States consumed 22.5 Trillion cubic feet (Tcf) of natural gas, which was approximately 20% of all the fossil fuel used. Further, the demand for natural gas is predicted to rise significantly in the future; specifically, more power plants are using natural gas to generate electricity, and more factories are using it both as a fuel and as a raw material for a variety of chemicals. These expanded operations are motivated by access to distributed gas pipelines and practically pollution-free utilization of this energy resource.

The United States has vast resources of natural gas available for extraction. The estimate of technically recoverable natural gas resources is 1,190 Tcf according to the Energy Information Administration, 1,779 Tcf according to the National Petroleum Council, and 1,090 Tcf according to the Potential Gas Committee [NaturalGas.org]. However, the estimated recoverable natural gas can only last 50 to 80 years at current consumption rate. Coalbed methane (CBM), an unconventional natural gas resource, has received significant attention since the 1990's. As reported by the United States Geological Survey, the in-place CBM resources of the United States are estimated to be

more than 700 Tcf, of which about 100 Tcf may be economically recoverable [USGS.gov]. Compared with the recoverable natural gas in the conventional gas reservoirs, the amount of recoverable CBM is significant. Currently, CBM constitutes about 7% of the natural gas production in the USA.

The majority of the coalbed methane is adsorbed in coal pore structures. The first stage in the production of CBM is called primary recovery and utilizes the high pressure in the reservoir to drive the methane out. The second stage is called enhanced coalbed methane (ECBM) recovery, which uses nitrogen (N_2) or carbon dioxide (CO_2) to enhance the CBM recovery processes. CO_2 enhanced recovery is more promising not only because CO_2 displaces more methane but also because CO_2 can be sequestered in coalbeds. CO_2 is a well-known greenhouse gas and the CO_2 concentration change in the atmosphere is believed to be the main cause of global warming; thus, CO_2 enhanced recovery provides the additional benefit of CO_2 sequestration.

Thermodynamic models for adsorption provide crucial information for designing processes to sequester CO_2 and recover natural gas from unminable coalbeds. These models can describe the quantity of gas initially residing in the coalbeds and how, through the process of ECBM recovery, reservoir changes in pressure, temperature, and gas composition affect the quantity and quality of the recovered natural gas.

CBM production and CO_2 sequestration are not the only applications of adsorption modeling. In industry, adsorption processes are used extensively in fluids separation and purification. Thus, research to develop more reliable adsorption models may have a significant economic impact.

2

Equilibrium models for gas adsorption relate the amount of adsorption to the pressure, temperature, and compositions in the gas phase. In 1918, Langmuir described the adsorption equilibrium from a kinetics point of view. The Langmuir model is still widely used because of its simplicity and its capability to model gas adsorption behavior at low pressures. Since then a number of adsorption models have been developed, including the BET (Brunauer, Emmett and Teller) model [Brunauer et al., 1938], the ideal adsorbed solution (IAS) model [Myers et al., 1965], the two-dimensional equations of state [see, e.g., Zhou et al., 1994], the simplified local density (SLD) model [see, e.g., Fitzgerald et al., 2003], the pore filling model [Dubinin, 1966], the local density model, and the lattice theory [see, e.g., Sudibandriyo, 2003].

The two-dimensional (2-D) equations of state (EOSs) are analogues of three-dimensional (3-D) EOSs. They depict the adsorbed phase as a two-dimensional interface, where the adsorbed molecules are assumed to be mobile and to have lateral interactions. In this work, we will focus on the 2-D EOSs because they offer several advantages, including:

1. Ease of implementation of a well-developed framework; the 2-D EOSs are analogues of the 3-D EOSs used for pressure-volume-temperature (PVT) behavior modeling

2. Availability of 2-D mixing rules for multicomponent mixtures in direct analogy to 3-D mixing theories

3. Similarity of the adsorption algorithms to vapor-liquid equilibrium (VLE) algorithms; thus the ability to facilitate CBM process simulations

In comparison with the Langmuir model, which calls for the localized adsorption assumption, the 2-D EOSs are equipped with better theory and, in practice, provide better quality of fit to adsorption data. However, attention to the 2-D EOSs was very limited, probably because of failures associated with applying the 3-D EOS parameters in 2-D EOS models. Considering that the adsorbent surface has significant interaction with the adsorbed molecules, it is quite understandable that direct application of the 3-D EOS parameters with simple modifications would not lead to satisfactory results.

In 2-D EOS theory, fluid-solid interactions are accounted for indirectly. More precisely, the fluid-solid interaction is implied in the regressed 2-D EOS parameters. Further, no sound theoretical treatment is currently available to facilitate 2-D EOS parameter determination based on 3-D EOS parameters values.

Our analysis indicates that the 2-D EOSs have the potential to describe the adsorption behavior using adsorbent characterization and gas properties. In the present work, capabilities of the 2-D EOSs were extended to pure-gas adsorption predictions based on adsorbent characterization, and mixture adsorption using Wong-Sandler mixing rules. Also, an iteration function method was developed to enhance the multicomponent adsorption calculations.

1.2 Objectives and Plans

The goal of the present work was to analyze, develop, and evaluate the 2-D EOS models and the associated equilibrium algorithms as they apply to pure-gas and multicomponent adsorption, especially the adsorption of CO_2, methane, and nitrogen on

4

carbon matrices including coals and activated carbons. The specific objectives for this project are:

1. Assemble an adsorption database, including pure-gas and multicomponent adsorption isotherms on carbon matrices at various temperatures, pressures, and compositions.

2. Conduct selected adsorption measurements for pure methane, nitrogen, CO_2, and their mixtures on an activated carbon (AC) and on selected coals at temperatures from 304 K to 320 K and pressures to 13.8 MPa. The newly-acquired data are used to enhance the assembled adsorption database.

3. Evaluate the capability of 2-D EOSs to model the pure-gas adsorptions.

4. Generalize the temperature relations for the 2-D EOS parameters, expecting predictions for pure-gas adsorption within three times the experimental uncertainties.

5. Evaluate the capability of one-fluid mixing rules to model the mixture adsorption.

6. Implement the Wong-Sandler mixing rules with Non-Random Two-Liquid (NTRL) model to the 2-D EOSs.

7. Develop a robust iteration function method for multicomponent adsorption calculations.

Chapter 2 contains a review of the fundamentals of adsorption. Chapter 3 outlines a number of relevant adsorption models and characterization of carbon adsorbents. Chapter 4 provides descriptions of the experimental work and the adsorption database used in this work. In Chapter 5, the two-dimensional equations of state are reviewed and discussed. In Chapter 6, the capabilities of the 2-D EOSs to model the pure-gas

5

adsorption are evaluated and temperature relationships for the 2-D EOS parameters are developed; pure-gas adsorption predictions based on adsorbent structure are also suggested in this chapter. Chapter 7 presents an evaluation of the capability of one-fluid mixing rules to model the mixture adsorption, and it summarizes the implementation of the Wong-Sandler mixing rules within the generalized 2-D EOS. Chapter 8 contains a description of a new iteration function method for multicomponent adsorption using 2-D EOSs, and Chapter 9 contains the conclusions and recommendations drawn from this study.

This study was part of an extensive research project dealing with high-pressure gas-adsorption modeling [Gasem, et al., 2003]. As such, materials included in Chapters 3 and 4, as well as the adsorption database used in the model development are a product of a collective effort involving the author, Mahmud Sudibandriyo (2003), and James Fitzgerald (2003).

CHAPTER 2

FUNDAMENTALS OF ADSORPTION

2.1 Phenomenon of Adsorption

When a certain number of gas molecules strike continually upon a surface and stay there for a certain length of time before re-evaporating, the concentration of the gas at this surface will be higher than that of the gas in the bulk phase [de Boer, 1968]. This condensed phase is called an adsorbed phase and this phenomenon is called adsorption.

The cause for the retention of gas molecules on the surface is due to the attractive forces provided by the surface. The four basic types of contributions to the adsorbate-adsorbent interactions are dispersion, repulsion, electrostatic, and chemical bond [Yang, 2003]. Chemical bonding will lead to chemical adsorption, which is not within the scope of this work. For physical adsorption, the adsorbate-adsorbent potential is:

$$\Phi = \Phi_D + \Phi_R + \Phi_{Ind} + \Phi_{F\mu} + \Phi_{\dot{F}Q} \qquad (2\text{-}1)$$

where Φ_D is dispersion energy, Φ_R is close-range repulsion energy, Φ_{Ind} is induction energy (interaction between an electric field and an induced dipole), $\Phi_{F\mu}$ is interaction between an electric field (F) and a permanent dipole (μ), $\Phi_{\dot{F}Q}$ is interaction between a field gradient ($\dot{F}$) and a quadrupole with a moment Q [Yang, 2003].

2.2 Fundamentals of Adsorption

The first and second laws of thermodynamics give the fundamental property relations for an adsorption system. Using these relations, the governing equations for multicomponent gas adsorption can be derived as [see, e.g., Zhou, 1994]:

$$T^g = T^a \text{ and } P^g = P^a$$

$$\mu_i^g = \mu_i^a \text{ for } i=1, NC \qquad (2-2)$$

where μ_i^g and μ_i^a are the chemical potentials of the component in the gas phase and the adsorbed phase, respectively; NC is the number of components in the adsorption system. Equation 2-2 states the equilibrium criteria for a closed adsorption system. Classical thermodynamics, statistical thermodynamics, and/or molecular simulations can be applied to calculate the chemical potential in the adsorbed phase. In all cases, however, knowledge of the interactions in the adsorption system is required for reliable descriptions of adsorption equilibria; although, it is often difficult to include all of the physical complexity into one model.

2.2.1 Classical Thermodynamics

Figure 2-1 illustrates a typical adsorption system, in which the adsorbed phase is a interface between the bulk gas phase and the solid adsorbent. To develop the working equilibrium equations in terms of fugacity, we employ the constructs of the fundamental property relations. The fundamental property relation for the adsorbed phase using the Gibbs approach [see, e.g., Zhou, 1994] is:

$$d(nG) = -(nS)dT + (na)d\pi + \sum_i \mu_i dn_i \qquad (2-3)$$

where π is spreading pressure, a is the molar area of the adsorbate, and the component chemical potential in the adsorbed phase may be given as:

$$\mu_i^a = \left[\frac{\partial(nG)}{\partial n_i}\right]_{T,\pi,n_j} = \overline{G}_i^a \tag{2-4}$$
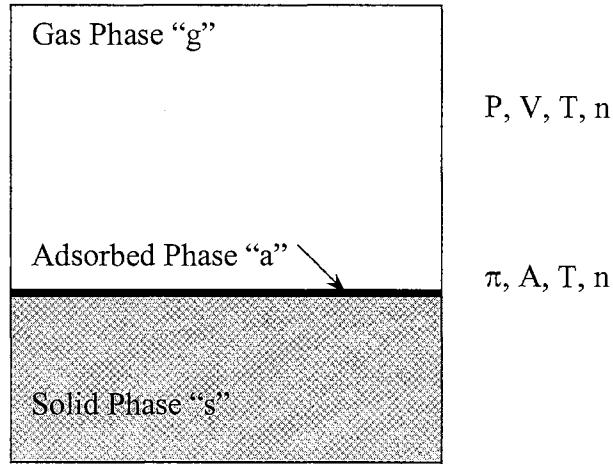
Figure 2-1. Adsorption Equilibrium System

Equation 2-2 can thus be expressed as:

$$\overline{G}_i^g = \overline{G}_i^a \tag{2-5}$$

Differentiating Equation 2-5, it leads to:

$$d\overline{G}_i^g = d\overline{G}_i^a \tag{2-6}$$

By definition, the Gibbs free energies in the adsorbed phase and bulk phase are:

$$d\overline{G}_i^a = RT d\ln \hat{f}_i^a \tag{2-7}$$

$$d\overline{G}_i^g = RT d\ln \hat{f}_i^g \tag{2-8}$$

Combining Equations 2-6 to 2-8, it yields:

$$d\ln \hat{f}_i^g = d\ln \hat{f}_i^a \tag{2-9}$$

Integrating both sides of Equation 2-9, it results in:

$$\int_{P^*}^{P} d \ln \hat{f}_i^g = \int_{\pi^*}^{\pi} d \ln \hat{f}_i^a \qquad (2\text{-}10)$$

or,

$$\ln \hat{f}_i^a (\pi) - \ln \hat{f}_i^a (\pi^*) = \ln \hat{f}_i^g (P) - \ln \hat{f}_i^g (P^*) \qquad (2\text{-}11)$$

At very low pressure, $\hat{f}_i^a (\pi^*) = \pi_i^*$ and $\hat{f}_i^g (P^*) = P_i^*$. Thus:

$$P_i^* \hat{f}_i^a (\pi) = \pi_i^* \hat{f}_i^g (P) \qquad (2\text{-}12)$$

For vapor-liquid equilibrium, the equal-chemical potential equations lead to the following equal-fugacity equations:

$$\hat{f}_i^L = \hat{f}_i^V \qquad (2\text{-}13)$$

The difference between Equations 2-12 and 2-13 is in the reference states used.

Implementation of Equation 2-12 requires a 3-D EOS for the gas phase and a 2-D EOS or an adsorption solution model for the adsorbed phase. Detailed discussion of this subject is given in Chapters 5 though 7.

2.2.2 Statistical Thermodynamics

Partition functions can be used to describe the state of adsorbed molecules. The partition function can account for both the adsorbate-adsorbate interaction and adsorbate-adsorbent interactions. Different assumptions can be made to derive the partition function. Once a partition function, Q, of a system containing N molecules occupying an area A is constructed, the chemical potential of a molecule is then obtained from the following relation [see, e.g., Do, 1998]:

$$\frac{\mu^a}{kT} = -\left(\frac{\partial \ln Q}{\partial N} \right)_{T,A} \qquad (2\text{-}14)$$

As stated earlier, at equilibrium, the chemical potential of an adsorbed molecule is equal to the chemical potential of a gas molecule. Thus, using different partition functions for the adsorbed phase and different models to calculate the chemical potential in the gas phase, various models can be derived.

2.2.3 Kinetics

The adsorption process can also be modeled from the point of view of kinetics [see, e.g., Zhou, 1994]. At equilibrium, the rate of adsorption, R_a, is equal to the rate of desorption, R_d,:

$$R_a = R_d \qquad (2\text{-}15)$$

The rate of adsorption is:

$$R_a = k_a P(1-\theta) \qquad (2\text{-}16)$$

where k_a is the adsorption rate constant, and θ is the fractional coverage. The rate of desorption is:

$$R_d = k_d \theta \qquad (2\text{-}17)$$

where k_d is the desorption rate constant. Thus, combining Equations 2-15 through 2-17 yields:

$$\theta = \frac{\omega}{L} = \frac{BP}{1+BP} \qquad (2\text{-}18)$$

where B is the Langmuir constant, and L is the maximum adsorption capacity. Equation 2-18 is the famous Langmuir model. A series of models have been developed based on a kinetics point of view, including the BET (Brunauer, Emmett and Teller) model [Brunauer et al., 1938].

CHAPTER 3

ADSORPTION THEORIES

3.1 Adsorption Models

Adsorption is determined mainly by the interactions among the gas molecules and the surface. The nature of the adsorbent and adsorbate will lead to different adsorption behaviors. For example, the characteristic of the adsorbent (e.g., whether it is porous or not) and the conditions of the adsorbate (e.g., whether it is in sub-critical or supercritical region) will affect the shape of the adsorption isotherms. Typically, there are five types of adsorption isotherms [Brunauer et al., 1940] as shown in Figure 3-1.

In 1918, Langmuir derived the first well-known adsorption model - the Langmuir model. Although the Langmuir model can only represent Type I adsorption, other models were developed based on this theory. In 1938, The BET (Brunauer, Emmett and Teller) model was developed, and it has the capability to represent Types I, II, and III adsorption. Modified BET models can represent all five adsorption types.

Although the models based on kinetics had success in representing adsorption behaviors, their semi-empirical nature limited their predictive capabilities. Thermodynamically rigorous models have also been developed. Models based on classical thermodynamics, for example, the ideal adsorption solution (IAS)

12

model, and models based on statistical thermodynamics, for example, the lattice theory, not only can represent the adsorption data, but they also have the capability to predict adsorption behavior.
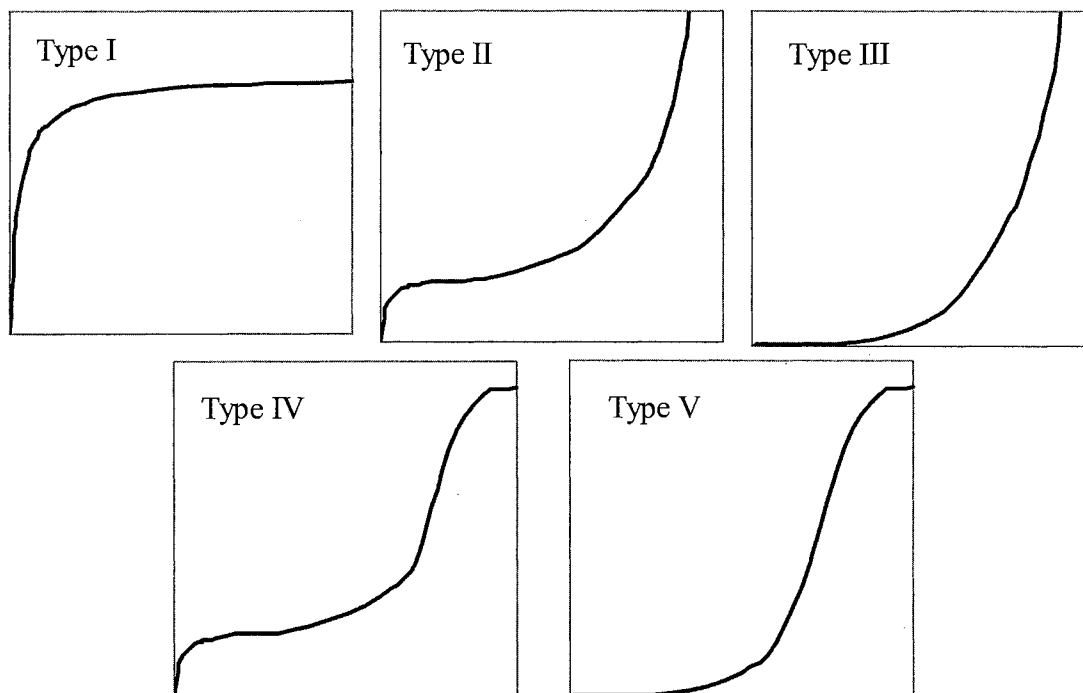
Figure 3-1. Types of Adsorption Isotherm

In this chapter, a number of adsorption models will be reviewed briefly, followed by a brief review of carbon adsorbents. Specifically, in this section, the following adsorption models will be outlined: the Langmuir model, the BET (Brunauer, Emmett and Teller) model, the ideal adsorbed solution (IAS) model, the two-dimensional equations of state, the pore filling model, the lattice theory, and the simplified local density model. Since the properties of the gas molecules are well known, they will be summarized in a table in Chapter 6 without detailed discussions.

The Langmuir Model

The Langmuir model is derived to describe adsorption on a flat surface as given by the kinetic theory. At equilibrium, a continual process of bombardment of molecules onto the surface and a corresponding evaporation of molecules from the surface maintain a zero rate of accumulation at the surface. The assumptions of the Langmuir model are [see, e.g., Do, 1998]:

1. The surface is homogeneous; that is, the adsorption energy is constant over all sites.

2. Adsorption on the surface is localized, which means that the atoms or molecules are adsorbed at definite, localized sites.

3. Each site can accommodate only one molecule or atom.

Based on the assumptions above, the Langmuir model can be derived as:

$$\theta = \frac{\omega}{L} = \frac{BP}{1+BP} \qquad (3\text{-}1)$$

where θ is the fractional coverage, ω is the amount adsorbed, B is the Langmuir constant, L is maximum adsorption capacity. When extended to mixture adsorption, the Langmuir model becomes:

$$\omega_i = \frac{L_i B_i P y_i}{1+\sum_j B_j P y_j} \qquad (3\text{-}2)$$

where subscript "i" represents component i, and y is the mole fraction in the gas phase. The extended Langmuir is not thermodynamically correct unless the maximum capacity L_i is the same for each component [see, e.g., Do, 1998].

The BET Model

The Langmuir model is for monolayer coverage. However, in the adsorption for sub-critical adsorbates, molecules first adsorb onto the solid surface in a layering process, and when the pressure is sufficiently high (about 0.1 of the vapor pressure) multiple layers are formed. The BET theory, which accounts for the layering process, was first developed by Brunauer et al. (1938). The assumptions of the BET model are:

1. The surface is homogeneous; that is, the adsorption energy is constant over all sites.

2. Adsorption on the surface is localized, which means that the atoms or molecules are adsorbed at definite, localized sites.

3. Each site can accommodate only one molecule or atom.

4. There is no limit to the numbers of layers.

The first three assumptions are the same as in Langmuir model. The BET model can be simplified and written as:

$$\frac{\omega}{L} = \frac{CP}{(P_o - P)[1 + (C - 1)(P / P_o)]} \qquad (3\text{-}3)$$

where P_o is the vapor pressure, L and C are model parameters. The BET model can represent the adsorption isotherms from Types I to III by adjusting the parameters L and C. However, it cannot represent the plateau in Types IV and V. Brunauer et al. (1940) modified the BET model to represent Type IV and V isotherms.

The BET model is widely used to determine the surface area for an adsorbent. Nitrogen adsorption at 77 K is commonly used to estimate the surface areas for carbon matrices.

15

The Ideal Adsorbed Solution (IAS) Model

The ideal adsorbed solution model is for the mixture adsorption only. It was developed by Myers and Prausnitz (1965). The IAS is an adsorption analog to the Raoult's Law for vapor-liquid equilibrium. The assumptions of the IAS model are [see, e.g., Zhou, 1994]:

1. The adsorbed solutions and the gas phase are ideal.

2. All activity coefficients in the adsorbed phase are unity.

   The equilibrium condition for the adsorbed phase and the gas phase is:

$$Py_i = x_i P_{o,i}(\pi) \tag{3-4}$$

where $P_{o,i}$ is the pressure of the equilibrium gas phase, which corresponds to the spreading pressure π for the adsorption of component i. To perform mixed-gas adsorption calculations, a pure-component model is needed. Any pure-component model can be utilized in the IAS calculation.

Two-Dimensional Equations of State

The 2-D EOS is analogous to the three-dimensional equations of state, simply by replacing the pressure, P, with the spreading pressure, π, and the specific volume, v, with the specific surface density, σ. The assumptions of the 2-D EOS model are [DeGance, 1992]:

1. The actual interfacial region, which itself is three-dimensional, can be treated as an imaginary mathematical surface, a two-dimensional phase with its own thermodynamic properties.

2. The adsorbent is supposed to be thermodynamically inert.

16

3. The adsorbent possesses a temperature-invariant area, which is equally accessible to all adsorbates.

4. The surface is homotattic, i.e., it is made up of many homogeneous sub-regions.

5. The absolute definition of adsorption applies; this definition differs from the Gibbs definition, which is the one usually employed for low-pressure data collected using volumetric methods, because it accounts for the volume occupied by the adsorbed phase.

The popular generalized cubic 3-D EOS used in vapor-liquid equilibrium calculations is given as:

$$\left[p + \frac{a\rho^2}{1 + Ub\rho + W(b\rho)^2} \right] [1 - b\rho] = \rho RT \tag{3-5}$$

where a and b are the traditional EOS parameters, and numerical values of U and W may be specified to give various forms of 3-D EOSs.

The general 2-D analog can be written as follows (with an additional parameter m for added model flexibility) [Zhou et al., 1994]:

$$\left[\pi + \frac{a_2\sigma^2}{1 + Ub_2\sigma + W(b_2\sigma)^2} \right] \left[1 - (b_2\sigma)^m \right] = \sigma RT \tag{3-6}$$

or,
$$\left[A\pi + \frac{\alpha\omega^2}{1 + U\beta\omega + W(\beta\omega)^2} \right] \left[1 - (\beta\omega)^m \right] = \omega RT \tag{3-7}$$

where A is the specific surface area, π is the spreading pressure, σ is the surface density of the adsorbate, $\omega = \sigma A$ is the specific amount adsorbed, and $\alpha = a_2/A$ and $\beta = b_2/A$ are model parameters.

17

The Pore Filling Model

Most of the models discussed above are based on the flat surface assumption. However, most of the adsorbents, especially carbon adsorbents, are porous. The theory of volume filling micropores (TVFM) was first introduced by Dubinin (1966). The assumptions of the TVFM model are [Dubinin, 1966]:

1. The adsorbate fills the micropores via a volume filling mechanism.

2. No discrete monolayer is formed in the pores.

Pure-component isotherm of Dubinin-Astakhov (D-A) equation is given as follows [see, e.g., Do, 1998]:

$$V = V_s \exp\left\{-\left(\frac{RT}{\beta E}\ln\frac{P_{o,i}}{P}\right)^n\right\} \qquad (3\text{-}8)$$

where parameter n describes the surface heterogeneity, V is the adsorption volume, V_s is the maximum volume, $P_{o,i}$ is the vapor pressure, E is a characteristic energy, and β is the coefficient of similarity. To extend TVFM to multicomponent adsorption, mixture equilibrium models such as IAS might be applied.

The Adsorption Lattice Theory

The statistical lattice theory concept was first proposed by Ono and Kondo in 1960. Aranovich et al. (1996, 1997, 2001) recently developed a more general formalism of this model, in the context of adsorption of solutes in liquid solutions. The assumptions for the lattice Ono-Kondo model are [see, e.g., Sudibandriyo, 2003]:

1. The fluid system is assumed to be composed of layers of lattice cells that contain fluid molecules and vacancies.

2. Molecular interactions are assumed to exist only between the nearest neighboring molecules.

3. Chemical equilibrium between the adsorbed layers and the bulk is given by the equality of the chemical potential in each layer and the bulk.

When the equilibrium exists between the gas phase and a multilayer adsorbed phase, the expression for the configurational free energy of the first and the tth adsorbed layer are:

$$A_{1st} = \sum_i^n N_i^s (\frac{c_p}{2} \varepsilon_{ii} + \varepsilon_{is}) + \sum_i^n \sum_j^n N_i^s x_{j,2nd} \varepsilon_{ij} + kT \sum_i^n N_i^s \ln x_i^s$$

$$+ \frac{c_p M^s T}{8} \sum_i^n \sum_j^n \Delta_{ij} x_i^s x_j^s \int_0^{1/T} (\Psi_{ij}^s + \Psi_{ji}^s) d(1/T)$$ (3-9)

and

$$A_{t^{th}} = \sum_i^n N_i^t (\frac{c_p}{2} \varepsilon_{ii}) + \frac{1}{2} \sum_i^n \sum_j^n N_i^t (x_{j,t-1} + x_{j,t+1}) \varepsilon_{ij} + kT \sum_i^n N_i^s \ln x_i^s$$

$$+ \frac{c_p M^t T}{8} \sum_i^n \sum_j^n \Delta_{ij} x_{i,t} x_{j,t} \int_0^{1/T} (\Psi_{ij}^t + \Psi_{ji}^t) d(1/T)$$ (3-10)

In these equations, N_i is the number of adsorbate molecules i, M is total number of lattice cells in the corresponding layer, x_i (= $N_{i,t}/M_t$) is the reduced density or fraction of sites occupied by adsorbed molecules i in layer t, and c_p is the coordination number in the parallel direction. The adsorbate-adsorbate energy interaction parameter is expressed by ε_{ii}; the adsorbate-adsorbent surface energy interaction parameter is expressed by ε_{is}, and $\Delta_{ij} \equiv 2 \varepsilon_{ij} - (\varepsilon_{ii} + \varepsilon_{jj})$. Ψ_{ij}, is the ratio of the probability for having a molecule i around an arbitrary molecule j, to the probability of molecule i occupying the lattice cell. T is the absolute temperature and k is Boltzmann's constant.

The condition for phase equilibrium between the adsorbed layers and the bulk phase is given by the equality of the chemical potential in each layer and the bulk phase,

$$\mu_{i,1} = \mu_{i,2} = \mu_{i,3} = \ldots = \mu_{i,m} = \mu_{i,b} \tag{3-11}$$

The chemical potential in each layer or the bulk is defined as:

$$\mu_{i,t} = \left(\frac{\partial A_{i,t}}{\partial N_{i,t}} \right)_{T,M,N_{n,t}} \tag{3-12}$$

Following the equilibrium expression, the Gibbs excess adsorption is defined as:

$$\Gamma_i = C_i \sum_{t=1}^{m} (x_{i,t} - x_{i,b}) \tag{3-13}$$

Here, the prefactor C_i represents the maximum capacity of the adsorbent for adsorbent "i" and might be presumed to be a parameter taking into account the fraction of the active pores of the adsorbent and other structural properties of the adsorbent. The number of layers, m, however, is specific to the adsorbate-adsorbent system and needs to be determined before the Ono-Kondo model can be applied. This number is usually chosen based on the best fit to the experimental adsorption data set [Sudibandriyo, 2003].
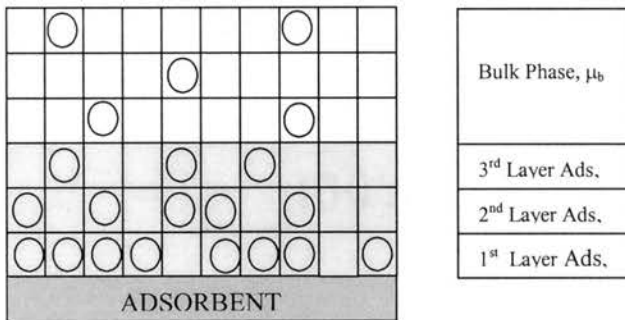
Figure 3-2. Multilayer Adsorption
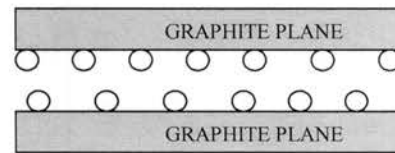
Figure 3-3. Monolayer Adsorption on Graphite Slit

A commonly used simplification of the model is the assumption of monolayer adsorption. Sudibandriyo et al. (2003) assumed that the adsorption process is directly mapped onto the two parallel graphite planes as shown in Figure 3-3.

Benard et al. (1997, 2001) used this approach for the adsorption of pure methane and hydrogen on activated carbon. In this approach, the equilibrium equation becomes:

$$\ln\left[x_{ads}(1-x_b)/x_b(1-x_{ads})\right] + ((c_p + c_v)x_{ads} - cx_b)\varepsilon/kT + \varepsilon_s/kT = 0 \qquad (3\text{-}14)$$

where $c_p = 6$, $c_v = 1$ and $c = 8$ for the hexagonal lattice cell.

For the pure adsorption inside the slit approach of Benard et al. (1997, 2001), the number of layers, m is equal to two and Equation 3-13 becomes:

$$\Gamma = 2C \ (x_{ads} - x_b) = 2C \left(\frac{\rho_{ads}}{\rho_{mc}} - \frac{\rho_b}{\rho_{mc}}\right) \qquad (3\text{-}15)$$

where ρ_{ads} is the adsorbed phase density, and ρ_{mc} is the adsorbed phase density at the maximum adsorption capacity. Here, the fractional coverage in each phase is related to its phase density, i.e., $x_{ads} = \rho_{ads}/\rho_{mc}$ and $x_b = \rho_b/\rho_{mc}$. The bulk density is calculated separately using an accurate equation of state. For the homogeneous structure, $2C/\rho_{mc}$ represents the specific adsorbed-phase volume of the adsorbent and the $2C\rho_{ads}/\rho_{mc}$ term in Equation 3-15 is the absolute adsorption.

The Simplified Local Density (SLD) Model

The local density models describe the adsorption behavior based on fluid-fluid and fluid-surface interactions. The assumptions of the simplified local density model are [see, e.g., Fitzgerald, 2003]:

21

1. The chemical potential at any point next to adsorbent surface is equal to the bulk phase chemical potential.

2. The chemical potential at any point above the surface is the sum of the fluid-fluid interaction and fluid-solid interaction potentials.

3. The chemical potential of the fluid for each point in space is estimated from mean field theory.

The SLD model is formulated in terms of the Gibbs excess adsorption (n_{Gibbs}), defined as the excess number of moles per unit mass of adsorbent, or:

$$n_{Gibbs} = A/2 \int_{\sigma_{ff}/2}^{L-\sigma_{ff}/2} (\rho(z) - \rho_b) dz \qquad (3\text{-}16)$$

For the slit geometry considered and as shown in Figure 3, the lower limit of integration $\sigma_{ff}/2$ is the center of the adsorbed molecule on the plane surface, and the upper limit, $L-\sigma_{ff}/2$, is the slit width adjusted by half of the fluid diameter σ_{ff}. Chen and Wong, Lee's partially integrated 10-4 Lennard-Jones potential is used to describe the fluid-solid interactions. The fluid-solid potential, represented by $\psi(z)$, is defined on a molecular basis by:

$$\mu_{fs}(z) = N_A \cdot \Psi(z) \qquad (3\text{-}17)$$

$$\Psi(z) = 4\pi \rho_{atoms} \varepsilon_{fs} \sigma_{fs}^2 \left(\frac{\sigma_{fs}^{10}}{5(z')^{10}} - \frac{1}{2} \sum_{i=1}^{4} \frac{\sigma_{fs}^4}{(z'+(i-1) \cdot \sigma_{ss})^4} \right) \qquad (3\text{-}18)$$

where ε_{fs} is the fluid-solid interaction energy parameter and $\rho_{atoms} = 0.382$ atoms/A^2. The molecular diameter of the adsorbate and the carbon interplanar distances are σ_{ff} and σ_{ss}, respectively. The carbon interplanar distance was adopted to be 0.335 nm [Chen et

22

al., 1997]. For convenience, the fluid-solid diameter σ_{fs} and the dummy coordinate z' are defined as $\sigma_{fs} = (\sigma_{ff} + \sigma_{ss})/2$ and $z' = z + \sigma_{ss}/2$.

The local density is determined by relating the fluid-fluid chemical potential to the fugacity in the gas phase as given by [Fitzgerald et al. 2003]:

$$\ln\left(\frac{f_{ff}[a(z),\rho(z)]}{f}\right) = -\left(\frac{\Psi(z) + \Psi(L-z)}{kT}\right)$$

(3-19)

An equation of state can be used to determine the bulk density, the bulk fugacity and fluid fugacity.

3.2 Review on Carbon Adsorbents

Alumina, silica gel, activated carbon, and zeolite are commonly used adsorbents. In this work, coals and activated carbons are of great interest. The following is taken closely from our previous work of Sudibandriyo (2003).

Activated carbon has the ability to adsorb various substances both from gas and liquid phases. It is a processed carbon material with a highly developed porous structure and a large internal specific surface area. It consists mainly of carbon (87-97%) and, in addition, contains such elements as hydrogen, oxygen, sulfur and nitrogen, as well as various compounds either originating from the raw material used or generated during its production. The pore volume of activated carbons usually greater than 0.2 cm^3/g; sometimes it even exceeds 1 cm^3/g. The inner specific surface area is generally greater than 400 m^2/g but in many instances it is greater than 1000 m^2/g.

The principal properties of manufactured activated carbons depend on the type and properties of the raw material used. Most important raw materials are wood

(sawdust), charcoal, peat, peat coke and coals. Coconut shells are also usually used to produce activated carbon with higher surface area. However, hard coals currently are the best raw materials. About 60% of activated carbon production in the United States is based on hard coal.

Among the activated carbon properties, the pore distribution is the most important one affecting its gas adsorption behavior. The volume of macropores (>50nm), mesopores (<50nm and >2nm), and micropores (<2nm) in activated carbons are usually in the range 0.2-0.8 cm^3/g, 0.1-0.5 cm^3/g and 0.2-0.6 cm^3/g. The surface area of the micropores, however, might contribute to 99% of the total surface area of the carbon [Kadlec et al., 1984].

Knowledge of coals is crucial for the adsorption modeling in coalbed methane recovery and CO_2 sequestration. The physical and chemical structural of coal are summarized by Meyers (1982) and listed below.

Table 3-1. Gross Open Pore Distribution in Coals

	Anthracite	Lignite
% Volume		
>30 nm	11.9	77.2
1.2-30 nm	13.1	3.5
<1.2 nm	75.0	19.3
% Area		
>30 nm	0.4	7.3
1.2-30 nm	1.1	1.2
<1.2 nm	98.5	91.5

Coal is a porous material. Table 3-1 shows the pore volumes in different diameter ranges for the highest (anthracite) and the lowest (lignite) rank of coal [Gan et al., 1972]. Pore volume contained in pores > 30 nm in diameter is estimated from mercury

porosimetry. Pore volume contained in pores in the diameter range 1.2-30 nm is estimated from the adsorption of the nitrogen isotherms using the Cranston and Inkey method (1957). Pore volume contained in pores < 1.2 nm in diameter is calculated by subtracting the total open volume accessible to helium from the volume obtained from both mercury porosimetry and nitrogen adsorption. The results show that the higher the coal rank is, the higher percent is the pore volume contained in the micropores (IUPAC defined macropores, mesopores, and micropores as pores in the diameter range of > 50 nm, 2-50 nm and < 2 nm, respectively). These results are also in good agreement with the pore size distribution obtained by Medek in 1977, who used the CO_2 adsorption isotherm in his method. The surface area distribution shown in Table 3-1 also indicates that the micropores play a major role for the adsorption of a small molecule.

The structure of coal at the molecular level of 10^{-9}-10^{-8} m consists of submicroscopic chemical species aggregated into crystalline and amorphous zones in both organic and mineral regions. This can be observed only by spectroscopic techniques and by effect on chemical reactivity. Listed below is the information observed using X-Ray diffraction for coals with a carbon content of 65-95% [Ergun et al., 1959]:

1. Carbon-carbon distances similar to those of graphite, with C-C bands about 0.14 nm in length

2. Interlayer distances between lamellae similar to those of graphite 0.343-0.354 nm for coals with carbon content of 84-94%

3. Polynuclear aromatic rings ranging from two to four condensed structures in coals with carbon content in the range 65-90%

25

CHAPTER 4

EXPERIMENTS AND ADSORPTION DATA

4.1 Review of Experimental Techniques

In this section, four widely used gas adsorption experimental techniques, volumetric, gravimetric, gas flow, and chromatographic techniques, are reviewed briefly.

The volumetric gas adsorption method calls for measuring the gas pressure in a calibrated constant volume cell, at a set temperature. The pressure and temperature of each dose of gas are measured and the gas is allowed to enter the adsorption bulk. After adsorption equilibrium has been established, the amount adsorbed is calculated from the change in pressure. This technique can only be used to measure the gas adsorption point-by-point, which is referred to as a discontinuous procedure. Also, when building a complete isotherm, additional successive errors might result from the dosing device. Because of its simplicity, however, many researchers use this technique [Reich et al., 1980; Vermesse et al., 1996; Krooss et al., 2002].

The gravimetric technique directly determines the amount adsorbed from the increase in mass measured by a balance. A simple gravimetric method uses a spring balance to determine the amount of gas adsorbed. However, in recent years spring balances have been largely superseded by electronic microbalance [Vaart et al., 2000; Salem et al., 1998; Beutekamp et al., 2002; Frére et al., 2002; Humayun et al., 2000].

An extremely sensitive gravimetric technique is based on the effect of change of mass on the resonance frequency of vibrating quartz crystal. In this case, the adsorbent must be firmly attached to the crystal [Krim et al., 1991].

In gas flow techniques, a flowmeter is used to determine the amount of gas adsorbed. The flowmeter can be a differential type [Nelsen et al., 1958] or a thermal detector [Pieters et al., 1984]. The thermal detector provides a signal, which depends on the heat capacity, the thermal conductivity, and the mass flow rate of the gas. These gas flow techniques can be used for either a continuous or discontinuous procedure.

The chromatographic technique involves a column packed with the adsorbent to separate the flowing species [Haydel et al., 1967]. The chromatographic analysis method is simple and fast in producing data but suffers from inherently larger errors [de Boer, 1968].

Detailed descriptions of the above experimental methods are given elsewhere [Sudibandriyo, 2003].

4.2 Experimental Method

Our experiments are based on the volumetric method. A brief description of the apparatus and procedures is as follows. The following is taken closely from our previous work of Gasem et al. (2003) and Sudibandriyo et al. (2003).

The experimental apparatus, shown schematically in Figure 4-1, has been used successfully in previous studies [Hall, 1993]. The pump and cell sections of the apparatus are maintained in a constant temperature air bath. The equilibrium cell has a volume of 110 cm^3 and is filled with the adsorbent to be studied. The cell is placed under

27
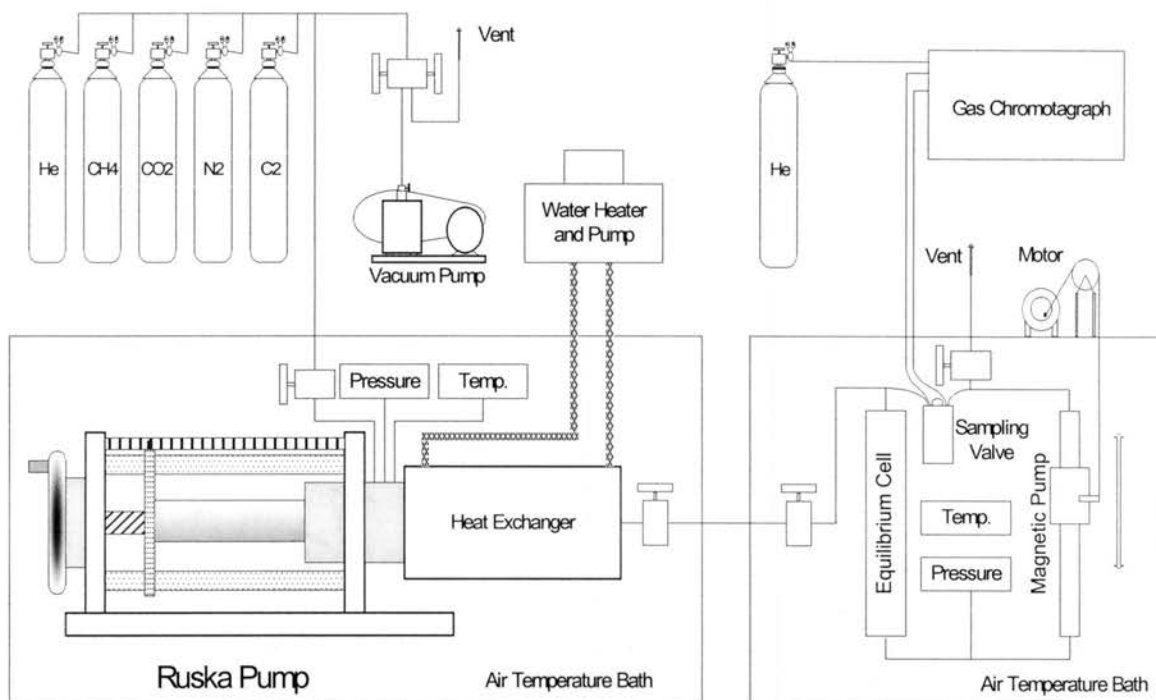
Figure 4-1. Schematic Diagram of the Experimental Apparatus

vacuum prior to gas injection. The void volume V_{void} in the equilibrium cell is then

determined by injecting known quantities of helium from a calibrated injection pump

(Ruska Pump). Since helium is not significantly adsorbed, the void volume can be

determined from measured values of temperature, pressure and amount of helium injected

into the cell. Several injections made into the cell at different pressures show consistency

in the calculated void volume. Generally, the void volume calculated from sequential

injections varies less than 0.3 cm^3 from the average value based on at least five

injections. The mass-balance equation, expressed in volumetric terms, is:

$$V_{void} = \frac{\left(\dfrac{P\Delta V}{ZT}\right)_{pump}}{\left(\dfrac{P_2}{Z_2 T} - \dfrac{P_1}{Z_1 T}\right)_{cell}} \tag{4-1}$$

where ΔV is the volume injected from the pump, Z is the compressibility factor of

helium, T is the temperature, P is the pressure, subscripts "cell" and "pump" refer to

conditions in the cell and pump sections of the apparatus, respectively, and "1" and "2" refer to conditions in the cell before and after injection of gas from the pump, respectively. This void volume is used in subsequent measurements of adsorption, as follows.

The Gibbs adsorption (also known as the excess adsorption) is calculated directly from experimental quantities. For pure-gas adsorption measurements, a known quantity, n_{inj}, of gas (e.g., methane) is injected from the pump section into the cell section. Some of the injected gas will be adsorbed, and the remainder, n_{unads}^{Gibbs}, will exist in the equilibrium bulk (gas) phase in the cell. A molar balance is used to calculate the amount adsorbed, n_{ads}^{Gibbs}, as:

$$n_{ads}^{Gibbs} = n_{inj} - n_{unads}^{Gibbs} \qquad (4\text{-}2)$$

The amount injected can be determined from pressure, temperature and volume measurements of the pump section:

$$n_{inj} = \left(\frac{P\Delta V}{ZRT}\right)_{pump} \qquad (4\text{-}3)$$

The amount of unadsorbed gas is calculated from conditions at equilibrium in the cell:

$$n_{unads}^{Gibbs} = \left(\frac{PV_{void}}{ZRT}\right)_{cell} \qquad (4\text{-}4)$$

In Equations 4-3 and 4-4, Z is the compressibility of the pure gas at the corresponding conditions of temperature and pressure.

The above steps are repeated sequentially at higher pressures to yield a complete adsorption isotherm. The amount adsorbed is usually presented as an intensive quantity (mmol adsorbed / g adsorbent or mmol/g) obtained by dividing n_{ads}^{Gibbs} by the mass of

adsorbent in the cell. Inspection of Equations 4-2 to 4-4 reveals that the amount adsorbed may be calculated in a straightforward manner from experimental measurements of pressures, temperatures and volumes, coupled with independent knowledge of the gas compressibility factors, Z (from experimental data or a suitably accurate equation of state).

For gas mixture adsorption measurements, a volumetrically prepared gas mixture of known composition (z_i) is injected; thus, the total amount of each component in the cell is known. A magnetic pump is used to circulate the fluid mixture to ensure that equilibrium is reached. The composition (y_i) of the gas phase in the cell at equilibrium is determined by chromatographic analysis. A pneumatically controlled sampling valve, contained in the air bath at cell temperature, sends a 20μL sample to the gas chromatograph (GC) for analysis. The amount of each individual component adsorbed is calculated using component material balances; for component "i" in the mixture, the relations are:

$$n_{ads(i)}^{Gibbs} = n_{inj(i)} - n_{unads(i)}^{Gibbs} = n_{inj} z_i - n_{unads}^{Gibbs} y_i \qquad (4\text{-}5)$$

where:

$$n_{inj(i)} = \left(\frac{P \Delta V}{ZRT} \right)_{pump} z_i \qquad (4\text{-}6)$$

and Z is the compressibility of the feed gas mixture at pump conditions, and

$$n_{unads(i)}^{Gibbs} = \left(\frac{P V_{void}}{ZRT} \right)_{cell} y_i \qquad (4\text{-}7)$$

where Z is the compressibility of the equilibrium gas mixture at cell conditions.

Calibrations were performed routinely during the course of the experiments. The temperature measuring devices were calibrated against a Minco platinum resistance

reference thermometer, and the pressure transducers were calibrated against a Ruska deadweight tester with calibration traceable to the National Institute of Science and Technology.

The gas chromatograph was calibrated against volumetrically prepared mixtures at the nominal feed-gas concentrations. The GC used for composition analysis is a Varian Chrompack CP-3800 with the helium carrier gas maintained at a 0.25-mL/s flow rate. A 10-ft Haysep D packed-column was used for CH_4+CO_2 and N_2+CO_2 systems, and a molecular sieve 13X column was used for the CH_4+N_2 system; column temperature was 353.2 K. A thermal conductivity detector was used for all of the binary systems studied; its bath temperature was set at 373.2 K. The chromatographic response factor, defined as $(A_2/A_1)/(y_2/y_1)$, where A is the GC response area, was found to depend slightly on pressure; as such, the GC was calibrated for each nominal composition at pressure intervals of 1.4 MPa.

4.3 Data Reduction

2-D EOSs model absolute adsorption. Calculations for the Gibbs and absolute adsorption differ in the manner by which n_{unads} is calculated. The Gibbs adsorption calculation, described above, neglects the volume occupied by the adsorbed phase in calculating the amount of unadsorbed gas (i.e., in Equation 4-4, the entire void volume, V_{void}, is viewed as being available to the unadsorbed gas).

Following is a discussion to clarify the relationships between the Gibbs and absolute adsorption and to highlight the approximate nature of the calculated absolute adsorption. In addition, expressions are presented which facilitate calculation of the

absolute component adsorption, $n^{abs}_{ads(i)}$, and the adsorbed-phase mole fraction, x^{abs}_i, in terms of the experimental Gibbs adsorption results. The following is taken closely from our previous work of Gasem et al. (2003) and Sudibandriyo et al. (2003).

In gas adsorption, various volumes can be used to characterize the state existing in the equilibrium cell. A representation that envisions two distinct, homogeneous fluid phases (bulk gas and adsorbed phase) expresses the total system volume V_{total} of the experimental apparatus as the sum of the volumes of solid adsorbent (V_{solid}), gas (V_{gas}), and adsorbed-phase (V_{ads}), as follows:

$$V_{total} = V_{solid} + V_{gas} + V_{ads} \tag{4-8}$$

The void volume, having been determined by helium injection, is related to these quantities as follows:

$$V_{void} = V_{gas} + V_{ads} = V_{total} - V_{solid} \tag{4-9}$$

Now, consider the amount of material adsorbed at equilibrium, which may be written in molar terms as follows:

$$n_{ads} = n_{total} - n_{unads} \tag{4-10}$$

The difference in the definitions of the Gibbs and total adsorption resides in the manner in which n_{unads} is related to the volume terms. As stated previously, in the Gibbs calculation, the volume occupied by the condensed phase is neglected in calculating n_{unads}, and the amount of unadsorbed gas is calculated using the entire void volume; thus, using Equation 4-9 for V_{void}, Equation 4-10 becomes:

$$n^{Gibbs}_{ads} = n_{total} - V_{void}\, \rho_{gas} \tag{4-11}$$

where ρ donates density. In the calculation of the absolute adsorption, n_{unads} is determined using the volume actually available to the bulk gas phase (accounting for the

reduction of volume accessible to the gas as a result of the volume occupied by the adsorbed phase):

$$n_{ads}^{Abs} = n_{total} - V_{gas} \, \rho_{gas} \tag{4-12}$$

Combining Equations 4-11 and 4-12 and eliminating n_{total}, the following relation between Gibbs and absolute adsorption is obtained:

$$n_{ads}^{Gibbs} = n_{ads}^{Abs} - V_{ads} \, \rho_{gas} \tag{4-13}$$

The volume of the adsorbed phase may be expressed in terms of the amount adsorbed and the density of the adsorbed phase as:

$$V_{ads} = n_{ads}^{Abs} / \rho_{ads} \tag{4-14}$$

Combining Equations 4-13 and 4-14 yields:

$$n_{ads}^{Gibbs} = V_{ads} \left(\rho_{ads} - \rho_{gas} \right) \tag{4-15}$$

Equation 4-15 clearly illustrates the physical interpretation of the Gibbs adsorption, namely, the amount adsorbed in excess of that which would be present if the adsorbed phase volume were filled with bulk gas. Combining Equations 4-14 and 4-15 leads to:

$$n_{ads}^{Abs} = n_{ads}^{Gibbs} \left(\frac{\rho_{ads}}{\rho_{ads} - \rho_{gas}} \right) \tag{4-16}$$

An important consideration in the calculation of the absolute adsorption is that it requires knowledge of the adsorbed phase density, ρ_{ads}, which is not readily available by experimental measurement. Thus, estimates of ρ_{ads} are usually employed. A commonly used approximation is the liquid density at the atmospheric pressure boiling point, as was done by Arri et al. (1992). In this work, the adsorbed phase density used is discussed in Chapter 5.

For mixture absolute adsorption, the component mole fractions in the adsorbed phase, x_i^{abs}, may be calculated from the component Gibbs adsorption; however, this requires some assumption regarding the density, ρ_{ads}, of the adsorbed phase mixture. In the following discussion, ρ_{ads} is approximated using the assumption of ideal mixing in the adsorbed phase, where the pure-component adsorbed-phase density estimates are used to calculate the mixture adsorbed-phase density. The component Gibbs adsorption (amount of component "i" in the adsorbed phase in excess of the amount that would be present if the bulk equilibrium gas mixture occupied the volume of the adsorbed phase) may be written using a component material balance as:

$$n_{ads(i)}^{Gibbs} = n_{ads}^{Abs} x_i^{Abs} - V_{ads} \rho_{gas} y_i = V_{ads} \left(\rho_{ads} x_i^{Abs} - \rho_{gas} y_i \right) \tag{4-17}$$

For convenience, we define a fractional component Gibbs adsorption, θ_i^{Gibbs}, as:

$$\theta_i^{Gibbs} = \frac{n_{ads(i)}^{Gibbs}}{n_{ads}^{Gibbs}} \tag{4-18}$$

(Note that, although Equation 4-18 has the appearance of a mole fraction, the Gibbs adsorption is an excess quantity, not a total quantity for a specified phase; thus θ, rather than x, is used to denote the quantity.)

Inserting this definition into Equation 4-17, we obtain:

$$n_{ads}^{Gibbs} \theta_i^{Gibbs} = n_{ads}^{Abs} x_i^{Abs} - y_i \frac{\rho_{gas}}{\rho_{ads}} \tag{4-19}$$

Combining Equation 4-16 with Equation 4-19, it yields:

$$x_i^{Abs} = \theta_i^{Gibbs} \left(1 - \frac{\rho_{gas}}{\rho_{ads}} \right) + y_i \frac{\rho_{gas}}{\rho_{ads}} \tag{4-20}$$

Equation 4-20 reveals that x_i^{abs} and θ_i^{Gibbs} become identical in the limit of low pressure (where ρ_{gas} becomes small).

Inspection of Equation 4-20 reveals that all quantities on the right hand side can be obtained directly from experimental measurements except ρ_{ads}, for which some approximation must be made. If ideal mixing is used to represent ρ_{ads} in terms of the pure component adsorbed-phase densities, we have:

$$\frac{1}{\rho_{ads}} = \sum_i^{NC} \frac{x_i^{Abs}}{\rho_{ads(i)}} \tag{4-21}$$

where the subscripts "i" refer to pure component i, NC is the number of components. Then, Equation 4-20 may be written as:

$$x_i^{Abs} = \theta_i^{Gibbs} - \sum_j^{NC} \frac{x_j^{Abs}}{\rho_{ads(j)}} \rho_{gas} \left(\theta_i^{Gibbs} - y_i \right) \tag{4-22}$$

x_i^{abs} can be solved from Equation 4-22 and the absolute component adsorption can be calculated as follows:

$$n_{ads(i)}^{Abs} = n_{ads}^{Abs} x_i^{Abs} \tag{4-23}$$

with Equation 4-16 used to calculate the total mixture adsorption, n_{ads}^{Abs}, where the densities, ρ_{ads} and ρ_{gas}, refer to mixtures of compositions x_i^{abs} and y_i, respectively.

As indicated by Equations 4-3 and 4-4, accurate gas-phase compressibility (Z) factors are required for methane, nitrogen, and CO_2 and their mixtures to properly analyze the experimental data. The compressibility factors for pure methane, nitrogen, and CO_2 were determined from highly accurate equations of state [Jaeschke et al., 1990; IUPAC, 1978; IUPAC, 1977; IUPAC, 1976]. For void volume determination, the helium compressibility factor is given by [see, e.g., Hall, 1993]:

$$Z_{He} = 1 + (0.001471 - 0.000004779T + 0.00000000492T^2)/P \qquad (4\text{-}24)$$

where T is in K and P is in atm.

A careful evaluation of the current literature led us to conclude that an adequate predictive capability for the mixture Z factors did not exist. Therefore, we elected to use available pure-fluid and binary mixture data to refit the Benedict-Webb-Rubin equation of state (BWR EOS) and improve its accuracy significantly. In general, the new BWR parameters yield deviations in the Z factors of less than 0.5%. This allowed us to address our compressibility factor needs for binary adsorption mixtures. Details of the BWR equation expressions are given in Appendix A.

4.4 Error Analysis

The uncertainties in the experimentally measured quantities after calibrations were estimated as follows: temperatures, 0.1 K; pressures, 7.0 kPa; injected gas volumes, 0.02 cm^3; gas mixture compositions, 0.002 mole fraction.

A detailed error propagation analysis was performed, which indicates that the average uncertainties for the pure adsorption measurements are approximately 1.8% (0.065-0.069 mmol/g) for methane adsorption, 2.3% (0.054-0.056 mmol/g) for nitrogen and 6.4 % (0.269-0.342 mmol/g) for CO_2 adsorption. The higher percentage uncertainty for CO_2 is due mainly to the lower value of the Gibbs adsorption for CO_2 at the higher pressure and the higher uncertainty in the CO_2 compressibility factor (due to proximity to its critical point).

The uncertainties for the binary mixture adsorption vary with composition. Uncertainties for all the binary gas total adsorption measurements are within 4%. The

percentage uncertainty of component gas adsorption, however, can become high at low concentrations of the less adsorbed gases (i.e., N_2 in the N_2+CO_2 system).

The detailed error propagation analyses are shown elsewhere [Hall, 1993].

4.5 Adsorption Database

Literature Data

The data in the literature on gas adsorption primarily concern two adsorbents: activated carbon and zeolites. Because the ultimate goal of this study is the modeling of gas adsorption on coals, attention is paid mainly to the data on carbon adsorbents (i.e. activated carbon). The experimental data for high-pressure gas adsorption on coals are scarce and complicated by (a) the difficulty in characterizing the coal matrix adequately and (b) assessing the effect of water (found in essentially all coalbeds) on the resulting data [Levy et al., 1997; Joubert et al., 1973; Hall et al., 1994]. Therefore, the gas adsorption data on activated carbon were used to evaluate the model prior to extending the model to include the effects of the complex adsorbent structure of coals and/or the presence of water.

The literature data for gas adsorption on activated carbon and other adsorbent are summarized in Tables 4-1 and 4-2. The data cover wide ranges of temperature, pressure and most pure and mixture components applicable for coalbed methane study. These data provide a useful source to evaluate the adsorption model for the whole range of total loadings. In addition, the data can also be used to evaluate the model capability of predicting multicomponent adsorption based on the data for pure-gas adsorption.

The literature database mainly includes coalbed methane gases, CH_4, CO_2, and N_2, adsorption on various activated carbons. It also includes C_2H_6, C_2H_4, C_3H_8, and H_2S adsorption on various activated carbons. The data cover wide ranges of temperature, pressure and provide a useful source to evaluate the adsorption model.

OSU Data

Table 4-3 documents the OSU CBM gas (CH_4, CO_2, and N_2) adsorption database. The database contains the pure, binary, and ternary mixture adsorption measurements conducted at Oklahoma State University. Included in the database are details regarding the adsorbates, the adsorbent, and the corresponding temperature and pressure ranges for each system. The following is taken closely from our previous work of Gasem et al. (2003).

Pure-gas adsorption measurements are reported for CH_4, N_2, C_2H_6, and CO_2 on ten solid matrices comprised of wet Fruitland coal (OSU #1 and OSU #2), wet Lower Basin Fruitland coal (OSU #3), wet / dry Illinois #6 coal, wet Tiffany coal, dry BeulahZap coal, dry Wyodak coal, dry Upper Freeport coal, dry Pocahontas coal, and dry activated carbon.

Binary adsorption measurements are presented for mixtures of methane, nitrogen and CO_2 at a series of compositions on four different matrices: Fruitland coal, Illinois #6 coal, Tiffany coal, and activated carbon. Ternary measurements are also presented for $CH_4+N_2+CO_2$ mixtures on wet, mixed Tiffany coal and on dry activated carbon.

38

Table 4-1. Literature Data Used for Pure-Gas Adsorption Model Evaluation

System No.	Adsorbent	Adsorbent Surf. area (m^2/g)	Adsorbate	Temp. Range (K)	Pressure Range (MPa)	Reference
1	AC, Columbia Grade L	1152	N_2	311 - 422	0.028 – 1.50	Ray (1950)
2	AC, Columbia Grade L	1152	CH_4	311 - 422	0.026 – 1.48	Ray (1950)
3	AC, Columbia Grade L	1152	C_2H_6	311 - 478	0.007 – 1.49	Ray (1950)
4	Charcoal	1157	CH_4	283 - 323	0.5 – 13.8	Payne (1968)
5	Charcoal	1157	C_3H_8	293 - 333	8×10^{-4} – 1.35	Payne (1968)
6	AC, BPL	988	CH_4	213 - 301	0.012 – 3.83	Reich (1980)
7	AC, BPL	988	C_2H_6	213 - 301	7×10^{-4} – 1.71	Reich (1980)
8	AC, BPL	988	C_2H_4	213 - 301	7×10^{-4} – 1.70	Reich (1980)
9	AC, BPL	988	CO_2	213 - 301	0.003 – 3.84	Reich (1980)
10	AC, PCB-Calgon Corp.	1150-1250	CH_4	296 - 480	0.27 – 6.69	Ritter (1987)
11	AC, PCB-Calgon Corp.	1150-1250	CO_2	296 - 480	0.11 – 3.67	Ritter (1987)
12	AC, F30/470, Chemviron Carbon	993.5	CO_2	278 - 328	0.05 – 3.35	Berlier (1997)
13	AC, Norit R1 Extra	1450	N_2	298	0.03 – 5.98	Dreisbach (1999)
14	AC, Norit R1 Extra	1450	CH_4	298	0.01 – 5.75	Dreisbach (1999)
15	AC, Norit R1 Extra	1450	CO_2	298	0.008 – 6.0	Dreisbach (1999)
16	AC, Coconut shell with KOH activation	3106 (CO_2 ads.)	CH_4	233 - 333	0.09 – 9.40	Zhou (2000)
17	AC, Calgon F-400	850	CO_2	303 - 318	0.02 – 20.2	Humayun (2000)
18	AC, Norit RB1	1100	CH_4	294 - 351	0.05 – 0.8	Vaart (2000)
19	AC, Norit RB1	1100	CO_2	294 - 348	0.05 – 0.8	Vaart (2000)
20	AC, Coconut shell with KOH activation	3106 (CO_2 ads.)	N_2	178 - 298	0.44 – 9.19	Zhou (2001)
21	AC, F30/470, Chemviron Carbon	993.5	N_2	303 - 383	0.39 – 9.5	Frére (2002)

Table 4-1. Literature Data Used for Pure-Gas Adsorption Model Evaluation - Cont'd

System No.	Adsorbent	Adsorbent Surf. area (m²/g)	Adsorbate	Temp. Range (K)	Pressure Range (MPa)	Reference
22	AC, F30/470, Chemviron Carbon	993.5	CH_4	303 - 383	0.44 – 8.98	Frére (2002)
23	AC, F30/470, Chemviron Carbon	993.5	C_3H_8	303 - 383	0.05 – 2.20	Frére (2002)
24	AC, Norit R1	1262	N_2	298	0.03 – 14.56	Beutekamp (2002)
25	AC, Norit R1	1262	CO_2	298	0.03 – 6.04	Beutekamp (2002)
26	Zeolite, Linde 13 X	525	N_2	298 - 348	0.35 – 8.23	Wakasugi (1981)
27	Zeolite, Linde 5A	~400	N_2	298 - 348	0.60 – 17.61	Wakasugi (1981)
28	Zeolite, Linde 5A	~400	CH_4	298 - 348	0.36 – 9. 18	Wakasugi (1981)
29	Zeolite, Linde 5A	~400	CO_2	298 - 348	0.03 – 11. 22	Wakasugi (1981)
30	Zeolite, Linde 5A	~400	C_2H_6	298 - 348	0.07 – 5.07	Wakasugi (1981)
31	H-Modernite, Norton Co: Type Z-900H	~300	CO_2	283 - 333	$3x10^{-4}$ – 0.29	Talu (1986)
32	H-Modernite, Norton Co: Type Z-900H	~300	H_2S	283 - 368	$4x10^{-4}$ – 0.10	Talu (1986)
33	H-Modernite, Norton Co: Type Z-900H	~300	C_3H_8	283 - 324	$2x10^{-5}$ – 0.21	Talu (1986)
34	Zeolite, G5	430	CH_4	283 - 303	0.13 – 1.15	Berlier (1995)
35	Zeolite, G5	430	C_2H_6	283 - 303	0.056 – 1.10	Berlier (1995)
36	Zeolite, G5	430	C_2H_4	283 - 303	0.056 – 1.10	Berlier (1995)
37	Zeolite, 13 X	383	CH_4	298	0.15 – 15.02	Beutekamp (2002)
38	Zeolite, 13 X	383	C_2H_6	298	0.14 – 3.95	Beutekamp (2002)

40

Table 4-2. Literature Data Used for Mixed-Gas Adsorption Model Evaluation

System No.	Adsorbent	Adsorbent Surf. area (m^2/g)	Adsorbate	Temp. Range (K)	Pressure Range (MPa)	Reference
39	AC, BPL	988	$CH_4 + C_2H_6$	301	0.13 – 2.01	Reich (1980)
40	AC, BPL	988	$CH_4 + C_2H_4$	301	0.12 – 2.03	Reich (1980)
41	AC, BPL	988	$C_2H_6 + C_2H_4$	301	0.14 – 1.98	Reich (1980)
42	AC, BPL	988	$CH_4 + C_2H_6 + C_2H_4$	301	0.12 – 2.97	Reich (1980)
43	AC, Norit R1 Extra	1450	$N_2 + CH_4$	298	0.03 – 6.00	Dreisbach (1999)
44	AC, Norit R1 Extra	1450	$CH_4 + CO_2$	298	0.03 – 6.00	Dreisbach (1999)
45	AC, Norit R1 Extra	1450	$N_2 + CO_2$	298	0.03 – 6.00	Dreisbach (1999)
46	AC, Norit R1 Extra	1450	$N_2 + CH_4 + CO_2$	298	0.03 – 6.00	Dreisbach (1999)

Table 4-3. The OSU Adsorption Database

System No.	Adsorbent	Adsorbate	Temp. (K)	Pressure Range (MPa)
47	Dry AC, Calgon F 400	N_2	318	0.7 – 13.7
48	Dry AC, Calgon F 400	CH_4	318	0.7 – 13.7
49	Dry AC, Calgon F 400	CO_2	318	0.7 – 13.7
50	Dry AC, Calgon F 400	C_2H_6	318	0.7 – 13.7
51	Dry AC, Calgon F 400	$N_2 + CH_4$	318	0.7 – 12.4
52	Dry AC, Calgon F 400	$CH_4 + CO_2$	318	0.7 – 12.4
53	Dry AC, Calgon F 400	$N_2 + CO_2$	318	0.7 – 12.4
54	Dry AC, Calgon F 400	$N_2 + CH_4 + CO_2$	318	0.7 – 12.4
55a	Wet Fruitland Coal OSU #1	N_2	319	0.7 – 12.4
56a	Wet Fruitland Coal OSU #1	CH_4	319	0.7 – 12.4
57a	Wet Fruitland Coal OSU #1	CO_2	319	0.7 – 12.4
55b	Wet Fruitland Coal OSU #2	N_2	319	0.7 – 12.4
56b	Wet Fruitland Coal OSU #2	CH_4	319	0.7 – 12.4
57b	Wet Fruitland Coal OSU #2	CO_2	319	0.7 – 12.4
58	Wet Fruitland Coal OSU #1	$N_2 + CH_4$	319	0.7 – 12.4
59	Wet Fruitland Coal OSU #1	$CH_4 + CO_2$	319	0.7 – 12.4
60	Wet Fruitland Coal OSU #1	$N_2 + CO_2$	319	0.7 – 12.4
61	Wet Illinois #6 Coal	N_2	319	0.7 – 12.4
62	Wet Illinois #6 Coal	CH_4	319	0.7 – 12.4
63	Wet Illinois #6 Coal	CO_2	319	0.7 – 12.4
64	Wet Illinois #6 Coal	$N_2 + CH_4$	319	0.7 – 12.4
65	Wet Illinois #6 Coal	$CH_4 + CO_2$	319	0.7 – 12.4
66	Wet Illinois #6 Coal	$N_2 + CO_2$	319	0.7 – 12.4
67	Wet Tiffany Coal	N_2	328	0.7 – 13.7
68	Wet Tiffany Coal	CH_4	328	0.7 – 13.7
69	Wet Tiffany Coal	CO_2	328	0.7 – 13.7
70	Wet Tiffany Coal	$N_2 + CH_4$	328	0.7 – 13.7
71	Wet Tiffany Coal	$CH_4 + CO_2$	328	0.7 – 13.7
72	Wet Tiffany Coal	$N_2 + CO_2$	328	0.7 – 13.7
73	Wet Tiffany Coal	$N_2 + CH_4 + CO_2$	328	0.7 – 13.7
74	Wet LB Fruitland Coal	N_2	319	0.7 – 12.4
75	Wet LB Fruitland Coal	CH_4	319	0.7 – 12.4
76	Wet LB Fruitland Coal	CO_2	319	0.7 – 12.4
77	Dry Illinois #6 Coal	CO_2	328	0.7 – 13.7
78	Dry Beulah Zap Coal	CO_2	328	0.7 – 13.7
79	Dry Wyodak Coal	CO_2	328	0.7 – 13.7
80	Dry Upper Freeport Coal	CO_2	328	0.7 – 13.7
81	Dry Pocahontas Coal	CO_2	328	0.7 – 13.7

Tables 4-4 and 4-5 present the compositional analyses for the various solid matrices considered. The activated carbon used was Filtrasorb 400, 12x40 mesh, from Calgon Carbon company. The activated carbon was dried under vacuum at 431.5 K for two days before the adsorption measurements. The nitrogen BET surface area at 77 K has been reported by Humayun et al. (2000) to be 850 m^2/g. The surface area value provided by the supplier, however, is 998 m^2/g.

Four different wet coals were prepared for adsorption measurements. The Fruitland coal is from the San Juan Basin; it is a medium volatile bituminous coal. This recently prepared sample (OSU #2) has a slightly different composition from the one used in previous measurements (OSU #1). The Lower Basin (LB) Fruitland coal is from the same coalbed seam as Fruitland coal, but it was taken from a different location. The Illinois #6 coal is a high volatile bituminous coal. Other coal samples are from BP Amoco Tiffany Injection Wells #1 and #10. The coal samples were ground to 200μm particles and moistened with water. This made the sample moisture content varies from 4 to 15% (by weight), which is higher than the equilibrium moisture content. Equilibrium moisture content was determined gravimetrically by exposing dry coal to 303.1 K air at 96-99% saturation.

In addition, five types of coal samples prepared by Argonne National Laboratory were used to study CO_2 adsorption on dry coals. The coals were dried under vacuum in an equilibrium cell at 353 K for 36 hours before being used in the adsorption measurements. Complete database is available in our report prepared for the U.S. Department of Energy [Gasem et al., 2003].

43

Table 4-4. Compositional Analysis of Solid Matrices Used in This Study

Analysis	Activated Carbon	Fruitland Amoco	Fruitland OSU #1	Fruitland OSU #2	Illinois-6	Lower Basin Fruitland OSU #3a	Lower Basin Fruitland OSU #3b	Tiffany Well #1	Tiffany Well #10
Ultimate*									
Carbon %	88.65	68.56	68.63	66.58	71.47	38.92	40.20	47.78	56.75
Hydrogen %	0.74	5.74	4.27	4.23	5.13	3.08	3.10	2.62	2.77
Oxygen %	3.01	7.19	0.89	5.08	9.85	3.75	2.87	6.19	5.16
Nitrogen %	0.40	1.40	1.57	1.47	1.46	0.87	0.89	0.92	1.02
Sulfur %	0.73	0.65	4.19	0.72	1.27	1.73	2.14	0.57	0.52
Ash %	6.46	16.45	20.45	21.92	10.81	51.66	50.81	49.71	47.74
Proximate*									
Vol. Matter %	3.68	19.12	20.2	20.33	30.61	20.01	14.00	15.48	15.35
Fixed Carbon %	89.86	64.42	59.35	57.75	55.90	28.33	35.19	34.82	36.91
Equil. Moisture Content (%)	35	2.3	2.2	2.2	3.9	4.0	4.0	3.8	3.7

* Huffman Laboratories, Inc., Golden, Colorado.

Table 4-5. Compositional Analysis of Coals from Argonne National Laboratory

Analysis*	Beulah Zap	Wyodak	Illinois-6	Upper Freeport	Pocahon-tas
Ultimate					
Carbon %	72.9	75.0	77.7	85.5	91.1
Hydrogen %	4.83	5.35	5.00	4.70	4.44
Oxygen %	20.3	18.0	13.5	7.5	2.5
Sulfur %	0.80	0.63	4.83	2.32	0.66
Ash %	9.7	8.8	15.5	13.2	4.8
Proximate					
Moisture %	32.2	28.1	8.0	1.1	0.7
Vol. Matter %	30.5	32.2	36.9	27. 1	18.5
Fixed Carbon %	30.7	33.0	40.9	58.7	76.1
Ash %	6.6	6.3	14.3	13.0	4.7

* Analyses were provided by the Argonne National Laboratory

CHAPTER 5

TWO-DIMENSIONAL EQUATIONS OF STATE

5.1 Review of Two-Dimensional Equations of State

Although several frameworks are used to describe the adsorption phenomena and correlate pure-gas and mixture adsorption isotherms, the 2-Ds EOS offer distinct advantages in modeling supercritical, high-pressure adsorption systems. The advantages include:

1. Ease of implementation of a well-developed framework; the 2-Ds EOS are analogues of the 3-D EOSs used for PVT behavior modeling

2. Availability of 2-D mixing rules for multi-component mixtures in direct analogy to 3-D mixing theories

3. Similarity of the adsorption algorithms to vapor-liquid equilibrium algorithms; thus the ability to facilitate CBM process simulations

Over the years, various researchers have applied the 2-D EOSs to gas adsorption. Hill (1946) and de Boer (1968) have used the van der Waals (VDW) EOS to correlate pure-gas adsorption. Hoory et al. (1967) extended the 2-D VDW EOS to mixtures by introducing mixing rules. More recently, DeGance (1992) used the 2-D virial and Eyring EOS to correlate high-pressure pure adsorption isotherms.

In early 1990's, we presented a generalized 2-D cubic EOS, which encompasses 2-D analogs of previous cubic EOS forms [Zhou et al., 1994]. The generalized 2-D EOS (with an additional parameter, m, for added model flexibility) is analogous to the popular three-dimensional equations of state used in vapor-liquid equilibrium calculations:

$$\left[\pi + \frac{a_2\sigma^2}{1 + Ub_2\sigma + W(b_2\sigma)^2}\right]\left[1 - (b_2\sigma)^m\right] = \sigma RT \tag{5-1}$$

where a_2 and b_2 are the 2-D EOS parameters, and numerical values of U, W, and m may be specified to give various forms of two-dimensional equations of state.

The general two-dimensional analog can be re-written as follows:

$$\left[A\pi + \frac{\alpha\omega^2}{1 + U\beta\omega + W(\beta\omega)^2}\right]\left[1 - (\beta\omega)^m\right] = \omega RT \tag{5-2}$$

where A is the specific surface area, π is the spreading pressure, σ is the surface density of the adsorbate, $\omega = \sigma A$ is the specific amount adsorbed, and $\alpha = a_2/A$ and $\beta = b_2/A$ are model parameters. The model coefficients, U, W, and m must be specified to obtain a specific form of the 2-D EOSs for application. For example, an analog of the van der Waals (VDW) EOS is obtained by setting m = 1 and U = W = 0; similarly for the Soave-Redlich-Kwong (SRK) (m = U = 1 and W = 0); the Peng-Robinson (PR) (m = 1, U = 2, and W = -1); and the Eyring (m = 1/2 and U = W = 0) EOS.

This general 2-D EOS can be used to investigate EOS behaviors by specifying various combinations of model coefficients. Selection of the model coefficient m is the most important among the EOS model coefficients because it is in the repulsive term and has a significant effect on the shape of the pure adsorption isotherm. Based on extensive

47

calculations, Zhou found that an equation with m = 1/3 and U = W = 0 (the Zhou-Gasem-Robinson (ZGR) EOS) promising [Zhou et al., 1994].

Among all the 2-D EOSs, we can divide them to two categories based on the value of the exponent m; i.e., m<1 or m=1. In this work, we evaluated two typical 2-D EOSs, the ZGR EOS and 2-D PR EOS, because each of them can well represent its category.

5.2 Equilibrium Relations

As elaborated in Chapter 2, at equilibrium, the chemical potential of species i in the adsorbed phase, μ_i^a, is equal to that in the gas phase, μ_i^g:

$$\mu_i^a = \mu_i^g \text{ and } d\mu_i^a = d\mu_i^g \tag{5-3}$$

Thus,

$$\int_{\pi^*}^{\pi} d\ln \hat{f}_i^a = \int_{P^*}^{P} d\ln \hat{f}_i^g \tag{5-4}$$

Integrating Equation 5-4, it yields:

$$\ln \hat{f}_i^a (\pi) - \ln \hat{f}_i^a (\pi^*) = \ln \hat{f}_i^g (P) - \ln \hat{f}_i^g (P^*) \tag{5-5}$$

At very low pressure, $\hat{f}_i^a (\pi^*) = \pi_i^*$ and $\hat{f}_i^g (P^*) = P_i^*$

$$P_i^* \hat{f}_i^a (\pi) = \pi_i^* \hat{f}_i^g (P) \tag{5-6}$$

At very low pressure, 2-D ideal gas law applies:

$$\pi_i^* A = \omega_i^* RT \tag{5-7}$$

Henry's constant is defined as:

$$k_i = \frac{\omega_i^*}{P_i^*} \tag{5-8}$$

48

So, substitution into Equation 5-6, we obtain:

$$A\hat{f}_i^a = Ax_i\pi\hat{\phi}_i^a = k_iRT\hat{f}_i^g \qquad (5-9)$$

For pure-gas adsorption, Equation 5-9 becomes:

$$\omega Z_a\phi^a = k_if^g \qquad (5-10)$$

The fugacity for the 2-D EOS is:

$$\ln\hat{\phi}_i^a = \int_0^\omega \left[\frac{1}{RT\omega} \frac{\partial(A\pi)}{\partial\omega_i}\bigg|_{T,M_s,n_j} - \frac{1}{\omega} \right]d\omega - \ln Z_a \qquad (5-11)$$

where ω is the amount adsorbed, Z_a is the 2-D compressibility factor, ϕ^a is the fugacity coefficient using the 2-D EOS, f^g is the fugacity for the gas phase. The 3-D PR EOS was used to calculate the gas fugacity. Detailed derivation of Equation 5-11 was provided by Zhou (1994).

5.3 Mixing Rules

One-fluid mixing rules were used in the 2-D EOS to describe mixture adsorption data:

$$\alpha = \sum_i\sum_j x_ix_j\alpha_{ij} \quad \text{and} \quad \beta = \sum_i\sum_j x_ix_j\beta_{ij} \qquad (5-12)$$

The combination rules below are chosen because they work best for adsorbed phase [Zhou et al., 1994]:

$$\alpha_{ij} = (\alpha_i + \alpha_j)(1 - C_{ij})/2 \qquad (5-13)$$

$$\beta_{ij} = \sqrt{\beta_i\beta_j}(1 + D_{ij})/2 \qquad (5-14)$$

However, other mixing rules can be applied to 2-D EOS to calculate the mixture adsorption.

49

5.4 Equilibrium Calculation Initialization Methods

Only physically meaningful parameters can serve as a rational basis for parameter generalizations. When we perform regressions for pure-gas adsorption using the 2-D EOS, random parameterization may lead to trivial solutions. Therefore, the initial guesses for α, β, and k are critical since the 2-D EOS parameter regressions involve nonlinear equations. For example, Zhou (1994) reported pure nitrogen adsorption on wet Fruitland coal at 319.3 K using the ZGR EOS with the percentage average absolute deviation (%AAD) of 1.7%. The model parameter α is equal to -1887 (bar cm^3 g/mmol / mol) and β is equal to 0.001 (mmol/g)$^{-1}$. However, β being equal to 0.001 (mmol/g)$^{-1}$ is physically incorrect because it means 1 gram of adsorbent can adsorb 1 mole of gas when the pressure is high, which is unrealistically high. The unrealistic-regressed parameters are due to the improper initial guesses.

The 2-D EOS adsorption calculation is an equal-fugacity calculation. To generate initial guesses, one can assume the fugacity in the bulk phase to be ideal. Thus, Gibbs isotherm can be derived as [see, e.g., Do, 1998]:

$$\left(\frac{d\pi}{d\ln P}\right)_T = \frac{n}{A}RT \tag{5-15}$$

Applying the generalized 2-D EOS into the above equation, the following expression is derived:

$$BP = \left(\frac{\theta^{1/m}}{1-\theta^{1/m}}\right)^m \exp\left(\frac{\theta^{1/m}}{1-\theta^{1/m}}\right)\exp(-c\theta) \tag{5-16}$$

where $\theta = \omega/L$; L, B and c are model parameters. Thus, the initial guesses for the 2-D EOS can be obtained from Equation 5-16. However, it is still not easy to get the initial

guesses from Equation 5-6. The Langmuir model is an alternative because of its simplicity, where:

$$BP = \frac{\theta}{1-\theta}$$ (5-17)

The empirical initial guesses can be related to Langmuir model parameters of the same isotherm:

$\alpha=200$ (bar cm^3 g/mmol / mol)

$\beta=1/(2L)$ (mmol/g)$^{-1}$

$k=5LB$ (mmol/g bar^{-1})

For the example above, by using this initial guess method, we can obtain L = 0.694 (mmol/g) and B = 0.0102 (bar^{-1}) for the Langmuir model, so the initial guess could be α =200 (bar cm^3 g/mmol/mol), β=0.72 (mmol/g)$^{-1}$, and k=0.0355 (mmol/g bar^{-1}). Upon regression, the parameters are: α=109450 (bar cm^3 g/mmol / mol), β=0.776 (mmol/g)$^{-1}$, and k=0.0311 (mmol/g bar^{-1}) with %AAD of 2.6%. Although the %AAD is slightly higher, the parameters are meaningful and thus can be used in the temperature dependence correlations and mixture calculations.

5.5 Two-Dimensional Equations of State for Gibbs Excess Adsorption

As described in the previous chapter, the experiment measures the Gibbs Excess adsorption, but the 2-D EOS uses absolute adsorption data in the calculation. The relation between Gibbs adsorption (ω^{Gibbs}) and absolute adsorption (ω^{Abs}) is:

$$\omega^{Abs} = \frac{\omega^{Gibbs}}{1 - \dfrac{\rho_{gas}}{\rho_{ads}}}$$ (5-19)

where ρ_{gas} and ρ_{ads} are bulk gas density and adsorbed-phase density.

In our previous calculations, we assumed ρ_{ads} is a known constant for a given adsorbate on different adsorbents and that it is pressure independent. The adsorbed-phase density is treated as equal to the saturated liquid density. The densities of saturated liquid nitrogen and methane at their normal boiling points are known. The saturated liquid densities of nitrogen and methane at atmospheric pressure are 0.808 g/cm^3 and 0.421 g/cm^3, respectively. For CO_2, we used its triple point density 1.18 g/cm^3 [Liang, 1999].

When Gibbs adsorption goes to zero (at high pressure), the adsorbed-phase density is equal to bulk phase density. Experimental results indicate that Gibbs adsorption isotherms approach zero when the bulk phase density is high enough. Thus, an alternative method to determine the adsorbed-phase density is to treat it as a parameter to be regressed from Gibbs adsorption data.

Even though the adsorbed-phase density can be regressed from experimental data, it is very sensitive to the uncertainties in the experimental data. For example, for CO_2 adsorption on dry Illinois #6 coal at 328.2 K, a 1% change in void volume, which is an experimentally measured value, could cause up to 40% difference in maximum adsorbed-phase density. Meanwhile, for low-pressure adsorption isotherms, Gibbs adsorption data do not reach a maximum, making it very hard to regress a reasonable adsorbed-phase density in these cases.

The 3-D VDW covolume for CO_2, N_2, and CH_4 are 0.0429, 0.0386, and 0.0431 liter/mole. Converted to density, they will be 1.027, 0.725, and 0.371 gram/cm^3, respectively. The regressed maximum densities for these three gases on activated carbon at 318.2 K are 0.982, 0.839, and 0.346 gram/cm^3. Thus, the 3-D VDW covolume

provides an alternative to estimate the maximum adsorbed-phase density and it is consistent when we use the EOS to do all the adsorption calculations.

In this work, when converting the Gibbs adsorption data into absolute adsorption data, we used Equation 5-19 with the adsorbed-phase densities being the inverse of the 3-D VDW covolume, unless mentioned otherwise.

CHAPTER 6

MODELING OF PURE-GAS ADSORPTION

In this chapter, we develop a new approach for estimating the 2-D EOS model parameters, and consequently, provide for generalized 2-D EOS pure-gas adsorption predictions. Specifically, correlations are developed to describe the temperature dependence of the 2-D EOS parameters, and the parameters are generalized in terms of adsorbate and adsorbent physical properties. The 2-D EOS correlative capabilities are evaluated, especially for coalbed gases, CH_4, CO_2, and N_2 adsorption on carbon adsorbents. Two specific 2-D EOS example models, the ZGR EOS and the 2-D PR EOS, are evaluated.

6.1 Database Used

A literature database (Table 4-1) and the OSU database (Table 4-3) are used to evaluate the modeling of pure-gas adsorption. All the systems documented in Table 4-1 and all the pure-gas adsorption systems from Table 4-3 are used.

The objective function, S, is used to correlate data with the 2-D EOSs. The function minimizes the sum of the squared-percentage deviations in predicted adsorption:

$$S = 100 \sqrt{ \frac{\sum_{i=1}^{NPTS} \left[\dfrac{\omega_i^c - \omega_i^e}{\omega_i^e} \right]^2}{NPTS} } \qquad (6\text{-}1)$$

where ω^c and ω^e are the calculated and experimental adsorption amount, respectively. NPTS is the number of data points. When the experimental uncertainties are available, the objective function, S_σ, is used to correlate data with the 2-D EOS models. The function minimizes the sum of the squared weighted deviations in predicted adsorption:

$$S_\sigma = \sqrt{\frac{\sum_{i=1}^{NPTS}\left[\frac{\omega_i^c - \omega_i^e}{\sigma_i^e}\right]^2}{NPTS}} \tag{6-2}$$

where, σ^e is the expected experimental uncertainty. The percentage average absolute deviation (%AAD) and root-mean-square error (RMSE) are used to evaluate the results:

$$\%AAD = \frac{100}{NPTS}\sum_{i=1}^{NPTS}\left|\frac{\omega_i^c - \omega_i^e}{\omega_i^e}\right| \tag{6-3}$$

$$RMSE = \sqrt{\frac{\sum_{i=1}^{NPTS}\left(\omega_i^c - \omega_i^e\right)^2}{NPTS}} \tag{6-4}$$

The weighted average absolute deviation (WAAD) is also used to quantify the model evaluations when the expected experimental uncertainties are available:

$$WAAD = \frac{1}{NPTS}\sum_{i=1}^{NPTS}\left|\frac{\omega_i^c - \omega_i^e}{\sigma_i^e}\right| \tag{6-5}$$

Typically, literature data do not provide the expected experimental uncertainty for each measurement; thus, the WAAD evaluation is not included in the corresponding tables.

6.2 Correlation of Pure-Gas adsorption

In this section, the correlative capabilities of the ZGR EOS and 2-D PR EOS are evaluated. In this case, the model parameters, α, β, and k, are regressed for each

isotherm. The units for the parameter, α, β, and k are (bar cm^3 mol^{-1} (mmol/g)$^{-1}$), (mmol/g)$^{-1}$, and (mmol/g bar^{-1}), respectively.

Table 6-1 presents summary results for the ZGR EOS representation of the literature data. The overall AAD for the 2363 literature data points is 1.7% and the overall RMSE is 0.096 mmol/g. As indicated by the results, N_2 adsorption on Columbia Grade L activated carbon at 422.0 K (System 1) has the worst quality of fit with an AAD of 6.9%, and N_2 adsorption on Coconut Shell activated carbon at 178.0 K (System 20) has the worst RMSE of 0.299 mmol/g.

Table 6-2 presents summary results for the 2-D PR EOS representation of the literature data. The overall AAD is 1.5% and the overall RMSE is 0.097 mmol/g. For this model, CO_2 adsorption on H-Modernite, Z-900H at 323.0 K (System 31) has the worst quality of fit with AAD of 5.9%. CO_2 adsorption on F30/470 Chemviron activated carbon at 278.0 K (System 12) has the worst RMSE of 0.273 mmol/g.

These results show that both the ZGR EOS and the 2-D PR EOS are capable of representing the pure-gas adsorption equilibrium data on the carbon adsorbents, as well as other adsorbents. Overall, the two models can represent the experimental data equally well. For a complete adsorption isotherm, the ZGR EOS represents the adsorption data better than the 2-D PR EOS at high pressures, while at lower pressures the 2-D PR EOS represents the data more precisely. Since the amount of adsorption is small at low pressure, small absolute errors will lead to large percentage errors. This explains why the ZGR EOS represents the data with slightly higher %AAD and a lower RMSE than for 2-D PR EOS.

Table 6-1. Regression Results for Pure-Gas Adsorption Using the ZGR EOS (Literature Data)

System No.	Adsorbent	Adsorbate	NPTS	T (K)	Parameters α	Parameters β	Parameters -ln(k)	%AAD	RMSE (mmol/g)
1	AC, Columbia Grade L	N_2	9	310.9	29044.0	0.1970	-0.1972	4.0	0.018
			5	338.7	38094.0	0.2317	0.2569	0.9	0.021
			9	366.5	65053.0	0.3304	0.8711	5.8	0.014
			8	394.3	92188.0	0.4234	1.2188	4.6	0.015
			5	422.0	165120.0	0.6722	1.5681	6.5	0.051
2	AC, Columbia Grade L	CH_4	12	310.9	12826.0	0.1027	-1.5128	4.6	0.035
			10	338.7	20396.0	0.1373	-0.9923	3.0	0.062
			8	366.5	36268.0	0.1938	-0.3557	3.2	0.063
			7	394.3	45037.0	0.2327	0.0464	3.4	0.039
			8	422.0	68579.0	0.3000	0.5199	3.7	0.033
3	AC, Columbia Grade L	C_2H_6	10	310.9	5088.1	0.0786	-4.8089	1.1	0.107
			9	338.7	8669.9	0.0941	-3.8745	0.4	0.016
			10	366.5	10854.0	0.0998	-3.0381	1.7	0.039
			10	394.3	10597.0	0.0953	-2.4349	2.4	0.022
			9	422.0	25601.0	0.1383	-1.6549	1.5	0.055
			5	449.8	19902.0	0.1197	-1.2724	0.6	0.022
			5	477.6	25903.0	0.1314	-0.6391	0.7	0.020
4	Charcoal	CH_4	8	283.2	3213.3	0.0455	-2.3149	0.1	0.007
			12	293.2	3499.3	0.0469	-2.0478	0.4	0.027
			12	303.2	5048.1	0.0535	-1.7118	0.3	0.022
			10	313.2	6795.5	0.0598	-1.2870	0.8	0.044
			13	323.2	7282.7	0.0627	-1.1558	0.8	0.027

57

Table 6-1. Regression Results for Pure-Gas Adsorption Using the ZGR EOS (Literature Data) - Cont'd.

System No.	Adsorbent	Adsorbate	NPTS	T (K)	Parameters			%AAD	RMSE (mmol/g)
					α	β	$-\ln(k)$		
5	Charcoal	C_3H_8	10	293.2	8094.2	0.0885	-6.5361	2.9	0.136
			11	303.2	2898.4	0.0769	-7.1687	1.0	0.056
			10	313.2	4564.9	0.0796	-6.4215	0.8	0.039
			11	323.2	6280.1	0.0845	-5.8480	0.6	0.032
			10	333.2	6449.8	0.0874	-5.7200	0.2	0.016
6	AC, BPL	CH_4	23	212.7	2488.2	0.0581	-4.2230	1.3	0.123
			24	260.2	4649.3	0.0638	-2.3138	1.0	0.039
			25	301.4	9887.4	0.0873	-1.1285	1.1	0.026
7	AC, BPL	C_2H_6	18	212.7	4260.2	0.0833	-8.1825	2.6	0.168
			15	260.2	2714.8	0.0752	-6.1280	0.9	0.056
			16	301.4	6583.2	0.0865	-4.1326	0.7	0.031
8	AC, BPL	C_2H_4	21	212.7	-1335.4	0.0518	-8.5283	2.9	0.163
			15	260.2	2473.5	0.0674	-5.4529	0.5	0.027
			16	301.4	5703.9	0.0783	-3.6855	0.6	0.028
9	AC, BPL	CO_2	21	212.7	3346.4	0.0481	-5.8453	1.0	0.056
			14	260.2	3944.4	0.0477	-3.5773	0.3	0.020
			25	301.4	5310.8	0.0509	-2.1118	0.9	0.054
10	AC, PCB-Calgon	CH_4	7	296.0	7504.7	0.0724	-1.8382	0.2	0.016
			8	373.0	10975.0	0.0847	-0.4204	0.7	0.025
			7	480.0	49443.0	0.1952	1.4678	1.5	0.036
11	AC, PCB-Calgon	CO_2	4	296.0	4566.7	0.0467	-2.9818	0.1	0.022
			4	373.0	9531.0	0.0634	-0.9731	1.1	0.048
			4	480.0	23246.0	0.1057	0.5901	1.2	0.028

Table 6-1. Regression Results for Pure-Gas Adsorption Using the ZGR EOS (Literature Data) - Cont'd.

System No.	Adsorbent	Adsorbate	NPTS	T (K)	Parameters			%AAD	RMSE (mmol/g)
					α	β	$-\ln(k)$		
12	AC, F30/470 Chemviron Carbon	CO_2	30	278.0	3770.1	0.0518	-3.8627	1.3	0.274
			19	288.0	2569.9	0.0441	-3.5255	1.1	0.156
			19	298.0	4217.3	0.0520	-3.0716	0.3	0.039
			19	303.0	4214.3	0.0520	-3.0045	0.4	0.028
			38	308.0	4193.7	0.0516	-2.9226	0.5	0.047
			19	318.0	4611.1	0.0532	-2.4638	0.5	0.039
			20	328.0	6329.5	0.0619	-2.1993	0.7	0.037
13	AC, Norit R1 Extra	N_2	10	298.0	13302.0	0.0999	-0.1924	5.0	0.074
14	AC, Norit R1 Extra	CH_4	12	298.0	6276.9	0.0600	-1.6807	2.9	0.028
15	AC, Norit R1 Extra	CO_2	12	298.0	3957.2	0.0377	-2.5799	3.4	0.042
16	AC, Coconut Shell	CH_4	21	233.0	1220.3	0.0191	-3.2053	0.8	0.205
			19	253.0	1670.1	0.0208	-2.6098	0.8	0.130
			22	273.0	2029.6	0.0228	-2.2061	0.9	0.105
			21	293.0	2648.1	0.0253	-1.7117	1.0	0.070
			20	313.0	3603.1	0.0292	-1.2143	1.5	0.076
			19	333.0	4512.7	0.0323	-0.8048	1.9	0.088
17	AC, Calgon F-400	CO_2	75	303.6	3575.1	0.0443	-2.5517	2.0	0.164
			74	305.2	4051.9	0.0444	-2.2401	3.1	0.216
			75	309.2	3731.1	0.0426	-2.1518	2.8	0.174
			76	313.2	2894.4	0.0388	-2.1469	2.7	0.126
			76	318.2	4939.2	0.0494	-1.9917	2.7	0.137

59

Table 6-1. Regression Results for Pure-Gas Adsorption Using the ZGR EOS (Literature Data) - Cont'd.

System No.	Adsorbent	Adsorbate	NPTS	T (K)	Parameters			%AAD	RMSE (mmol/g)
					α	β	-ln(k)		
18	AC, Norit RB1	CH_4	16	304.9	7147.5	0.0798	-2.1724	0.2	0.005
			16	311.4	11509.0	0.1019	-1.6680	0.5	0.008
			16	331.3	17080.0	0.1266	-1.2123	0.7	0.010
			16	350.5	24887.0	0.1604	-0.8182	0.9	0.009
19	AC, Norit RB1	CO_2	16	305.2	4969.1	0.0544	-3.0951	0.1	0.005
			16	311.2	6392.0	0.0615	-2.5513	0.2	0.007
			16	329.5	8877.3	0.0733	-2.0516	0.5	0.011
			16	348.3	13363.0	0.0951	-1.6172	0.7	0.017
20	AC, Coconut Shell	N_2	10	178.0	619.8	0.0192	-3.8980	1.8	0.299
			11	198.0	1320.8	0.0233	-3.0557	0.8	0.139
			10	218.0	2044.5	0.0279	-2.3677	0.5	0.061
			10	233.0	2550.2	0.0305	-1.7953	0.2	0.023
			11	258.0	3185.9	0.0333	-1.3115	0.2	0.021
			10	278.0	3213.5	0.0336	-0.9952	0.8	0.060
			9	298.0	4605.2	0.0397	-0.5387	1.5	0.063
21	AC F30/470	N2	25	303.0	18796.0	0.1437	-0.1909	1.7	0.072
			19	323.0	22313.0	0.1597	0.1145	1.5	0.052
			24	343.0	28079.0	0.1818	0.5169	1.1	0.036
			24	363.0	34520.0	0.2072	0.8146	1.0	0.024
			24	383.0	38952.0	0.2264	0.9946	0.8	0.017
22	AC F30/470	CH_4	24	303.0	14642.0	0.1055	-1.1040	2.3	0.133
			24	323.0	15027.0	0.1093	-0.9850	1.9	0.111
			25	343.0	17710.0	0.1203	-0.6642	2.2	0.121
			25	363.0	20496.0	0.1323	-0.4041	2.3	0.111
			24	383.0	24589.0	0.1458	-0.0205	1.5	0.058

Table 6-1. Regression Results for Pure-Gas Adsorption Using the ZGR EOS (Literature Data) - Cont'd.

System No.	Adsorbent	Adsorbate	NPTS	T (K)	Parameters α	Parameters β	Parameters $-\ln(k)$	%AAD	RMSE (mmol/g)
23	AC F30/470	C_3H_8	11	303.0	-12807.0	0.0197	-8.6208	1.4	0.129
			15	323.0	-10732.0	0.0270	-7.2295	0.8	0.061
			19	343.0	-11627.0	0.0222	-6.4518	0.5	0.037
			23	363.0	156.0	0.0826	-5.7327	0.3	0.021
			34	383.0	12755.0	0.1140	-3.9619	1.1	0.077
24	AC, Norit R1	N_2	31	298.0	11388.0	0.0880	-0.3194	3.5	0.078
25	AC, Norit R1	CO_2	29	298.0	3121.7	0.0325	-2.5906	0.8	0.070
26	Zeolite, Linde 13X	N_2	8	298.0	22294.0	0.1938	-0.1936	1.4	0.032
			8	323.0	28568.0	0.2166	0.4122	1.6	0.031
			8	348.0	36158.0	0.2412	0.9510	1.9	0.035
27	Zeolite, Linde 5A	N_2	9	298.0	19781.0	0.1930	-0.7314	1.1	0.047
			9	323.0	19652.0	0.1902	-0.2451	1.0	0.032
			9	348.0	24782.0	0.2067	0.3614	0.8	0.021
28	Zeolite, Linde 5A	CH_4	10	298.0	22175.0	0.1912	-1.2523	0.7	0.033
			10	323.0	24259.0	0.1993	-0.7701	0.5	0.015
			8	348.0	31317.0	0.2195	-0.0772	0.8	0.027
29	Zeolite, Linde 5A	CO_2	11	298.0	-12794.0	0.1109	-10.5178	1.4	0.101
			15	323.0	-1151.9	0.1378	-7.9717	1.0	0.077
			15	348.0	9972.5	0.1547	-5.6726	1.1	0.054
30	Zeolite, Linde 5A	C_2H_6	9	298.0	66146.0	0.3125	-0.6473	1.0	0.031
			9	323.0	43444.0	0.3027	-2.9976	1.9	0.053
			9	348.0	43720.0	0.3024	-2.4501	1.6	0.043
31	H-Modernite, Z-900H	CO_2	18	283.0	-6929.0	0.0724	-6.2860	3.0	0.037
			41	303.0	-4483.4	0.0784	-5.1929	2.9	0.028
			34	323.0	-2785.1	0.0809	-4.1891	4.4	0.042

Table 6-1. Regression Results for Pure-Gas Adsorption Using the ZGR EOS (Literature Data) – Cont'd.

System No.	Adsorbent	Adsorbate	NPTS	T (K)	Parameters			%AAD	RMSE (mmol/g)
					α	β	-ln(k)		
32	H-Mordenite, Z-900H	H_2S	17	283.0	-6258.7	0.1294	-9.5782	0.6	0.011
			22	303.0	-1703.3	0.0647	-8.5757	0.9	0.017
			23	338.0	-2856.9	0.1389	-6.8738	2.7	0.030
			7	368.0	3036.0	0.1564	-5.6114	1.1	0.020
33	H-Mordenite, Z-900H	C_3H_8	30	283.0	21704.0	0.4829	-8.2104	3.9	0.026
			34	303.0	56053.0	0.5645	-6.4374	5.5	0.044
			28	324.0	37815.0	0.5194	-5.9894	3.1	0.021
34	Zeolite G5	CH_4	32	283.0	22835.0	0.1720	-1.1616	1.2	0.024
			19	303.0	27753.0	0.1873	-0.5527	2.1	0.021
35	Zeolite G5	C_2H_6	22	283.0	-26948.0	0.0788	-10.9893	0.3	0.013
			18	303.0	27114.0	0.2083	-3.8318	0.5	0.018
36	Zeolite G5	C_2H_4	17	283.0	-10429.0	0.1515	-12.2849	0.2	0.008
			17	303.0	-10351.0	0.1501	-10.5168	0.1	0.006
37	Zeolite 13X	CH_4	18	298.0	25505.0	0.1829	-0.4517	1.2	0.032
38	Zeolite 13X	C_2H_6	11	298.0	-32229.0	0.0260	-8.4180	1.0	0.042
Overall			2363					1.7	0.096

Table 6-2. Regression Results for Pure-Gas Adsorption Using the 2-D PR EOS (Literature Data)

System No.	Adsorbent	Adsorbate	NPTS	T (K)	Parameters			%AAD	RMSE (mmol/g)
					α	β	-ln(k)		
1	AC, Columbia Grade L	N_2	9	310.9	-5823.9	0.0049	1.0671	1.2	0.010
			5	338.7	-5247.7	0.0520	1.5164	1.8	0.022
			9	366.5	-4242.8	0.0622	2.0429	1.2	0.010
			8	394.3	-3604.4	0.0676	2.4025	1.3	0.007
			5	422.0	2521.0	0.4125	2.8236	1.7	0.009
2	AC, Columbia Grade L	CH_4	12	310.9	-2716.9	0.0926	-0.1800	1.8	0.019
			10	338.7	-3558.7	0.0677	0.3407	1.5	0.041
			8	366.5	-869.5	0.1119	0.9124	1.0	0.010
			7	394.3	-5698.4	0.0448	1.3431	0.6	0.004
			8	422.0	-912.1	0.1134	1.7408	1.3	0.011
3	AC, Columbia Grade L	C_2H_6	10	310.9	-7140.1	0.0959	-3.4615	1.4	0.110
			9	338.7	-7520.5	0.1090	-2.0708	1.0	0.032
			10	366.5	-8642.1	0.0945	-1.7652	0.7	0.023
			10	394.3	-10455.0	0.0595	-1.1522	1.9	0.035
			9	422.0	-8499.3	0.0552	-0.4691	3.0	0.076
			5	449.8	-8503.0	0.0343	0.1080	0.4	0.016
			5	477.6	-8661.0	0.0484	0.6463	0.7	0.016
4	Charcoal	CH_4	8	283.2	-2417.2	0.0571	-0.7802	0.1	0.007
			12	293.2	-3142.5	0.0550	-0.6690	0.7	0.048
			12	303.2	-2640.0	0.0602	-0.3389	0.8	0.047
			10	313.2	-1858.5	0.0645	0.0765	0.3	0.033
			13	323.2	-1800.8	0.0689	0.2787	0.4	0.028

Table 6-2. Regression Results for Pure-Gas Adsorption Using the 2-D PR EOS (Literature Data) - Cont'd.

System No.	Adsorbent	Adsorbate	NPTS	T (K)	Parameters			%AAD	RMSE (mmol/g)
					α	β	-ln(k)		
5	Charcoal	C_3H_8	10	293.2	-2956.4	0.1079	-5.0547	2.3	0.133
			11	303.2	-10126.0	0.0964	-5.9586	0.6	0.051
			10	313.2	-7893.2	0.0999	-5.0624	0.7	0.038
			11	323.2	-6510.6	0.1049	-4.4225	0.5	0.032
			10	333.2	-7810.1	0.1080	-4.3602	0.3	0.015
6	AC, BPL	CH_4	23	212.7	-3984.9	0.0652	-2.8962	1.0	0.077
			24	260.2	-3582.1	0.0678	-0.9421	0.5	0.029
			25	301.4	-2928.2	0.0782	0.2505	0.5	0.027
7	AC, BPL	C_2H_6	18	212.7	-3799.5	0.1030	-6.6951	2.7	0.177
			15	260.2	-7281.1	0.0967	-4.7486	0.9	0.059
			16	301.4	-5848.5	0.1039	-2.7450	0.6	0.025
8	AC, BPL	C_2H_4	21	212.7	-8625.6	0.0724	-7.3931	2.9	0.163
			15	260.2	-6457.1	0.0871	-4.0783	0.4	0.029
			16	301.4	-5615.7	0.0933	-2.2765	0.3	0.017
9	AC, BPL	CO_2	21	212.7	-1195.6	0.0563	-4.4091	1.0	0.071
			14	260.2	-1453.0	0.0551	-2.0637	0.4	0.019
			25	301.4	-2155.4	0.0484	-0.7352	0.4	0.026
10	AC, PCB-Calgon	CH_4	7	296.0	-514.4	0.0890	-0.1958	0.1	0.014
			8	373.0	-5613.6	0.0594	0.9424	0.8	0.041
			7	480.0	9130.4	0.1748	2.8932	1.6	0.022
11	AC, PCB-Calgon	CO_2	4	296.0	-1177.2	0.0557	-1.4443	0.0	0.005
			4	373.0	-2574.4	0.0457	0.3618	0.1	0.004
			4	480.0	-5103.1	0.0341	1.8489	1.1	0.047

Table 6-2. Regression Results for Pure-Gas Adsorption Using the 2-D PR EOS (Literature Data) - Cont'd.

System No.	Adsorbent	Adsorbate	NPTS	T (K)	Parameters α	Parameters β	Parameters $-\ln(k)$	%AAD	RMSE (mmol/g)
12	AC, F30/470 Chemviron Carbon	CO_2	30	278.0	-2526.9	0.0639	-2.3348	1.3	0.273
			19	288.0	-3492.1	0.0547	-2.0851	1.1	0.153
			19	298.0	-2952.5	0.0606	-1.6232	0.3	0.030
			19	303.0	-2876.2	0.0620	-1.5121	0.3	0.028
			38	308.0	-3126.3	0.0601	-1.3528	0.5	0.044
			19	318.0	-3689.0	0.0574	-1.0777	0.5	0.032
			20	328.0	-3930.5	0.0602	-0.8708	0.5	0.023
13	AC, Norit R1 Extra	N_2	10	298.0	-2097.7	0.0854	0.9155	0.7	0.016
14	AC, Norit R1 Extra	CH_4	12	298.0	-3214.4	0.0540	-0.4825	1.5	0.041
15	AC, Norit R1 Extra	CO_2	12	298.0	-2257.3	0.0301	-1.4047	2.1	0.086
16	AC, Coconut Shell	CH_4	21	233.0	-1234.3	0.0186	-2.0298	1.2	0.262
			19	253.0	-961.6	0.0221	-1.3383	0.5	0.110
			22	273.0	-876.9	0.0241	-0.7778	0.4	0.145
			21	293.0	-744.8	0.0266	-0.2791	0.4	0.067
			20	313.0	-675.4	0.0281	0.1668	0.3	0.027
			19	333.0	-616.1	0.0282	0.5690	0.2	0.017
17	AC, Calgon F-400	CO_2	75	303.6	-2320.1	0.0545	-1.0368	2.1	0.161
			74	305.2	-1458.9	0.0548	-0.6420	3.2	0.218
			75	309.2	-1975.7	0.0513	-0.6175	2.9	0.173
			76	313.2	-2869.2	0.0457	-0.6995	2.8	0.128
			76	318.2	-1796.8	0.0587	-0.4876	2.7	0.139

Table 6-2. Regression Results for Pure-Gas Adsorption Using the 2-D PR EOS (Literature Data) - Cont'd.

System No.	Adsorbent	Adsorbate	NPTS	T (K)	Parameters			%AAD	RMSE (mmol/g)
					α	β	$-\ln(k)$		
18	AC, Norit RB1	CH_4	16	304.9	-5487.1	0.0418	-0.8024	0.3	0.006
			16	311.4	-5340.8	0.0434	-0.2723	0.3	0.005
			16	331.3	-5345.4	0.0450	0.1594	0.6	0.008
			16	350.5	-5233.7	0.0486	0.5498	0.7	0.008
19	AC, Norit RB1	CO_2	16	305.2	-2566.0	0.0571	-1.6572	0.3	0.011
			16	311.2	-3182.2	0.0507	-1.1489	0.3	0.011
			16	329.5	-4007.2	0.0310	-0.6668	0.3	0.006
			16	348.3	-4290.4	0.0334	-0.2316	0.5	0.009
20	AC, Coconut Shell	N_2	10	178.0	-415.0	0.0273	-1.7709	0.8	0.181
			11	198.0	-288.2	0.0311	-1.2972	0.8	0.142
			10	218.0	-484.4	0.0325	-0.8288	0.4	0.078
			10	233.0	-341.4	0.0359	-0.1951	0.3	0.039
			11	258.0	-224.7	0.0383	0.2782	0.2	0.027
			10	278.0	-320.5	0.0398	0.6564	0.2	0.019
			9	298.0	-262.5	0.0417	1.0418	0.1	0.009
21	AC F30/470	N_2	25	303.0	4199.7	0.1709	1.5391	2.1	0.079
			19	323.0	5030.7	0.1909	1.8136	1.7	0.057
			24	343.0	7517.0	0.2136	2.2385	1.7	0.044
			24	363.0	5810.4	0.2260	2.3756	1.4	0.037
			24	383.0	6225.7	0.2480	2.6005	1.3	0.027
22	AC F30/470	CH_4	24	303.0	6139.7	0.1286	0.8751	2.2	0.129
			24	323.0	2408.0	0.1350	0.7221	1.9	0.110
			25	343.0	5518.8	0.1472	1.2113	2.3	0.121
			25	363.0	2803.0	0.1532	1.2136	2.7	0.122
			24	383.0	4319.2	0.1679	1.5901	1.9	0.069

Table 6-2. Regression Results for Pure-Gas Adsorption Using the 2-D PR EOS (Literature Data) - Cont'd.

System No.	Adsorbent	Adsorbate	NPTS	T (K)	Parameters			%AAD	RMSE (mmol/g)
					α	β	$-\ln(k)$		
23	AC F30/470	C_3H_8	11	303.0	-22639.0	0.0380	-8.4472	1.4	0.128
			15	323.0	-21576.0	0.0496	-6.7439	0.8	0.061
			19	343.0	-21591.0	0.0424	-5.9305	0.5	0.036
			23	363.0	-19220.0	0.1051	-4.7216	0.3	0.020
			34	383.0	-5670.3	0.1402	-2.4304	1.0	0.076
24	AC Norit R1	N_2	31	298.0	-2210.9	0.0797	0.8482	1.1	0.063
25	AC Norit R1	CO_2	29	298.0	-1750.1	0.0313	-1.2601	1.1	0.123
26	Zeolite, Linde 13X	N_2	8	298.0	-643.0	0.2221	1.3707	1.3	0.033
			8	323.0	-703.5	0.2330	1.9173	1.5	0.034
			8	348.0	-1693.1	0.2286	2.3920	1.6	0.041
27	Zeolite, Linde 5A	N_2	9	298.0	-1234.3	0.2366	0.9751	1.1	0.046
			9	323.0	-4798.5	0.2305	1.3662	1.1	0.033
			9	348.0	-4348.5	0.2462	1.9319	0.7	0.020
28	Zeolite, Linde 5A	CH_4	10	298.0	2821.6	0.2338	0.4996	0.7	0.033
			10	323.0	1874.2	0.2448	0.9549	0.6	0.016
			8	348.0	3868.1	0.2578	1.5963	0.9	0.031
29	Zeolite, Linde 5A	CO_2	11	298.0	-4528.7	0.1478	-10.3027	1.4	0.107
			15	323.0	-3483.7	0.1692	-7.4362	1.0	0.077
			15	348.0	-2141.0	0.1866	-4.7231	1.1	0.055
30	Zeolite, Linde 5A	C_2H_6	9	298.0	48548.0	0.3594	1.1395	1.0	0.030
			9	323.0	6541.0	0.3551	-1.5561	1.7	0.054
			9	348.0	22648.0	0.3792	-0.0522	1.5	0.035

Table 6-2. Regression Results for Pure-Gas Adsorption Using the 2-D PR EOS (Literature Data) - Cont'd.

System No.	Adsorbent	Adsorbate	NPTS	T (K)	Parameters			%AAD	RMSE (mmol/g)
					α	β	$-\ln(k)$		
31	H-Mordenite, Z-900H	CO_2	18	283.0	-22578.0	0.1031	-5.2764	3.4	0.040
			41	303.0	-21586.0	0.1022	-4.1524	4.1	0.037
			34	323.0	-21115.0	0.0999	-3.1440	5.9	0.055
32	H-Mordenite, Z-900H	H_2S	17	283.0	-30904.0	0.1941	-8.4583	0.6	0.011
			22	303.0	-36701.0	0.1507	-7.7711	0.9	0.072
			23	338.0	-30397.0	0.2084	-5.5962	2.6	0.030
			7	368.0	-31427.0	0.1762	-4.3822	1.1	0.018
33	H-Mordenite, Z-900H	C_3H_8	30	283.0	-43102.0	0.6193	-6.6863	3.7	0.030
			34	303.0	-9152.4	0.6941	-4.7923	4.8	0.048
			28	324.0	-37630.0	0.06569	-4.4838	3.0	0.022
34	Zeolite G5	CH_4	32	283.0	3851.8	0.1791	0.4151	1.0	0.022
			19	303.0	2944.3	0.1620	0.9453	0.4	0.006
35	Zeolite G5	C_2H_6	22	283.0	-60077.0	0.1433	-11.2153	0.3	0.013
			18	303.0	5414.2	0.2498	2.1866	0.6	0.021
36	Zeolite G5	C_2H_4	17	283.0	-57999.0	0.1823	-13.2865	0.2	0.008
			17	303.0	-54555.0	0.1872	-10.6898	0.1	0.006
37	Zeolite 13X	CH_4	18	298.0	6817.9	0.2135	1.2033	1.1	0.041
38	Zeolite 13X	C_2H_6	11	298.0	-55086.0	0.08225	-8.9521	1.0	0.042
Overall			**2363**					**1.5**	**0.097**

Table 6-3 presents summary results for the ZGR EOS representation of the OSU pure-gas adsorption database. The overall AAD for all 549 OSU experimental data points is 4.3% and the overall RMSE is 0.075 mmol/g. The overall WAAD is 0.6, which means the ZGR EOS can, on average, represent the experimental data within the expected experimental uncertainties. As shown in the table, CO_2 adsorption on wet Illinois #6 coal at 319.3 K (System 63) has the worst quality of fit with an AAD of 10.3% (WAAD of 1.7), and C_2H_6 adsorption on Calgon F-400 activated carbon at 318.2 K (System 50) has the worst RMSE of 0.154 mmol/g.

Table 6-4 presents summary results of the 2-D PR EOS representation of the OSU pure-gas adsorption database. The overall AAD for all 549 OSU experimental data points is 4.4% and the overall RMSE is 0.077 mmol/g. The overall WAAD is 0.6, which means the 2-D PR EOS can also, on average, represent the experimental data within the expected experimental uncertainties. As shown in the table, CO_2 adsorption on wet Illinois #6 coal at 319.3 K (System 63) has the worst quality of fit with AAD of 11.5% (WAAD of 1.7), and C_2H_6 adsorption on Calgon F-400 activated carbon at 318.2 K (System 50) has the worst RMSE of 0.154 mmol/g.

In general, adsorption on wet coals is more difficult to model than adsorption on activated carbons. As shown in Tables 6-3 and 6-4, CO_2 adsorption on wet coals, in particular, is the most difficult to model. This is attributed in part to how the moisture content is accounted for in the adsorption experiments for wet coals. To account for moisture effects in the current adsorption data reduction procedures, part of the CO_2 is assumed to dissolve in water. However, no account is made for how the water molecules

Table 6-3. Regression Results for Pure-Gas Adsorption Using the ZGR EOS (OSU Data)

System No.	Adsorbent	Adsor-bate	NPTS	T (K)	Parameters α	Parameters β	Parameters $-\ln(k)$	%AAD	RMSE (mmol/g)	WAAD
47	AC, Calgon F-400	N_2	22	318.2	12520.0	0.1076	0.0110	0.4	0.011	0.3
48	AC, Calgon F-400	CH_4	22	318.2	8362.7	0.0824	-1.2223	0.5	0.024	0.7
49	AC, Calgon F-400	CO_2	52	318.2	4732.1	0.0497	-2.1677	2.0	0.110	0.5
50	AC, Calgon F-400	C_2H_6	21	318.2	1829.1	0.0744	-4.4025	6.4	0.154	0.7
55	Wet Fruitland Coal	N_2	37	319.3	109450.0	0.7762	3.4687	2.6	0.006	0.4
56	Wet Fruitland Coal	CH_4	40	319.3	46902.0	0.3988	1.7932	1.1	0.007	0.4
57	Wet Fruitland Coal	CO_2	57	319.3	1050.0	0.0879	0.8713	8.7	0.123	0.9
61	Wet Illinois # 6 Coal	N_2	20	319.3	309330.0	1.9798	4.4610	3.3	0.003	0.1
62	Wet Illinois # 6 Coal	CH_4	20	319.3	104130.0	0.8249	2.6973	1.9	0.005	0.3
63	Wet Illinois # 6 Coal	CO_2	40	319.3	11155.0	0.1324	1.6826	10.3	0.109	1.7
67	Wet Tiffany Coal	N_2	21	327.5	203370.5	1.4192	4.3040	2.3	0.002	0.5
68	Wet Tiffany Coal	CH_4	34	327.5	115540.0	0.8394	2.8661	3.1	0.011	1.1
69	Wet Tiffany Coal	CO_2	16	327.5	62560.0	0.5405	1.2459	4.0	0.026	0.2
74	Wet LB Fruitland Coal	N_2	17	319.3	95972.0	0.7332	4.7916	2.9	0.003	0.2
75	Wet LB Fruitland Coal	CH_4	16	319.3	22837.0	0.3143	3.2584	2.2	0.007	0.4
76	Wet LB Fruitland Coal	CO_2	48	319.3	103750.0	0.7905	1.5904	7.1	0.040	0.5
77	Dry Illinois # 6 Coal	CO_2	11	328.0	5262.1	0.0679	1.0575	2.5	0.034	0.4
78	Dry Beulah Zap Coal	CO_2	22	328.0	374.7	0.0526	0.3864	5.8	0.112	0.7
79	Dry Wyodak Coal	CO_2	11	328.0	3467.4	0.0516	0.8258	6.7	0.123	0.8
80	Dry Upper Freeport Coal	CO_2	11	328.0	-4205.3	0.1049	0.5818	4.2	0.044	0.4
81	Dry Pocahontash Coal	CO_2	11	328.0	-1497.0	0.1077	0.1747	2.7	0.036	0.2
Overall			**549**					**4.3**	**0.075**	**0.6**

Table 6-4. Regression Results for Pure-Gas Adsorption Using the 2-D PR EOS (OSU Data)

System No.	Adsorbent	Adsor-bate	NPTS	T (K)	Parameters			%AAD	RMSE (mmol/g)	WAAD
					α	β	$-\ln(k)$			
47	AC, Calgon F-400	N_2	22	318.2	-1567.6	0.1229	1.5551	0.4	0.015	0.3
48	AC, Calgon F-400	CH_4	22	318.2	-2197.6	0.1004	0.3673	0.5	0.026	0.7
49	AC, Calgon F-400	CO_2	52	318.2	-1781.7	0.0607	-0.5787	2.0	0.113	0.5
50	AC, Calgon F-400	C_2H_6	21	318.2	-11251.0	0.0972	-3.1076	6.4	0.154	0.7
55	Wet Fruitland Coal	N_2	37	319.3	-22832.0	0.2393	4.8530	2.4	0.006	0.3
56	Wet Fruitland Coal	CH_4	40	319.3	-15173.0	0.3381	3.2015	0.9	0.005	0.4
57	Wet Fruitland Coal	CO_2	57	319.3	-16950.0	0.0988	2.0134	8.9	0.125	0.9
61	Wet Illinois # 6 Coal	N_2	20	319.3	-6047.6	1.1211	5.8409	1.6	0.001	0.0
62	Wet Illinois # 6 Coal	CH_4	20	319.3	-18408.0	0.7455	4.1531	1.8	0.006	0.3
63	Wet Illinois # 6 Coal	CO_2	40	319.3	-16580.0	0.1221	2.7488	11.5	0.120	1.7
67	Wet Tiffany Coal	N_2	21	327.5	-43152.0	0.4537	5.7062	2.8	0.003	0.5
68	Wet Tiffany Coal	CH_4	34	327.5	-12437.0	0.7180	4.2980	3.4	0.011	1.2
69	Wet Tiffany Coal	CO_2	16	327.5	-2378.7	0.6593	2.9396	4.1	0.026	0.3
74	Wet LB Fruitland Coal	N_2	17	319.3	-63209.0	0.4550	5.8280	3.8	0.004	0.3
75	Wet LB Fruitland Coal	CH_4	16	319.3	-35702.0	0.2746	4.4951	2.9	0.009	0.5
76	Wet LB Fruitland Coal	CO_2	48	319.3	12269.0	0.9151	3.2636	7.0	0.039	0.5
77	Dry Illinois # 6 Coal	CO_2	11	328.0	-8979.7	0.0639	2.1918	3.0	0.037	0.5
78	Dry Beulah Zap Coal	CO_2	22	328.0	-10799.0	0.0622	1.5280	6.3	0.116	0.8
79	Dry Wyodak Coal	CO_2	11	328.0	-8496.1	0.0541	1.7575	7.1	0.134	0.9
80	Dry Upper Freeport Coal	CO_2	11	328.0	-27349.0	0.1261	1.7071	4.4	0.044	0.4
81	Dry Pocahontash Coal	CO_2	11	328.0	-23825.0	0.1074	1.3737	2.7	0.036	0.2
Overall			**549**					**4.4**	**0.077**	**0.6**

71

would affect adsorption. This means the current data reduction procedures may not yield highly accurate adsorption results on wet coals.

6.3 Temperature Dependence of 2-D EOS Model Parameters

The results shown in the previous section are based on separate regressions for each individual isotherm. The regressed parameters show a definite temperature dependence. Therefore, temperature relations for each 2-D EOS parameter, α, β, and k, are essential to facilitate adsorption predictions.

Temperature relations for the 2-D EOS parameters can be either empirically or theoretically based. Empirical correlations (e.g., linear relations) can be used to describe the temperature dependence. However, they are rather arbitrary and may not work well for a broad temperature range. In this work, the effort was focused on theory-based relations.

de Boer (1968) related 2-D EOS parameters, a_2 and b_2, with the 3-D EOS parameters, a and b, through:

$$a_2 = \frac{3a}{8d} \tag{6-6}$$

$$b_2 = \frac{3b}{4d} \tag{6-7}$$

where d is the diameter of the gas molecule. In doing so, he assumed that the adsorbent is inert to adsorption. Thus, he could derive the critical temperature, T_{c2}, for the 2-D EOS:

$$T_{c2} = \frac{T_c}{2} \tag{6-8}$$

where T_c is the critical temperature. However, because surface interactions with the gas molecules exist in the 2-D phase, the simple transformations of model parameters from 3-D EOS to 2-D EOS had few successful applications. In other words, the 2-D critical properties are not only gas dependent, but also depend on the adsorbent. If the above relations are used, we obtain:

$$\frac{\alpha}{\beta} = \frac{a_2}{b_2} = \frac{a}{2b} \qquad (6\text{-}9)$$

As indicated in Tables 6-2 and 6-4, the value of α for the 2-D VDW-type EOS is negative. Although the ZGR EOS forces α to be positive by revising the repulsive term in the EOS, Equation 6-9 is still invalid.

In this work, a different route was taken to generate the temperature relations for the 2-D EOS parameters. Here, we rely on the Ono-Kondo lattice theory and other theories to generate the temperature relations for the 2-D EOS parameters.

6.3.1 Temperature Dependence of β

For the surface density of the adsorbate, σ_m (mmol/m^2), the relation below was used by Sudibandriyo (2003):

$$\frac{d\sigma_m / dT}{\sigma_m} = -\delta \qquad (6\text{-}10)$$

where δ is the thermal expansion coefficient for the adsorbed gas.

β in the 2-D EOS is the inverse of the maximum adsorption capacity:

$$\beta = \frac{1}{(\sigma_m A)} \qquad (6\text{-}11)$$

Combining Equations 6-6 and 6-7 and integrating yields:

$$\ln\left(\frac{1}{\beta A}\right) - \ln\left(\frac{1}{\beta_0 A}\right) = -\delta(T - T_0) \tag{6-12}$$

or

$$\ln(\beta) = \delta T - \lfloor \delta T_0 + \ln \sigma_{m,0} + \ln A \rfloor \tag{6-13}$$

where T_0 is set at the normal boiling point of the adsorbate (triple point for CO_2), and

$\sigma_{m,0}$ is the maximum surface density of the adsorbate at T_0 [Sudibandriyo, 2003].

6.3.2 Temperature Dependence of Henry's Constant

The Henry's constant k is defined as:

$$k = \frac{d\omega^{Abs}}{dP}\bigg|_{P=0} \tag{6-14}$$

From the Ono-Kondo lattice theory [see, e.g., Sudibandriyo, 2003], x_{abs} is given as:

$$\ln[x_{ads}(1 - x_b)/x_b(1 - x_{ads})] + ((c_p + c_v)x_{ads} - cx_b)\varepsilon_{ff}/kT + \varepsilon_{fs}/kT = 0 \tag{6-15}$$

where $x_{ads} = \dfrac{\rho_{ads}}{\rho_{mc}}$, $x_b = \dfrac{\rho_b}{\rho_{mc}}$, ρ_{ads} is the adsorbed phase density, ρ_b is the bulk gas

phase density, ρ_{mc} is the maximum density defined as: $\rho_{mc} = \sigma_{m,0}/d$, ε_{ff} is the

adsorbate-adsorbate interaction energy, ε_{fs} is the adsorbate-adsorbent interaction energy,

and c_p, c_v, and c are model constants.

The absolute adsorption, ω^{Abs}, is defined as:

$$\omega^{Abs} = Cx_{ads} = C\frac{\rho_{ads}}{\rho_{mc}} \tag{6-16}$$

where C is the maximum adsorption capacity. Taking the derivative of Equation 6-15

with respect to pressure at the zero pressure limit yields:

74

$$\frac{dx_{ads}}{dP}\bigg|_{P=0} = \left(\frac{x_{ads}}{x_b}\frac{dx_b}{dP}\right)\bigg|_{P=0} \tag{6-17}$$

Thus, Henry's constant is derived as:

$$k = \frac{d\omega^{Abs}}{dP}\bigg|_{P=0} = C\frac{dx_{ads}}{dP}\bigg|_{P=0} = C\frac{x_{ads}}{x_b}\frac{dx_b}{dP}\bigg|_{P=0} = C\frac{x_{ads}}{x_b}\frac{1}{\rho_{mc}RT} \tag{6-18}$$

Meanwhile, Equation 6-15 can be simplified at low pressure to yield:

$$\ln[x_{ads}/x_b] + \varepsilon_{fs}/kT = 0 \tag{6-19}$$

Combining Equations 6-18 and 6-19, and identifying that C in the OK model is equivalent to $1/\beta$ in 2-D EOS yields:

$$k = \frac{1}{\beta\rho_{mc}RT}\exp\left(\frac{-\varepsilon_{fs}}{kT}\right) \tag{6-20}$$

where ε_{fs} is the adsorbate-adsorbent or fluid-solid interaction energy.

The fluid-solid energy parameter, ε_{fs}/k, may be expressed in terms of the interaction of a single molecule with a single lattice plane. If z is the distance between the adsorbate molecule i and the lattice carbon plane, the potential energy can be written as follows [see, e.g., Do, 1998]:

$$\Phi = 4\pi\rho_{atom}\varepsilon_{fs}^*\sigma_{fs}^2\left[\frac{1}{5}\left(\frac{\sigma_{fs}}{z}\right)^{10} - \frac{1}{2}\left(\frac{\sigma_{fs}}{z}\right)^4\right] \tag{6-21}$$

This potential energy has a minimum and its depth is given by:

$$\varepsilon_{fs} = \frac{6}{5}\pi\rho_{atom}\varepsilon_{fs}^*\sigma_{fs}^2 \tag{6-22}$$

where ρ_{atom} is the solid atom density of the adsorbent, $\sigma_{fs} = (\sigma_{ff} + \sigma_{fs})/2$ is the fluid-solid collision diameter, and $\varepsilon_{fs}^* = \sqrt{\varepsilon_{ff}^* \varepsilon_{ss}^*}$ is the fluid-solid well depth potential. For carbon adsorbent, $\rho_{atom} = 0.382$ atom/Å^2 [see, e.g., Do, 1998].

6.3.3 Temperature Dependence of α

In 2-D EOS, only the interactions within the adsorbed phase are considered. To estimate the attractive term in the 2-D EOS, de Boer (1968) used Equation 6-23 to estimate a_2:

$$a_2 = \frac{N_a^2}{2} \int_{\sigma_{ff}}^{\infty} \frac{4\varepsilon_{ff}^* \sigma_{ff}^6}{r^6} 2\pi r dr \tag{6-23}$$

However, in the 2-D phase, the attractive interactions are affected by the attractive force from the adsorbent surface. To estimate the attractive energy among the adsorbate molecules, a correction for the Equation 6-23 is necessary to discount the influence of the surface interactions.

A method to evaluate a more realistic attractive term for the adsorbed gas is to deduct the attractive energy of the adsorbate-adsorbent from Equation 6-23. Although this is not a rigorous method, it does provide a reasonable approximation. In this study, an expression is derived for the total attractive energy between the adsorbed molecules and the solid surface, a_2', given as:

$$a_2' = \frac{N_a^2}{2} \int_{\sigma_{fs}}^{\infty} \frac{2\pi \rho_{atom} \varepsilon_{fs}^* \sigma_{fs}^6}{r^4} 2r dr \tag{6-24}$$

Since α is the total attractive energy per surface area, then after correcting for the surface interactions, we obtain:

$$\alpha = \frac{a_2 - a_2'}{A} = \left(\frac{N_a^2}{2} \int_{\sigma_{ff}}^{\infty} \frac{4\varepsilon_{ff}^* \sigma_{ff}^6}{r^6} 2\pi r dr - \frac{N_a^2}{2} \int_{\sigma_{fs}}^{\infty} \frac{2\pi\rho_{atom}\varepsilon_{fs}^* \sigma_{fs}^6}{r^4} 2 r dr \right) \Big/ A \quad (6\text{-}25)$$

or

$$\alpha = \left(N_a^2 \pi \varepsilon_{ff}^* \sigma_{ff}^2 - N_a^2 2\pi\rho_{atom}\varepsilon_{fs}^* \sigma_{fs}^4 / 3 \right) \Big/ A \quad (6\text{-}26)$$

Usually, the adsorbate-adsorbent attractive energy is larger than the adsorbate-adsorbate attractive energy, which explains why the regressed parameter, α, in the 2-D PR EOS is mostly negative.

However, Equation 6-26 only works for 2-D VDW type of EOS. For the other 2-D EOS, such as Eyring EOS and ZGR EOS, the repulsive term was revised to obtain positive α values. The empirical revision of the repulsive term makes it more difficult to estimate α, because in both equations, α is also correlated with β. That is, empirically, α and β tend to exhibit a linear relation for a moderate temperate range.

6.3.4 Results for Generalization of Model Temperature Dependence

Based on the above analyses, the temperature relations for the 2-D PR EOS parameters are generalized, as they relate to some of the gas properties and adsorbent characteristics. In this study, the 2-D PR EOS is used to demonstrate the efficacy of the new temperature relations for the 2-D EOS parameters.

Table 6-5 summarizes the physical properties of the adsorbates investigated in this work. For the gas adsorption on activated carbons, the solid-solid interaction, ε_{ss}, the maximum surface density of the adsorbate at T_0, $\sigma_{m,0}$, and the thermal expansion coefficient, δ, are regressed for each adsorption system at various temperatures. The specific adsorbent surface area, A, is not a directly measured value. Consequently, it is

Table 6-5. Physical Properties of Adsorbates

Adsorbate	MW	P_c (MPa)	T_c (K)	Normal Boiling Point (K)	Reciprocal van der Waals co-volume (mol/liter)	σ_{ff} (10^{-10} m)	$\varepsilon_{ff}*/k$ (K)
H_2	2.02	1.31	33.19	20.4	38.16	2.827	59.7
N_2	28.01	3.40	126.20	77.3	25.89	3.798	71.4
H_2S	34.08	8.96	373.53	212.8	23.08	3.623	301.1
CO_2	44.01	7.38	304.21	216.6 [a]	23.34	3.941	195.2
CH_4	16.04	4.60	190.56	111.7	23.37	3.758	148.6
C_2H_4	28.05	5.04	282.34	169.4	17.39	4.163	224.7
C_2H_6	30.07	4.87	305.32	184.6	15.41	4.443	215.7
C_3H_8	44.10	4.25	369.83	231.1	11.07	5.118	237.1
i- C_4H_{10}	58.12	3.65	408.14	261.4	8.60	5.278	330.1

[a] : Triple point temperature

inferred from adsorption measurements using selected models. In this study, the N_2 BET

surface area at 77 K is used due to availability and standardization.

Figure 6-1 shows the effect of variation in surface area on the adsorption

representations. The adsorption in this sample calculation is for CO_2 adsorption on

activated carbon measured at OSU. From the figure, we see that a 10% variation in the

surface area yields no significant difference in the correlation results; albeit, different

surface area estimates produce different regressed model parameter values.

Table 6-6 presents summary results for the 2-D PR EOS representation of the

pure-gas adsorption data on various activated carbons (Systems 1 to 25 and Systems 47

to 50). Adsorption on Zeolites was not included here, since characterization data for

these adsorbents are not available. The overall AAD for the 1922 data points is 2.4% and

the overall RMSE is 0.199 mmol/g. In comparison, the overall AAD and RMSE for the

adsorption on activated carbon from Tables 6-2 and 6-4 are 1.4% and 0.108 mmol/g,

respectively. While the errors have doubled, use of the temperature relations provides for

adsorption predictions over the desired temperature range.

Unlike activated carbons, the coals we investigated do not have the commercial

surface area data available. Since each system includes only one isotherm, we fixed the

surface density and thermal expansion coefficient for the gas adsorption on coals. Only

the surface area and the solid-solid interaction are regressed in this case.

For the maximum surface density, we used the hexagon to represent the minimum

area occupied by the gas molecules on the adsorbent surface, thus the maximum surface

density:
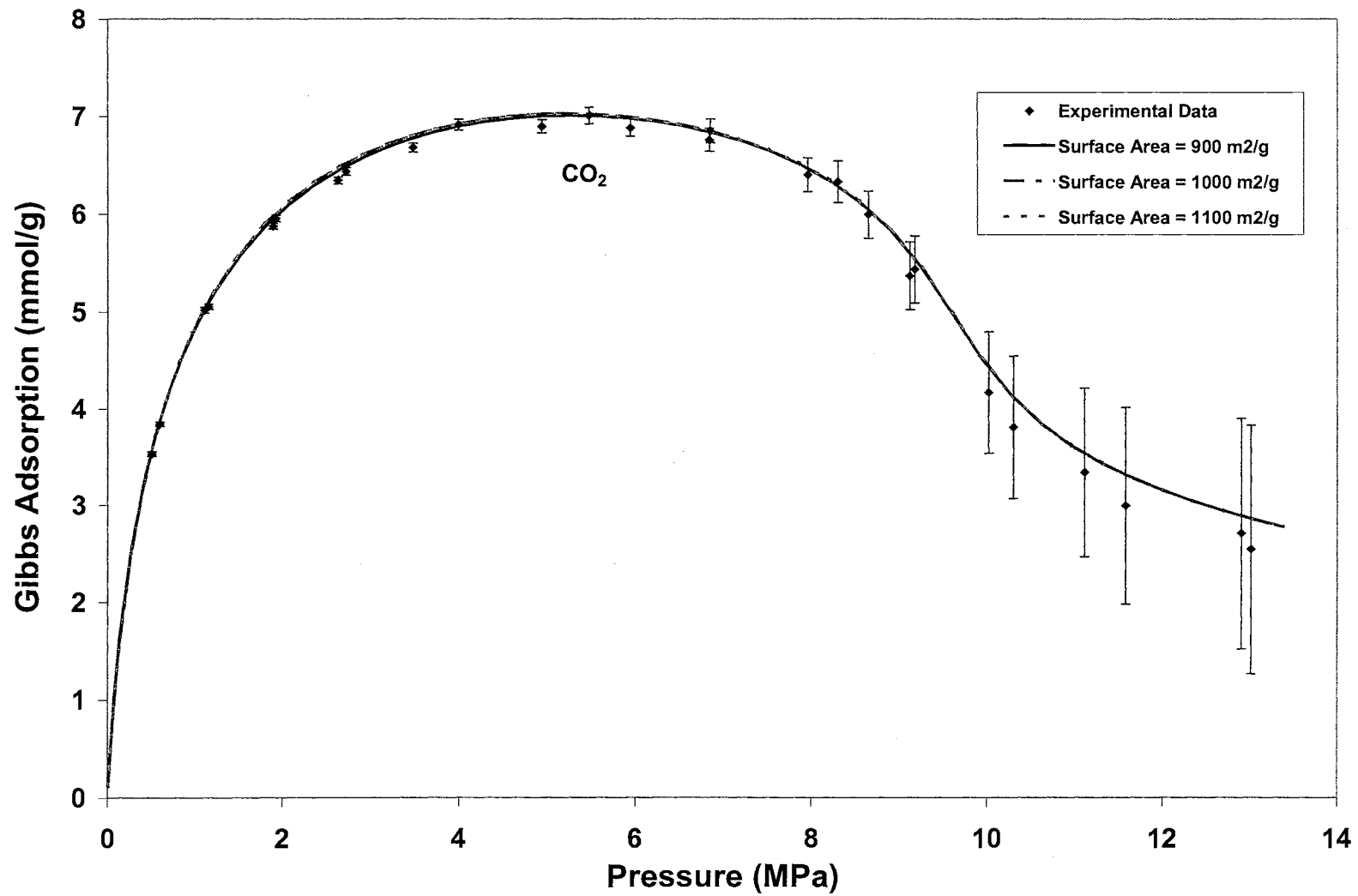
Figure 6-1. Effect of Surface Area on Pure CO_2 Adsorption on Activated Carbon at 318.2 K

Table 6-6. Regression Results for Pure-Gas Adsorption on Activated Carbons Using the New Temperature Relations

System No.	Adsorbent	Adsorbate	NPTS	Regressed Parameters				%AAD	RMSE (mmol/g)
				A (m^2/g)	ε_{ss}/k(K)	$\sigma_{m,0}$ (mmol/m^2)	δ (1/K)		
1	AC, Columbia Grade L	N_2	36	1152.0	53.01	0.0168	0.00295	3.7	0.029
2	AC, Columbia Grade L	CH_4	45	1152.0	45.82	0.0158	0.00287	3.1	0.057
3	AC, Columbia Grade L	C_2H_6	58	1152.0	49.59	0.0117	0.00317	4.5	0.152
4	Charcoal	CH_4	55	1157.0	45.86	0.0275	0.00350	0.9	0.053
5	Charcoal	C_3H_8	52	1157.0	45.68	0.0095	0.00248	3.8	0.133
6	AC, BPL	CH_4	72	988.0	39.12	0.0189	0.00319	2.5	0.115
7	AC, BPL	C_2H_6	49	988.0	46.25	0.0112	0.00313	4.4	0.207
8	AC, BPL	C_2H_4	52	988.0	48.43	0.0173	0.00308	4.3	0.218
9	AC, BPL	CO_2	60	988.0	47.40	0.0962	0.01100	3.7	0.336
10	AC, PCB-Calgon	CH_4	21	1200.0	41.65	0.0166	0.00264	1.8	0.059
11	AC, PCB-Calgon	CO_2	12	1200.0	38.85	0.0245	0.00561	1.8	0.187
12	AC, F30/470 Chemviron Carbon	CO_2	164	993.5	49.52	0.0340	0.00502	2.6	0.241
13	AC, Norit R1 Extra	N_2	10	1450.0	57.21	0.0231	0.00476	0.7	0.016
14	AC, Norit R1 Extra	CH_4	12	1450.0	72.63	0.0889	0.01099	1.7	0.036

Table 6-6. Regression Results for Pure-Gas Adsorption on Activated Carbons Using the New Temperature Relations - Cont'd.

System No.	Adsorbent	Adsorbate	NPTS	Regressed Parameters				%AAD	RMSE (mmol/g)
				A (m^2/g)	ε_{ss}/k (K)	$\sigma_{m,0}$ ($mmol/m^2$)	δ (1/K)		
15	AC, Norit R1 Extra	CO_2	12	1450.0	53.32	0.0905	0.01328	2.1	0.086
16	AC, Coconut Shell	CH_4	122	3106.0	23.70	0.0175	0.00277	2.0	0.242
17	AC, Calgon F-400	CO_2	374	1200.0	43.35	0.0587	0.00994	2.7	0.286
18	AC, Norit RB1	CH_4	64	1100.0	48.17	0.0152	0.00295	1.3	0.026
19	AC, Norit RB1	CO_2	64	1100.0	47.05	0.0281	0.00570	1.0	0.033
20	AC, Coconut Shell	N_2	71	3106.0	32.20	0.0183	0.00385	2.1	0.267
21	AC F30/470	N_2	116	993.5	60.17	0.0216	0.00373	2.2	0.065
22	AC F30/470	CH_4	122	993.5	46.23	0.0216	0.00307	1.9	0.104
23	AC F30/470	C_3H_8	102	993.5	40.25	0.0102	0.00223	1.5	0.106
24	AC Norit R1	N_2	31	1262.0	51.28	0.0188	0.00288	1.1	0.064
25	AC Norit R1	CO_2	29	1262.0	40.03	0.0417	0.00489	1.1	0.121
47	AC, Calgon F-400	N_2	22	950.0	31.93	0.0089	0.00001	0.4	0.018
48	AC, Calgon F-400	CH_4	22	950.0	41.06	0.0180	0.00250	0.5	0.025
49	AC, Calgon F-400	CO_2	52	950.0	32.83	0.0175	0.00001	1.4	0.144
50	AC, Calgon F-400	C_2H_6	21	950.0	40.55	0.0099	0.00146	5.5	0.394
Overall			1922					2.4	0.199

$$\sigma_{m,0} = 1 \Big/ \left[\frac{3\sqrt{3}}{2} \left(\frac{\sigma_{ff}}{2} \right)^2 N_a \right] \qquad (6\text{-}27)$$

The thermal expansion coefficient is fixed to be 0.0024 (1/K), as suggested by Sudibandriyo (2003).

Table 6-7 presents summary results for the 2-D PR EOS representation of the pure-gas adsorption on wet and dry coals using the generalized temperature relations of Equations 6-13, 6-20, and 6-26. The overall AAD for the 432 data points is 4.7%; the overall RMSE is 0.050 mmol/g; and the over WAAD is 0.6. As indicated in the table, CO_2 adsorption on dry Illinois #6 coal (System 77) has the worst quality of fit with AAD of 10.2% and RMSE of 0.155 mmol/g. CH_4 adsorption on wet Tiffany coal (System 68) has the worst WAAD of 1.3.

Regressing the surface area of a given matrix using various adsorbates leads to different area estimates. In addition, the value of the regressed surface area is affected by the values chosen for the maximum surface density and the thermal expansion coefficient. The results indicate that among the CBM gases (CH_4, CO_2, and N_2), N_2 accesses the least surface area and has the lowest fluid-solid interaction energy, while CO_2 accesses the most surface area and has the highest fluid-solid interaction energy.

Overall, the regression results described above using the temperature relations show that the 2-D PR EOS can be applied successfully within the experimental uncertainties (WAAD of 0.6). However, CO_2 adsorption on coals produces less favorable results. As discussed in the previous section, adsorption on wet coals is difficult to model, partly because the current procedures do not account effectively for

Table 6-7. Regression Results for Pure-Gas Adsorption on Coals Using the New Temperature Relations

System No.	Adsorbent	Adsor-bate	NPTS	T (K)	Regressed Parameters				% AAD	RMSE (mmol/g)	WAAD
					A (m^2/g)	ε_{ss}/k (K)	$\sigma_{m,0}$ $(mmol/m^2)$	δ (1/K)			
55	Wet Fruitland Coal	N_2	37	319.3	131.4	16.47	0.0177	0.0024	2.4	0.006	0.4
56	Wet Fruitland Coal	CH_4	40	319.3	158.8	23.85	0.0181	0.0024	1.3	0.007	0.5
57	Wet Fruitland Coal	CO_2	57	319.3	211.1	36.63	0.0165	0.0024	6.5	0.075	0.7
61	Wet Illinois # 6 Coal	N_2	20	319.3	70.6	11.74	0.0177	0.0024	1.6	0.001	0.0
62	Wet Illinois # 6 Coal	CH_4	20	319.3	84.0	19.47	0.0181	0.0024	1.9	0.006	0.3
63	Wet Illinois # 6 Coal	CO_2	40	319.3	190.1	24.27	0.0165	0.0024	4.1	0.038	1.2
67	Wet Tiffany Coal	N_2	21	327.5	68.1	14.98	0.0177	0.0024	2.8	0.003	0.5
68	Wet Tiffany Coal	CH_4	34	327.5	87.6	20.04	0.0181	0.0024	3.7	0.012	1.3
69	Wet Tiffany Coal	CO_2	16	327.5	121.5	35.83	0.0165	0.0024	9.5	0.055	0.7
74	Wet LB Fruitland Coal	N_2	17	319.3	54.0	12.55	0.0177	0.0024	4.2	0.004	0.3
75	Wet LB Fruitland Coal	CH_4	16	319.3	75.2	16.51	0.0181	0.0024	2.4	0.007	0.4
76	Wet LB Fruitland Coal	CO_2	48	319.3	85.1	40.94	0.0165	0.0024	8.9	0.039	0.5
77	Dry Illinois # 6 Coal	CO_2	11	328.0	352.5	25.87	0.0165	0.0024	10.2	0.155	0.9
78	Dry Beulah Zap Coal	CO_2	22	328.0	363.4	37.29	0.0165	0.0024	4.6	0.080	0.6
79	Dry Wyodak Coal	CO_2	11	328.0	403.5	31.17	0.0165	0.0024	3.9	0.067	0.6
80	Dry Upper Freeport Coal	CO_2	11	328.0	174.3	48.64	0.0165	0.0024	5.2	0.057	0.4
81	Dry Pocahontash Coal	CO_2	11	328.0	213.4	49.18	0.0165	0.0024	7.1	0.093	0.5
Overall			432						4.7	0.050	0.6

the moisture affects in the data reduction procedures. In this case, it may also be that the thermal expansion coefficient for CO_2 is underestimated.

6.4 Predictions for Pure-Gas Adsorption on Activated Carbons

Predictions of pure-gas adsorption on activated carbon require: the surface area of the adsorbent, the solid-solid interaction of the adsorbent, the maximum surface density of the adsorbate, and the thermal expansion coefficient of the adsorbate. Surface area of the adsorbent was taken as the N_2 BET surface area, which was available for each activated carbon.

The solid-solid interaction of the adsorbent is highly dependent on the matrix structure. However, for most of the activated carbons with the surface area of about 1000 m^2/g, the solid-solid interaction parameter is approximately 40 K [Sudibandriyo, 2003]. However, an activated carbon with higher surface area tends to have weaker solid-solid interaction, thus lower values for the solid-solid interaction parameter are used. For example, we use a parameter value of 20 K for the activated carbon made from Coconut Shell, which has a surface area of 3106 m^2/g. Moreover, for the surface area for Charcoal in Systems 4 and 5, we use 45 K for the solid-solid interaction. All these solid-solid interaction energy values were fixed empirically from the regressed values in Table 6-6.

The maximum surface density can be calculated approximately from the molecular size. The maximum surface density is defined in previous section as:

$$\sigma_{m,0} = 1 \Bigg/ \left[\frac{3\sqrt{3}}{2} \left(\frac{\sigma_{ff}}{2} \right)^2 N_a \right] \tag{6-27}$$

Also, a value of 0.0024 (1/K) is used for the thermal expansion coefficient for all the gases considered.

Table 6-8 presents the 2-D PR EOS summary results for representing the pure-gas adsorption on various activated carbons. The overall AAD for the 1922 data points is 8.6% and the overall RMSE is 0.617 mmol/g. As shown in the table, CO_2 adsorption on Calgon F-400 activated carbon (System 49) has the worst quality of fit with AAD of 18.6%, and CO_2 adsorption on Norit R1 activated carbon (System 25) has the worst RMSE of 1.861 mmol/g.

Overall, the generalized model predictions yield less than 10.0 %AAD for pure-gas adsorption data on activated carbons. The results indicate that CO_2 adsorption on activated carbons are the most difficult to predict. To achieve better prediction for all the systems of interest, improved estimates for the fluid-solid interaction and the thermal expansion coefficient of the gas are required.

6.5 Discussion

Table 6-9 represents the overall results for the pure-gas modeling using 2-D EOSs. Indicated by the error profiles for the data regressions, the temperature relations for the 2-D PR EOS are effective in representing the pure-gas adsorption data. Further, the pure-gas adsorption predictions for activated carbons are reasonably accurate with AAD of 8.6%, corresponding to a WAAD less than 3.0.

Figure 6-2 illustrates the capabilities of 2-D EOS to represent and *a priori* predict pure CO_2, CH_4, N_2, and C_2H_6 adsorption on activated carbon at 318.2 K. As indicated the EOS can describe the experimental data within the expected experimental

Table 6-8. Prediction Results for Pure-Gas Adsorption on Activated Carbons

System No.	Adsorbent	Adsorbate	NPTS	Parameters				%AAD	RMSE (mmol/g)
				A (m^2/g)	ε_{ss}/k(K)	$\sigma_{m,0}$ (mmol/m^2)	δ (1/K)		
1	AC, Columbia Grade L	N_2	36	1152.0	40.0	0.0177	0.0024	17.8	0.106
2	AC, Columbia Grade L	CH_4	45	1152.0	40.0	0.0181	0.0024	8.0	0.074
3	AC, Columbia Grade L	C_2H_6	58	1152.0	40.0	0.0130	0.0024	14.7	0.292
4	Charcoal	CH_4	55	1157.0	45.0	0.0181	0.0024	6.5	0.501
5	Charcoal	C_3H_8	52	1157.0	45.0	0.0098	0.0024	4.5	0.154
6	AC, BPL	CH_4	72	988.0	40.0	0.0181	0.0024	9.6	0.346
7	AC, BPL	C_2H_6	49	988.0	40.0	0.0130	0.0024	11.6	0.546
8	AC, BPL	C_2H_4	52	988.0	40.0	0.0148	0.0024	13.9	0.572
9	AC, BPL	CO_2	60	988.0	40.0	0.0165	0.0024	16.9	1.092
10	AC, PCB-Calgon	CH_4	21	1200.0	40.0	0.0181	0.0024	6.9	0.296
11	AC, PCB-Calgon	CO_2	12	1200.0	40.0	0.0165	0.0024	12.7	0.550
12	AC, F30/470 Chemviron Carbon	CO_2	164	993.5	40.0	0.0165	0.0024	10.8	0.945
13	AC, Norit R1 Extra	N_2	10	1450.0	40.0	0.0177	0.0024	8.3	0.318
14	AC, Norit R1 Extra	CH_4	12	1450.0	40.0	0.0181	0.0024	11.4	0.639

Table 6-8. Prediction Results for Pure-Gas Adsorption on Activated Carbons - Cont'd.

System No.	Adsorbent	Adsorbate	NPTS	Parameters				%AAD	RMSE (mmol/g)
				A (m^2/g)	ε_{ss}/k(K)	$\sigma_{m,0}$ (mmol/m^2)	δ (1/K)		
15	AC, Norit R1 Extra	CO_2	12	1450.0	40.0	0.0165	0.0024	14.8	0.553
16	AC, Coconut Shell	CH_4	122	3106.0	20.0	0.0181	0.0024	4.2	0.428
17	AC, Calgon F-400	CO_2	374	1200.0	40.0	0.0165	0.0024	7.4	0.739
18	AC, Norit RB1	CH_4	64	1100.0	40.0	0.0181	0.0024	8.5	0.122
19	AC, Norit RB1	CO_2	64	1100.0	40.0	0.0165	0.0024	5.3	0.216
20	AC, Coconut Shell	N_2	71	3106.0	20.0	0.0177	0.0024	7.4	0.971
21	AC F30/470	N_2	116	993.5	40.0	0.0177	0.0024	6.2	0.153
22	AC F30/470	CH_4	122	993.5	40.0	0.0181	0.0024	4.4	0.194
23	AC F30/470	C_3H_8	102	993.5	40.0	0.0098	0.0024	4.9	0.262
24	AC Norit R1	N_2	31	1262.0	40.0	0.0177	0.0024	12.3	0.250
25	AC Norit R1	CO_2	29	1262.0	40.0	0.0165	0.0024	16.1	1.861
47	AC, Calgon F-400	N_2	22	950.0	40.0	0.0177	0.0024	7.2	0.189
48	AC, Calgon F-400	CH_4	22	950.0	40.0	0.0181	0.0024	1.1	0.061
49	AC, Calgon F-400	CO_2	52	950.0	40.0	0.0165	0.0024	18.6	0.500
50	AC, Calgon F-400	C_2H_6	21	950.0	40.0	0.0130	0.0024	11.5	0.707
	Overall		1922					8.6	0.617

uncertainties. Similarly, excellent predictions are obtained for CH_4, N_2, and C_2H_6 adsorption on activated carbon. However, accurate predictions for CO_2 can be obtained when the surface area is increased form 950 to 1200 m^2/g.

Table 6-9. Summaries of the Results for Pure-Gas Adsorption

Cases	NPTS	%AAD	RMSE	WAAD
Regressions Based on Individual Isotherms				
ZGR EOS for Literature Data	2363	1.7	0.096	
2-D PR EOS for Literature Data	2363	1.5	0.097	
ZGR EOS for OSU Data	549	4.3	0.075	0.6
2-D PR EOS for OSU Data	549	4.4	0.077	0.6
Regressions Based on Systems				
2-D PR EOS for Activated Carbons	1922	2.4	0.199	
2-D PR EOS for Coals	432	4.7	0.050	0.6
Predictions				
2-D PR EOS for Activated Carbons	1922	8.6	0.617	

A sample calculation is given to demonstrate the 2-D PR EOS predictions involving different isotherms. In this case, CH_4 adsorption data (System 16, 12 data points) up to 5.7 MPa at 233 K were regressed to obtain the EOS parameters, the surface area and fluid-solid interaction. Using this information, the model predicted, as shown in Figure 6-3, the higher-pressure adsorption of the same isotherm as well as the other adsorption isotherms over the full pressure range (System 16, 110 data points). The overall AAD and RMSE of 3.0% and 0.361 mmol/g, respectively, were obtained compared to 2.0% and 0.242 mmol/g, using parameters regressed from all the data.

These preliminary results indicate the effectiveness of the (a) newly-developed 2-D PR EOS temperature relations, and (b) parameter-calibrated predictions.
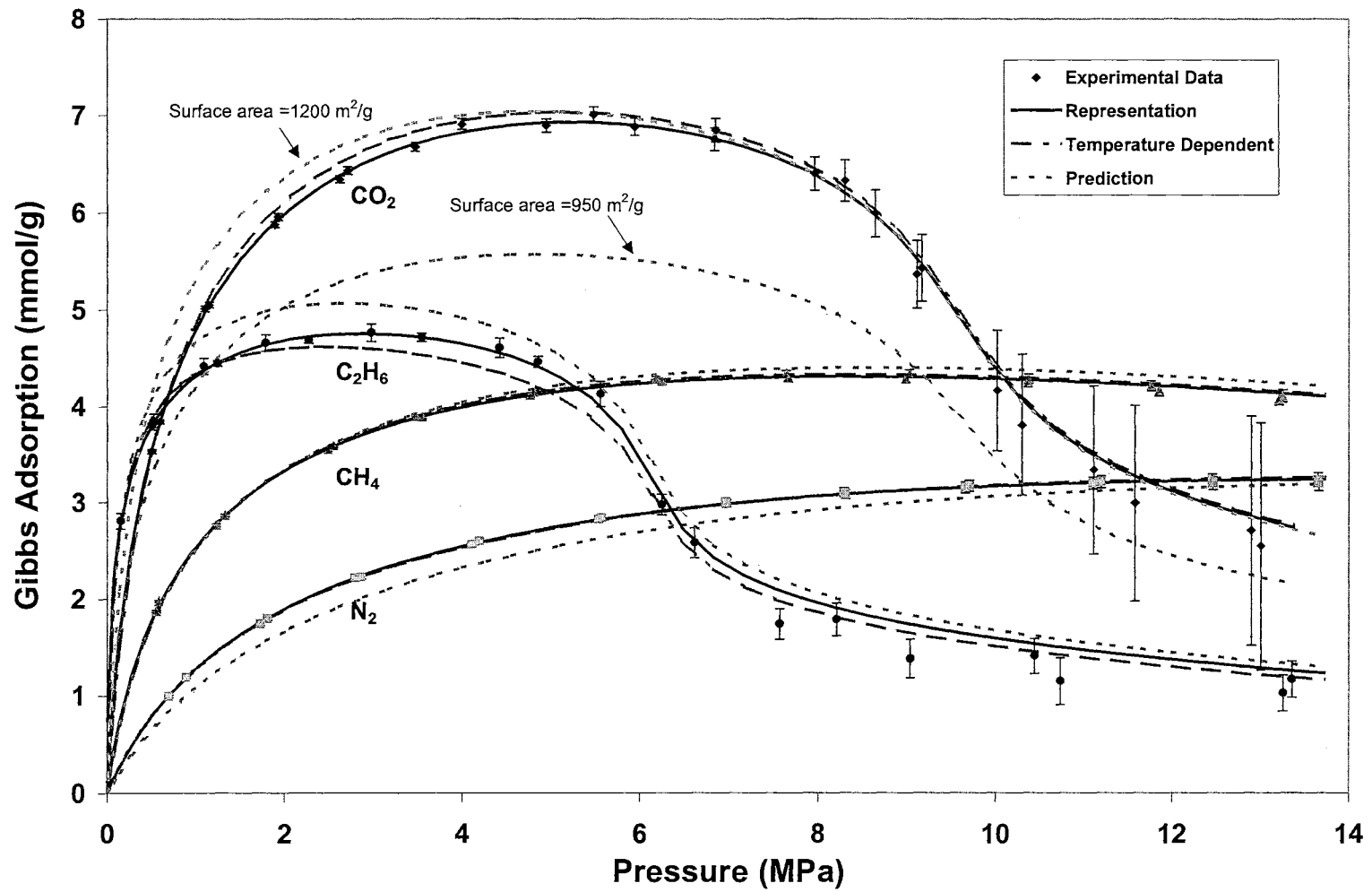
Figure 6-2. Representation and Prediction of Pure-Gas Adsorption on Activated Carbon at 318.2 K
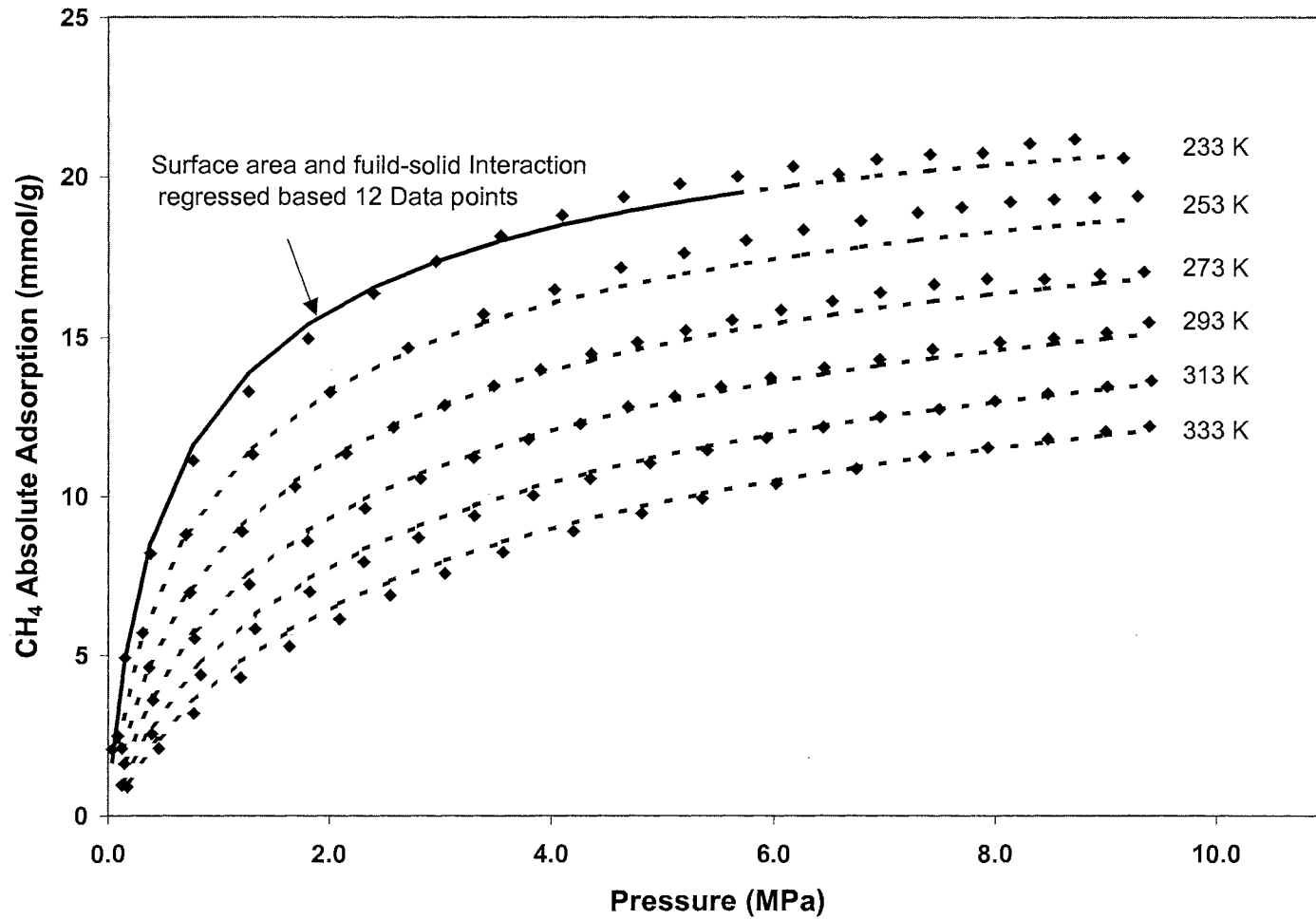
Figure 6-3. 2-D PR EOS Prediction of CH₄ Absolute Adsorption on Activated Carbon (Zhou, 2000)

Figure 6-4 shows the representation and prediction results for pure CO_2 adsorption on activated carbon at four different temperatures. Both methods are capable of accurately representing the experimental data; however, the EOS predictions underestimate the adsorption for low-temperature isotherms, and overestimate the adsorption for high-temperature isotherms. This is primarily due to the value used for the thermal expansion coefficient. As can be seen from Table 6-6, the regressed thermal expansion coefficient for this system is 0.0057, but a smaller value of 0.0024 is used in the prediction.

Figure 6-5 shows the representation results for the pure CO_2, CH_4, and N_2 adsorption on wet Fruitland coal at 319.3 K. The representations are within the expected experimental uncertainties.

The results of this study indicate that the surface area, fluid-solid interaction, maximum surface density, and thermal expansion coefficient provide effective input for EOS parameter generalization, which could facilitate *a priori* adsorption predictions.

Although the surface area for an individual adsorbent should be a unique value, different adsorbates may access different surface areas; especially when the adsorbent is porous. From the data regressions for gas adsorption on coals, we obtain similar surface areas for N_2 and CH_4 while surface areas regressed from CO_2 adsorption are usually much higher. This may also explain, in part, why the CO_2 adsorption predictions are less satisfactory compared to the other gases.

The maximum surface density of the adsorbate is relatively independent of the adsorbent. However, the thermal expansion coefficient is highly dependent on the
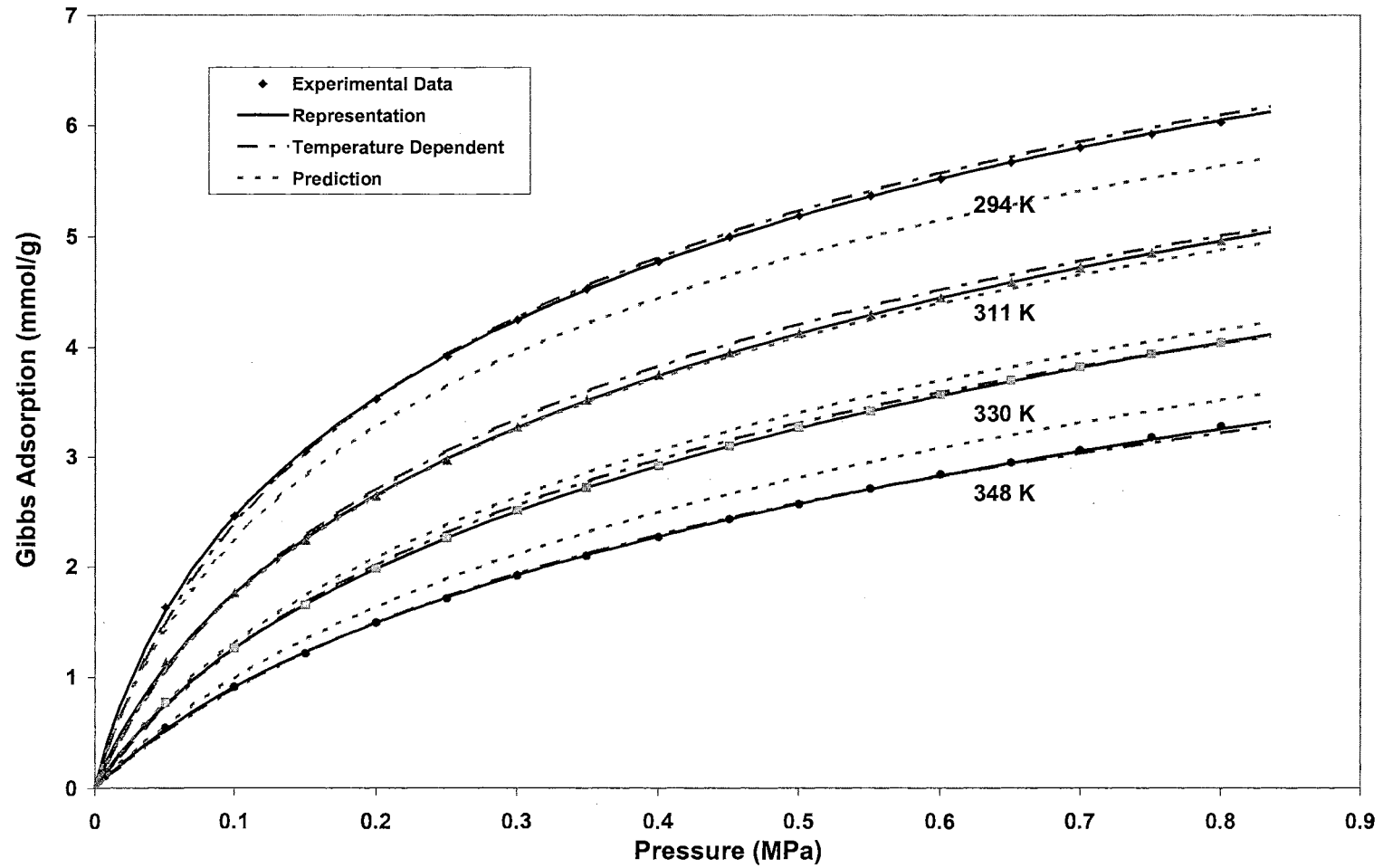
Figure 6-4. Representation and Prediction of CO_2 Adsorption on Activated Carbon
at Four Different Temperatures (Vaart, 2000)
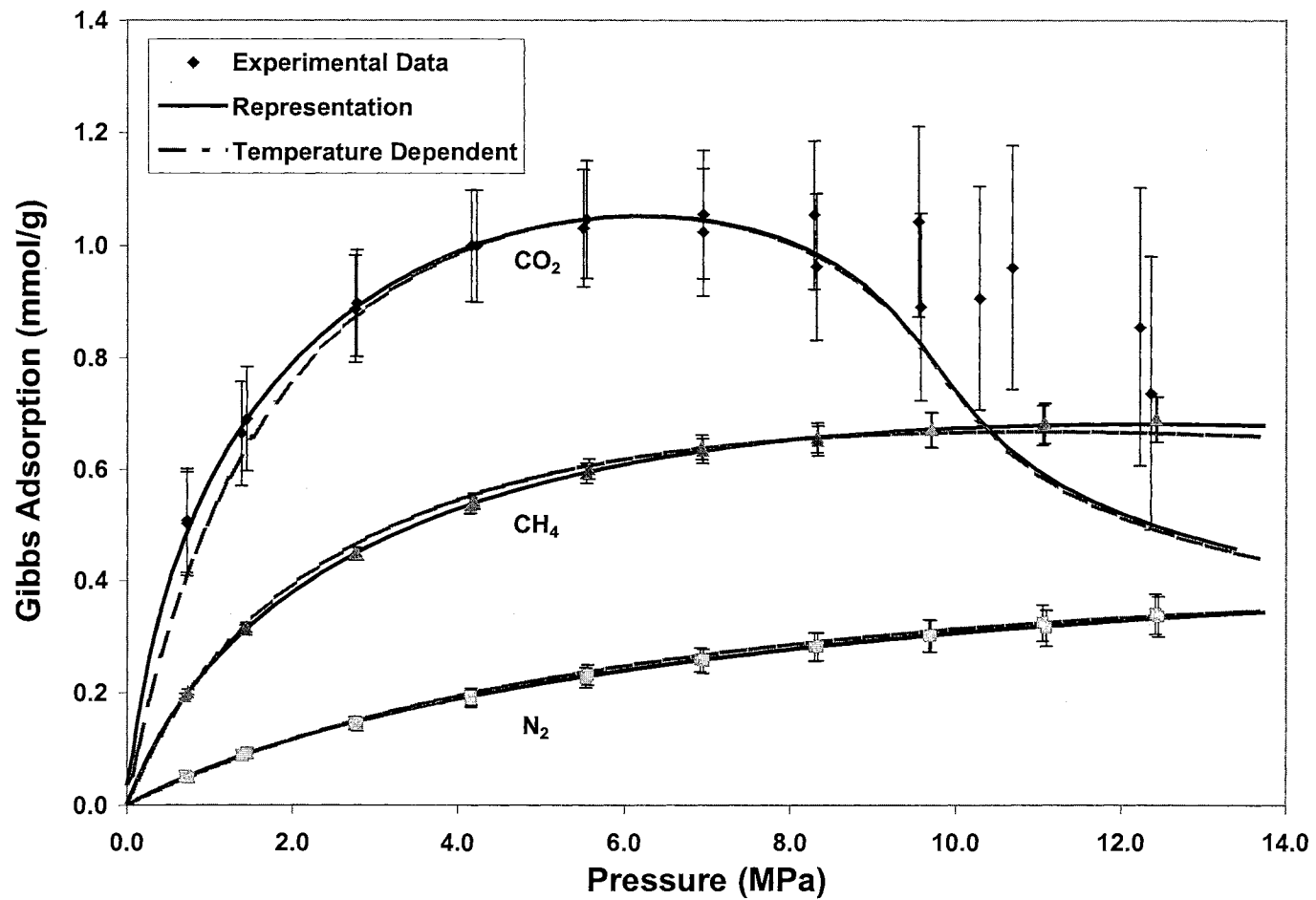
Figure 6-5. Representation of Pure-Gas Adsorption on Wet Fruitland Coal at 319.3 K

characteristics of the adsorbent and adsorbate. In the present predictions, a fixed value of 0.0024 is used. Thus, to predict adsorption with higher accuracy, the thermal expansion coefficient should be derived based on both the adsorbent and adsorbate properties.

For the fluid-solid interaction, we only considered the interaction of the adsorbate with carbon atoms in the adsorbent. However, different activated carbons have different additional functional groups, which may have significant impact on the adsorption.

In addition to the four model parameters discussed above, other adsorbate and adsorbent characteristics are also important for accurate adsorption predictions. For example, the carbon atom density in the adsorbent will influence the fluid-solid interaction. In this work, the carbon atom density is set to the value of graphite; albeit, this property varies for different carbon adsorbents.

Although a generalized capability has not been fully developed for wet coals the results obtained for the activated carbon are encouraging. However, to realize this objective, attention is required to address the effect of moisture on coalbed adsorption behavior. We believe developing reliable generalized models is not complete without a proper understanding of, and rigorous accounting for, the effects of moisture on adsorption capacity, adsorbed-phase densities, and the competitive adsorption in mixtures. In fact, as stated earlier, we need to address this issue before we can develop structure-based characterizations. At present, confusion relating to the proper accounting for moisture content significantly limits the value of the existing literature data for developing generalized predictions.

In summary, the 2-D EOS modeling results for pure-gas adsorption indicate that:

1. In general, both the ZGR EOS and the 2-D PR EOS can represent the pure-gas adsorption precisely within the expected experimental uncertainties of about 2%. Overall, the new temperature relations for the 2-D PR EOS enable us to represent the pure-gas adsorption within the expected experimental uncertainties without the need to regress each isotherm.

2. The revised attractive term for the 2-D PR EOS works well for all the data considered in this work; however, it does not account for temperature variations. To describe the molecular attraction more accurately, we need to delineate temperature dependence of the α function.

3. On average, the 2-D PR EOS is capable of predicting pure-gas adsorption on activated carbons with AAD of 9%. The results are comparable to the predications using the OK model, which yields 8 %AAD [Sudibandriyo 2003]. Moreover, improved estimates for the surface area and fluid-solid interaction could be helpful in achieving higher prediction accuracy.

4. Although a generalized capability to predict CBM-type adsorption on wet coals has not been fully developed, the results obtained for the activated carbons demonstrate a realistic potential for doing so.

CHAPTER 7

MODELING OF MULTICOMPONENT ADSORPTION

In this chapter, we incorporated the excess Gibbs free energy mixing rules in the 2-D EOSs. In so doing, we recognize differences in the molecular affinity between the adsorbate and the adsorption surface, which can result in non-random mixing. One-fluid mixing rules are also evaluated for comparison purposes.

7.1 Case Studies Conducted

Four cases were studied as follows:

1. Prediction capability ($C_{ij}=D_{ij}=0$) of the ZGR EOS and the 2-D PR EOS using one-fluid mixing rules

2. Representation capability (C_{ij} and D_{ij} are regressed) of the ZGR EOS and the 2-D PR EOS using one-fluid mixing rules

3. Prediction capability of the ZGR EOS and the 2-D PR EOS using Wong-Sandler mixing rules, where the binary interaction parameter, C_{ij}, and three parameters in NTRL (α_{12}, τ_{12}, and τ_{21}) are set to zero

4. Representation capability of the ZGR EOS and the 2-D PR EOS using Wong-Sandler mixing rules, where all four adjustable parameters are regressed

In addition, two prediction cases were performed for ternary mixtures:

5. Prediction capability of the ZGR EOS and the 2-D PR EOS using one-fluid mixing rules, where C_{ij} and D_{ij} are from Case 2

6. Prediction capability of the ZGR EOS and the 2-D PR EOS using Wong-Sandler mixing rules, where all four adjustable parameters are from Case 4

The mixture adsorption data are listed in Tables 4-2 and 4-3. In Table 7-1 these mixture adsorption systems are relisted to include the feed molar compositions. Systems 39 through 46 and 51 through 54 are gas adsorption on dry activated carbons; Systems 58 through 60, 64 through 66, and 70 through 73 are gas adsorption on wet coals. These data cover a wide pressure range at temperatures close to typical CBM reservoir temperatures.

The objective function, S, was used to correlate the data. The function minimizes the sum of the squared-percentage deviations in predicted adsorption:

$$S = 100 \sqrt{\sum_{j=1}^{NC} \sum_{i=1}^{NPTS} \left[\frac{\omega_j^e(i) - \omega_j^c(i)}{\omega_j^e(i)} \right]^2} \qquad (7\text{-}1)$$

where ω_j^e and ω_j^c are the experimental and calculated adsorption amounts for component j, respectively, NC is the number of gas components in the mixture, and NPTS is the number of data points for each component. In addition, the percentage average absolute deviation (%AAD ω_j) and root-mean-square error (RMSE ω_j) are presented to assist in evaluating the results:

$$\%\text{AAD } \omega_j = \frac{100}{NPTS} \sum_{i=1}^{NPTS} \left| \frac{\omega_j^e(i) - \omega_j^c(i)}{\omega_j^e(i)} \right| \qquad (7\text{-}2)$$

$$\text{RMSE } \omega_j = \sqrt{\frac{\sum_{i=1}^{NPTS} \left(\omega_j^e(i) - \omega_j^c(i) \right)^2}{NPTS}} \qquad (7\text{-}3)$$

Table 7-1. Data Used for Mixed-Gas Adsorption Model Evaluation

System No.	Adsorbent	Adsorbate	Temp. (K)	Pressure Range (MPa)	Feed Molar Composition	Sources
39	AC, BPL	$CH_4 + C_2H_6$	301	0.13 – 2.01	0.267,0.499,0.745*	Reich (1980)
40	AC, BPL	$CH_4 + C_2H_4$	301	0.12 – 2.03	0.260,0.534,0.745*	Reich (1980)
41	AC, BPL	$C_2H_6 + C_2H_4$	301	0.14 – 1.98	0.240,0.472,0.682*	Reich (1980)
42	AC, BPL	$CH_4 + C_2H_6 + C_2H_4$	301	0.12 – 2.97	0.624+0.174+0.202* 0.230+0.520+0.250* 0.200+0.192+0.608*	Reich (1980)
43	AC Norit R1 Extra	$N_2 + CH_4$	298	0.03 – 6.00	Not available	Dreisbach (1999)
44	AC Norit R1 Extra	$CH_4 + CO_2$	298	0.03 – 6.00	Not available	Dreisbach (1999)
45	AC Norit R1 Extra	$N_2 + CO_2$	298	0.03 – 6.00	Not available	Dreisbach (1999)
46	AC Norit R1 Extra	$N_2 + CH_4 + CO_2$	298	0.03 – 6.00	Not available	Dreisbach (1999)
51	Dry AC – F 400	$N_2 + CH_4$	318	0.7 – 12.4	0.2, 0.4, 0.6, 0.8	OSU
52	Dry AC – F 400	$CH_4 + CO_2$	318	0.7 – 12.4	0.2, 0.4, 0.6, 0.8	OSU
53	Dry AC – F 400	$N_2 + CO_2$	318	0.7 – 12.4	0.2, 0.4, 0.6, 0.8	OSU
54	Dry AC – F 400	$N_2 + CH_4 + CO_2$	318	0.7 – 12.4	0.1+0.4+0.5	OSU
58	Wet Fruitland Coal	$N_2 + CH_4$	319	0.7 – 12.4	0.2, 0.4, 0.6, 0.8	OSU
59	Wet Fruitland Coal	$CH_4 + CO_2$	319	0.7 – 12.4	0.2, 0.4, 0.6, 0.8	OSU
60	Wet Fruitland Coal	$N_2 + CO_2$	319	0.7 – 12.4	0.2, 0.4, 0.6, 0.8	OSU
64	Wet Illinois #6 Coal	$N_2 + CH_4$	319	0.7 – 12.4	0.2, 0.4, 0.6, 0.8	OSU
65	Wet Illinois #6 Coal	$CH_4 + CO_2$	319	0.7 – 12.4	0.2, 0.4, 0.6, 0.8	OSU
66	Wet Illinois #6 Coal	$N_2 + CO_2$	319	0.7 – 12.4	0.2, 0.4, 0.6, 0.8	OSU
70	Wet Tiffany Coal	$N_2 + CH_4$	328	0.7 – 13.7	0.2, 0.4, 0.6, 0.8	OSU
71	Wet Tiffany Coal	$CH_4 + CO_2$	328	0.7 – 13.7	0.2, 0.4, 0.6, 0.8	OSU
72	Wet Tiffany Coal	$N_2 + CO_2$	328	0.7 – 13.7	0.2, 0.4, 0.6, 0.8	OSU
73	Wet Tiffany Coal	$N_2 + CH_4 + CO_2$	328	0.7 – 13.7	0.1+0.4+0.5	OSU

* Gas-phase mole fraction of the first-named component at equilibria

The weighted average-absolute deviation (WAAD ω_j) is also used to evaluate results when the expected experimental uncertainties, σ_j^e, are available:

$$\text{WAAD}\,\omega_j = \frac{1}{\text{NPTS}} \sum_{i=1}^{\text{NPTS}} \left| \frac{\omega_j^e(i) - \omega_j^c(i)}{\sigma_j^e(i)} \right| \tag{7-4}$$

7.2 One-Fluid Mixing Rules

Mixing rules for the model parameters are crucial for extending the 2-D EOS from pure-gas adsorption to mixture adsorption. One-fluid mixing rules are widely used in 3-D EOS applications, where the 3-D EOS parameters, a and b, for mixtures are given by:

$$a = \sum_i \sum_j x_i x_j a_{ij} \quad \text{and} \quad b = \sum_i \sum_j x_i x_j b_{ij} \tag{7-5}$$

and:

$$a_{ij} = \sqrt{a_i a_j}\left(1 - C_{ij}\right)/2 \tag{7-6}$$

$$b_{ij} = \left(b_i + b_j\right)\left(1 + D_{ij}\right)/2 \tag{7-7}$$

where C_{ij} and D_{ij} are binary interaction parameters.

However, the combination rule for "a" of Equation 7-6 is not applicable in 2-D EOS because α values can be either positive or negative. Thus, based on practical considerations, Zhou et al. (1994) used an arithmetic mean for parameter α and geometric mean for β. The one-fluid mixing rules used are expressed empirically as:

$$\alpha = \sum_i \sum_j x_i x_j \alpha_{ij} \quad \text{and} \quad \beta = \sum_i \sum_j x_i x_j \beta_{ij} \tag{7-8}$$

and:

100

$$\alpha_{ij} = (\alpha_i + \alpha_j)(1 - C_{ij})/2 \qquad\qquad (7\text{-}9)$$

$$\beta_{ij} = \sqrt{\beta_i \beta_j}(1 + D_{ij})/2 \qquad\qquad (7\text{-}10)$$

7.3 Wong-Sandler Mixing Rules to 2-D EOS

As indicated in the previous section, in order to represent mixture adsorption, a set of non-conventional combination rules (Equations 7-9 and 7-10) were used in the one-fluid mixing rules. In the regression cases, geometric or arithmetic mean for the combination rules work identically, except that the values of the regressed interaction parameters, C_{ij} and D_{ij}, are different. For the prediction cases ($C_{ij}=D_{ij}=0$), however, different combination rules will lead to different results. Moreover, we recognize differences in the molecular affinity between the adsorbate and the adsorption surface, which can result in non-random mixing. Thus, we applied the Wong-Sandler mixing rules to the 2-D EOSs.

Wong-Sandler mixing rules were developed for 3-D cubic EOSs. They equate the excess Helmholtz free energy at infinite pressure from the chosen equation of state to that from an activity coefficient model. Use of the Helmholtz free energy ensures that the second virial coefficient calculated from the equation of state has quadratic composition dependence, as required by statistical mechanics [Wong et al., 1992].

The Wong-Sandler mixing rules for 3-D cubic EOSs are [Wong et al., 1992]:

$$b - \frac{a}{RT} = \sum_i \sum_j x_i x_j \left(b - \frac{a}{RT} \right)_{ij} \qquad\qquad (7\text{-}11)$$

$$\frac{A_\infty^E}{FRT} = -\frac{a}{bRT} + \sum_i x_i \frac{a_i}{b_i RT} \qquad\qquad (7\text{-}12)$$

where the cross term:

$$\left(b - \frac{a}{RT}\right)_{ij} = \frac{1}{2}\left[\left(b_i - \frac{a_i}{RT}\right) + \left(b_j - \frac{a_j}{RT}\right)\right]\left(1 - C_{ij}\right) \tag{7-13}$$

and F in Equation 7-12 is a constant specific to the EOS chosen.

The Wong-Sandler mixing rules for 2-D EOS are listed below. (Details are in Appendix B.)

$$\beta - \frac{\alpha}{RT} = \sum_i \sum_j x_i x_j \left(\beta - \frac{\alpha}{RT}\right)_{ij} \tag{7-14}$$

$$\frac{A_\infty^E}{RT} = -\frac{\alpha}{F\beta RT} + \sum_i x_i \frac{\alpha_i}{F\beta_i RT} + (\frac{1}{m} - 1)\sum_i x_i \ln\frac{\beta}{\beta_i} \tag{7-15}$$

where:

$$\left(\beta - \frac{\alpha}{RT}\right)_{ij} = \frac{1}{2}\left[\left(\beta_i - \frac{\alpha_i}{RT}\right) + \left(\beta_j - \frac{\alpha_j}{RT}\right)\right]\left(1 - C_{ij}\right) \tag{7-16}$$

and $F = \sqrt{U^2 - 4W} \Big/ \ln\left(\frac{1 + \left(U - \sqrt{U^2 - 4W}\right)\big/2}{1 + \left(U + \sqrt{U^2 - 4W}\right)\big/2}\right)$

If U=W=0, then F=1.

The Non-Random Two-Liquid (NRTL) model [see, e.g., Tester, 1996] was used to estimate the Helmholtz free energy, A_∞^E for the adsorbed phase:

$$\frac{A_\infty^E}{RT} \approx \frac{\Delta G^E}{RT} = \sum_{l=1}^{NC}\left[\frac{x_l \sum_{j=1}^{NC}\tau_{jl}G_{jl}x_j}{\sum_{k=1}^{NC}G_{kl}x_k}\right] = \frac{1}{\omega}\sum_{l=1}^{NC}\left[\frac{\omega_l \sum_{j=1}^{NC}\tau_{jl}G_{jl}\omega_j}{\sum_{k=1}^{NC}G_{kl}\omega_k}\right] \tag{7-17}$$

where $\tau_{ii} = 0$ and $G_{ji} = \exp\left(-\alpha_{ji}\tau_{ji}\right)$ with $\alpha_{ji} = \alpha_{ij}$.

7.4 Results for Mixture Adsorption on Activated Carbons

This section presents the results of the ZGR EOS and 2-D PR EOS modeling of mixture adsorption on three dry activated carbons.

Tables 7-2 through 7-4 show the prediction results for binary mixture adsorption on activated carbons using Case 1. On average, both the ZGR EOS and 2-D PR EOS predict the component and total adsorption within three times the expected experimental uncertainties using one-fluid mixing rules. However, the ZGR EOS yields larger errors than the 2-D PR EOS. Typically, for the lower-adsorption component, the errors are larger than those of the higher-adsorption component.

Tables 7-5 through 7-7 show the representation results for binary mixture adsorption on activated carbons using Case 2. As expected, by regressing two binary interaction parameters, C_{ij} and D_{ij}, both EOSs yield better results than those in Case 1. The binary interactions, C_{ij} and D_{ij}, are larger in the 2-D PR EOS than in ZGR EOS, especially for C_{ij}. However, even with the large regressed values for C_{ij}, the results do not show significant improvement over the prediction mode. This indicates the calculated mixture adsorption is insensitive to the binary interaction parameters using the 2-D PR EOS for these systems.

Tables 7-8 through 7-10 show the prediction results for the ternary mixtures on activated carbons using Case 1 and Case 5. As expected, the prediction results for the ternary mixture are worse than those for binary mixture. Unexpectedly, the prediction results based on the pure-gas adsorption parameters and binary interaction parameters (Case 5) are worse than the prediction based only on pure-gas adsorption parameters (Case 1).

Table 7-2. The 2-D EOS Predictions of Binary Mixture Adsorption on Activated Carbon at 301.4 K (Reich, 1980) – One-Fluid Mixing Rules

Systems	NPTS	%AAD	RMSE (mmol/g)	WAAD
ZGR EOS				
$CH_4+C_2H_6$				
Methane	14	38.0	0.328	–
Ethane	14	2.6	0.097	–
Total	14	5.2	0.269	–
$CH_4+C_2H_4$				
Methane	15	31.8	0.289	–
Ethylene	15	3.1	0.111	–
Total	15	4.7	0.212	–
$C_2H_6+C_2H_4$				
Ethane	12	4.1	0.097	–
Ethylene	12	6.5	0.184	–
Total	12	4.1	0.214	–
2-D PR EOS				
$CH_4+C_2H_6$				
Methane	14	37.4	0.323	–
Ethane	14	2.5	0.095	–
Total	14	5.0	0.257	–
$CH_4+C_2H_4$				
Methane	15	30.5	0.284	–
Ethylene	15	2.8	0.105	–
Total	15	4.7	0.209	–
$C_2H_6+C_2H_4$				
Ethane	12	4.3	0.091	–
Ethylene	12	7.4	0.193	–
Total	12	4.1	0.208	–

Table 7-3. The 2-D EOS Predictions of Binary Mixture Adsorption on Activated Carbon at 298.0 K (Dreisbach, 1999) – One-Fluid Mixing Rules

Systems	NPTS	%AAD	RMSE (mmol/g)	WAAD
ZGR EOS				
CH$_4$+N$_2$				
Methane	24	6.8	0.224	–
Nitrogen	24	16.5	0.143	–
Total	24	4.9	0.154	–
CH$_4$+CO$_2$				
Methane	24	10.1	0.291	–
CO$_2$	24	22.6	0.362	–
Total	24	3.6	0.323	–
N$_2$+CO$_2$				
Nitrogen	24	44.3	0.308	–
CO$_2$	24	3.7	0.376	–
Total	24	5.3	0.478	–
2-D PR EOS				
CH$_4$+N$_2$				
Methane	24	9.2	0.255	–
Nitrogen	24	11.8	0.112	–
Total	24	3.5	0.174	–
CH$_4$+CO$_2$				
Methane	24	9.9	0.310	–
CO$_2$	24	20.2	0.302	–
Total	24	3.3	0.313	–
N$_2$+CO$_2$				
Nitrogen	24	10.4	0.064	–
CO$_2$	24	3.0	0.238	–
Total	24	2.9	0.264	–

Table 7-4. The 2-D EOS Predictions of Binary Mixture Adsorption on Activated Carbon at 318.2 K – One-Fluid Mixing Rules

Systems	NPTS	%AAD	RMSE (mmol/g)	WAAD
ZGR EOS				
CH_4+N_2				
Methane	40	5.2	0.172	2.0
Nitrogen	40	4.7	0.063	1.1
Total	40	3.4	0.149	1.4
CH_4+CO_2				
Methane	40	6.3	0.156	1.3
CO_2	40	11.4	0.277	2.9
Total	40	2.5	0.155	0.8
N_2+CO_2				
Nitrogen	40	13.1	0.132	2.1
CO_2	40	11.9	0.233	2.7
Total	40	6.9	0.306	2.1
2-D PR EOS				
CH_4+N_2				
Methane	40	6.5	0.188	2.5
Nitrogen	40	4.9	0.056	1.2
Total	40	3.8	0.164	1.6
CH_4+CO_2				
Methane	40	4.6	0.123	1.0
CO_2	40	7.4	0.188	1.8
Total	40	1.4	0.090	0.4
N_2+CO_2				
Nitrogen	40	5.5	0.068	1.0
CO_2	40	5.3	0.120	1.2
Total	40	3.3	0.148	1.0

106

Table 7-5. The 2-D EOS Representations of Binary Mixture Adsorption on Activated Carbon at 301.4 K (Reich, 1980) – One-Fluid Mixing Rules

Systems	NPTS	%AAD	RMSE (mmol/g)	WAAD	C_{12}	D_{12}
ZGR EOS						
$CH_4+C_2H_6$					0.6072	-0.4775
Methane	14	15.0	0.105	–		
Ethane	14	2.7	0.100	–		
Total	14	2.6	0.129	–		
$CH_4+C_2H_4$					-0.0615	-0.1028
Methane	15	7.6	0.061	–		
Ethylene	15	3.4	0.115	–		
Total	15	2.2	0.104	–		
$C_2H_6+C_2H_4$					0.4573	-0.2039
Ethane	12	4.6	0.096	–		
Ethylene	12	5.4	0.160	–		
Total	12	3.2	0.157	–		
2-D PR EOS						
$CH_4+C_2H_6$					-0.2291	-1.0485
Methane	14	8.1	0.070	–		
Ethane	14	4.7	0.195	–		
Total	14	2.9	0.163	–		
$CH_4+C_2H_4$					0.0459	-0.6458
Methane	15	6.6	0.045	–		
Ethylene	15	3.7	0.146	–		
Total	15	2.2	0.109	–		
$C_2H_6+C_2H_4$					-0.2398	-0.3148
Ethane	12	4.5	0.092	–		
Ethylene	12	6.1	0.142	–		
Total	12	2.5	0.111	–		

Table 7-6. The 2-D EOS Representations of Binary Mixture Adsorption on Activated Carbon at 298.0 K (Dreisbach, 1999) – One-Fluid Mixing Rules

Systems	NPTS	%AAD	RMSE (mmol/g)	WAAD	C_{12}	D_{12}
ZGR EOS						
CH_4+N_2						
Methane	24	9.0	0.219	—	0.3335	-0.1926
Nitrogen	24	6.6	0.094	—		
Total	24	5.6	0.201	—		
CH_4+CO_2						
Methane	24	19.6	0.437	—	0.9357	-0.5183
CO_2	24	14.3	0.254	—		
Total	24	4.6	0.339	—		
N_2+CO_2						
Nitrogen	24	9.9	0.099	—	0.4180	-0.2567
CO_2	24	3.2	0.298	—		
Total	24	3.6	0.348	—		
2-D PR EOS						
CH_4+N_2						
Methane	24	10.8	0.262	—	-0.2546	-0.0516
Nitrogen	24	4.5	0.081	—		
Total	24	4.6	0.225	—		
CH_4+CO_2						
Methane	24	19.5	0.485	—	0.1131	0.5462
CO_2	24	13.5	0.226	—		
Total	24	4.6	0.451	—		
N_2+CO_2						
Nitrogen	24	5.8	0.043	—	-0.9042	-1.4192
CO_2	24	3.1	0.224	—		
Total	24	2.6	0.227	—		

Table 7-7. The 2-D EOS Representations of Binary Mixture Adsorption on Activated Carbon at 318.2 K – One-Fluid Mixing Rules

Systems	NPTS	%AAD	RMSE (mmol/g)	WAAD	C_{12}	D_{12}
ZGR EOS						
CH_4+N_2						
Methane	40	5.3	0.165	2.1	0.0753	-0.0309
Nitrogen	40	2.7	0.055	0.7		
Total	40	4.0	0.169	1.7		
CH_4+CO_2						
Methane	40	7.9	0.174	1.8	0.2271	-0.0779
CO_2	40	8.1	0.201	2.0		
Total	40	0.7	0.058	0.2		
N_2+CO_2						
Nitrogen	40	5.3	0.058	0.8	0.2851	-0.1200
CO_2	40	9.5	0.207	2.2		
Total	40	3.7	0.171	1.1		
2-D PR EOS						
CH_4+N_2						
Methane	40	6.8	0.169	2.5	-0.6386	-0.1277
Nitrogen	40	2.7	0.036	0.6		
Total	40	4.0	0.154	1.6		
CH_4+CO_2						
Methane	40	4.3	0.091	0.9	-0.6382	-0.1470
CO_2	40	4.8	0.140	1.2		
Total	40	1.0	0.075	0.3		
N_2+CO_2						
Nitrogen	40	5.0	0.071	0.9	-1.0744	-0.2790
CO_2	40	4.6	0.154	1.2		
Total	40	3.0	0.167	0.9		

Table 7-8. The 2-D EOS Predictions of Ternary Mixture Adsorption on Activated Carbon at 301.4 K (Reich, 1980) – One-Fluid Mixing Rules

Systems	NPTS	%AAD	RMSE (mmol/g)	WAAD
ZGR EOS Based on Pure Gas Parameters				
Methane	14	49.4	0.461	—
Ethane	14	4.4	0.079	—
Ethylene	14	3.8	0.120	—
Total	14	6.2	0.459	—
2-D PR EOS Based on Pure Gas Parameters				
Methane	14	49.1	0.450	—
Ethane	14	5.1	0.090	—
Ethylene	14	3.6	0.120	—
Total	14	6.0	0.438	—
ZGR EOS Based on Pure Gas and Binary Mixture Parameters				
Methane	14	29.5	0.206	—
Ethane	14	5.2	0.096	—
Ethylene	14	3.9	0.125	—
Total	14	2.6	0.226	—
2-D PR EOS Based on Pure Gas and Binary Mixture Parameters				
Methane	14	25.7	0.189	—
Ethane	14	7.7	0.170	—
Ethylene	14	3.9	0.099	—
Total	14	2.6	0.170	—

Table 7-9. The 2-D EOS Predictions of Ternary Mixture Adsorption on Activated Carbon at 298.0 K (Dreisbach, 1999) – One-Fluid Mixing Rules

Systems	NPTS	%AAD	RMSE (mmol/g)	WAAD
ZGR EOS Based on Pure Gas Parameters				
Methane	40	17.9	0.767	–
Nitrogen	40	36.1	0.436	–
CO_2	40	22.8	0.673	–
Total	40	4.9	0.594	–
2-D PR EOS Based on Pure Gas Parameters				
Methane	40	17.3	0.733	–
Nitrogen	40	47.0	0.562	–
CO_2	40	19.4	0.581	–
Total	40	5.6	0.696	–
ZGR EOS Based on Pure Gas and Binary Mixture Parameters				
Methane	40	21.7	0.915	–
Nitrogen	40	73.0	0.811	–
CO_2	40	21.2	0.739	–
Total	40	9.3	0.835	–
2-D PR EOS Based on Pure Gas and Binary Mixture Parameters				
Methane	40	21.1	0.912	–
Nitrogen	40	43.6	0.519	–
CO_2	40	17.7	0.560	–
Total	40	7.1	0.818	–

Table 7-10. The 2-D EOS Predictions of Ternary Mixture Adsorption on Activated Carbon at 318.2 K – One-Fluid Mixing Rules

Systems	NPTS	%AAD	RMSE (mmol/g)	WAAD
ZGR EOS Based on Pure Gas Parameters				
Methane	11	3.6	0.024	0.3
Nitrogen	11	13.2	0.272	2.3
CO_2	11	13.6	0.646	3.5
Total	11	5.8	0.370	1.9
2-D PR EOS Based on Pure Gas Parameters				
Methane	11	3.8	0.023	0.4
Nitrogen	11	18.7	0.358	3.4
CO_2	11	11.7	0.595	2.8
Total	11	3.5	0.237	1.0
ZGR EOS Based on Pure Gas and Binary Mixture Parameters				
Methane	11	8.9	0.053	0.8
Nitrogen	11	24.0	0.398	4.6
CO_2	11	13.9	0.701	3.5
Total	11	3.7	0.257	1.1
2-D PR EOS Based on Pure Gas and Binary Mixture Parameters				
Methane	11	6.2	0.039	0.5
Nitrogen	11	19.7	0.360	3.7
CO_2	11	13.7	0.683	3.3
Total	11	4.5	0.294	1.3

112

Tables 7-11 through 7-13 show the prediction results for binary mixture adsorption on activated carbons using Case 3. The results are similar to those obtained using one-fluid mixing rules; the ZGR EOS has larger errors than the 2-D PR EOS. The 2-D PR EOS predicts the lower-adsorption component with better accuracy than the ZGR EOS.

Tables 7-14 through 7-16 show the representation results for binary mixture adsorption on activated carbons using Case 4. In this case, both EOSs can represent most of the systems within AAD of 10%. However, the NTRL parameters are not the same as those from the vapor-liquid equilibrium (VLE) calculations. This is due largely to the presence of the adsorbent surface, which changes the local densities in the adsorbed phase. In other words, the NTRL parameters for the 2-D EOS are no longer dependent only on the gas molecules but also depend indirectly on the properties of the adsorbent.

Tables 7-17 through 7-19 show the prediction results for the ternary mixture adsorption on activated carbons using Case 3 and Case 6. Similar to the study using one-fluid mixing rules, the prediction results based on the pure-gas adsorption parameters and binary parameters (Case 6) do not improve predictions over those based only on the pure-gas adsorption parameters (Case 3).

7.5 Results for Mixture Adsorption on Coals

This section presents the results of the ZGR EOS and 2-D PR EOS modeling of mixture adsorption on three wet coals.

Tables 7-20 through 7-22 show the prediction results for binary mixture adsorption on wet coals using Case 1. Both EOSs predict the lower-adsorption

Table 7-11. The 2-D EOS Predictions of Binary Mixture Adsorption on Activated Carbon at 318.2 K (Reich, 1980) – Wong-Sandler Mixing Rules

Systems	NPTS	%AAD	RMSE (mmol/g)	WAAD
ZGR EOS				
$CH_4+C_2H_6$				
Methane	14	38.3	0.330	–
Ethane	14	2.6	0.097	–
Total	14	5.2	0.270	–
$CH_4+C_2H_4$				
Methane	15	39.5	0.344	–
Ethylene	15	3.1	0.123	–
Total	15	5.2	0.250	–
$C_2H_6+C_2H_4$				
Ethane	12	4.0	0.096	–
Ethylene	12	6.6	0.185	–
Total	12	4.2	0.218	–
2-D PR EOS				
$CH_4+C_2H_6$				
Methane	14	38.5	0.332	–
Ethane	14	2.5	0.095	–
Total	14	5.1	0.266	–
$CH_4+C_2H_4$				
Methane	15	35.7	0.316	–
Ethylene	15	2.8	0.113	–
Total	15	4.9	0.232	–
$C_2H_6+C_2H_4$				
Ethane	12	4.3	0.091	–
Ethylene	12	7.4	0.193	–
Total	12	4.1	0.208	–

Table 7-12. The 2-D EOS Predictions of Binary Mixture Adsorption on Activated Carbon at 298.0 K (Dreisbach, 1999) – Wong-Sandler Mixing Rules

Systems	NPTS	%AAD	RMSE (mmol/g)	WAAD
ZGR EOS				
CH_4+N_2				
Methane	24	9.7	0.237	–
Nitrogen	24	5.9	0.068	–
Total	24	6.3	0.240	–
CH_4+CO_2				
Methane	24	10.9	0.307	–
CO_2	24	21.4	0.344	–
Total	24	3.7	0.335	–
N_2+CO_2				
Nitrogen	24	25.2	0.123	–
CO_2	24	3.2	0.278	–
Total	24	3.3	0.332	–
2-D PR EOS				
CH_4+N_2				
Methane	24	9.1	0.252	–
Nitrogen	24	12.5	0.126	–
Total	24	3.6	0.164	–
CH_4+CO_2				
Methane	24	10.7	0.318	–
CO_2	24	19.7	0.295	–
Total	24	3.4	0.319	–
N_2+CO_2				
Nitrogen	24	11.5	0.067	–
CO_2	24	2.9	0.233	–
Total	24	2.9	0.262	–

Table 7-13. The 2-D EOS Predictions of Binary Mixture Adsorption on Activated Carbon at 318.2 K – Wong-Sandler Mixing Rules

Systems	NPTS	%AAD	RMSE (mmol/g)	WAAD
ZGR EOS				
CH_4+N_2				
Methane	40	5.4	0.169	2.1
Nitrogen	40	2.6	0.059	0.7
Total	40	4.2	0.179	1.8
CH_4+CO_2				
Methane	40	5.3	0.159	1.2
CO_2	40	9.8	0.237	2.5
Total	40	1.5	0.097	0.4
N_2+CO_2				
Nitrogen	40	8.7	0.081	1.2
CO_2	40	8.7	0.195	2.0
Total	40	2.9	0.123	0.8
2-D PR EOS				
CH_4+N_2				
Methane	40	6.4	0.186	2.5
Nitrogen	40	5.3	0.057	1.3
Total	40	3.7	0.156	1.6
CH_4+CO_2				
Methane	40	4.3	0.119	1.0
CO_2	40	7.1	0.181	1.8
Total	40	1.3	0.085	0.4
N_2+CO_2				
Nitrogen	40	5.9	0.078	1.1
CO_2	40	5.2	0.120	1.2
Total	40	3.6	0.162	1.1

116

Table 7-14. The 2-D EOS Representations of Binary Mixture Adsorption on Activated Carbon at 301.4 K (Reich, 1980) – Wong-Sandler Mixing Rules

Systems	NPTS	%AAD	RMSE (mmol/g)	WAAD	C_{12} α_{12}	τ_{12} τ_{21}
ZGR EOS						
$CH_4+C_2H_6$					0.4387	-0.2614
Methane	14	14.5	0.118	–	0.1851	-0.5461
Ethane	14	3.0	0.116	–		
Total	14	2.3	0.120	–		
$CH_4+C_2H_4$					0.0784	-0.2540
Methane	15	5.1	0.042	–	0.9573	-1.1439
Ethylene	15	3.3	0.119	–		
Total	15	2.5	0.123	–		
$C_2H_6+C_2H_4$					-0.2835	-0.3029
Ethane	12	3.0	0.060	–	12.932	-0.2098
Ethylene	12	2.2	0.062	–		
Total	12	1.8	0.104	–		
2-D PR EOS						
$CH_4+C_2H_6$					0.2124	0.4684
Methane	14	8.3	0.074	–	1.0316	-3.6814
Ethane	14	4.6	0.192	–		
Total	14	2.9	0.161	–		
$CH_4+C_2H_4$					0.2447	0.0282
Methane	15	6.5	0.042	–	0.3000	-1.9522
Ethylene	15	3.6	0.132	–		
Total	15	2.1	0.099	–		
$C_2H_6+C_2H_4$					-0.0349	-0.7695
Ethane	12	3.7	0.079	–	8.9906	0.0116
Ethylene	12	3.4	0.079	–		
Total	12	2.5	0.122	–		

Table 7-15. The 2-D EOS Representations of Binary Mixture Adsorption on Activated Carbon at 298.0 K (Dreisbach, 1999) – Wong-Sandler Mixing Rules

Systems	NPTS	%AAD	RMSE (mmol/g)	WAAD	C_{12} α_{12}	τ_{12} τ_{21}
ZGR EOS						
CH_4+N_2					0.4169 0.5827	-0.0029 5.8449
Methane	24	7.9	0.183	—		
Nitrogen	24	6.6	0.062	—		
Total	24	6.4	0.211	—		
CH_4+CO_2					1.1056 0.2437	4.2900 -0.0034
Methane	24	9.8	0.305	—		
CO_2	24	6.9	0.202	—		
Total	24	4.0	0.287	—		
N_2+CO_2					0.7672 0.2682	-0.5311 0.7104
Nitrogen	24	6.5	0.050	—		
CO_2	24	3.5	0.310	—		
Total	24	3.3	0.336	—		
2-D PR EOS						
CH_4+N_2					-0.1490 0.1749	-2.0331 14.477
Methane	24	8.6	0.238	—		
Nitrogen	24	3.3	0.065	—		
Total	24	5.2	0.233	—		
CH_4+CO_2					0.0912 0.1437	9.1701 -0.9318
Methane	24	10.5	0.376	—		
CO_2	24	7.5	0.235	—		
Total	24	4.0	0.354	—		
N_2+CO_2					-0.0076 0.4456	-11.141 -0.7837
Nitrogen	24	5.9	0.045	—		
CO_2	24	3.1	0.220	—		
Total	24	2.6	0.226	—		

118

Table 7-16. The 2-D EOS Representations of Binary Mixture Adsorption on Activated Carbon at 318.2 K – Wong-Sandler Mixing Rules

Systems	NPTS	%AAD	RMSE (mmol/g)	WAAD	C_{12} α_{12}	τ_{12} τ_{21}
ZGR EOS						
CH_4+N_2						
Methane	40	1.8	0.042	0.6	-0.2502	-0.1743
Nitrogen	40	2.7	0.048	0.8	20.0	-0.2677
Total	40	0.9	0.041	0.4		
CH_4+CO_2						
Methane	40	3.0	0.060	0.6	-0.4465	-0.0028
CO_2	40	4.0	0.092	1.0	20.0	-0.3256
Total	40	2.1	0.134	0.6		
N_2+CO_2						
Nitrogen	40	5.0	0.052	0.8	-0.1000	-0.0949
CO_2	40	8.6	0.179	2.0	20.0	-0.1500
Total	40	4.2	0.174	1.2		
2-D PR EOS						
CH_4+N_2						
Methane	40	4.2	0.091	1.5	-0.1206	-0.0988
Nitrogen	40	1.9	0.027	0.5	20.0	-0.2643
Total	40	2.0	0.081	0.8		
CH_4+CO_2						
Methane	40	3.0	0.069	0.6	-0.1405	-0.0947
CO_2	40	2.7	0.074	0.7	20.0	-0.2448
Total	40	1.3	0.099	0.4		
N_2+CO_2						
Nitrogen	40	3.4	0.041	0.5	-0.1194	-0.1314
CO_2	40	5.1	0.165	1.3	20.0	-0.0056
Total	40	2.8	0.151	0.9		

119

Table 7-17. The 2-D EOS Predictions of Ternary Mixture Adsorption on Activated Carbon at 301.4 K (Reich, 1980) – Wong-Sandler Mixing Rules

Systems	NPTS	%AAD	RMSE (mmol/g)	WAAD
ZGR EOS Based on Pure Gas Parameters				
Methane	14	50.4	0.473	–
Ethane	14	4.5	0.082	–
Ethylene	14	3.6	0.119	–
Total	14	6.4	0.470	–
2-D PR EOS Based on Pure Gas Parameters				
Methane	14	49.8	0.459	–
Ethane	14	5.1	0.089	–
Ethylene	14	3.7	0.120	–
Total	14	6.1	0.446	–
ZGR EOS Based on Pure Gas and Binary Mixture Parameters				
Methane	14	31.6	0.239	–
Ethane	14	10.4	0.204	–
Ethylene	14	3.3	0.121	–
Total	14	3.9	0.233	–
2-D PR EOS Based on Pure Gas and Binary Mixture Parameters				
Methane	14	26.2	0.195	–
Ethane	14	10.3	0.252	–
Ethylene	14	4.1	0.117	–
Total	14	2.8	0.195	–

Table 7-18. The 2-D EOS Predictions of Ternary Mixture Adsorption on Activated Carbon at 298.0 K (Dreisbach, 1999) – Wong-Sandler Mixing Rules

Systems	NPTS	%AAD	RMSE (mmol/g)	WAAD
ZGR EOS Based on Pure Gas Parameters				
Methane	40	16.8	0.705	–
Nitrogen	40	53.8	0.656	–
CO_2	40	20.8	0.634	–
Total	40	5.8	0.705	–
2-D PR EOS Based on Pure Gas Parameters				
Methane	40	17.3	0.734	–
Nitrogen	40	46.9	0.562	–
CO_2	40	19.0	0.571	–
Total	40	5.6	0.703	–
ZGR EOS Based on Pure Gas and Binary Mixture Parameters				
Methane	40	20.9	0.844	–
Nitrogen	40	48.9	0.584	–
CO_2	40	29.3	0.852	–
Total	40	5.9	0.585	–
2-D PR EOS Based on Pure Gas and Binary Mixture Parameters				
Methane	40	16.7	0.700	–
Nitrogen	40	41.9	0.553	–
CO_2	40	22.6	0.665	–
Total	40	4.7	0.565	–

Table 7-19. The 2-D EOS Predictions of Ternary Mixture Adsorption on Activated Carbon at 318.2 K – Wong-Sandler Mixing Rules

Systems	NPTS	%AAD	RMSE (mmol/g)	WAAD
ZGR EOS Based on Pure Gas Parameters				
Methane	11	3.8	0.022	0.4
Nitrogen	11	28.2	0.468	5.4
CO_2	11	13.4	0.676	3.4
Total	11	3.1	0.210	0.9
2-D PR EOS Based on Pure Gas Parameters				
Methane	11	3.8	0.023	0.4
Nitrogen	11	17.8	0.343	3.2
CO_2	11	11.7	0.596	2.8
Total	11	3.7	0.252	1.1
ZGR EOS Based on Pure Gas and Binary Mixture Parameters				
Methane	11	5.9	0.037	0.6
Nitrogen	11	22.0	0.398	4.1
CO_2	11	12.0	0.613	3.0
Total	11	3.0	0.197	0.9
2-D PR EOS Based on Pure Gas and Binary Mixture Parameters				
Methane	11	7.1	0.048	0.6
Nitrogen	11	21.5	0.396	4.0
CO_2	11	13.6	0.688	3.3
Total	11	3.7	0.252	1.0

Table 7-20. The 2-D EOS Predictions of Binary Mixture Adsorption on Wet Fruitland Coal at 319.3 K – One-Fluid Mixing Rules

Systems	NPTS	%AAD	RMSE (mmol/g)	WAAD
ZGR EOS				
CH_4+N_2				
Methane	41	5.3	0.022	0.6
Nitrogen	41	20.9	0.022	1.5
Total	41	2.3	0.011	0.3
CH_4+CO_2				
Methane	40	24.4	0.062	2.2
CO_2	40	10.8	0.062	1.5
Total	40	9.4	0.103	1.8
N_2+CO_2				
Nitrogen	50	109.5	0.113	3.5
CO_2	50	15.4	0.115	1.9
Total	50	22.7	0.225	3.2
2-D PR EOS				
CH_4+N_2				
Methane	41	4.0	0.017	0.4
Nitrogen	41	23.0	0.027	1.7
Total	41	3.4	0.014	0.4
CH_4+CO_2				
Methane	40	8.6	0.021	0.8
CO_2	40	5.6	0.044	0.8
Total	40	3.7	0.046	0.7
N_2+CO_2				
Nitrogen	50	25.2	0.028	0.9
CO_2	50	5.9	0.037	0.6
Total	50	3.1	0.025	0.3

Table 7-21. The 2-D EOS Predictions of Binary Mixture Adsorption on Wet Illinois #6 Coal at 319.3 K – One-Fluid Mixing Rules

Systems	NPTS	%AAD	RMSE (mmol/g)	WAAD
ZGR EOS				
CH_4+N_2				
Methane	40	24.7	0.028	0.6
Nitrogen	40	29.7	0.012	0.4
Total	40	15.2	0.034	0.5
CH_4+CO_2				
Methane	40	11.7	0.019	0.5
CO_2	40	18.2	0.090	1.4
Total	40	13.0	0.091	1.2
N_2+CO_2				
Nitrogen	–	–	–	–
CO_2	–	–	–	–
Total	–	–	–	–
2-D PR EOS				
CH_4+N_2				
Methane	40	14.9	0.017	0.4
Nitrogen	40	15.3	0.005	0.3
Total	40	7.9	0.016	0.3
CH_4+CO_2				
Methane	40	17.7	0.021	0.7
CO_2	40	11.7	0.054	0.8
Total	40	6.4	0.050	0.6
N_2+CO_2				
Nitrogen	40	69.1	0.017	0.7
CO_2	40	10.4	0.046	0.7
Total	40	8.0	0.046	0.5

Table 7-22. The 2-D EOS Predictions of Binary Mixture Adsorption on Wet Tiffany Coal at 327.6 K – One-Fluid Mixing Rules

Systems	NPTS	%AAD	RMSE (mmol/g)	WAAD
ZGR EOS				
CH_4+N_2				
Methane	11	10.7	0.024	1.6
Nitrogen	11	5.5	0.004	0.4
Total	11	9.0	0.025	1.5
CH_4+CO_2				
Methane	11	26.6	0.037	4.4
CO_2	11	12.7	0.057	2.7
Total	11	3.1	0.021	0.7
N_2+CO_2				
Nitrogen	11	33.9	0.012	1.2
CO_2	11	5.9	0.043	1.0
Total	11	4.4	0.032	0.9
2-D PR EOS				
CH_4+N_2				
Methane	11	12.3	0.025	1.8
Nitrogen	11	4.4	0.004	0.3
Total	11	10.5	0.028	1.7
CH_4+CO_2				
Methane	11	24.1	0.036	3.7
CO_2	11	10.0	0.052	1.9
Total	11	3.1	0.018	0.7
N_2+CO_2				
Nitrogen	11	52.8	0.019	1.8
CO_2	11	7.5	0.049	1.4
Total	11	5.4	0.033	1.2

component with larger error in terms of AAD and WAAD. On average, the 2-D PR EOS can predict the component and total adsorption within two times the expected experimental uncertainties except for the methane adsorption in CH_4+CO_2 mixture on wet Tiffany coal. Overall, the ZGR EOS has a worse quality of fit than the 2-D PR EOS.

The ZGR EOS cannot predict N_2+CO_2 mixture adsorption as well as CH_4+N_2 and CH_4+CO_2 mixture adsorption on wet Fruitland coal. This is because pure N_2 and CO_2 parameters are substantially different using the ZGR EOS. The pure-gas adsorption parameters, α and β, for N_2 are about ten times larger than those of CO_2 in the ZGR EOS. In other words, the ZGR EOS interprets N_2 and CO_2 as a highly non-ideal pair, which leads to large errors in the adsorption prediction. In fact, the calculations failed to converge for the N_2+CO_2 mixture on the wet Illinois #6 coal, where the pure-gas adsorption parameter, α, for N_2 is about thirty times larger than that of CO_2. This disparity in parameter values caused the lack of convergence in adsorption predictions.

Tables 7-23 through 7-25 show the representation results for binary mixture adsorption on wet coals using Case 2. By regressing two binary interaction parameters, C_{ij} and D_{ij}, the ZGR EOS can represent the experimental data within three times the expected experimental uncertainties for the adsorption on wet Tiffany coals and two times the expected experimental uncertainties for the adsorption on wet Fruitland coal and wet Illinois #6 coal. The 2-D PR EOS can represent the experimental data within two times the expected experimental uncertainties for the adsorption on wet Tiffany coal and within the expected experimental uncertainties for the wet Fruitland coal and wet Illinois #6 coal. However the binary interaction parameters are unrealistically large for the 2-D PR EOS.

Table 7-23. The 2-D EOS Representations of Binary Mixture Adsorption on Wet Fruitland Coal at 319.3 K – One-Fluid Mixing Rules

Systems	NPTS	%AAD	RMSE (mmol/g)	WAAD	C_{12}	D_{12}
ZGR EOS						
CH_4+N_2						
Methane	41	7.6	0.029	0.8	0.5263	-0.4743
Nitrogen	41	8.2	0.009	0.6		
Total	41	3.8	0.025	0.5		
CH_4+CO_2						
Methane	40	5.2	0.015	0.5	0.3769	-0.0985
CO_2	40	5.5	0.041	0.7		
Total	40	2.8	0.040	0.5		
N_2+CO_2						
Nitrogen	50	12.0	0.013	0.5	0.2291	0.0364
CO_2	50	7.4	0.054	0.9		
Total	50	5.0	0.052	0.7		
2-D PR EOS						
CH_4+N_2						
Methane	41	4.6	0.016	0.5	1.9927	1.8136
Nitrogen	41	7.6	0.010	0.5		
Total	41	3.1	0.017	0.4		
CH_4+CO_2						
Methane	40	3.7	0.013	0.4	-0.1725	0.0159
CO_2	40	4.4	0.040	0.6		
Total	40	2.5	0.043	0.4		
N_2+CO_2						
Nitrogen	50	15.4	0.014	0.4	0.2649	0.2556
CO_2	50	6.0	0.038	0.6		
Total	50	3.3	0.031	0.4		

Table 7-24. The 2-D EOS Representations of Binary Mixture Adsorption on Wet Illinois #6 Coal at 319.3 K – One-Fluid Mixing Rules

Systems	NPTS	%AAD	RMSE (mmol/g)	WAAD	C_{12}	D_{12}
ZGR EOS						
CH_4+N_2					0.5478	-0.3753
Methane	40	19.6	0.020	0.5		
Nitrogen	40	20.9	0.008	0.4		
Total	40	7.6	0.014	0.2		
CH_4+CO_2					0.4422	-0.3346
Methane	40	11.9	0.016	0.5		
CO_2	40	12.7	0.087	1.4		
Total	40	12.0	0.083	1.1		
N_2+CO_2					–	–
Nitrogen	–	–	–	–		
CO_2	–	–	–	–		
Total	–	–	–	–		
2-D PR EOS						
CH_4+N_2					3.7989	1.2195
Methane	40	14.2	0.016	0.4		
Nitrogen	40	14.9	0.007	0.3		
Total	40	6.6	0.013	0.2		
CH_4+CO_2					-0.0314	0.4156
Methane	40	15.0	0.021	0.6		
CO_2	40	11.8	0.054	0.8		
Total	40	5.3	0.041	0.4		
N_2+CO_2					-0.7207	0.7357
Nitrogen	40	51.7	0.034	0.9		
CO_2	40	9.9	0.043	0.7		
Total	40	4.0	0.016	0.3		

128

Table 7-25. The 2-D EOS Representations of Binary Mixture Adsorption on Wet Tiffany Coal at 327.6 K – One-Fluid Mixing Rules

Systems	NPTS	%AAD	RMSE (mmol/g)	WAAD	C_{12}	D_{12}
ZGR EOS						
CH_4+N_2						
Methane	11	10.3	0.023	1.5	0.0265	-0.0392
Nitrogen	11	6.1	0.004	0.4		
Total	11	7.9	0.022	1.3		
CH_4+CO_2						
Methane	11	7.6	0.011	1.4	-0.1116	-0.0170
CO_2	11	13.3	0.057	3.0		
Total	11	8.3	0.051	2.1		
N_2+CO_2						
Nitrogen	11	10.2	0.003	0.4	0.2548	-0.2723
CO_2	11	5.9	0.043	1.0		
Total	11	5.4	0.041	1.0		
2-D PR EOS						
CH_4+N_2						
Methane	11	7.0	0.011	1.0	-1.0973	-3.0000
Nitrogen	11	5.5	0.004	0.4		
Total	11	4.7	0.010	0.8		
CH_4+CO_2						
Methane	11	7.2	0.014	1.0	4.9538	0.03890
CO_2	11	7.7	0.038	1.6		
Total	11	5.0	0.029	1.3		
N_2+CO_2						
Nitrogen	11	6.7	0.002	0.3	0.6113	-0.4547
CO_2	11	7.4	0.048	1.3		
Total	11	6.9	0.048	1.3		

Table 7-26 shows the prediction results for the ternary mixture on wet Tiffany coal using Case 1 and Case 5. As expected, because of the presence of methane, the prediction results for nitrogen and CO_2 component adsorption results in this ternary mixture are worse than those in N_2+CO_2 binary mixture adsorption. Similar to the ternary adsorption results on activated carbons, the prediction results based on the pure-gas adsorption parameters and binary interaction parameters do not show much improvement over the prediction based on pure-gas adsorption parameters only.

Tables 7-27 through 7-29 show the prediction results for binary mixture adsorption on wet coals using Case 3. The results are similar to those obtained using one-fluid mixing rules; the ZGR EOS has larger errors than the 2-D PR EOS. The 2-D PR EOS predicts the lower adsorbed component better than ZGR EOS does. The ZGR EOS does not converge for N_2+CO_2 adsorption on wet Fruitland coal and wet Illinois #6 coal. This failure to converge is partly due to reasons discussed in the one-fluid mixing rules for the adsorption and to other causes, which will be addressed in the discussion section.

Tables 7-30 through 7-32 show the representation results for binary mixture adsorption on wet coals using Case 4. The results are similar to those obtained using one-fluid mixing rules (Case 1).

Table 7-33 shows the prediction results for the ternary mixture on wet Tiffany coal using Case 2 and Case 6. These results also indicate that use of the binary mixture information does not improve the ternary mixture adsorption results.

Table 7-26. The 2-D EOS Predictions of Ternary Mixture Adsorption on Wet Tiffany Coal at 327.6 K – One-Fluid Mixing Rules

Systems	NPTS	%AAD	RMSE (mmol/g)	WAAD
ZGR EOS Based on Pure Gas Parameters				
Methane	11	24.4	0.007	1.0
Nitrogen	11	46.2	0.030	3.0
CO_2	11	19.4	0.075	3.6
Total	11	6.6	0.038	1.4
2-D PR EOS Based on Pure Gas Parameters				
Methane	11	19.3	0.006	0.8
Nitrogen	11	57.3	0.040	3.5
CO_2	11	15.9	0.074	2.8
Total	11	5.2	0.031	1.1
ZGR EOS Based on Pure Gas and Binary Mixture Parameters				
Methane	11	16.2	0.005	0.6
Nitrogen	11	29.8	0.019	2.0
CO_2	11	20.1	0.076	3.7
Total	11	11.4	0.062	2.6
2-D PR EOS Based on Pure Gas and Binary Mixture Parameters				
Methane	11	44.1	0.018	1.3
Nitrogen	11	20.9	0.011	1.5
CO_2	11	15.6	0.068	2.8
Total	11	12.1	0.076	2.8

Table 7-27. The 2-D EOS Predictions of Binary Mixture Adsorption on Wet Fruitland Coal at 319.3 K – Wong-Sandler Mixing Rules

Systems	NPTS	%AAD	RMSE (mmol/g)	WAAD
ZGR EOS				
CH$_4$+N$_2$				
Methane	41	3.9	0.019	0.5
Nitrogen	41	29.9	0.034	2.1
Total	41	3.8	0.019	0.5
CH$_4$+CO$_2$				
Methane	40	41.9	0.087	3.6
CO$_2$	40	10.9	0.063	1.5
Total	40	8.8	0.095	1.5
N$_2$+CO$_2$				
Nitrogen	–	–	–	–
CO$_2$	–	–	–	–
Total	–	–	–	–
2-D PR EOS				
CH$_4$+N$_2$				
Methane	41	4.1	0.018	0.5
Nitrogen	41	22.9	0.026	1.7
Total	41	3.3	0.014	0.4
CH$_4$+CO$_2$				
Methane	40	5.7	0.018	0.6
CO$_2$	40	4.9	0.042	0.7
Total	40	3.4	0.045	0.6
N$_2$+CO$_2$				
Nitrogen	50	25.8	0.029	0.9
CO$_2$	50	5.9	0.037	0.6
Total	50	3.2	0.025	0.4

Table 7-28. The 2-D EOS Predictions of Binary Mixture Adsorption on Wet Illinois #6 Coal at 319.3 K – Wong-Sandler Mixing Rules

Systems	NPTS	%AAD	RMSE (mmol/g)	WAAD
ZGR EOS				
CH_4+N_2				
Methane	40	19.6	0.020	0.5
Nitrogen	40	21.5	0.008	0.4
Total	40	8.0	0.016	0.3
CH_4+CO_2				
Methane	40	13.1	0.022	0.5
CO_2	40	19.2	0.090	1.5
Total	40	15.0	0.101	1.4
N_2+CO_2				
Nitrogen	—	—	—	—
CO_2	—	—	—	—
Total	—	—	—	—
2-D PR EOS				
CH_4+N_2				
Methane	40	14.9	0.018	0.4
Nitrogen	40	15.4	0.005	0.3
Total	40	8.0	0.017	0.3
CH_4+CO_2				
Methane	40	15.5	0.021	0.6
CO_2	40	11.7	0.053	0.8
Total	40	5.6	0.042	0.5
N_2+CO_2				
Nitrogen	40	49.1	0.027	0.7
CO_2	40	10.3	0.045	0.8
Total	40	4.5	0.023	0.4

Table 7-29. The 2-D EOS Predictions of Binary Mixture Adsorption on Wet Tiffany Coal at 327.6 K – Wong-Sandler Mixing Rules

Systems	NPTS	%AAD	RMSE (mmol/g)	WAAD
ZGR EOS				
CH_4+N_2				
Methane	11	11.2	0.025	1.7
Nitrogen	11	7.0	0.006	0.5
Total	11	10.4	0.030	1.7
CH_4+CO_2				
Methane	11	34.2	0.048	5.5
CO_2	11	12.7	0.058	2.7
Total	11	2.0	0.012	0.5
N_2+CO_2				
Nitrogen	11	69.4	0.023	2.4
CO_2	11	6.6	0.049	1.2
Total	11	4.4	0.029	1.0
2-D PR EOS				
CH_4+N_2				
Methane	11	11.9	0.024	1.7
Nitrogen	11	4.2	0.004	0.3
Total	11	10.1	0.026	1.6
CH_4+CO_2				
Methane	11	24.6	0.037	3.8
CO_2	11	10.0	0.052	1.9
Total	11	3.0	0.018	0.7
N_2+CO_2				
Nitrogen	11	43.4	0.015	1.5
CO_2	11	7.7	0.050	1.4
Total	11	5.8	0.037	1.2

Table 7-30. The 2-D EOS Representations of Binary Mixture Adsorption on Wet Fruitland Coal at 319.3 K – Wong-Sandler Mixing Rules

Systems	NPTS	%AAD	RMSE (mmol/g)	WAAD	C_{12} α_{12}	τ_{12} τ_{21}
ZGR EOS						
CH$_4$+N$_2$					1.0552	-1.0275
Methane	41	5.8	0.021	0.6	7.3922	-0.1558
Nitrogen	41	6.4	0.007	0.5		
Total	41	3.3	0.021	0.4		
CH$_4$+CO$_2$					0.6039	-0.4831
Methane	40	5.4	0.016	0.6	0.9791	-0.9208
CO$_2$	40	5.5	0.039	0.6		
Total	40	2.8	0.041	0.5		
N$_2$+CO$_2$					–	–
Nitrogen	–	–	–	–		
CO$_2$	–	–	–	–		
Total	–	–	–	–		
2-D PR EOS						
CH$_4$+N$_2$					0.4095	4.3366
Methane	41	5.7	0.023	0.6	0.6000	1.9299
Nitrogen	41	7.8	0.008	0.5		
Total	41	3.8	0.023	0.5		
CH$_4$+CO$_2$					-0.0814	0.8474
Methane	40	3.3	0.012	0.4	0.2000	-0.9230
CO$_2$	40	4.2	0.040	0.6		
Total	40	2.5	0.043	0.4		
N$_2$+CO$_2$					0.1853	4.4766
Nitrogen	50	15.2	0.014	0.5	0.0117	0.3705
CO$_2$	50	6.0	0.038	0.4		
Total	50	3.3	0.031	0.2		

135

Table 7-31. The 2-D EOS Representations of Binary Mixture Adsorption on Wet Illinois #6 Coal at 319.3 K – Wong-Sandler Mixing Rules

Systems	NPTS	%AAD	RMSE (mmol/g)	WAAD	C_{12} α_{12}	τ_{12} τ_{21}
ZGR EOS						
CH_4+N_2						
Methane	40	19.4	0.019	0.5	0.7060	4.4244
Nitrogen	40	19.8	0.008	0.4	0.2688	-2.1379
Total	40	7.8	0.014	0.2		
CH_4+CO_2						
Methane	40	11.3	0.019	0.4	0.5460	-0.8312
CO_2	40	7.9	0.031	0.5	6.1977	0.2455
Total	40	3.8	0.021	0.3		
N_2+CO_2						
Nitrogen	–	–	–	–	–	–
CO_2	–	–	–	–		
Total	–	–	–	–		
2-D PR EOS						
CH_4+N_2						
Methane	40	13.4	0.016	0.4	0.9307	6.6286
Nitrogen	40	13.9	0.007	0.3	0.2942	1.4992
Total	40	6.9	0.013	0.2		
CH_4+CO_2						
Methane	40	14.9	0.021	0.6	-0.0177	1.8158
CO_2	40	11.9	0.054	0.8	0.2104	6.4210
Total	40	5.3	0.040	0.4		
N_2+CO_2						
Nitrogen	40	51.8	0.033	0.9	-0.1918	-6.0733
CO_2	40	9.0	0.037	0.6	1.6000	1.9089
Total	40	3.4	0.014	0.3		

136

Table 7-32. The 2-D EOS Representations of Binary Mixture Adsorption on Wet Tiffany Coal at 327.6 K – Wong-Sandler Mixing Rules

Systems	NPTS	%AAD	RMSE (mmol/g)	WAAD	C_{12} α_{12}	τ_{12} τ_{21}
ZGR EOS						
CH₄+N₂						
Methane	11	3.7	0.008	0.6	0.1615	-0.0009
Nitrogen	11	5.5	0.004	0.4	5.9316	-0.6006
Total	11	3.2	0.008	0.5		
CH₄+CO₂						
Methane	11	8.7	0.012	1.5	-0.8419	0.2038
CO₂	11	4.9	0.019	1.2	3.6242	-1.2087
Total	11	3.0	0.016	0.9		
N₂+CO₂						
Nitrogen	11	7.1	0.002	0.3	0.5544	-0.3085
CO₂	11	6.2	0.045	1.1	2.2711	-2.4618
Total	11	5.7	0.044	1.1		
2-D PR EOS						
CH₄+N₂						
Methane	11	9.0	0.016	1.3	0.1468	-7.1169
Nitrogen	11	4.4	0.003	0.3	5.3000	-0.4682
Total	11	7.0	0.016	1.2		
CH₄+CO₂						
Methane	11	4.9	0.009	0.8	0.5815	0.5183
CO₂	11	7.7	0.041	1.6	0.9097	1.0000
Total	11	5.5	0.034	1.3		
N₂+CO₂						
Nitrogen	11	6.8	0.002	0.3	0.5430	1.1419
CO₂	11	7.4	0.049	1.4	0.0135	0.3716
Total	11	6.9	0.048	1.3		

Table 7-33. The 2-D EOS Predictions of Ternary Mixture Adsorption on Wet Tiffany Coal at 327.6 K – Wong-Sandler Mixing Rules

Systems	NPTS	%AAD	RMSE (mmol/g)	WAAD
ZGR EOS Based on Pure Gas Parameters				
Methane	11	30.9	0.010	1.2
Nitrogen	11	69.4	0.048	4.3
CO_2	11	19.8	0.078	3.6
Total	11	4.2	0.024	0.9
2-D PR EOS Based on Pure Gas Parameters				
Methane	11	19.7	0.006	0.8
Nitrogen	11	53.3	0.037	3.3
CO_2	11	16.5	0.077	2.9
Total	11	6.1	0.037	1.3
ZGR EOS Based on Pure Gas and Binary Mixture Parameters				
Methane	11	15.0	0.004	0.8
Nitrogen	11	17.9	0.009	1.3
CO_2	11	18.0	0.068	3.3
Total	11	10.5	0.059	2.4
2-D PR EOS Based on Pure Gas and Binary Mixture Parameters				
Methane	11	37.5	0.016	1.1
Nitrogen	11	21.3	0.012	1.5
CO_2	11	31.1	0.144	5.5
Total	11	23.4	0.149	5.3

7.6 Discussion

Because of the extra exponent (1/m) in the repulsive term in the ZGR EOS, the ZGR EOS is not actually cubic in nature. The second virial coefficient calculated from the ZGR EOS is infinite in the limit of low pressure, which is shown in the following discussion. For the generalized 2-D EOS:

$$\left[\pi + \frac{a_2\sigma^2}{1 + Ub_2\sigma + W(b_2\sigma)^2}\right]\left[1 - (b_2\sigma)^m\right] = \sigma RT \tag{7-18}$$

Re-writing the above equation yields:

$$Z = \frac{\pi}{\sigma RT} = \frac{1}{\left[1 - (b_2\sigma)^m\right]} - \frac{a_2\sigma}{RT\left[1 + Ub_2\sigma + W(b_2\sigma)^2\right]} \tag{7-19}$$

Taking the derivative of Z with respect to σ gives:

$$\frac{\partial Z}{\partial \sigma} = \frac{mb_2{}^m\sigma^{m-1}}{\left[1 - (b_2\sigma)^m\right]^2} - \frac{a_2}{RT\left[1 + Ub_2\sigma + W(b_2\sigma)^2\right]} + \frac{a_2\sigma\left(Ub_2 + 2Wb_2{}^2\sigma\right)}{RT\left[1 + Ub_2\sigma + W(b_2\sigma)^2\right]}$$

For the 2-D EOS where m=1:

$$B = \frac{\partial Z}{\partial \sigma}\bigg|_{\sigma=0} = b_2 - \frac{a_2}{RT}$$

However, for the ZGR EOS where m=1/3:

$$\frac{\partial Z}{\partial \sigma}\bigg|_{\sigma=0} = \left(\frac{b_2{}^{1/3}\sigma^{-2/3}}{3\left[1 - (b_2\sigma)^{1/3}\right]^2} - \frac{a_2}{RT}\right)\bigg|_{\sigma=0} = \infty$$

Thus, when using the ZGR EOS with Wong-Sandler mixing rules, the ZGR EOS does not meet the quadratic composition dependence for the second virial coefficient, although reasonable results are obtained for most mixture calculations.

Equation 7-15 relates the Helmholtz free energy with the generalized 2-D EOS:

$$\frac{A_\infty^E}{RT} = -\frac{\alpha}{\beta RT} + \sum_i x_i \frac{\alpha_i}{\beta_i RT} + (\frac{1}{m} - 1)\sum_i x_i \ln\frac{\beta}{\beta_i} \qquad (7\text{-}15)$$

Again, because of the exponent 1/3 in the ZGR EOS, the term, $(\frac{1}{m} - 1)\sum_i x_i \ln\frac{\beta}{\beta_i}$, will be

large if values of β_i differ significantly from each other, which may cause the calculation

to diverge. This term is the main reason why $N_2 + CO_2$ mixture adsorption on wet

Fruitland coal and wet Illinois #6 coal failed to converge using the ZGR EOS with

Wong-Sandler mixing rules.

To summarize the results of mixture adsorption using different mixing rules and

different EOSs, Table 7-34 compares the results for binary mixture adsorption on

activated carbons. Overall, the ZGR EOS with Wong-Sandler mixing rules predicts

mixture adsorption better than that with one-fluid mixing rules. For 2-D PR EOS, the two

mixing rules do not show significant difference. For the data correlation, Wong-Sandler

mixing rules show better results than one-fluid mixing rules for both EOS, but they have

more regressed parameters. Overall, the 2-D PR EOS show better results than the ZGR

EOS in predicting and representing the mixture adsorption for both one-fluid mixing

rules and Wong-Sandler mixing rules.

Table 7-35 compares the results for the binary mixture adsorption on wet coals.

The results of $N_2 + CO_2$ adsorption data on wet Fruitland coal and wet Illinois #6 coal are

excluded because ZGR EOS failed to converge in the calculation. Overall, the ZGR EOS

with Wong-Sandler mixing rules provides worse predictions for mixture adsorption than

that with the one-fluid mixing rules. These ZGR EOS predictions may be attributable to

the β_i parameter values for pure gases, which are significantly different. For the 2-D PR

Table 7-34. Summary of Mixture Adsorption on Activated Carbons

	L. A. C. *		H. A. C. *		Total	
	%AAD	RMSE	%AAD	RMSE	%AAD	RMSE
Predictions Using One-Fluid Mixing Rules						
ZGR EOS	16.0	0.202	9.0	0.253	4.4	0.265
2-D PR EOS	10.3	0.166	7.3	0.199	3.3	0.198
Predictions Using Wong-Sandler Mixing Rules						
ZGR EOS	12.2	0.180	8.3	0.224	3.7	0.222
2-D PR EOS	11.1	0.173	7.2	0.196	3.3	0.200
Regressions Using One-Fluid Mixing Rules						
ZGR EOS	8.1	0.171	7.3	0.206	3.3	0.205
2-D PR EOS	6.3	0.169	6.4	0.186	3.0	0.211
Regressions Using Wong-Sandler Mixing Rules						
ZGR EOS	5.5	0.113	5.0	0.164	3.0	0.189
2-D PR EOS	4.6	0.131	4.7	0.165	2.7	0.183

* L. A. C. means lower-adsorption component (233 data points)

* H. A. C. means higher-adsorption component (233 data points)

141

Table 7-35. Summary of Mixture Adsorption on Wet Coals

	L. A. C. *		H. A. C. *		Total	
	%AAD	RMSE	%AAD	RMSE	%AAD	RMSE
Predictions Using One-Fluid Mixing Rules						
ZGR EOS	21.7	0.033	13.9	0.055	9.2	0.065
2-D PR EOS	18.0	0.021	9.2	0.038	5.5	0.034
Predictions Using Wong-Sandler Mixing Rules						
ZGR EOS	28.4	0.045	12.8	0.055	8.3	0.065
2-D PR EOS	16.5	0.020	9.0	0.038	5.3	0.032
Regressions Using One-Fluid Mixing Rules						
ZGR EOS	10.9	0.012	11.1	0.050	6.6	0.047
2-D PR EOS	9.6	0.013	8.5	0.036	4.6	0.032
Regressions Using Wong-Sandler Mixing Rules						
ZGR EOS	10.1	0.013	8.8	0.029	4.3	0.026
2-D PR EOS	9.2	0.012	8.7	0.037	4.9	0.033

* L. A. C. means lower-adsorption component (194 data points)

* H. A. C. means higher-adsorption component (194 data points)

EOS, the Wong-Sandler mixing rules predict slightly better than one-fluid mixing rules. In the regression mode, however, the two mixing rules show comparable quality of fit.

Figures 7-1 through 7-3 show the comparison of one-fluid mixing rules and Wong-Sandler mixing rules for representing the CH_4+CO_2 mixture adsorption on activated carbon at 318.2 K using the ZGR EOS. From Figures 7-2 and 7-3, it can be seen that Wong-Sandler mixing rules represent the component adsorption better than one-fluid mixing rules. Using one-fluid mixing rules, the model underestimates the adsorption for CH_4 and overestimates CO_2. More generally, one-fluid mixing rules tend to underestimate the lower adsorption component and overestimate the higher adsorption component.

Figures 7-4 through 7-6 show comparisons of the ZGR EOS and 2-D PR EOS representation of N_2+CO_2 mixture adsorption on activated carbon at 318.2 K using Wong-Sandler mixing rules. The figures indicate that both models represent the adsorption with no significant difference.

In summary, the results of mixture adsorption modeling using 2-D EOS indicate:

1. Overall, both the ZGR EOS and the 2-D PR EOS can represent the binary mixture adsorption sets within an AAD of 12% using Wong-Sandler mixing rules and one-fluid mixing rules. Among the cases studied, 2-D PR EOS with Wong-Sandler mixing provides marginally better quality of fit, which suggests that the mixing in the adsorbed phase may be non-random, or that the additional model parameters in these mixing rules provide better precision.
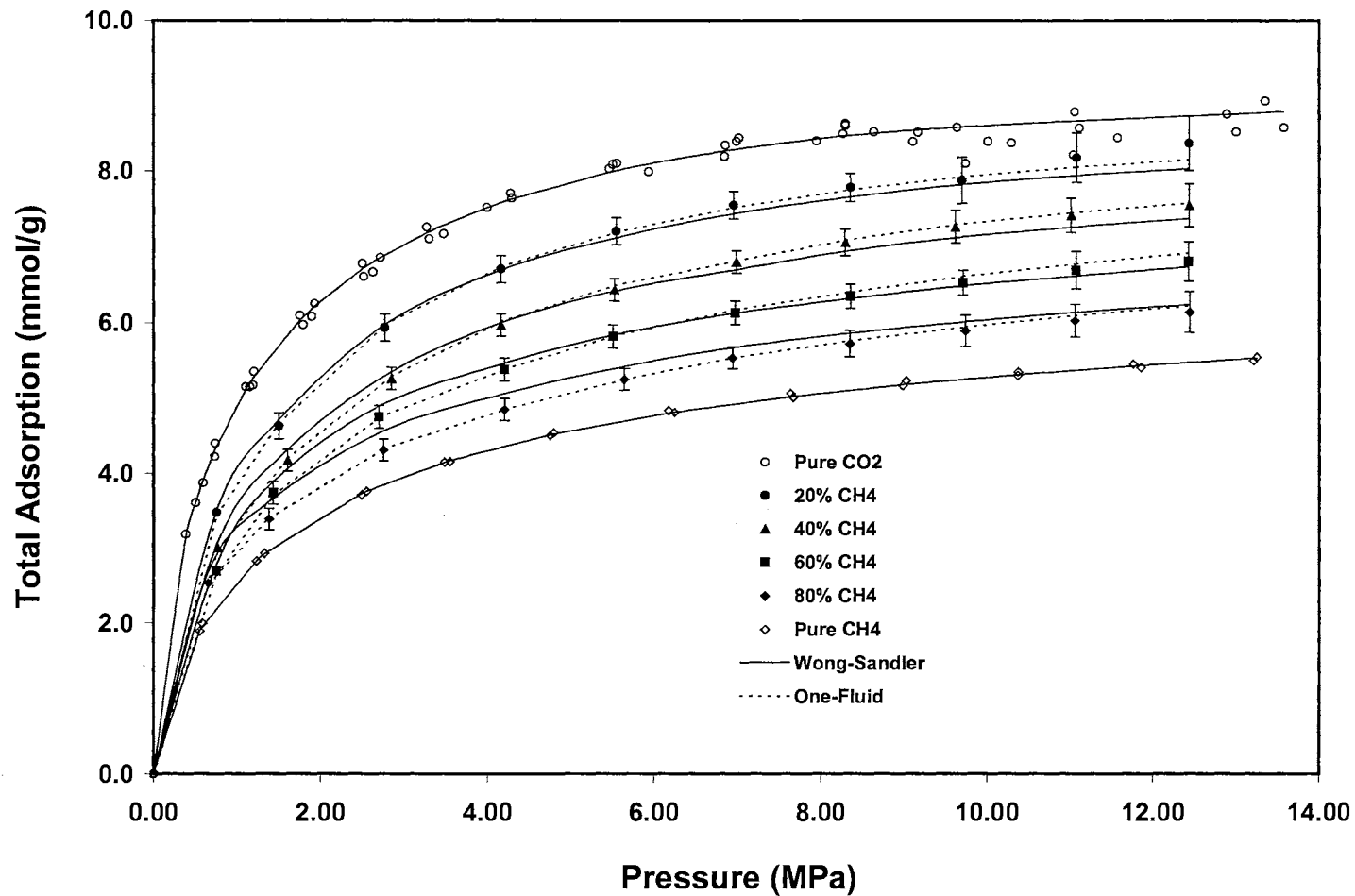
Figure 7-1. Representation of CH_4+CO_2 Mixture Adsorption on Activated Carbon at 318.2 K: Total Adsorption Using the ZGR EOS
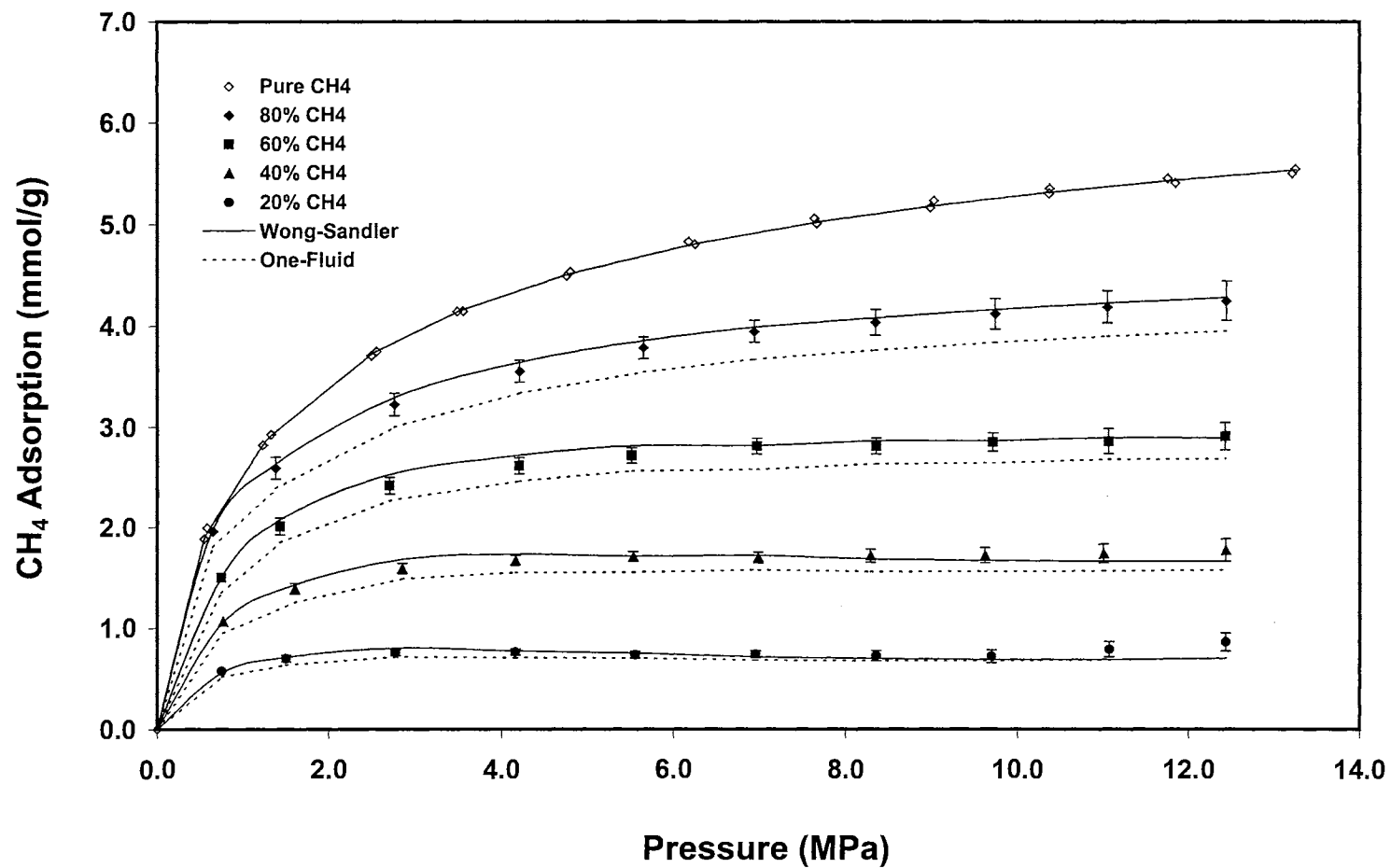
Figure 7-2. Representation of CH_4+CO_2 Mixture Adsorption on Activated Carbon at 318.2 K: CH_4 Component Adsorption Using the ZGR EOS
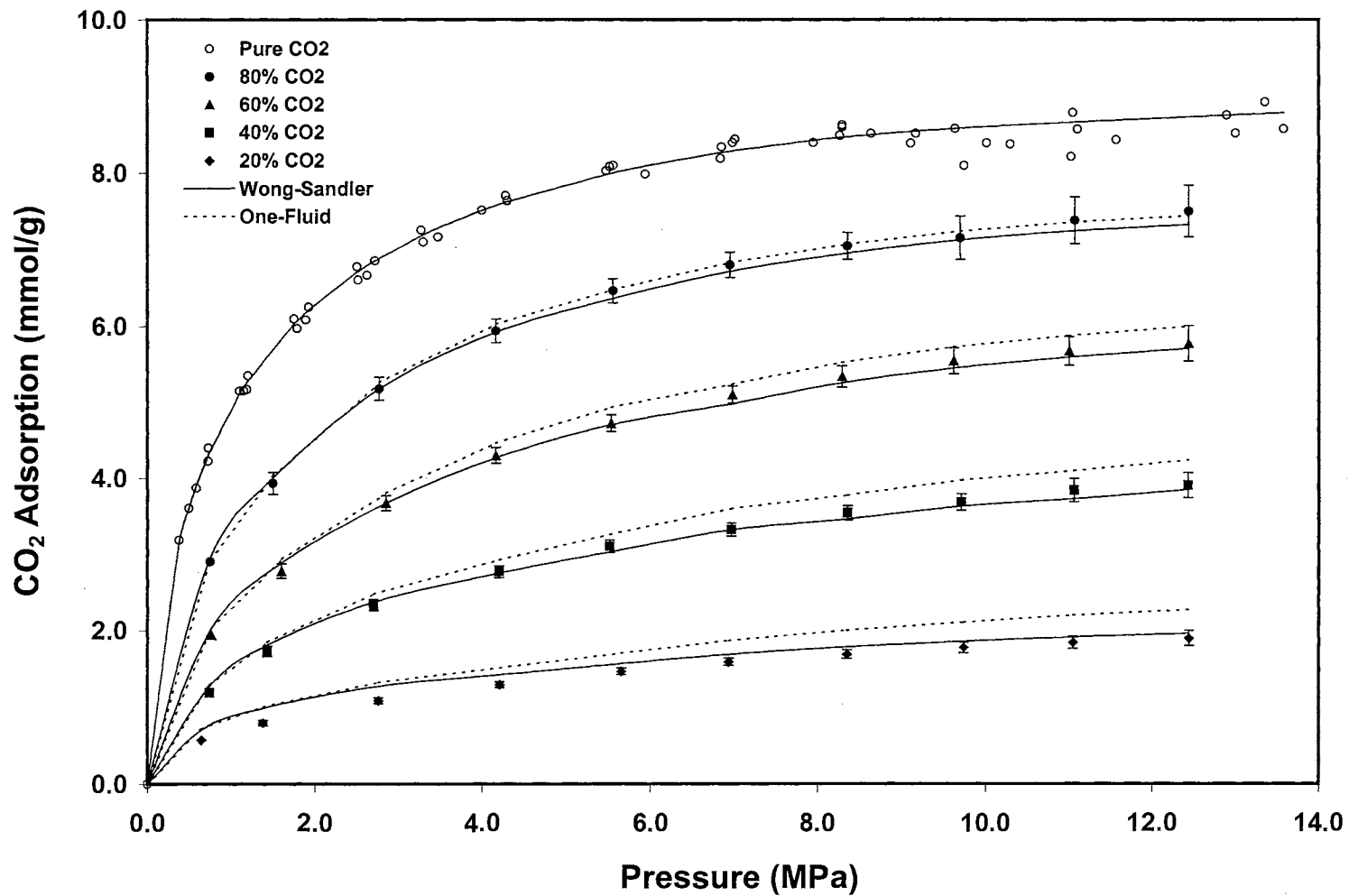
Figure 7-3. Representation of CH_4+CO_2 Mixture Adsorption on Activated Carbon at 318.2 K:
CO_2 Component Adsorption Using the ZGR EOS
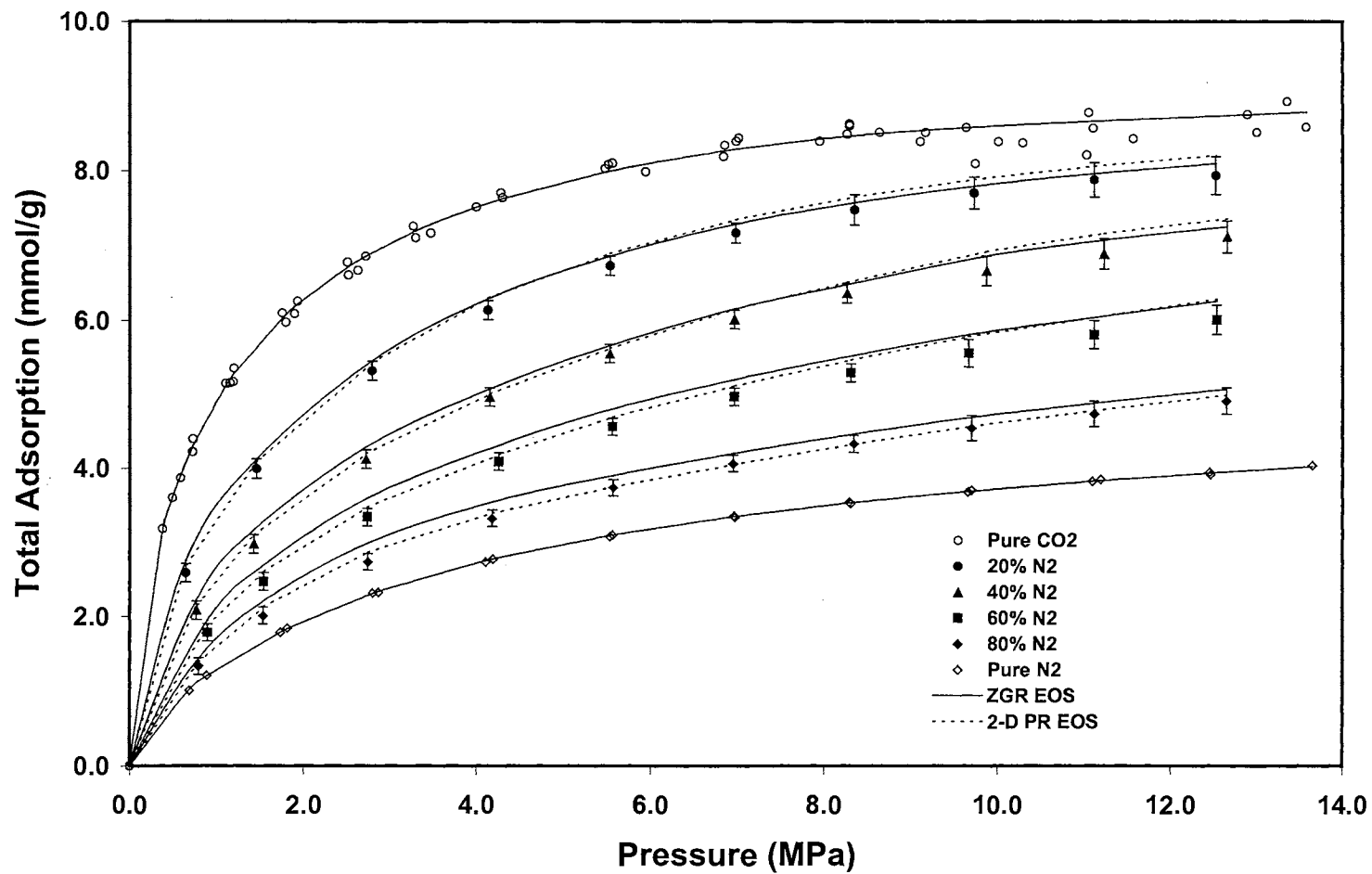
Figure 7-4. Representation of N_2+CO_2 Mixture Adsorption on Activated Carbon at 318.2 K:
Total Adsorption Using Wong-Sandler Mixing Rules
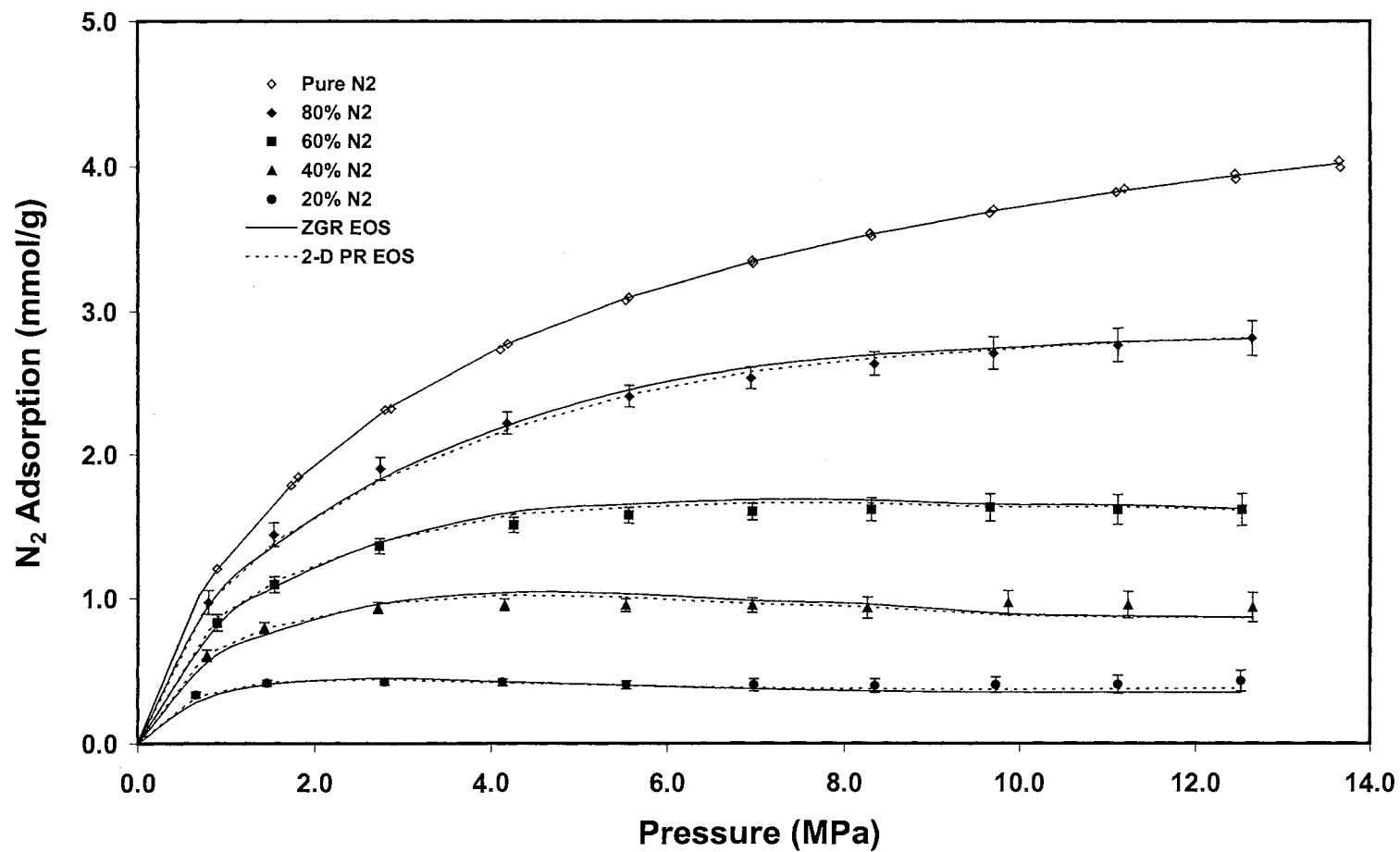
Figure 7-5. Representation of N_2+CO_2 Mixture Adsorption on Activated Carbon at 318.2 K:
N_2 Component Adsorption Using Wong-Sandler Mixing Rules
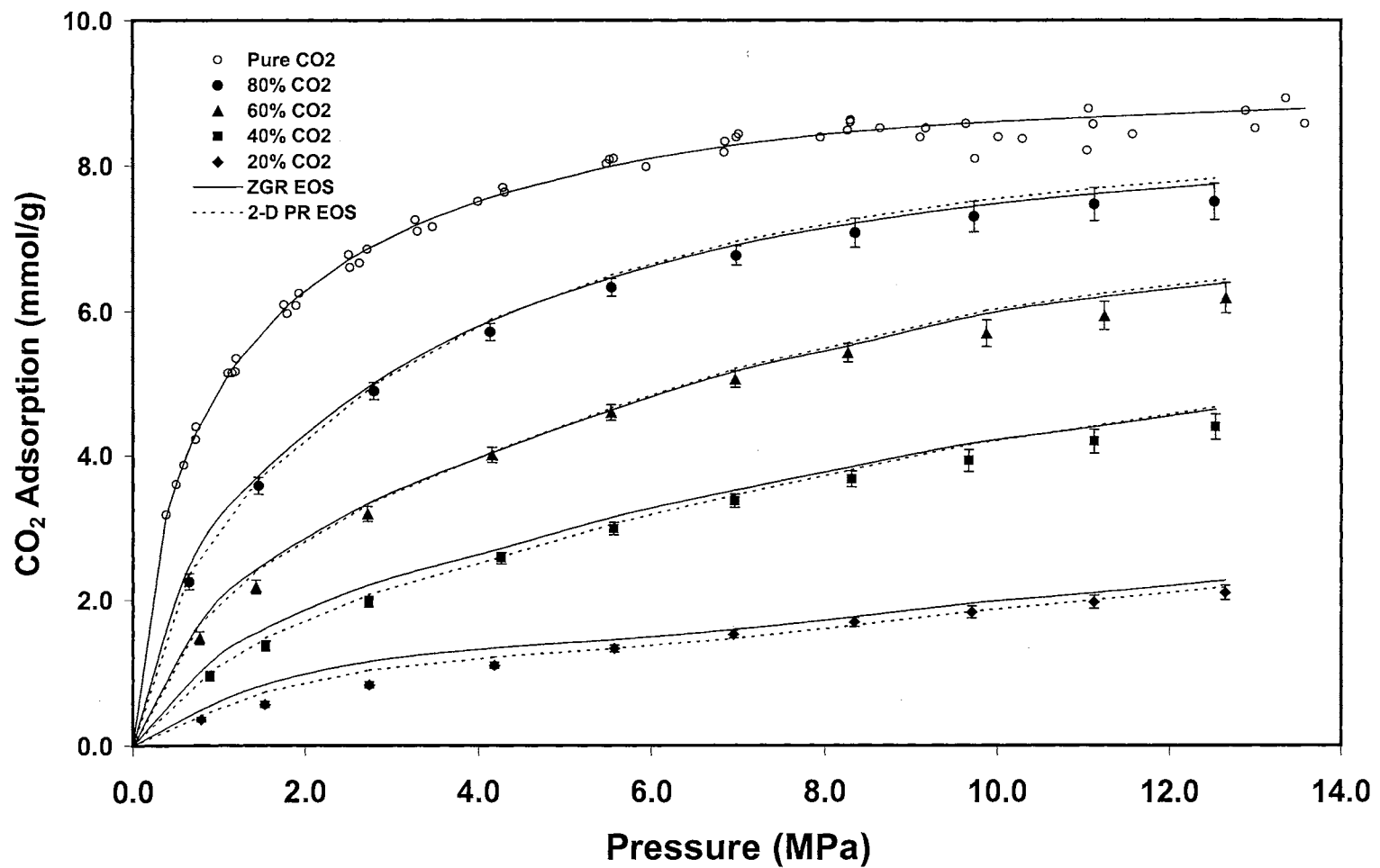
Figure 7-6. Representation of N_2+CO_2 Mixture Adsorption on Activated Carbon at 318.2 K: CO_2 Component Adsorption Using Wong-Sandler Mixing Rules

2. 2-D PR EOS predicts the binary adsorption better than ZGR EOS. Further, for all the cases studied, the 2-D PR EOS with Wong-Sandler mixing rules provides more accurate binary mixture adsorption predictions. However, both EOSs predict the lower-adsorption component with higher AAD than the higher-adsorption component.

3. Use of both pure-gas and binary mixture parameters does not result in any improvement in the prediction of the ternary mixture adsorption, when compared to using only pure-gas parameters.

4. Because of the revised repulsive term in ZGR EOS, mixture calculations may fail, especially when the model parameter, β_i, varies significantly among the mixture components. This may limit the use of ZGR EOS in calculating mixture adsorption.

CHAPTER 8

ALGORITHM FOR MULTICOMPONENT ADSORPTION

8.1 Multiphase Calculation Algorithms

Mixture adsorption calculations are essential in CBM recovery operations and CO_2 sequestration processes. In addition to accurate adsorption models, implementations of these processes require robust computational algorithms. For multiphase calculations, three methods may be used [see, e.g., Sofyan et al. 2003]:

1. Simultaneous solution of mass and equilibrium relations

2. Iteration function method (IFM)

3. Gibbs energy minimization (GEM) method

In our previous studies involving adsorption mixtures, the simultaneous solution method was used to perform such calculations based on experimental gas-phase compositions, y_i [Zhou, 1994]. However, in many mixture adsorption calculations, the bulk phase compositions are not available. Moreover, the use of experimental gas phase compositions leads to some inconsistency in the equilibrium calculations attributed to errors in the experimental gas compositions.

The most commonly used algorithm for a known phase distribution is the equal-chemical potential or equal-fugacity iteration function method, where feed gas compositions, z_i, are used to perform the calculations. In this chapter, an iteration

function method (IFM) for mixture adsorption equilibrium calculations is developed for 2-D EOS, and its robustness is evaluated for CBM-type systems.

8.2 IFM for Mixture Adsorption Calculations

In principle, the Rice-Rachford iteration function, or a similar function, can be used to perform two-phase equilibrium calculations. However, when dealing with adsorption systems, an additional degree of freedom is imposed by the presence of an adsorption matrix. For example, Smith et al. (1975) provided a phase rule for gas adsorption equilibrium to account for the spreading pressure:

$$F = N - \pi + 3 = N - 2 + 3 = N + 1 \tag{8-1}$$

where F is the degrees of freedom, N is the number of components, and π is the number of the phases. The phase number π for a gas adsorption system is two. However, a more generalized point of view regards the adsorbed phase as an interface [Ross et al., 1964], where:

$$F = N - \pi + 2 + i \tag{8-2}$$

and i is the number of interfaces. Thus, for a pure-gas adsorption on one adsorbent, there are two degrees of freedom, which means, two variables, for example, T and P must be fixed independently to establish an equilibrium state. Similarly, for a binary gas adsorption system, the degrees of freedom are three, and so on.

The total and component mass balances for a two-phase, gas-adsorption system are as follows:

$$N = N_{gas} + N_{ads} \tag{8-3}$$

$$Nz_i = N_{gas} y_i + N_{ads} x_i \tag{8-4}$$

152

where N is the total number of moles in the system, N_{ads} and N_{gas} are the number of moles of the adsorbed phase and gas phase, respectively. z_i, y_i, and x_i are the mole fractions of the feed, equilibrium gas phase, and equilibrium adsorbed phase, respectively.

The equilibrium requirements for a closed system at given temperature and pressure may be expressed as [Zhou, 1994]:

$$Z_a \hat{\phi}_i^a \omega x_i = k_i \hat{\phi}_i^g P y_i \tag{8-5}$$

where, Z_a is the compressibility factor for the adsorbed phase, $\hat{\phi}_i^a$ and $\hat{\phi}_i^g$ are the fugacity coefficient for the adsorbed phase and the gas phase, respectively, k_i is Henry's constant, and ω is the total amount adsorbed per mass of adsorbent.

By definition the equilibrium constant (K-value) is:

$$K_i = \frac{y_i}{x_i} = \frac{Z_a \hat{\phi}_i^a \omega}{k_i \hat{\phi}_i^g P} \tag{8-6}$$

Now, we use Equations 8-3, 8-4, and 8-6 to solve for x_i and y_i:

$$x_i = \frac{z_i}{\dfrac{N_{ads}}{N} + \left(1 - \dfrac{N_{ads}}{N}\right)K_i} \quad \text{and} \quad y_i = \frac{K_i z_i}{\dfrac{N_{ads}}{N} + \left(1 - \dfrac{N_{ads}}{N}\right)K_i} \tag{8-7}$$

Similar to vapor-liquid equilibrium, we obtain the equivalent to the VLE Rice-Rachford iteration function [see, e.g., Sofyan et al., 2003]:

$$F = \sum_i x_i - y_i = \sum_i \frac{(1 - K_i)z_i}{\dfrac{N_{ads}}{N} + \left(1 - \dfrac{N_{ads}}{N}\right)K_i} \equiv 0 \tag{8-8}$$

For the adsorbed phase, the number of moles adsorbed, N_{ads}, is calculated as:

$$N_{ads} = \omega M_s \tag{8-9}$$

where ω is the total amount adsorbed per mass of the adsorbent, and M_s is the mass of adsorbent. The number of moles in the gas phase, N_{gas}, is:

$$N_{gas} = \rho_{gas} V_{gas} \tag{8-10}$$

where ρ_{gas} and V_{gas} are the density and total volume of the gas phase, respectively. In adsorption systems, the total volume available for the gas phase is affected by the amount adsorbed [Sudibandriyo et al., 2003]; specifically,

$$V_{gas} = V_{void} - \omega M_s / \rho_{ads} \tag{8-11}$$

where V_{void} is the total volume available for the gas phase when there is no adsorption, and ρ_{ads} is the adsorbed-phase density.

Expressing the adsorbed-phase molar ratio in terms of the amount adsorbed, densities and volumes, we get:

$$\frac{N_{ads}}{N} = \frac{N_{ads}}{N_{ads} + N_{gas}} = \frac{\omega M_s}{\omega M_s + \rho_{gas} V_{gas}} = \frac{\omega M_s}{\omega M_s + \rho_{gas}\left(V_{void} - \omega M_s / \rho_{ads}\right)} \tag{8-12}$$

Now, if we define the void volume per mass of adsorbent as:

$$v_{void} = \frac{V_{void}}{M_s} \tag{8-13}$$

Equation 8-12 can be rewritten as:

$$\frac{N_{ads}}{N} = \frac{\omega}{\omega + \rho_{gas}\left(v_{void} - \omega / \rho_{ads}\right)} \tag{8-14}$$

and, the working iteration function becomes:

$$F\left(\frac{\omega}{\omega + \rho_{gas}\left(v_{void} - \omega / \rho_{ads}\right)}\right) = \sum_i \frac{\left(\omega + \rho_{gas}\left(v_{void} - \omega / \rho_{ads}\right)\right)\left(1 - K_i\right)z_i}{\omega + \left[\rho_{gas}\left(v_{void} - \omega / \rho_{ads}\right)\right]K_i} \equiv 0 \tag{8-15}$$

This means that having the feed composition at a given temperature and pressure, we can solve iteratively for the adsorbed-phase molar ratio, provided we have an adequate adsorption model for calculating the K-values.

The IFM iterative scheme for an adsorption equilibrium calculation is as follows:

1. Set initial estimates for x_i, y_i and the total adsorbed amount ω

2. Calculate the component fugacity coefficients of the adsorbed phase and the vapor phase

3. Use a numerical method to solve for N_{ads}/N from Equation 8-8

4. Calculate x_i, y_i and the total adsorbed amount ω

5. Calculate K_i for each component

6. If $\left| K_i^k - K_i^{k+1} \right| > \varepsilon$, where $\varepsilon = 0.00001$, go back to Step 2; otherwise print results

8.3 Algorithm Robustness Analyses

The Newton-Raphson approach is used to solve for the molar adsorption ratio, N_{ads}/N, in Equation 8-8 using the iteration expression:

$$\left(\frac{N_{ads}}{N} \right)_{i+1} = \left(\frac{N_{ads}}{N} \right)_i - \frac{F}{F'} \tag{8-16}$$

$$F' = -\sum_i \frac{(1-K_i)^2 z_i}{\left[\frac{N_{ads}}{N} + \left(1 - \frac{N_{ads}}{N} \right) K_i \right]^2} \tag{8-17}$$

However, implementation of the IFM iterative scheme outlined above using the Newton-Raphson method resulted in poor convergence characteristics; i.e., frequent convergence failures. Our analysis indicates that the iterative values generated by the algorithm for the total amount adsorbed, ω, are the main cause for calculation failure. In

155

the adsorption IFM scheme, unlike the VLE IFM, an estimate for the total amount

adsorbed is required to initiate the calculations. Unfortunately, an error in the ω estimate

is magnified in each iteration loop resulting in divergence and, thus, calculation failure.

Accordingly, a new robust algorithm was developed as outlined below.

Following extensive analysis of several iterative schemes, we propose the

following new iteration function for multicomponent adsorption equilibrium calculations:

$$F(\omega) = \sum_i \frac{(1 - \dfrac{Z_a \hat{\phi}_i^a \omega}{k_i \hat{\phi}_i^g P}) z_i}{\dfrac{\omega}{\omega + \rho_{gas}\left(v_{void} - \omega/\rho_{ads}\right)} + \left(1 - \dfrac{\omega}{\omega + \rho_{gas}\left(v_{void} - \omega/\rho_{ads}\right)}\right) \dfrac{Z_a \hat{\phi}_i^a \omega}{k_i \hat{\phi}_i^g P}} \equiv 0$$

(8-18)

In this scheme, we solve for ω instead of the N_{ads}/N ratio. Thus, ω is the iteration

variable, which we found to have excellent convergence characteristics.

Figure 8-1 shows a typical variation of the iteration function $F(\omega)$ with the

amount adsorbed ω. As indicated, $F(\omega)$ is a monotonic function. Although the Newton-

Raphson method could be used, we elected instead to use the secant method to avoid

deriving the iteration function derivative, $F'(\omega)$. As such, the iteration step for solving

Equation 8-18 is:

$$\omega_{i+1} = \omega_i - \frac{F(\omega_i)(\omega_i - \omega_{i-1})}{F(\omega_i) - F(\omega_{i-1})}$$

(8-19)

The algorithm for implementing the new IFM iterative scheme for adsorption
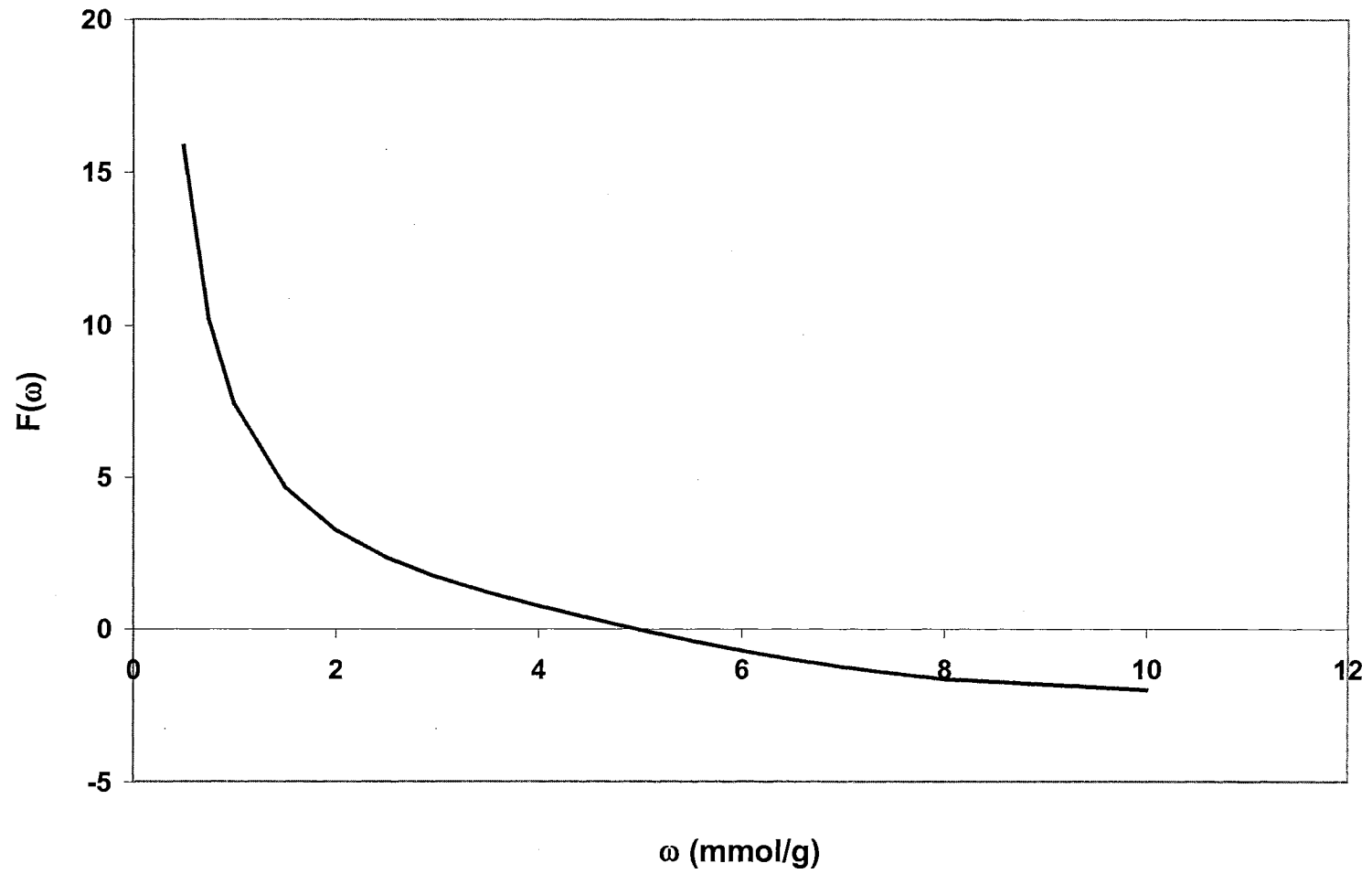
equilibrium calculation is as follows:

156

Figure 8-1. A Sample Plot for the Functional Behavior of Function F(ω)

157

1. Set the initial values of x_i, y_i and the total adsorbed amount ω; initial values of x_i and y_i are set equal to z_i, and that of ω as $\sum_{j=1}^{NC} z_j \omega_j$, where NC is the number of the components, and ω_j is the pure-gas adsorption for component j.

2. Calculate the component fugacity coefficients of the adsorbed phase and the vapor phase

3. Use a numerical method to solve for ω from Equation 8-18

4. Calculate N_{ads}/N

5. Calculate x_i, y_i and the total adsorbed amount ω

6. Calculate K_i for each component

7. If $\left| K_i^k - K_i^{k+1} \right| > \varepsilon$, go back to Step 2; otherwise print results

8.4 Results and Discussion

The 2-D PR EOS with one-fluid mixing rules was used to demonstrate the effectiveness of the new IFM algorithm for adsorption. Several case studies were conducted involving EOS predictions ($C_{ij}=D_{ij}=0$) and model parameter regressions (regressed C_{ij} and D_{ij}). Following our previous study, the following mixture adsorption data were selected to assess the robustness of the new IFM for CBM-type systems:

1. System 51 to 54: OSU data for mixtures of methane, nitrogen, and CO_2 on activated carbon at 318.2 K

2. System 58 to 60: OSU data for mixtures of methane, nitrogen, and CO_2 on wet Fruitland coal at 319.3 K

158

3. System 64to 66: OSU data for mixtures of methane, nitrogen, and CO_2 on Wet Illinois #6 Coal 319.3 K

4. System 70 to 73: OSU data for mixtures of methane, nitrogen, and CO_2 on wet Tiffany coal at 328.2 K

In the IFM scheme, we need the feed gas compositions and v_{void} in the calculation. Only the systems summarized above were used because they included that information. Equation 7-1 was used as the objective function. Equations 7-2 through 7-4 were used to evaluate the results.

Tables 8-1 to 8-8 present the results for each system using the IFM algorithm. For all the systems considered totaling 404 data points, the equilibrium adsorption calculations were successful.

Typically, fewer than ten iterations are required to solve $F(\omega)$ for ω using the secant method; two iterations for adsorption at pressures less than 1.0 MPa and about twenty iterations at pressures greater that 12.0 MPa.

Table 8-9 presents the overall comparison of the two calculation schemes: the simultaneous solution method using the gas phase compositions, and the IFM method using the feed compositions. Overall, the IFM algorithm produces slightly better results than the simultaneous solution method because it avoids errors introduced by imprecise gas-phase compositions. Figure 8-2 shows the comparison of the experimental and the calculated gas-phase composition for the CH_4+CO_2 mixture adsorption on activated carbon at 318.2 K. Excellent agreement is observed for all feed compositions.

Table 8-1. The 2-D PR EOS Predictions of Binary Mixture Adsorption on Activated Carbon at 318.2 K – IFM Calculations

Systems	NPTS	%AAD	RMSE (mmol/g)	WAAD
CH_4-N_2				
Methane	40	3.9	0.137	1.6
Nitrogen	40	2.9	0.052	0.8
Total	40	3.1	0.139	1.3
CH_4-CO_2				
Methane	40	2.5	0.064	0.5
CO_2	40	3.3	0.104	0.8
Total	40	1.0	0.076	0.3
N_2-CO_2				
Nitrogen	40	5.2	0.064	1.0
CO_2	40	2.8	0.104	0.8
Total	40	3.1	0.151	1.0

Table 8-2. The 2-D PR EOS Representations of Binary Mixture Adsorption on Activated Carbon at 318.2 K – IFM Calculations

Systems	NPTS	%AAD	RMSE (mmol/g)	WAAD	C_{12}	D_{12}
CH_4-N_2						
Methane	40	3.8	0.132	1.5	-0.0801	-0.0425
Nitrogen	40	3.6	0.047	0.9		
Total	40	2.6	0.117	1.1		
CH_4-CO_2						
Methane	40	2.6	0.074	0.6	-0.0856	0.0192
CO_2	40	2.3	0.077	0.6		
Total	40	0.6	0.052	0.2		
N_2-CO_2						
Nitrogen	40	4.1	0.043	0.6	-0.1213	0.0243
CO_2	40	2.5	0.106	0.7		
Total	40	2.1	0.106	0.7		

160

Table 8-3. The 2-D PR EOS Predictions of Binary Mixture Adsorption on Wet Fruitland Coal at 319.3 K – IFM Calculations

Systems	NPTS	%AAD	RMSE (mmol/g)	WAAD
CH₄-N₂				
Methane	41	3.2	0.009	0.3
Nitrogen	41	25.9	0.033	1.9
Total	41	7.8	0.040	1.0
CH₄-CO₂				
Methane	40	7.6	0.019	0.7
CO₂	40	5.5	0.042	0.8
Total	40	4.3	0.049	0.8
N₂-CO₂				
Nitrogen	50	30.2	0.038	1.1
CO₂	50	2.3	0.033	0.3
Total	50	4.7	0.051	0.6

Table 8-4. The 2-D PR EOS Representations of Binary Mixture Adsorption on Wet Fruitland Coal at 319.3 K – IFM Calculations

Systems	NPTS	%AAD	RMSE (mmol/g)	WAAD	C_{12}	D_{12}
CH₄-N₂						
Methane	41	3.4	0.013	0.3	0.7344	-0.0202
Nitrogen	41	6.6	0.007	0.4		
Total	41	3.0	0.015	0.4		
CH₄-CO₂						
Methane	40	3.8	0.014	0.4	-0.1154	0.2582
CO₂	40	4.0	0.038	0.6		
Total	40	2.4	0.040	0.4		
N₂-CO₂						
Nitrogen	50	14.4	0.013	0.4	0.0361	-0.0968
CO₂	50	3.0	0.037	0.4		
Total	50	2.0	0.038	0.3		

161

Table 8-5. The 2-D PR EOS Predictions of Binary Mixture Adsorption on Wet Illinois #6 Coal at 319.3 K – IFM Calculations

Systems	NPTS	%AAD	RMSE (mmol/g)	WAAD
CH$_4$-N$_2$				
Methane	40	13.4	0.017	0.4
Nitrogen	40	14.9	0.005	0.3
Total	40	7.1	0.016	0.3
CH$_4$-CO$_2$				
Methane	40	13.0	0.017	0.5
CO$_2$	40	9.5	0.054	0.7
Total	40	6.4	0.053	0.6
N$_2$-CO$_2$				
Nitrogen	40	49.4	0.024	0.7
CO$_2$	40	5.1	0.025	0.4
Total	40	2.7	0.019	0.3

Table 8-6. The 2-D PR EOS Representations of Binary Mixture Adsorption on Wet Illinois #6 Coal at 319.3 K – IFM Calculations

Systems	NPTS	%AAD	RMSE (mmol/g)	WAAD	C$_{12}$	D$_{12}$
CH$_4$-N$_2$						
Methane	40	13.7	0.017	0.4	0.2223	0.1834
Nitrogen	40	15.3	0.005	0.3		
Total	40	7.0	0.014	0.2		
CH$_4$-CO$_2$						
Methane	40	11.7	0.017	0.4	-0.1598	0.0979
CO$_2$	40	9.2	0.053	0.7		
Total	40	4.8	0.043	0.4		
N$_2$-CO$_2$						
Nitrogen	40	50.3	0.033	0.9	-0.5296	0.4556
CO$_2$	40	4.9	0.024	0.4		
Total	40	2.3	0.021	0.3		

Table 8-7. The 2-D PR EOS Predictions of Binary Mixture Adsorption on Wet Tiffany Coal at 327.6 K – IFM Calculations

Systems	NPTS	%AAD	RMSE (mmol/g)	WAAD
CH_4-N_2				
Methane	11	13.2	0.029	1.6
Nitrogen	11	4.8	0.005	0.4
Total	11	11.3	0.033	1.6
CH_4-CO_2				
Methane	11	27.2	0.041	3.6
CO_2	11	9.0	0.047	2.0
Total	11	2.6	0.012	0.8
N_2-CO_2				
Nitrogen	11	54.4	0.019	1.9
CO_2	11	7.6	0.051	1.4
Total	11	5.2	0.034	1.1

Table 8-8. The 2-D PR EOS Representations of Binary Mixture Adsorption on Wet Tiffany Coal at 327.6 K – IFM Calculations

Systems	NPTS	%AAD	RMSE (mmol/g)	WAAD	C_{12}	D_{12}
CH_4-N_2						
Methane	11	11.8	0.025	1.4	0.1205	-0.3286
Nitrogen	11	7.5	0.005	0.4		
Total	11	8.2	0.021	1.1		
CH_4-CO_2						
Methane	11	15.0	0.023	2.7	0.5129	-0.1328
CO_2	11	9.7	0.050	2.2		
Total	11	4.6	0.028	1.1		
N_2-CO_2						
Nitrogen	11	23.5	0.008	0.8	0.2398	-0.4310
CO_2	11	7.4	0.050	1.3		
Total	11	6.1	0.043	1.2		

163

Table 8-9. Comparison of Mixture Adsorption Using Simultaneous Solution Method and IFM

	L. A. C. *			H. A. C. *			Total		
	%AAD	RMSE	WAAD	%AAD	RMSE	WAAD	%AAD	RMSE	WAAD
Predictions									
Sim. Sol.	20.1	0.051	1.0	8.1	0.097	1.1	4.7	0.081	0.7
IFM	18.2	0.039	0.9	5.7	0.070	0.7	4.6	0.077	0.7
Regressions									
Sim. Sol.	12.8	0.041	0.6	7.4	0.090	1.0	3.8	0.079	0.6
IFM	12.8	0.034	0.6	5.5	0.065	0.7	3.2	0.059	0.5

* L. A. C. means lower-adsorption component (404 data points)

* H. A. C. means higher-adsorption component (404 data points)
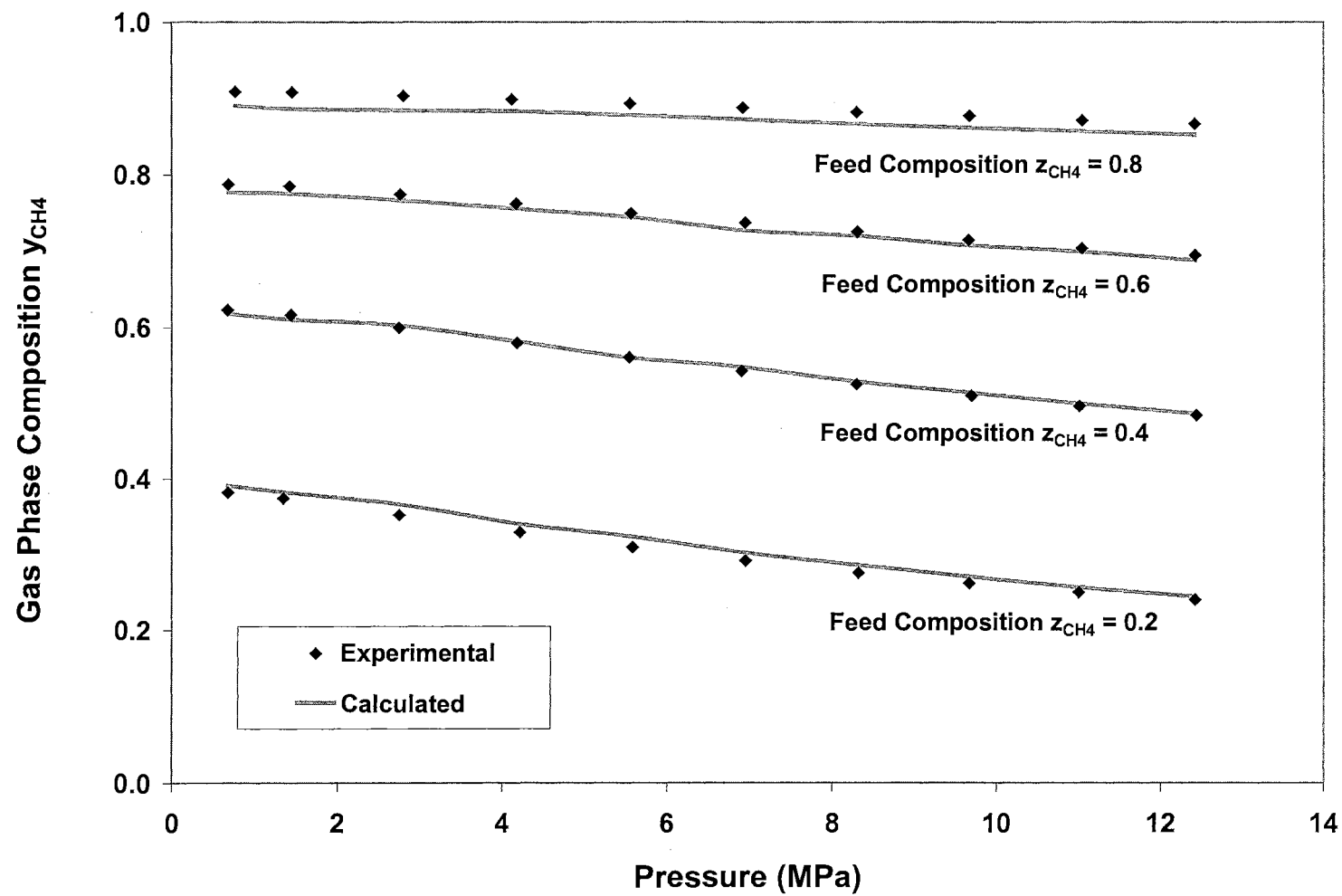
Figure 8-2. Comparison of the Experimental and Calculated Gas-Phase Compositions:
CH_4+CO_2 Adsorption on Activated Carbon at 318.2 K

Figure 8-3 provides an IFM algorithm sample calculation involving the 80%N_2+20%CO_2 mixture adsorption on activated carbon at 318.2 K. The results indicate that the IFM calculations provide smooth predictions (the solid line) in comparison to comparable results from the simultaneous solution method using experimental vapor compositions (the dash line).

In summary, analysis of results involving many CBM adsorption systems indicate that the new IFM algorithm for the 2-D EOS is effective in performing equilibrium mixture adsorption calculations based on feed compositions. Further, use of an equivalent formulation to the Rice-Rachford VLE iteration function, where the molar adsorption ratio is the iteration variable, leads to frequent adsorption calculation failures. Excellent convergence characteristics are obtained using the new IFM.
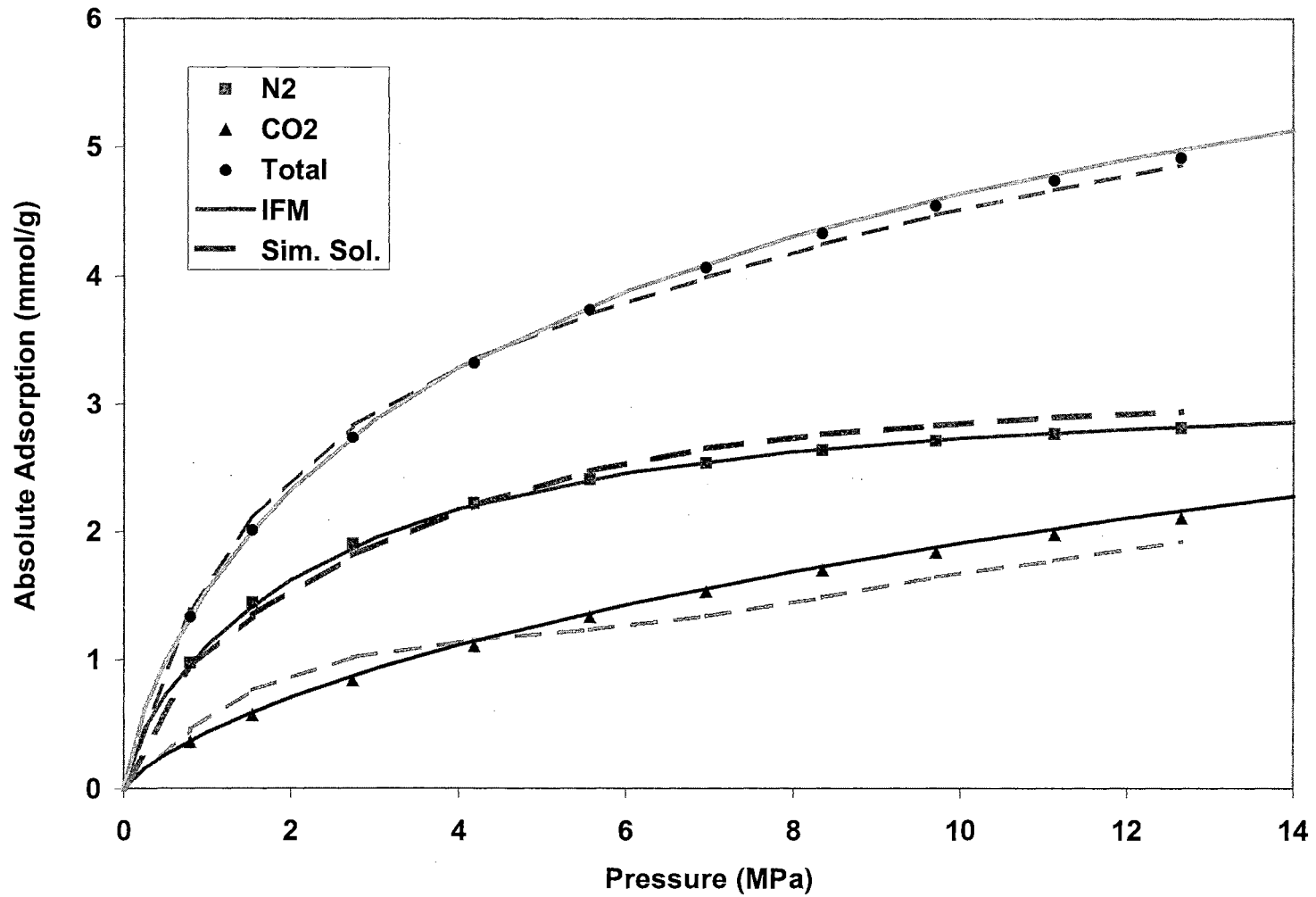
Figure 8-3. Comparison of the IFM and Simultaneous Solution Method:
80%N₂+20%CO₂ Adsorption on Activated Carbon at 318.2 K

CHAPTER 9

CONCLUSIONS AND RECOMMENDATIONS

The main goal of this work was to evaluate and extend the capability of 2-D EOSs to represent and predict the pure-gas and mixture adsorption on carbon matrices. Investigation of generalized temperature relations for the 2-D EOS parameters was undertaken to make the 2-D EOSs more attractive in CBM process calculations. New mixing rules and a new computational algorithm for the mixture adsorption were also developed to enhance its applications. Following are the specific conclusions and recommendations made based on this work.

9.1 Conclusions

The conclusions from this work are:

1. In general, regressing the model parameters for each isotherm, both the ZGR EOS and the 2-D PR EOS can represent pure-gas adsorption precisely (within the expected experimental uncertainties of about 2%). Overall, the two EOSs can represent the experimental data equally well. For a given adsorption isotherm, the ZGR EOS represents the adsorption data better than the 2-D PR EOS at high pressure, while at lower pressures the 2-D PR EOS represents the data more precisely.

2. Temperature relations for the 2-D PR EOS parameters were developed. Overall, the new temperature relations for the 2-D PR EOS enabled us to represent the pure-gas adsorption within the expected experimental uncertainties without the need to regress each isotherm. More importantly, the temperature relations for the 2-D PR EOS parameters are related to the properties of the adsorbent and adsorbate, thus facilitating generalized adsorption predictions.

3. On average, the 2-D PR EOS is capable of predicting pure-gas adsorption on activated carbons within AAD of 9%. However, improved estimates for the surface area and fluid-solid interaction are needed to achieve better accuracy.

4. Currently, the revised attractive term for the 2-D PR EOS works well for all the data considered in this work; however, it does not account for temperature variation. Moreover, the temperature relations for the 2-D PR EOS could not be applied to the ZGR EOS because of the empirical revision of the repulsive term in the ZGR EOS.

5. One-fluid mixing rules can represent the total adsorption precisely, but they do not represent the component adsorption equally well.

6. Wong-Sandler mixing rules provide an effective formulation for extending 2-D EOS models to mixtures. These mixing rules produce slightly better results than those obtained using the one-fluid mixing rules.

7. Because of the revised repulsive term in ZGR EOS, mixture calculations may fail, especially when the model parameter, β_i, varies significantly from component to component. This may limit the use of ZGR EOS in calculating mixture adsorption.

8. An iteration function method (IFM) was developed. Our analysis and the preliminary results indicate that the new IFM algorithm for the 2-D EOS is effective in performing equilibrium mixture adsorption calculations based on feed gas compositions.

9.2 Recommendations

The recommendations for future work are:

1. Investigative and rigorously account for the presence of moisture on adsorption behavior.

2. Further develop the α function in 2-D PR EOS to delineate the temperature dependence of the 2-D EOS.

3. Explore the potential use of NRTL parameters from VLE data for adsorption calculations.

BIBLIOGRAPHY

Arri, L. E., Yee, D., *Modeling Coalbed Methane Production With Binary Gas Sorption*, SPE Paper 24363, presented at the SPE Rocky Mountain Regional Meeting, Casper, Wyoming, May, 18-21, 1992.

Aranovich, G. L., Donohue, M. D., *Adsorption of Supercritical Fluids*, J. Colloid and Interface Sci., 180, 537-541, 1996.

Aranovich, G. L., Donohue, M. D., *Predictions of Multilayer Adsorption Using Lattice Theory*, J. Colloid and Interface Sci., 189, 101-108, 1997.

Aranovich, G. L., Donohue, M. D., *Surface Compression in Adsorption Systems*, Colloid and Surfaces A., 187-188, 95-108, 2001.

Benard, P., Chahine, R., *Modelling of High-Pressure Adsorption Isotherms above the Critical Temperature on Microporous Adsorbents: Application to Methane*, Langmuir, 13(4), 808-813, 1997.

Benard, P., Chahine, R., *Modeling of Adsorption Storage of Hydrogen on Activated Carbons*, International Journal of Hydrogen Energy, 26(8), 849-855, 2001

Berlier, K., Frere, M., *Adsorption of CO_2 on Microporous Materials. 1. On Activated Carbon and Silica Gel*, J. Chem. Eng. Data, 42, 533-537, 1997.

Berlier, K., Olivier, M. G., Jadot, R., *Adsorption of Methane, Ethane, and Ethylene on Zeolite*, J. Chem. Eng. Data, 40, 1206-1208, 1995.

Beutekamp, S., Harting, P., *Experimental Determination and Analysis of High Pressure Adsorption Data of Pure Gases and Gas Mixture*, Adsorption, 8, 255-269, 2002.

Bishnoi, P. R., Robinson, D. B., *Mixing Rules Improve BWR Use*, Hydrocarbon Processing, 11, 152-156, 1972.

Brugge, H. B., Holste, J. C. and Hall, K. R., Gammon, B. E. and Marsh, K. N., *Densities of Carbon Dioxide + Nitrogen from 225 K to 450 K at Pressures up to 70 MPa*, J. Chem. Eng. Data, 42, 903-907, 1997.

Brugge, H. B., Hwang, C. A., Rogers, W. J., Holste, J. C., Hall, K. R., Lemming, W., Esper, G. J., Marsh, K. N., Gammon, B. E., *Experimental Cross Virial Coefficients for Binary Mixtures of Carbon Dioxide with Nitrogen, Methane and Ethane at 300 and 320 K*, Physica A156, 382-416, North-Holland, Amsterdam, 1989.

171

Brunauer, S., Emmet, P. H., Teller, E. J., *Adsorption of Gases in Multimolecular Layers*, Am.Chem.Soc., 60, 309-319, 1938.

Brunauer, S., Deming, L. S., Deming, E., Teller, E. J., *On A Theory of the van der Waals Adsorption of Gases*, Am.Chem.Soc., 62, 1723-1732, 1940.

Chen, J. H., Wong, D. S. H., Tan, C. S., Subramanian, R., Lira, C. T., Orth, M., *Adsorption and Desorption of Carbon Dioxide onto and from Activated Carbon at High Pressures,* I&EC Research, 36, 2808-2815, 1997.

Cranston, R. W., Inkley, F. A., Advances in Catalysis, Vol. 9, Academic Press, New York, 1957.

de Boer, J. H., The Dynamical Character of Adsorption, 2nd Ed., Oxford at The Clarendon Press, London, 1968.

DeGance, A. E., *Multicomponent High-Pressure Adsorption Equilibria on Carbon Substrates: Theory and Data,* Fluid Phase Equilibria, 78, 99-137, 1992.

Do, D. D., Adsorption Analysis: Equilibria and Kinetics, Imperial College Press, London, 1998.

Dreisbach, F., Staudt, R., Keller, J. U., *High Pressure Adsorption Data of Methane, Nitrogen, Carbon Dioxide and Their Binary and Ternary Mixtures on Activated Carbon,* Adsorption, 5, 215-227, 1999.

Duarte-Garza, H., Brugge, H. B., Hwang, C-A., Eubank, P. T., Holste, J. C., Hall, K. R., *Research Report RR-140 Thermodynamic Properties of CO_2+N_2 Mixtures,* Project 842 GRI Contract No. 5087-260-1449, June 1995.

Dubinin, M. M., Chemistry and Physics of Carbon, Vol. 2, Walker, P. L., Eds., Jr. Edward Arnold Ltd., New York, 1966.

Ergun, S., Tiensuu, V. H., *Tetrahedral Structures in Amorphous Carbon*, Acta Crystallogr, 12, 1050-1051, 1959.

Ely, J. F., Magee, J. W., Haynes, W. M., *Research Report RR-110 Thermophysical Properties for Special High CO_2 Content Mixtures,* National Bureau of Standards Boulder, Colorado, May 1987.

Fitzgerald, J. E., Sudibandriyo, M., Pan, Z., Robinson, Jr., R. L., Gasem, K. A. M., *Modeling the Adsorption of Pure Gases on Coals with The SLD Model,* Carbon, 41, 2203-2216, 2003.

Frére, M. G., De Weireld, G. F., *High-Pressure and High-Temperature Excess Adsorption Isotherms of N_2, CH_4, and C_3H_8 on Activated Carbon,* J. Chem. Eng. Data, 47, 823-829, 2002.

Gan, H., Nandi, S. P., Walker, P. L., Jr., *Nature of the Porosity in American Coals*, Fuel, 51, 272-277, 1972.

Gasem, K. A. M., Robinson, Jr., R. L., Fitzgerald, J. E., Pan, Z., Sudibandriyo, M., *Sequestering Carbon Dioxide in Coalbeds*, Final Report, 1999-2003, Prepared for the U.S. Department of Energy, 2003.

Hall, F. E., Jr., *Adsorption of Pure and Multicomponent Gases on Wet Fruitland Coal*, M. S. Thesis, Oklahoma State University, Stillwater, Oklahoma, 1993.

Hall, F., Zhou, C., Gasem, K. A. M., Robinson, Jr., R. L., *Adsorption of Pure Methane, Nitrogen, and Carbon Dioxide and Their Binary Mixtures on Wet Fruitland Coal*, presented at the Eastern Regional Conference & Exhibition, Charleston, November 8-10, 1994.

Haydel, J. J., Kobayashi, R., *Adsorption Equilibria in the Methane-Propane-Silica Gel System at High Pressures*, I&EC Fundamentals, 6, 546-554, 1967.

Hill, T. L., *Theory of Multimolecular Adsorption From a Mixture of Gases*, J. Chem. Phys., 14, 268, 1946.

Hoory, S. E., Prausnitz, J. M., *Monolayer Adsorption of Gas Mixtures on Homogeneous and Heterogeneous Solids,* Chemical Engineering Science, 22, 1025-1033, 1967.

http://energy.cr.usgs.gov/oilgas/cbmethane/

http://www.naturalgas.org/overview/resources.asp

Hwang, C. A., Iglesias-Silva, G. A., Holste, J. C., and Hall, K. R., Gammon, B. E. and Marsh, K. N., *Densities of Carbon Dioxide + Methane Mixtures from 225 K to 350 K at Pressures up to 35 MPa,* J. Chem. Eng. Data, 42, P897-899, 1997.

Humayun, R., Tomasko, D. L., *High-Resolution Adsorption Isotherms of Supercritical Carbon Dioxide on Activated Carbon*, AIChE J., 46, 2065-2075, 2000.

International Thermodynamic Tables of the Fluid State: Carbon Dioxide, International Union of Pure and Applied Chemistry, 1976.

International Thermodynamic Tables of the Fluid State: Methane, International Union of Pure and Applied Chemistry, 1978.

International Thermodynamic Tables of the Fluid State: Nitrogen, International Union of Pure and Applied Chemistry, 1977.

Jaeschke, M., Humphreys, A. E., *The GERG Databank of High Accuracy Compressibility Factor Measurements*, GEGR Technical Monograph 4, 1990.

Joubert, J. I., Grein, C. T., Bienstock, D., *Sorption of Methane in Moist Coal*, Fuel, 52, 181-185, 1973.

Kadlec, O., Choma, J., Jankowska, H., *Analysis of the Pore Structure of Adsorbents and Its Characterization by a Numerical Method*, Chem. Comm., 49(12), 2721-2738, 1984.

Krim, J., Watts, E. T., Third International Conference on Fundamentals of Adsorption, Mersmann, A. B., Scholl, S. E., Eds., Engineering Foundation, New York, 1991.

Krooss, B. M., van Bergen, F., Gensterblum, Y., Siemons, N., Pagnier, H. J. M., David, P., *High-pressure Methane and Carbon Dioxide Adsorption on Dry and Moisture-equilibrated Pennsylvanian Coals,* International Journal of Coal Geology, 51, 69-92, 2002.

Langmuir, I., *The Adsorption of Gases on Plane Surfaces of Glass, Mica, and Platinum*, J. Am. Chem. Soc., 40, 1361, 1918.

Levy, J. H, Day, S. J, Killingley, J. S., *Methane capacities of Bowen Basin coals related to coal properties*, Fuel, 76(9), 813-819, 1997.

Liang, X., *Adsorption of Pure and Multicomponent Gases on Wet Coal*, M. S. Thesis, Oklahoma State University, Stillwater, Oklahoma, 1999.

Lielmezs, J., *Comparison of Benedict-Webb-Rubin and Starling Equations of State for Use in P-V-T Calculations of Binary Mixtures,* Thermochimica Acta, Volume 152, Issue 2, P341-358, October, 1989.

Magee, J. W., Howley, J. A., Ely, J. F., *A Predictive Model for the Thermophysical Properties of Carbon Dioxide Rich Mixtures*, Research report RR-136, March, 1994.

Medek, J., *Possibility of Micropore Analysis of Coal and Coke from the Carbon Dioxide Isotherm*, Fuel, 56, 131-133, 1977.

Meyers, R. A., Coal Structure, Academic Press, New York, 1982.

Myers, A. L., Prausnitz, J. M., *Thermodynamics of Mixed-Gas Adsorption,* AIChE J.,11, 121-129, 1965.

Nelsen, F. M., Eggertsen, F. T., *Determination of Surface Area: Adsorption Measurements by a Continuous Flow Method*, Anal. Chem., 30, 1387, 1958.

Ono, S., Kondo, S., *Molecular Theory of Surface Tension in Liquids*, Encyclopedia of Physics (S. Flugge, Ed.), Vol. X., Springer-Verlag, Gottingen, 1960.

Payne, H. K., Sturdevant, G. A., Leland, T. W., *Improved Two-Dimensional Equation of State to Predict Adsorption of Pure and Mixed Hydrocarbons,* I&EC Fundamentals, 7, 363-374, 1968.

Pieters, W. J. M., Gates, W. E., US Patent 4 489, 593, 1984.

Ray, G. C., Box, E. O., *Adsorption of Gases on Activated Carbon,* I&EC, 42, 1315-1318, 1950.

Reich, R., Ziegler, W. T., Rogers, K. A., *Adsorption of Methane, Ethane, and Ethylene Gases and Their Binary and Ternary Mixtures and Carbon Dioxide on Activated Carbon at 212-301 K and Pressures to 35 Atmosphers,* Ind. Eng.Chem. Process Des. Dev.,19, 336, 1980.

Ritter, J. A., Yang, R. T., *Equilibrium Adsorption of Multicomponent Gas Mixtures at Elevated Pressures,* Ind. Eng. Chem. Res., 26, 1679-1686, 1987.

Ross, S., Olivier, J. P., On Physical Adsorption, Interscience Publishers, New York, 1964.

Salem, M. M. K., Braeuer, P., Szombathely M., Heuchel, M., Harting, P., Quitzsch, K., *Thermodynamics of High-Pressure Adsorption of Argon, Nitrogen, and Methane on Microporous Adsorbents,* Langmuir, 14, 3376-3389, 1998.

Smith, J. M., and Van Ness, H. C., Introduction to Chemical Engineering Thermodynamics, McGraw-Hill, New York, 1975.

Sofyan, Y., Ghajar, A. J., and Gasem, K. A. M., *Multiphase Equilibrium Calculations Using Gibbs Minimization Techniques,* Ind. Eng. Chem. Res., 42, 2786-3801, 2003.

Sudibandriyo, M., Pan, Z., Fitzgerald, J. E., Robinson, Jr., R. L., Gasem, K. A. M., *Adsorption of Methane, Nitrogen, Carbon Dioxide and their Binary Mixtures on Dry Activated Carbon at 318.2 K and Pressures to 13.6 MPa,* Langmuir 19(13), 2003.

Sudibandriyo, M., *A Generalized Ono-Kondo Lattice Model for High-Pressure Adsorption on Carbon Adsorbents,* Ph.D Dissertation, Oklahoma State University, Stillwater, Oklahoma, 2003.

Talu, O., Zwiebel, I., *Multicomponent Adsorption Equilibria of Nonideal Mixtures,* AIChE J , 32, 1263-1276, 1986.

Tester, J. W., Modell, M., Thermodynamics and Its Applications, 3rd Edition, Prentice Hall PTR, 1996.

van der Vaart, R., Huiskes, C., Bosch, H., Reith, T., *Single and Mixed Gas Adsorption Equilibria of Carbon Dioxide/Methane on Activated Carbon,* Adsorption, 6, 311-323, 2000.

Vermesse, J., Vidal, D., Malbrunot, P., *Gas Adsorption on Zeolites at High Pressure,* Langmuir, 12, 4190-4196, 1996.

Wakasugi, Y., Ozawa, S., Ogino, Y., *Physical Adsorption of Gases at High Pressure, V. An Extension of a Generalized Adsorption Equation to System with Polar Adsorbents*, Journal of Colloid and Interface Science, 79, 399-409, 1981.

Wong, D. H., Sandler, S. I., *A Theoretically Correct Mixing Rule for Cubic Equations of State*, AIChE J., 38(5), 671-680, 1992.

Yang, R. T., Adsorbents: Fundamentals and Applications, Wiley-Interscience, Hoboken, N.J., 2003.

Younglove, B. A., *Thermophysical Properties of Fluids. I. Argon, Ethylene, Parahydrogen, Nitrogen, Nitrogen Trifluoride, and Oxygen*, J. Phys. Chem. Ref. Data. Vol. 11, Suppl. 1, 1982.

Zhou, C., Hall, F., Gasem, K. A. M., Robinson, Jr., R. L., *Predicting Gas Adsorption Using Two-Dimensional Equations of State*, I&EC Research, 33, 1280-1289, 1994.

Zhou, C., *Modeling and Prediction of Pure and Multicomponent Gas Adsorption*, Ph.D Dissertation, Oklahoma State University, Stillwater, Oklahoma, 1994.

Zhou, L., Zhou, Y., Li, M., Chen., P., and Wang., Y., *Experimental and Modeling Study of the Adsorption of Supercritical Methane on a High Surface Activated Carbon*, Langmuir, 16, 5955-5959, 2000.

Zhou, L., Zhou, Y., Bai, S., Lu, C., Yang, B., *Determination of the Adsorbed Phase Volume and Its Application in Isotherm Modeling for the Adsorption of Supercritical Nitrogen on Activated Carbon*, Journal of Colloid and Interface Science, 239, 33-38, 2001.

APPENDIX A

Benedict-Webb-Rubin (BWR) Equation of State for Mixture Compressibility Calculation

A.1 Introduction

Adsorption equilibrium models are essential in process simulators used to optimize coalbed methane production and carbon dioxide (CO_2) sequestration processes. To develop reliable adsorption models, accurate pure and mixture adsorption data are required. In turn, proper reduction of experimental adsorption data requires accurate gas-phase compressibility (Z) factors for methane (CH_4), nitrogen (N_2), CO_2 and their mixtures.

A careful evaluation of the current literature led us to conclude that an adequate predictive capability for mixture compressibility factors does not exist. Therefore, we elected to develop such a capability using the Benedict-Webb-Rubin (BWR) equation of state.

Specifically, we have used the available pure-fluid and binary mixture data to refit the parameters in the BWR equation to improve its compressibility factor predictions based on (a) the available experimental volumetric data from the literature, and (b) supplementary measurements we have conducted. Experimental data at temperatures from 300 to 350 K and pressures to 20 MPa were used to evaluate and further develop the BWR EOS. These data reflect coalbed reservoir temperature and pressure conditions.

A.2 Background

Our experimental technique for measuring adsorption isotherms employs a mass balance method, utilizing volumetric accounting principles; therefore, accurate gas-phase compressibility (Z) factors from outside sources are required for methane, nitrogen and CO_2 and their mixtures to properly analyze our experimental adsorption data [Hall,

178

1993]. Our objective has been to minimize the uncertainties in our reported adsorption results that are caused by errors in the input information on compressibility factors.

To illustrate the need for accurate compressibility factors, Figures A-1 and A-2 show the impact of uncertainties in the compressibility factor on the adsorption results for both pure CO_2 and CO_2 component adsorption in a CH_4+CO_2 binary mixture adsorbing on activated carbon at 318.2 K. The figures present, as a function of pressure, the effects of uncertainties in Z on the uncertainty in the amount adsorbed. Figure A-1 presents results for pure CO_2, and Figure A-2 shows similar results for the amount of CO_2 adsorbed from a CH_4+CO_2 mixture at a feed gas composition of 60% CO_2. These figures reveal that significant errors begin to occur in the amount adsorbed when the compressibility factor errors are as low as about 0.5%. The apparent "breaks" in the smoothness of the curves as a function of pressure are the result of the detailed experimental protocol used in the experiments illustrated; e.g., the point at which the injection pump had to be refilled part way through the experiment.

Since we are engaged in adsorption measurements involving pure, binary and ternary gas systems, we require compressibility factors of such gas systems. Following is a brief description of how we met our needs in recent studies.

For pure methane, nitrogen and CO_2, we employ highly accurate equations of state from the literature [Jaeschke et al., 1990; IUPAC, 1978; IUPAC, 1977; IUPAC, 1976]. These EOS models predict the compressibility factors within 0.1% AAD.

For gas mixtures, we have used available pure-fluid and binary mixture data to refit the BWR equation and improve its accuracy significantly; in general, the new BWR
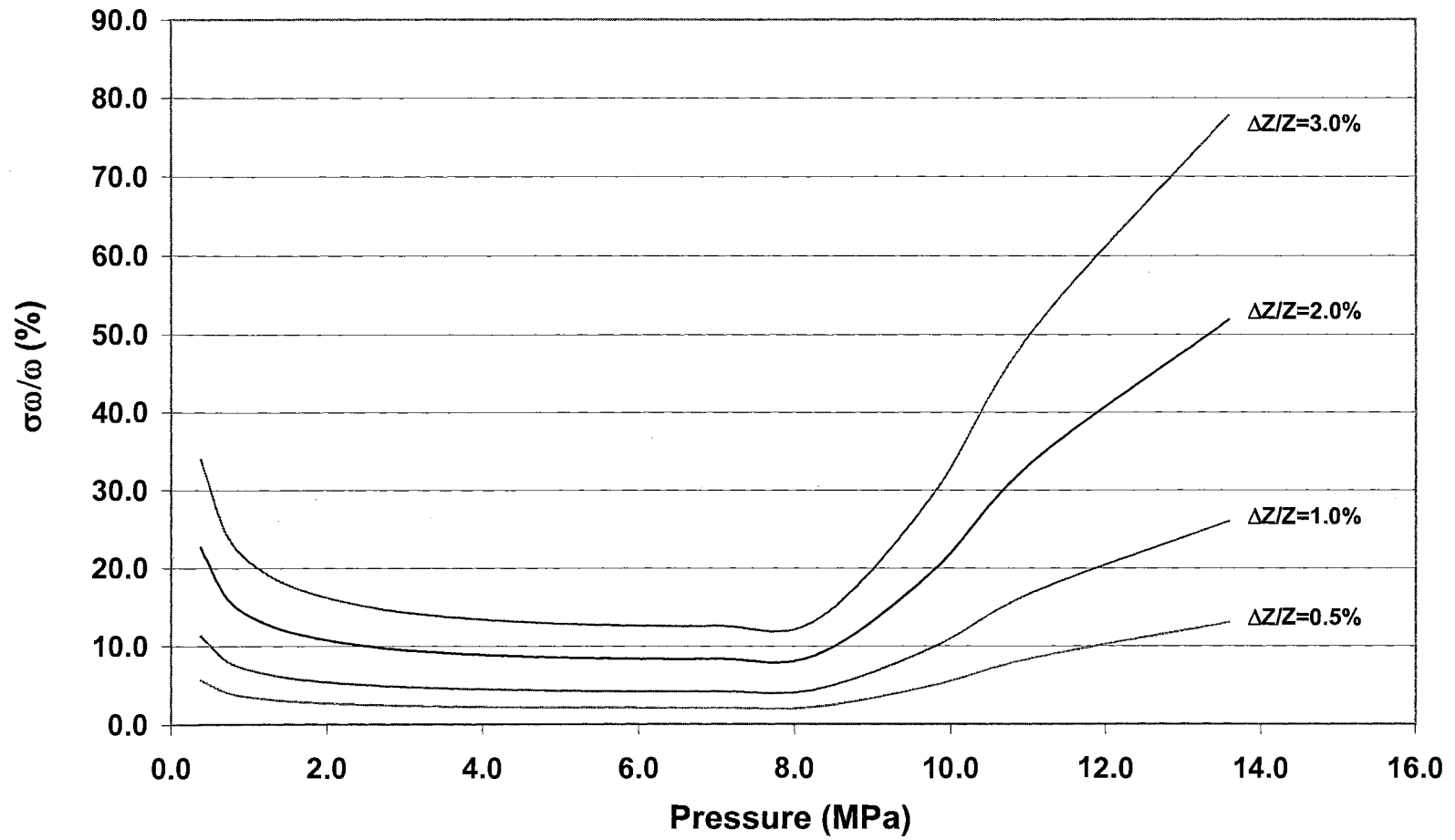
Figure A-1. Effect of Compressibility Factor Uncertainty on the Expected Uncertainties in Adsorption: Pure CO_2 on Activated Carbon at 318.2 K
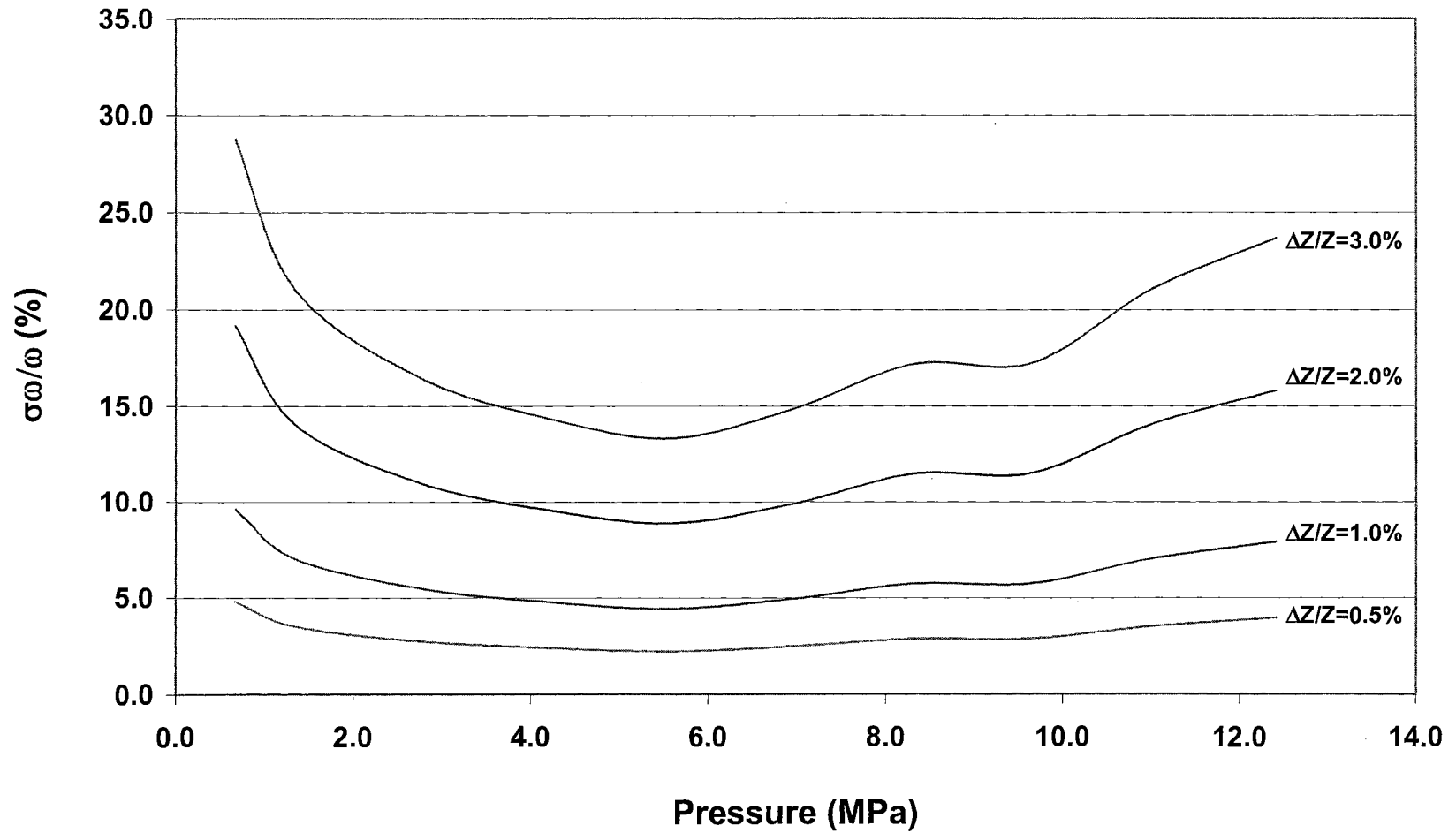
Figure A-2. Effect of Compressibility Factor Uncertainty on the expected Uncertainties in Adsorption: CO_2 Component Adsorption in 40%CH_4+60%CO_2 on Activated Carbon at 318.2 K

181

EOS parameters yield deviations in the compressibility factor within 0.5%. This level of accuracy is deemed satisfactory for our needs.

The present study was motivated by our need to reduce adsorption data for ternary gas systems, where we encountered the fact that ternary Z data were extremely scarce. As a result, we decided to perform a limited number of binary (CH_4+N_2) and ternary ($CH_4+N_2+CO_2$) compressibility factor measurements at 326.7 K and pressures to 13.8 MPa. These newly acquired data were combined with available data from the literature on pure substances and binary systems to improve the BWR EOS compressibility factor predictions.

A.3 Model Development

The BWR EOS is widely used in the hydrocarbon industry for correlating and predicting fluid densities [Bishnoi et al., 1972]. In this study, we employ the eight-parameter BWR EOS to correlate the PVT data of coalbed gases methane, nitrogen, CO_2 and their mixtures [Bishnoi et al., 1972]:

$$Z = 1 + \left(B_0 - \frac{A_0}{RT} - \frac{C_0}{RT^3} \right)\rho + \left(b - \frac{a}{RT} \right)\rho^2 + \frac{a\alpha}{RT}\rho^5 + \frac{c\rho^2}{RT^3}\left(1 + \gamma\rho^2 \right)e^{-\gamma\rho^2} \qquad (A-1)$$

where T is temperature, ρ is density, R is the universal gas constant, and a-c, A_0-C_0, and α and γ are EOS parameters. To apply the BWR to mixtures, mixing and combination rules are required. A variety of combinations rules were evaluated, including those employing composition-dependent interaction parameters [Lielmezs, 1989]; however, for simplicity, we have used the following mixing rules suggested by Bishnoi et al. (1972):

$$B_0 = \sum_{i=1}^{n} \sum_{j=1}^{n} x_i x_j B_{0ij} \qquad \text{where } B_{0ij} = \sqrt{B_{0i} B_{0j}}$$

$$A_0 = \sum_{i=1}^{n} \sum_{j=1}^{n} x_i x_j A_{0ij} \qquad \text{where } A_{0ij} = \sqrt{A_{0i} A_{0j}}\,(1 - k_{ij})$$

$$C_0 = \sum_{i=1}^{n} \sum_{j=1}^{n} x_i x_j C_{0ij} \qquad \text{where } C_{0ij} = \sqrt{C_{0i} C_{0j}}\,(1 - k_{ij})^3$$

$$b = \sum_{i=1}^{n} \sum_{j=1}^{n} \sum_{k=1}^{n} x_i x_j x_k (b_{ij} b_{jk} b_{ik})^{1/3} \qquad \text{where } b_{ij} = \sqrt{b_i b_j}$$

$$a = \sum_{i=1}^{n} \sum_{j=1}^{n} \sum_{k=1}^{n} x_i x_j x_k (a_{ij} a_{jk} a_{ik})^{1/3} \qquad \text{where } a_{ij} = \sqrt{a_i a_j}\,(1 - k_{ij})$$

$$c = \sum_{i=1}^{n} \sum_{j=1}^{n} \sum_{k=1}^{n} x_i x_j x_k (c_{ij} c_{jk} c_{ik})^{1/3} \qquad \text{where } c_{ij} = \sqrt{c_i c_j}\,(1 - k_{ij})^3$$

$$\alpha = \sum_{i=1}^{n} \sum_{j=1}^{n} \sum_{k=1}^{n} x_i x_j x_k (\alpha_{ij} \alpha_{jk} \alpha_{ik})^{1/3} \qquad \text{where } \alpha_{ij} = \sqrt{\alpha_i \alpha_j}$$

$$\gamma = \sum_{i=1}^{n} \sum_{j=1}^{n} x_i x_j \gamma_{ij} \qquad \text{where } \gamma_{ij} = \sqrt{\gamma_i \gamma_j} \qquad (A\text{-}2)$$

Here, n is the number of components, x_i is the mole fraction of component i in the gas phase, and k_{ij} is the binary interaction parameter. Following customary notation, for a given parameter β, $\beta_{ii} = \beta_i$, and the pure-fluid interaction parameters are equal to zero (or $k_{ii} = k_{jj} = 0$).

A.4 Database Used and Data Reduction

Literature Data: Table A-1 presents the literature data used in this work. Pure-gas and mixture data ranging in temperature from 279 to 350 K and pressures to 20.4 MPa are included.

183

Table A-1. Experimental Data Used

System No.	System	Temperature Range, (K)	Pressure Range, (MPa)	Composition Range, 1st Component	NPTS	Reference
1	CH_4	300.0 - 350.0	0.03 - 15.01	1.0000	27	[IUPAC, 1978]
2	N_2	300.0 - 350.0	0.01 - 20.01	1.0000	68	[Younglove, 1982]
3	CO_2	300.0 - 350.0	0.01 - 15.01	1.0000	55	[IUPAC, 1976]
4	$CH_4 + N_2$	327.6	3.78 - 13.44	0.1912 - 0.8237	12	[This Work]
5		308.4 - 330.0	0.39 - 12.00	0.1354 - 0.8976	391	[Jaeschke, 1990]
6	$CH_4 + CO_2$	315.0 - 330.0	2.45 - 19.31	0.0205 - 0.1011	57	[Magee, 1994]
7		300.0 - 350.0	2.11 - 13.87	0.0989 - 0.9017	38	[Hwang, 1997]
8		300.0 - 330.0	0.08 - 12.00	0.5239 - 0.8052	200	[Jaeschke, 1990]
9		300.0 - 310.0	2.25 - 15.65	0.0205 - 0.1011	34	[Magee, 1994]
10		320.0	0.19 - 9.47	0.0999 - 0.9001	80	[Brugge, 1989]
11	$N_2 + CO_2$	300.0 - 350.0	1.11 - 17.66	0.0908 - 0.8944	130	[Brugge, 1997]
12		273.1 - 330.0	0.09 - 11.91	0.5530 - 0.8990	168	[Jaeschke, 1990]
13		320.0	0.84 - 16.24	0.0908 - 0.8944	71	[Duarte-Garza, 1995]
14		305.0 - 330.0	2.26 - 15.05	0.0180 - 0.8237	48	[Ely, 1987]
15	Ternary	327.6	6.27 - 13.89	0.1510 - 0.4520	14	[This Work]
16		279.4 - 308.4	3.73 - 6.27	0.2482, 0.2497*	33	[Jaeschke, 1990]
17		300.0 - 340.0	3.99 - 20.41	0.9595, 0.0201*	16	[Magee, 1994]

* Single measurement compositions: y_{CO2}, y_{N2}

New Measurements: Our experimental Z factor measurements were done in the same apparatus used for adsorption studies (but with no adsorbent in the equilibrium cell). The technique employs a mass balance method, utilizing volumetric accounting principles. The experimental apparatus, shown schematically in Figure A-1, has been used successfully in our previous adsorption measurements [Hall, 1994]. Brief descriptions of the experimental apparatus and procedures follow.

The entire apparatus (both Pump and Cell sections) is maintained in a constant temperature air bath. A highly accurate variable-volume Ruska pump is used for the injections of the pure gases from the Ruska pump into the equilibrium cell (EC, Figure 4-1); the injections are made at constant pressure and temperature. A magnetic pump circulates the gas to ensure proper mixing. The temperature and pressure are recorded at equilibrium.

The equilibrium cell is placed under vacuum prior to gas injection. The volume of the equilibrium cell and associated tubing, V_{cell}, is then determined by injecting a known quantity of helium from a calibrated injection pump, as follows:

$$V_{cell} = n_{H_e} \left(Z_{H_e} RT / P \right)_{cell} \tag{A-3}$$

$$n_{H_e} = (PV/Z_{H_e} RT)_{pump} \tag{A-4}$$

In these equations, n_{He} is the number of moles of helium injected into the cell, V is the volume of gas injected from the pump, Z_{He}, is the compressibility factor of helium, R is the universal gas constant, T is the temperature, P is the pressure, and the subscripts "cell" and "pump" refer to conditions in the cell and pump sections of the apparatus, respectively. In these calibration measurements, values of Z_{He} were taken Equation 4-24.

Once V_{cell} was determined from multiple replications of the experimental technique, the targeted gas(es) was injected and allowed to reach equilibrium. For the mixtures, pure gases were injected in sequence, with the pump cleaned and evacuated prior to introduction of each gas. The total amount of each gas injected was thus known, and the gas composition in the equilibrium cell could be calculated by mass balance, based on the amount of each gas injected. For example, in the CH_4+N_2 system, CH_4 might be injected first to reach some desired initial pressure in EC, and then sequential injections of N_2 could be made, with equilibrium established after each injection. Thus, the pressure would increase after each N_2 injection, as would the total amount of gas, n_{total}, and the mole fraction of N_2 in the EC mixture. The compressibility factor for the mixture in the EC was calculated after each injection step as:

$$Z = \frac{PV_{cell}}{n_{total}RT} \tag{A-5}$$

The estimated uncertainties in each of the experimentally measured quantities are as follows: temperature 0.1 K, pressure 0.1 bar, injected gas volumes 0.02 cc, gas-phase composition 0.001 in mole fraction. The expected uncertainties in the compressibility factors are estimated using error propagation in all the measured variables and confirmed by duplicate runs.

The newly acquired PVT measurements for the selected mixtures and the associated expected experimental uncertainties appear in Table A-2. (Note that the experimental technique used leads to changing gas composition (mole fraction) as the pressure changes.) These data, combined with the literature data, were used to regress the BWR parameters and conduct our model evaluations.

Table A-2. Experimental Compressibility Factors for Mixtures at 327.6 K

Pressure (Psia)	y_{CH_4}	y_{CO_2}	y_{N_2}	Z_{exp}	Experimental Uncertainty in Z (%)
CH$_4$+N$_2$ System					
3.776	0.6662	0.0000	0.3338	0.9764	0.6
5.569	0.4548	0.0000	0.5452	0.9831	0.5
8.492	0.3013	0.0000	0.6987	0.9932	0.5
11.284	0.2296	0.0000	0.7704	1.0056	0.4
13.713	0.1912	0.0000	0.8088	1.0176	0.4
3.982	0.2964	0.0000	0.7036	0.9942	0.6
6.133	0.6422	0.0000	0.3578	0.9731	0.5
10.721	0.7530	0.0000	0.2470	0.9400	0.4
13.438	0.8064	0.0000	0.1936	0.9234	0.4
5.085	0.8237	0.0000	0.1763	0.9571	0.5
6.425	0.6555	0.0000	0.3445	0.9623	0.5
9.020	0.4727	0.0000	0.5273	0.9743	0.5
CH$_4$+CO$_2$+N$_2$ System					
6.487	0.4800	0.5200	0.0000	0.86446	0.5
6.929	0.0000	0.7897	0.2103	0.81313	0.5
6.884	0.0000	0.5164	0.4836	0.90761	0.5
6.479	0.2428	0.7572	0.0000	0.80687	0.5
6.482	0.0000	0.5840	0.4160	0.89179	0.5
8.236	0.2322	0.7678	0.0000	0.74606	0.5
6.275	0.4092	0.4883	0.1024	0.88580	0.5
7.855	0.4010	0.4345	0.1645	0.87463	0.5
11.666	0.4053	0.4696	0.1251	0.81424	0.4
9.006	0.4520	0.4582	0.0898	0.84397	0.5
8.283	0.1755	0.4258	0.3987	0.90046	0.5
10.282	0.1610	0.5020	0.3371	0.84894	0.4
8.416	0.2371	0.4455	0.3174	0.88338	0.5
13.894	0.1510	0.4994	0.3496	0.81858	0.4

Data Reduction: The percentage root-mean-square error (%RMSE) was used as an objective function to correlate the data with the BWR EOS. The function minimizes the sum of the squared-percentage deviations in compressibility factors:

$$\%RMSE = 100\sqrt{\frac{\sum_{i=1}^{NPTS}\left(\frac{Z_{exp} - Z_{calc}}{Z_{exp}}\right)_i^2}{NPTS}} \qquad (A-6)$$

Here, NPTS is the number of data points, Z_{calc} and Z_{exp} are the calculated and the experimental compressibility factor for datum point "i". The average absolute deviation (%AAD) and the root-mean-square error (RMSE) are also presented to further quantify our regressed parameter evaluations:

$$\%AAD = \frac{100}{NPTS}\sum_{i=1}^{NPTS}\left|\frac{Zcal - Zexp}{Zexp}\right|_i \qquad (A-7)$$

$$RMSE = \sqrt{\frac{\sum_{i=1}^{NPTS}(Z_{exp} - Z_{calc})_i^2}{NPTS}} \qquad (A-8)$$

A.5 Case Studies

Four different parameter-optimization scenarios were evaluated to ensure the best BWR quality fit for the data. Specifically, we conducted the following case studies:

Case 1: This is the base case; the original BWR model parameters were used, as reported by Bishnoi and Robinson (1992). Both their pure component parameters and binary interaction parameters were employed.

Case 2: Sequential parameter regressions were conducted. First the pure-component BWR parameters were regressed from pure PVT data for each of the Systems 1,

2 and 3; then the binary interaction parameters were regressed using both binary and ternary data simultaneously (Systems 4 to17).

Case 3: Simultaneous parameter regressions were conducted. Both the pure-component BWR parameters and the binary interaction parameters were regressed simultaneously using all the data (Systems 1 to 17).

Case 4: Regressions were done for a restricted range of conditions. Simultaneous parameter regressions were conducted covering only the temperature range of primary interest (307 to 338 K). Both pure-component BWR parameters and binary interaction parameters were regressed from all data points at temperatures from 307 K to 338 K and pressures up to 13.7 MPa.

A.6 Results and Discussion

The BWR EOS parameters for the various case studies are listed in Table A-3. An overall summary of results generated by these parameters is presented in Table A-4. These results indicated that the overall %AAD range from 0.1 to 0.4 for the cases considered and the maximum percentage deviations range from –5.9% to 14.6% (Case 2). As expected, Case 4, where we conducted simultaneous regression of pure, binary, and ternary data covering our experimental temperature and pressure range, produces the best overall fit and the least maximum deviation (0.07 %AAD and -1.5% maximum deviation).

Tables A-5 to A-8 present detailed results for Cases 1-4. The three binary systems show comparable quality of fit for the best cases (Cases 3 and 4). The largest errors tend to occur at high CO_2 compositions, particularly at conditions near the CO_2

Table A-3. BWR EOS Parameters for Pure Gases

Component	$B_0 \times 10^2$	A_0	$C_0 \times 10^{-5}$	$b \times 10^3$	a	$\alpha \times 10^5$	$c \times 10^{-4}$	$\gamma \times 10^3$	$k_{ij} \times 10^2$ *
Case 1									
CH_4	4.3203	1.8712	0.2350	3.9787	0.0692	9.6836	0.3018	5.7118	3.0000
CO_2	3.2015	1.8367	1.7603	6.2536	0.2420	4.8784	1.9008	4.2808	3.0000
N_2	4.0743	1.0536	0.0806	2.3277	0.0251	12.7200	0.0728	5.3000	3.0000
Case 2									
CH_4	4.3658	1.7825	0.3034	3.4320	0.0728	39.7800	0.4220	14.4131	3.1025
CO_2	3.1735	1.9668	1.6296	2.8034	0.0844	10.4177	1.2458	5.0744	8.4725
N_2	4.0681	0.9599	0.1386	2.0797	0.0279	29.0908	0.1107	0.0000	-2.2938
Case 3									
CH_4	4.4122	1.8538	0.2407	4.7569	0.1128	11.0522	0.4852	6.3824	2.4740
CO_2	3.2649	1.8396	1.7706	6.2334	0.2441	5.3636	1.9339	4.5487	2.8084
N_2	4.2007	1.0946	0.0466	2.6731	0.0374	7.8119	0.0868	4.4634	-5.5230
Case 4									
CH_4	4.8871	2.0094	0.2042	4.0428	0.0943	22.2778	0.4791	10.4556	2.0940
CO_2	3.2518	1.8450	1.7621	6.2767	0.2450	5.3354	1.9330	4.5528	1.2785
N_2	4.3979	1.1378	0.0414	2.0963	0.0244	20.4833	0.0668	9.0570	-6.7309

*k_{13}, k_{12}, k_{23}

T: K
P: atm
ρ: mol/liter

Table A-4. Overall Quality of BWR Compressibility Factor Predictions

| Case | Errors in Predicted Z Factor | | | |
	RMSE (X1000)	%RMS	%AAD	Range of % Deviations
1	5.0	0.84	0.38	-3.3 to 7.5
2	5.1	1.10	0.41	-5.8 to 14.6
3	1.3	0.18	0.10	-1.4 to 1.4
4	1.0	0.13	0.07	-1.5 to 0.8

Table A-5. Quality of BWR Compressibility Factor Predictions: Case 1

System No.	System	Errors in Predicted Z Factor			
		RMS (X1000)	%RMS	%AAD	Range of % Deviations
1	CH_4	1.6	0.18	0.17	-0.3 to 0.0
2	N_2	1.6	0.16	0.14	-0.3 to 0.0
3	CO_2	3.2	0.70	0.35	-3.1 to 0.5
4	$CH_4 + N_2$	4.0	0.41	0.33	-1.0 to 0.0
5		1.8	0.19	0.18	-0.5 to 0.4
6	$CH_4 + CO_2$	2.7	0.53	0.41	-1.9 to 0.9
7		2.4	0.34	0.27	-1.2 to 0.4
8		0.6	0.08	0.05	-0.3 to 0.1
9		3.2	0.83	0.54	-3.3 to 1.0
10		0.8	0.09	0.06	-0.3 to 0.1
11	$N_2 + CO_2$	12.4	2.25	1.48	-0.6 to 7.5
12		5.4	0.62	0.39	0.0 to 2.8
13		9.3	1.44	0.93	-0.5 to 4.1
14		3.2	0.94	0.69	-1.3 to 2.6
15	Ternary	5.3	0.62	0.53	-0.9 to 1.4
16		1.0	0.11	0.10	0.1 to 0.1
17		2.9	0.77	0.57	-0.8 to 1.9
	Overall	5.0	0.84	0.38	-3.3 to 7.5

Table A-6. Quality of BWR Compressibility Factor Predictions: Case 2

System No.	System	Errors in Predicted Z Factor			
		RMS (X1000)	%RMS	%AAD	Range of % Deviations
1	CH_4	0.3	0.03	0.02	-0.1 to 0.0
2	N_2	0.2	0.02	0.01	0.0 to 0.0
3	CO_2	1.1	0.18	0.12	-0.5 to 0.7
4	$CH_4 + N_2$	2.6	0.27	0.21	-0.7 to 0.2
5		0.5	0.05	0.03	-0.3 to 0.6
6	$CH_4 + CO_2$	3.2	0.62	0.51	-1.8 to 1.5
7		4.9	0.70	0.52	-1.4 to 1.9
8		4.3	0.54	0.34	0.0 to 2.2
9		7.2	2.03	1.38	-5.9 to 3.3
10		2.7	0.33	0.20	0.0 to 1.2
11	$N_2 + CO_2$	11.8	2.75	1.40	-2.5 to 14.6
12		4.5	0.53	0.33	-2.8 to 0.0
13		7.3	1.35	0.73	-1.6 to 7.3
14		7.3	2.25	1.48	-1.1 to 5.9
15	Ternary	6.0	0.70	0.54	-1.5 to 0.1
16		1.9	0.21	0.20	0.1 to 0.3
17		6.4	1.96	1.38	-0.4 to 4.3
	Overall	5.1	1.10	0.41	-5.9 to 14.6

193

Table A-7. Quality of BWR Compressibility Factor Predictions: Case 3

System No.	System	Errors in Predicted Z Factor			
		RMS (X1000)	%RMS	%AAD	Range of % Deviations
1	CH_4	0.7	0.08	0.07	-0.1 to 0.2
2	N_2	0.5	0.05	0.04	-0.1 to 0.1
3	CO_2	2.0	0.30	0.21	-0.6 to 0.9
4	$CH_4 + N_2$	2.7	0.28	0.21	-0.8 to 0.2
5		0.5	0.06	0.03	-0.3 to 0.6
6	$CH_4 + CO_2$	2.0	0.28	0.22	-0.7 to 0.6
7		1.6	0.25	0.15	-1.0 to 0.5
8		0.5	0.06	0.05	-0.1 to 0.2
9		2.0	0.47	0.35	-1.2 to 1.4
10		0.6	0.08	0.05	-0.1 to 0.2
11	$N_2 + CO_2$	2.1	0.25	0.18	-0.7 to 0.7
12		0.7	0.07	0.05	-0.1 to 0.2
13		1.2	0.14	0.10	-0.5 to 0.2
14		1.3	0.30	0.24	-0.7 to 0.5
15	Ternary	5.3	0.63	0.56	-1.4 to -0.2
16		0.7	0.08	0.08	0.1 to 0.1
17		1.5	0.32	0.23	-0.8 to 0.4
	Overall	1.3	0.18	0.10	-1.4 to 1.4

Table A-8. Quality of BWR Compressibility Factor Predictions: Case 4*

System No.	System	Errors in Predicted Z Factor			
		RMS (X1000)	%RMS	%AAD	Range of % Deviations
1	CH$_4$	1.1	0.12	0.10	-0.1 to 0.3
2	N$_2$	0.7	0.07	0.04	-0.3 to 0.1
3	CO$_2$	1.9	0.29	0.21	-0.4 to 0.8
4	CH$_4$ + N$_2$	2.7	0.27	0.22	-0.7 to 0.2
5		0.5	0.05	0.02	-0.3 to 0.6
6	CH$_4$ + CO$_2$	1.8	0.26	0.20	-0.6 to 0.6
7		1.7	0.23	0.19	-0.7 to 0.4
8		0.4	0.05	0.03	-0.2 to 0.2
9		2.6	0.68	0.49	-1.7 to 1.9
10		0.4	0.05	0.03	-0.2 to 0.2
11	N$_2$ + CO$_2$	2.6	0.41	0.25	-2.3 to 0.8
12		0.4	0.04	0.03	-0.1 to 0.2
13		1.2	0.13	0.09	-0.6 to 0.2
14		1.1	0.25	0.19	-0.6 to 0.7
15	Ternary	6.0	0.71	0.65	-1.5 to -0.2
16		0.1	0.02	0.01	0.0 to 0.0
17		1.5	0.35	0.27	-0.8 to 0.4
	Overall	1.4	0.22	0.10	-2.3 to 1.9

*Results for predictions for complete T, P ranges of data, based on parameters from fits to reduced ranges of Case 4

195

critical point. The ternary data is also well represented, with data from the present work showing the highest deviations (about 0.6 %AAD). This is not unexpected, since those data covered the widest composition range and had higher estimated experimental uncertainties than the other two sources of ternary data.

Figures A-3, to A-6 show deviation plots for the Z factors for the various mixtures for each of the case studies. A gradual improvement in the quality of fit is observed proceeding from Case 1 to Case 4. The figures indicate that the N_2+CO_2 binary data tend to exhibit the largest deviations, although this is less pronounced in the best cases (cases 3 and 4).

Figures A-7 to A-10 show the deviation plots for the pure components for the various case studies. These plots are useful in comparing the quality of the fit for the pure components, and especially to reveal potential loss of accuracy when conducting simultaneous regressions (Cases 3 and 4). Our objective was to gain model flexibility through simultaneous treatment of all data, but not at any significant expense to the pure-component predictions.

The pure-component deviation plots indicate that CO_2 (System 3) consistently exhibits the largest deviations in all scenarios. For pure gases, the BWR EOS can predict compressibility factors for CH_4 and N_2 within 0.3% for all four cases. However, for CO_2, the absolute deviations are as much as 3% for Case 1 and within 0.8% for Cases 2 to 4. The CO_2 Z factors are most difficult to represent as a result of the near-critical behavior of CO_2 in the range of temperatures and pressures of interest in this work.

Our recent adsorption isotherm measurements for the CH_4+CO_2 binary on dry activated carbon are used to demonstrate how compressibility factors in the bulk phase
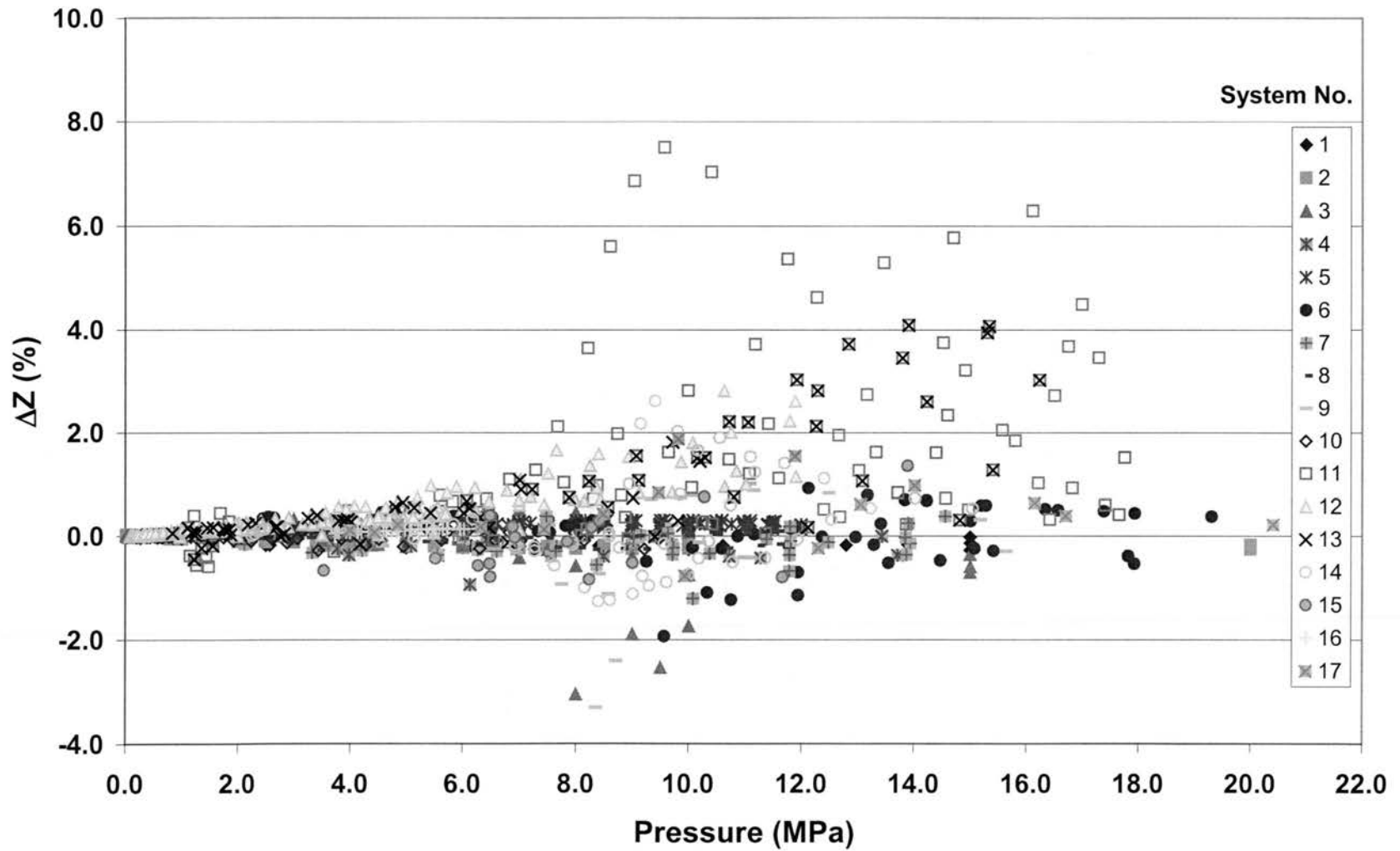
Figure A-3. Overall Summary Results for Case 1
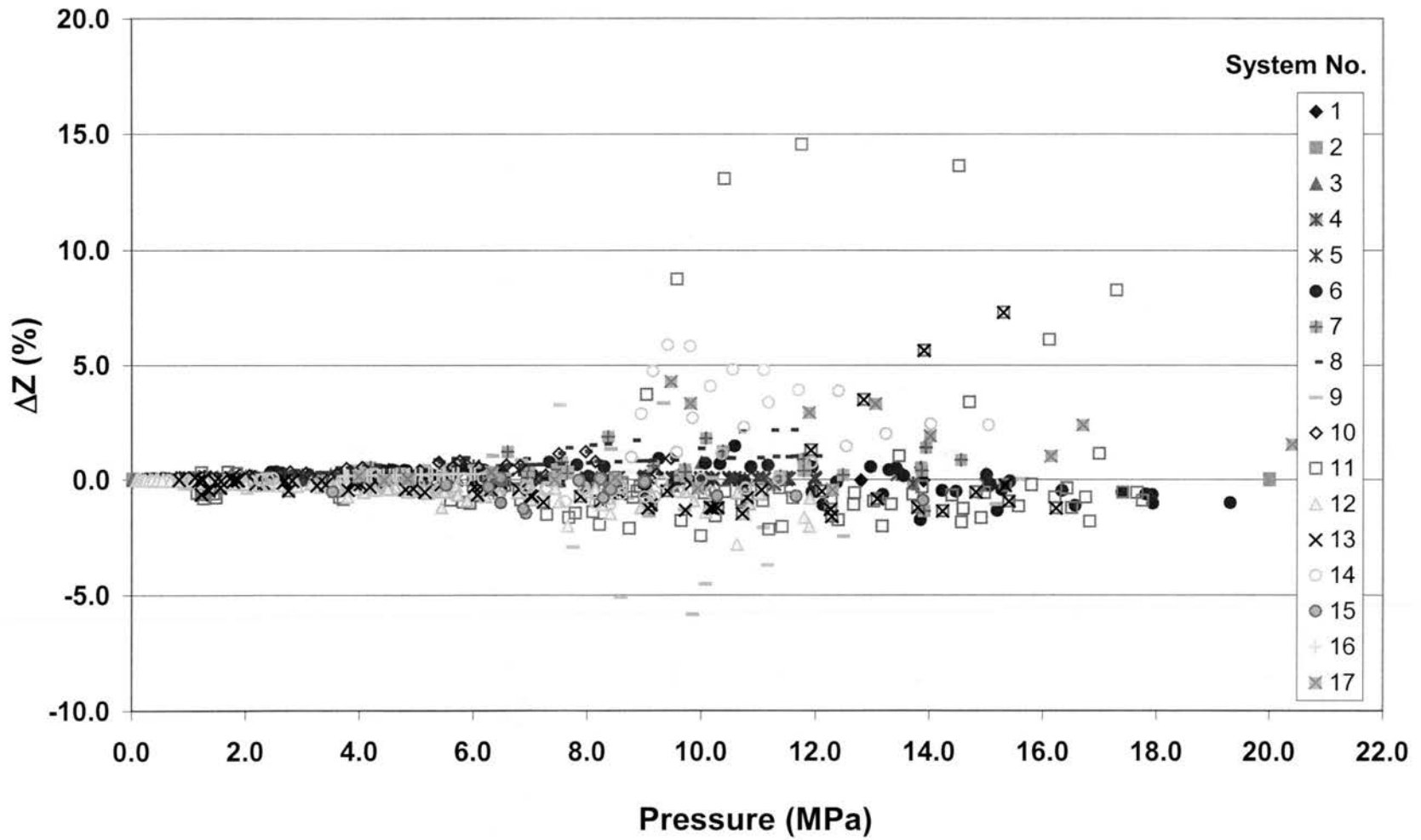
Figure A-4. Overall Summary Results for Case 2
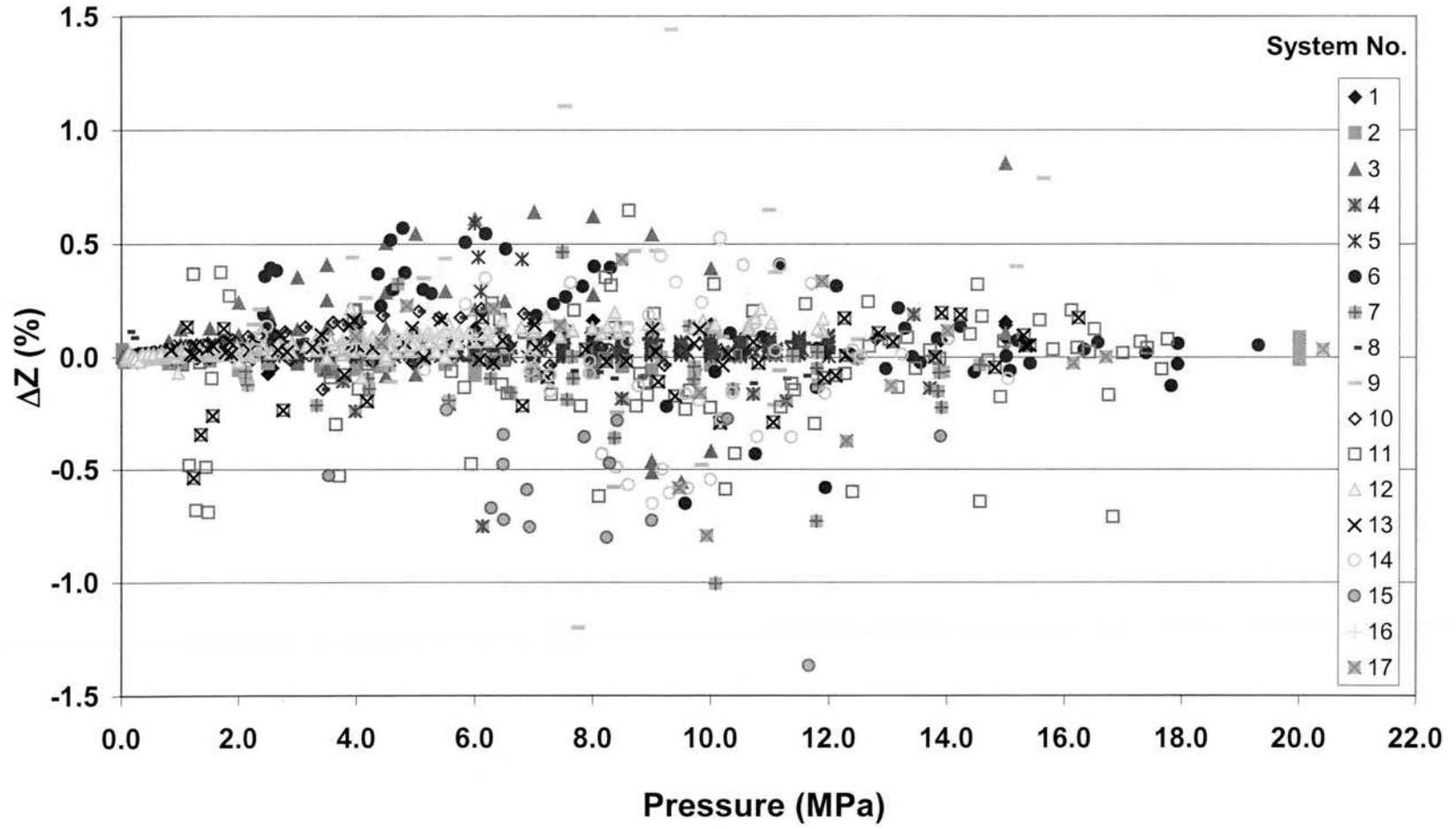
Figure A-5. Overall Summary Results for Case 3
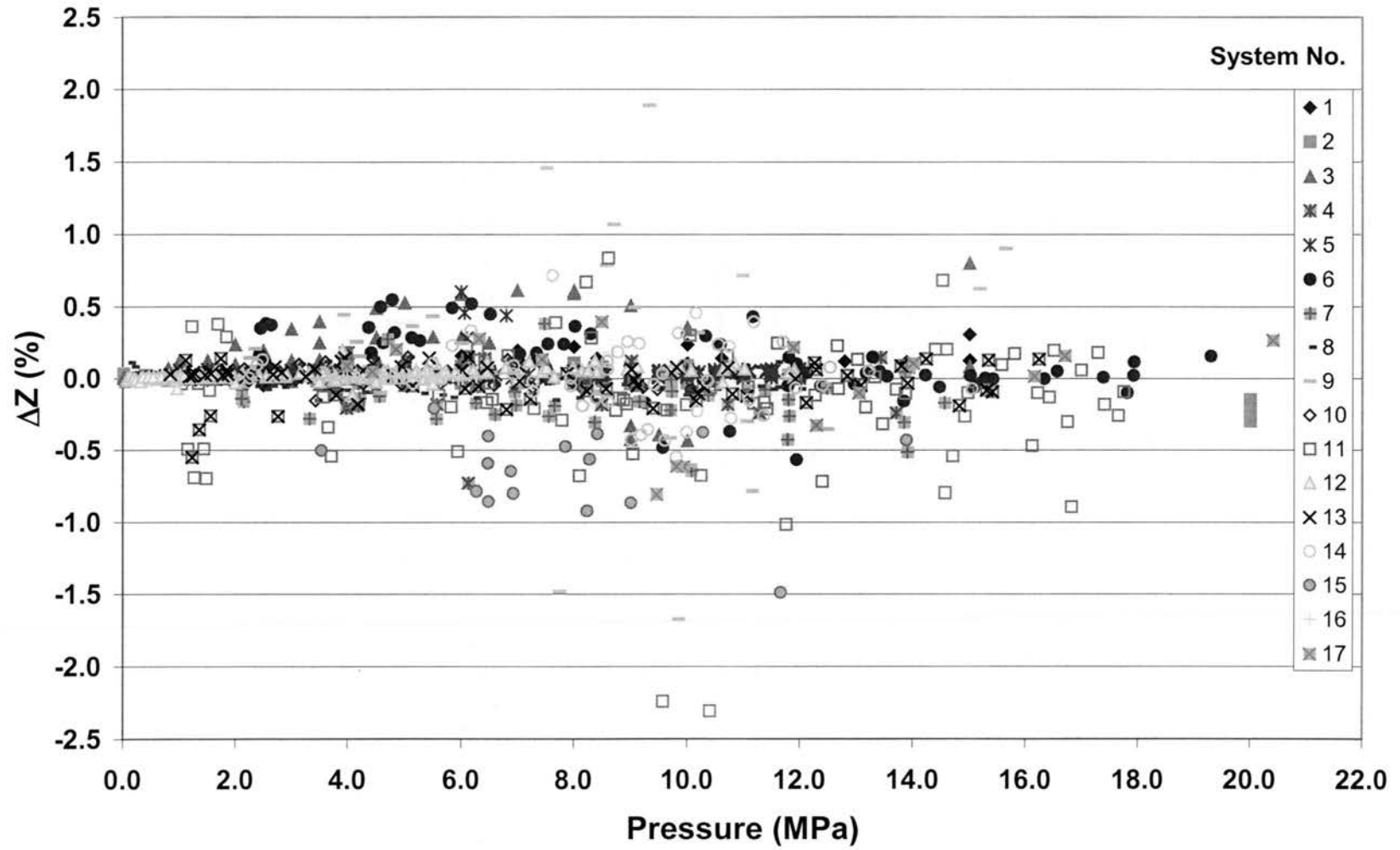
Figure A-6. Overall Summary Results for Case 4
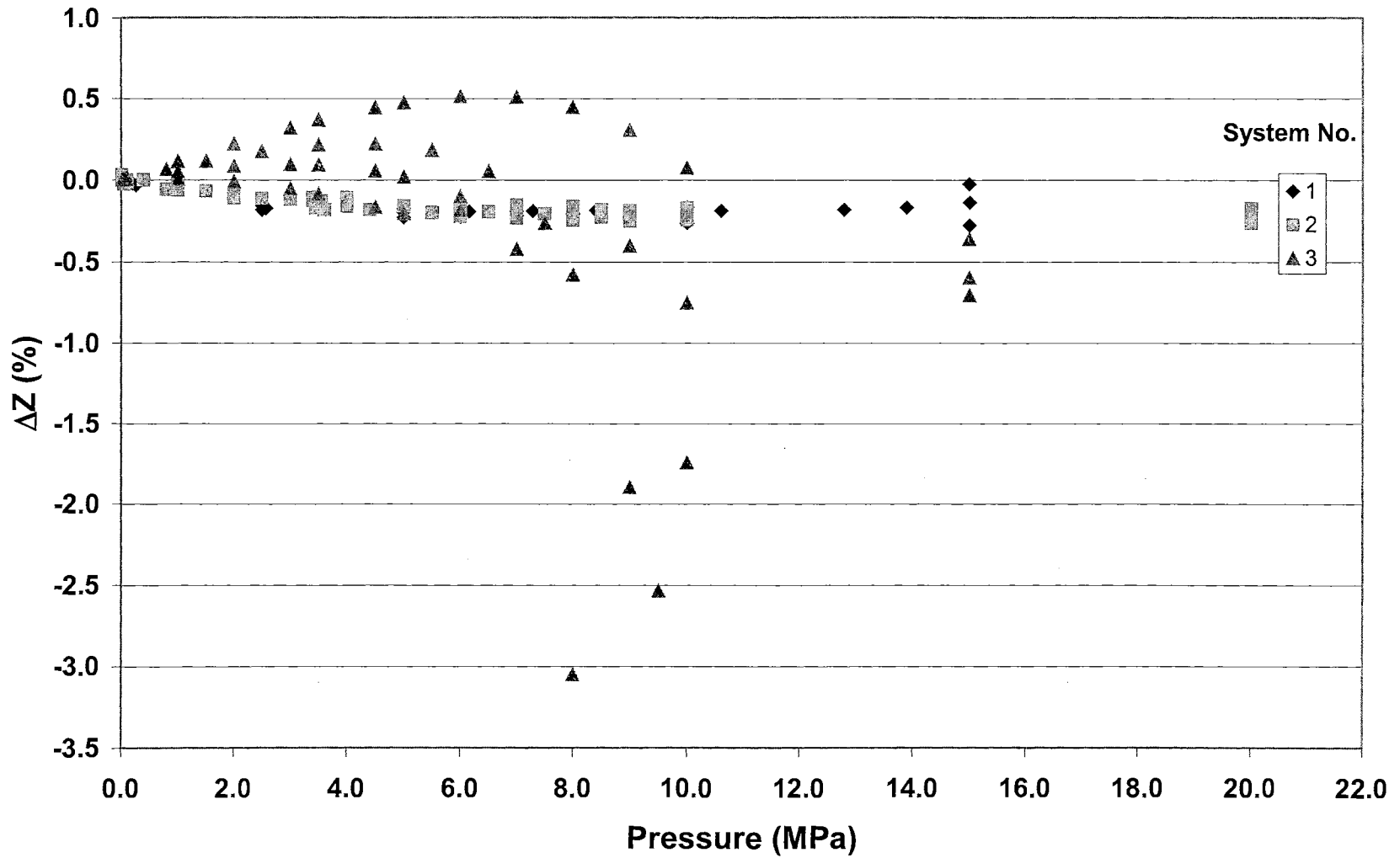
Figure A-7. Pure-Component Summary Results for Case 1
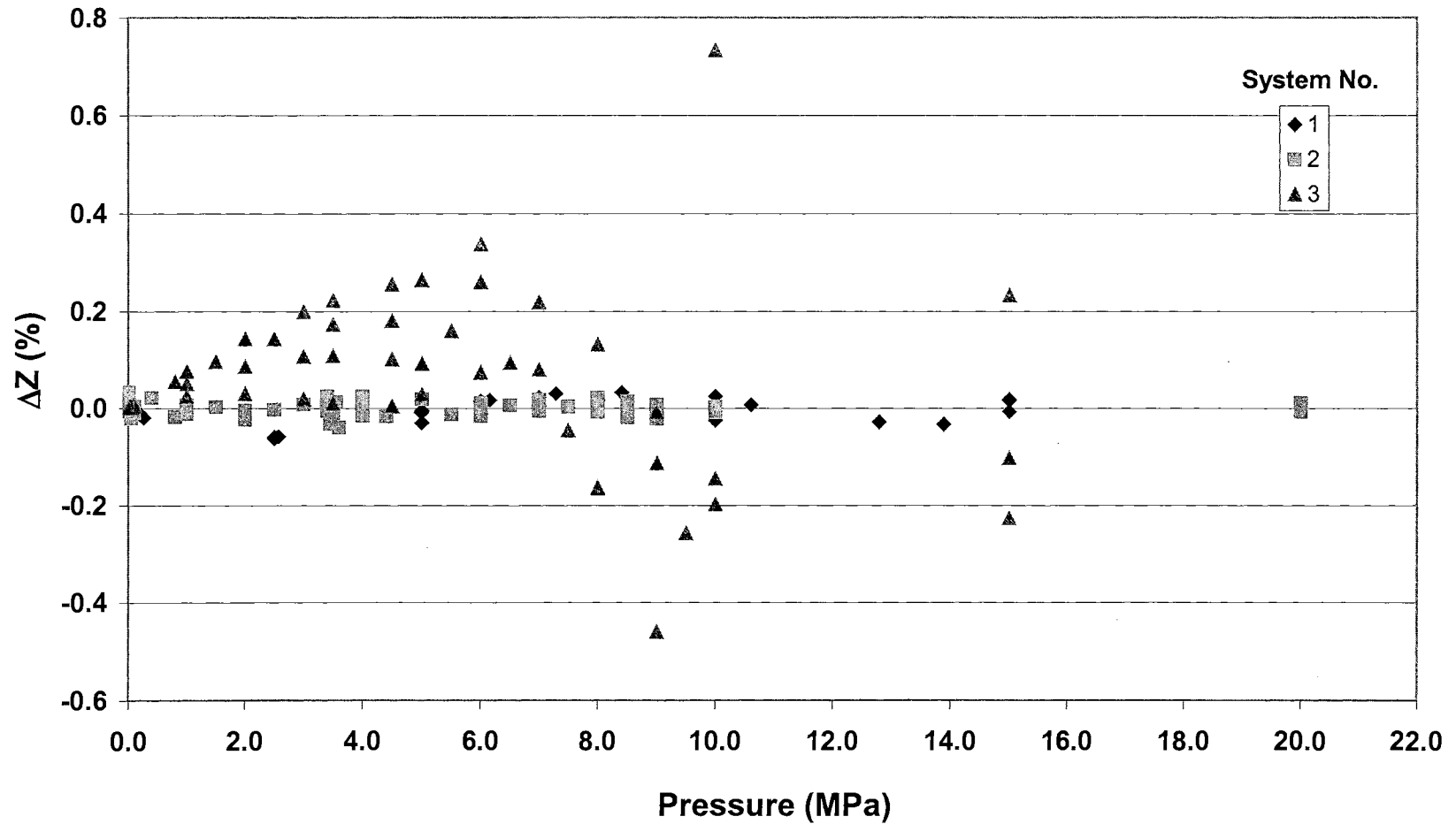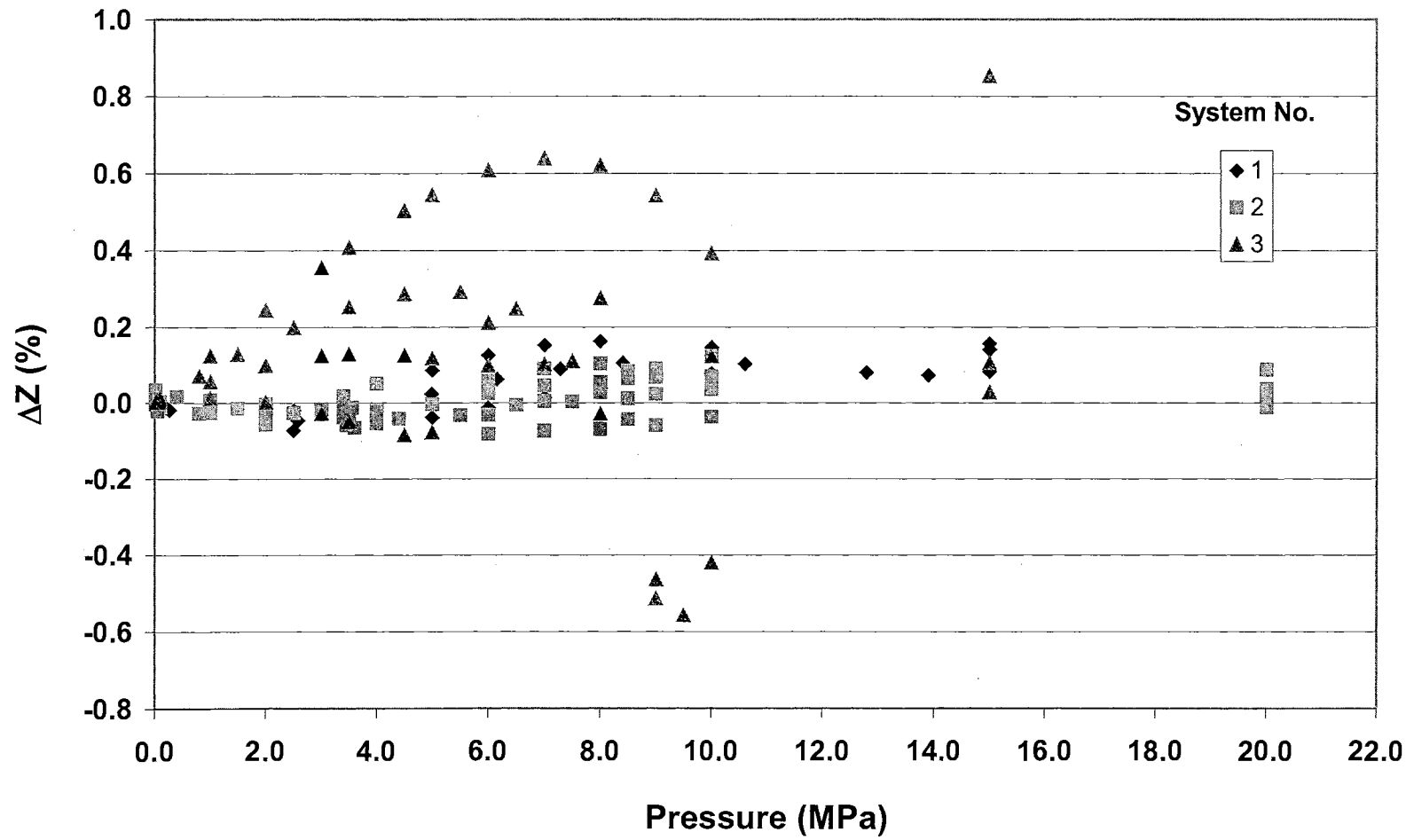
Figure A-8. Pure-Component Summary Results for Case 2

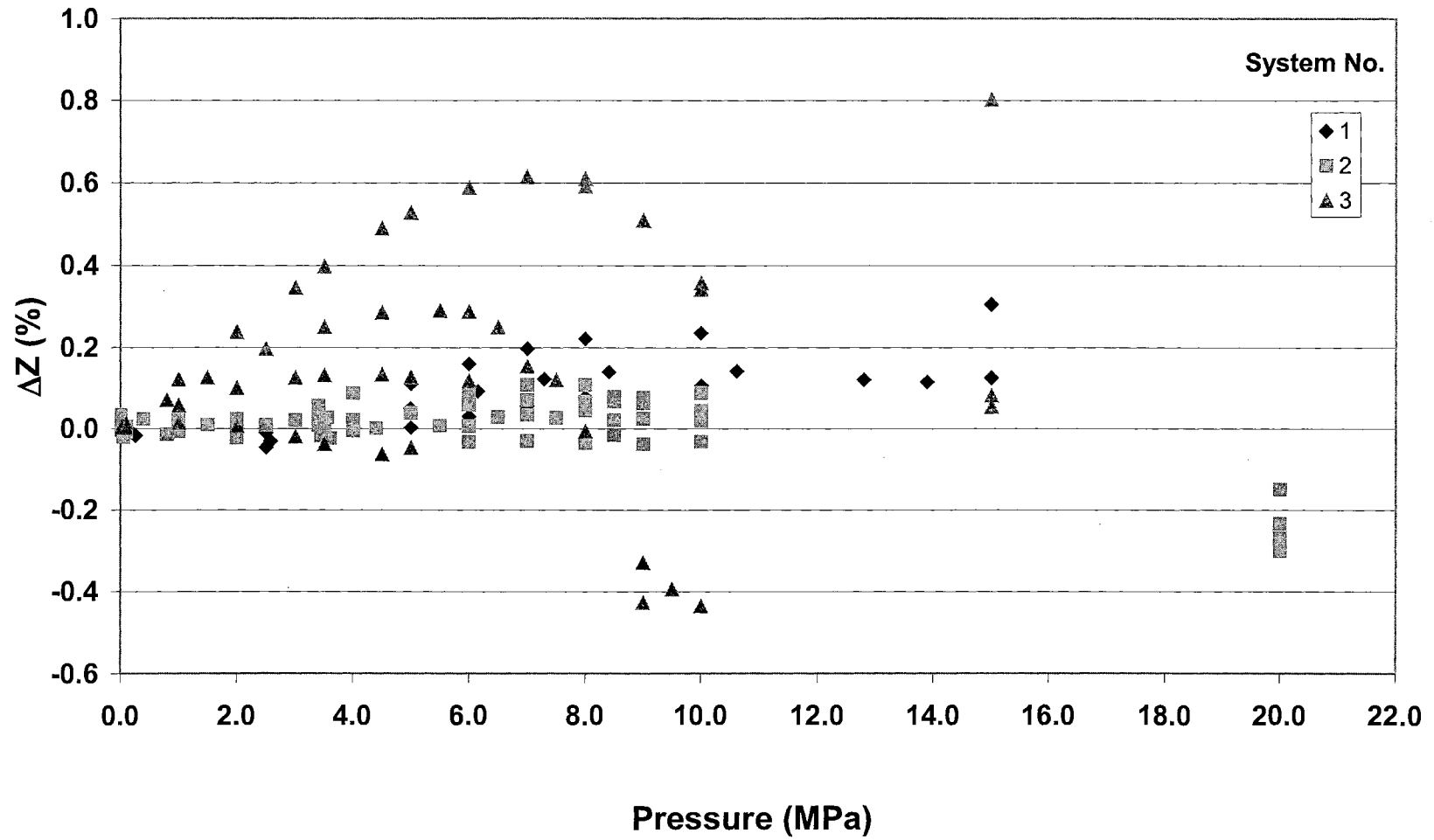Figure A-9. Pure-Component Summary Results for Case 3

Figure A-10. Pure-Component Summary Results for Case 4

affect the total adsorption as well as the component adsorption in mixtures [Sudibandriyo et al., 2003]. The molar feed composition of the mixture is 40% methane, and the equilibrium temperature is 3318.2 K. Figure A-11 shows the effect of 0.5%, 1.0% and 2.0% change in the compressibility factor on the total and the component CO_2 *Gibbs* adsorption. The observed percentage change in the amount adsorbed ranges corresponding to 0.5 and 2.0% variability in the compressibility factor are: from 1.6 to 6.2% in total adsorption, from 0.9 to 3.7% in CO_2 component adsorption and from 5.9 to 23.1% in CH_4 component adsorption.

Similar plots are given in Figure A-12 for the effect of 0.5%, 1.0% and 2.0% change in the compressibility factor on the total and the component CO_2 *absolute* adsorption. The observed percentage change in the amount adsorbed ranges corresponding to 0.5 and 2.0% variability in the compressibility factor are: from 1.4 to 5.4% in total adsorption, from 0.9 to 3.6% in CO_2 component adsorption and from 2.8 to 11.1% in CH_4 component adsorption.

A.7 Conclusions

The major conclusions of this study are:

1. Mixture adsorption calculations are sensitive to the accuracy of compressibility factor predictions.

2. Regressing the BWR EOS parameters using both pure and mixture PVT data simultaneously yielded improved compressibility factor predictions without the need for complicated combination and/or mixing rules.
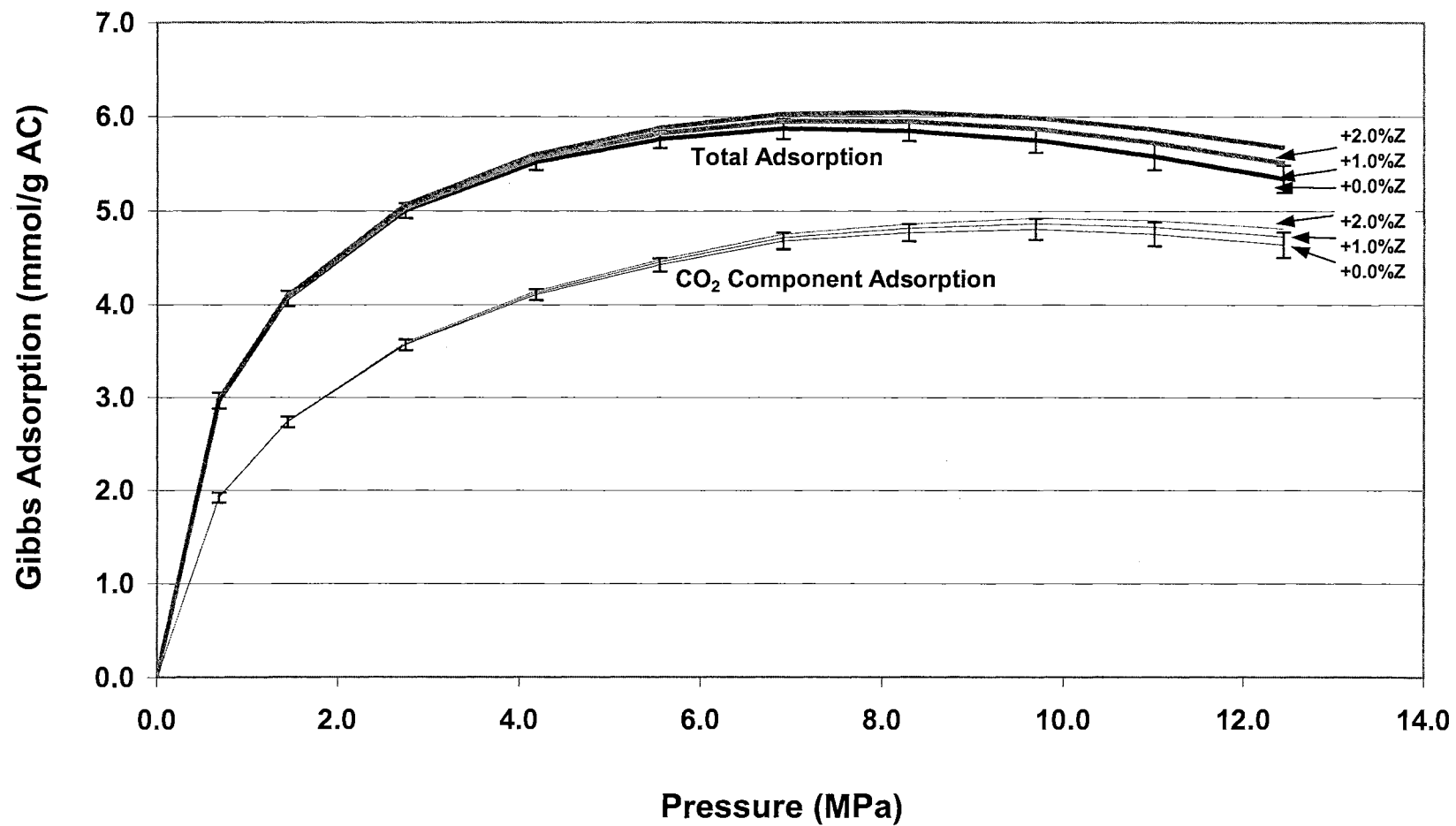
Figure A-11. Gibbs Adsorption Sensitivity to Variability in Compressibility Factor:
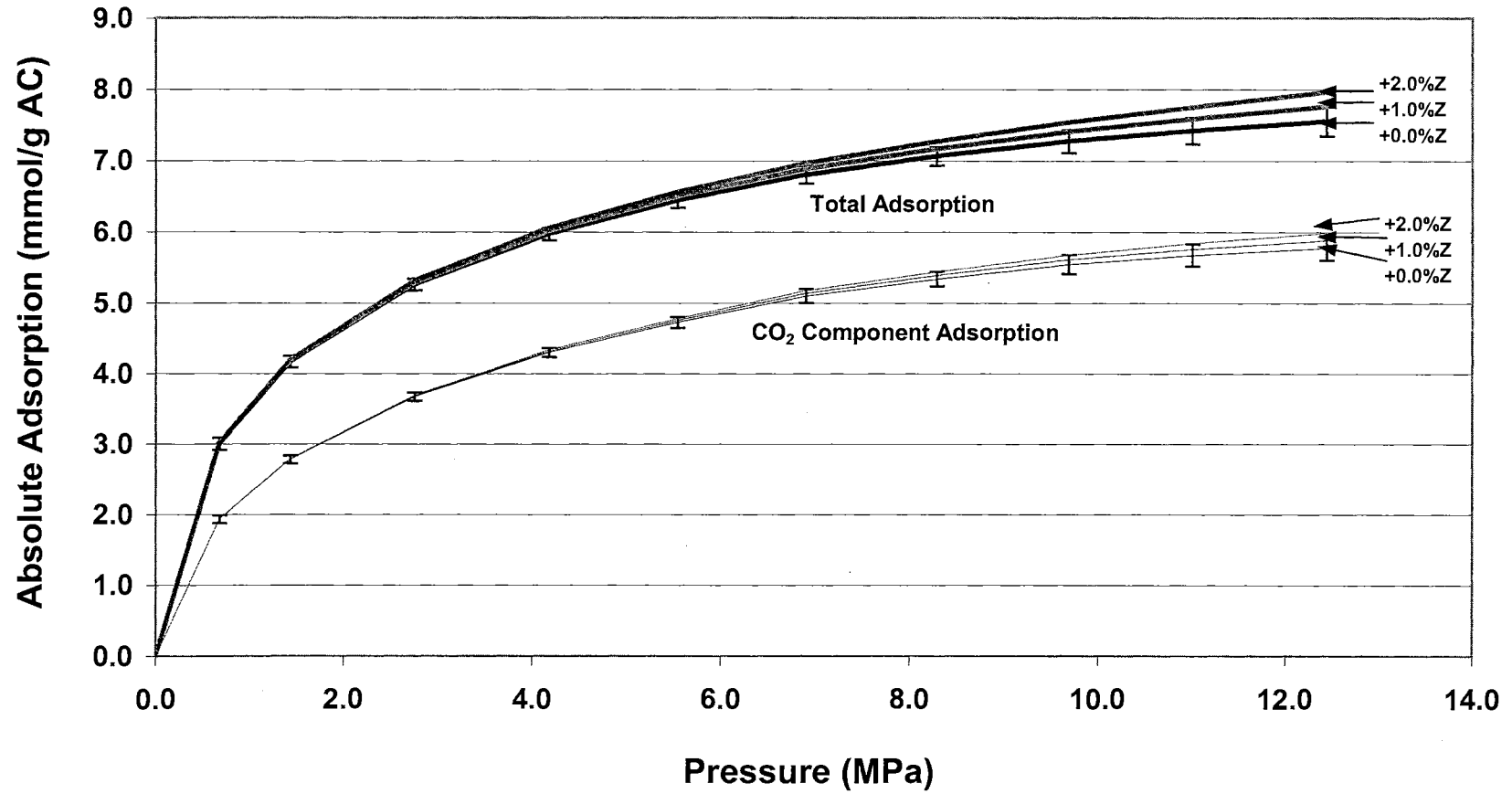$40\%CH_4+60\%CO_2$ on Activated Carbon at 318.2 K

Figure A-12. Absolute Adsorption Sensitivity to Variability in Compressibility Factor: 40%CH₄+60%CO₂ on Activated Carbon at 318.2 K

3. The modified BWR parameters (Cases 3 and 4) yield Z factors that are adequate for coalbed adsorption data reductions.

APPENDIX B

Fugacity Derivation for the Generalized 2-D EOS with Wong-Sandler Mixing Rules

B.1 Wong-Sandler Mixing Rules for 3-D Cubic EOS

Wong-Sandler mixing rules were developed for 3-D cubic equations of state. It equates the excess Helmholtz free energy at infinite pressure from the chosen equation of state to that from an activity coefficient model. Use of the Helmholtz free energy ensures that the second virial coefficient calculated from the equation of state has quadratic composition dependence, as required by statistical mechanics [Wong et al., 1992].

The Wong-Sandler mixing rules for 3-D cubic EOS are [Wong et al., 1992]:

$$b - \frac{a}{RT} = \sum_i \sum_j x_i x_j \left(b - \frac{a}{RT} \right)_{ij} \tag{B-1}$$

$$\frac{A_\infty^E}{FRT} = -\frac{a}{bRT} + \sum_i x_i \frac{a_i}{b_i RT} \tag{B-2}$$

Where the cross term:

$$\left(b - \frac{a}{RT} \right)_{ij} = \frac{1}{2} \left[\left(b_i - \frac{a_i}{RT} \right) + \left(b_j - \frac{a_j}{RT} \right) \right] (1 - C_{ij}) \tag{B-3}$$

F is constant specific to the EOS chosen.

B.2 Wong-Sandler Mixing Rules for the Generalized 2-D EOS

For 2-D EOSs, the parameter definitions ($b = \beta A$ and $a = \alpha A$) assume the surface area is same for different components. Accordingly, the Wong-Sandler mixing rule can be extended to the generalized 2-D EOS as follows:

$$\beta - \frac{\alpha}{RT} = \sum_i \sum_j x_i x_j \left(\beta - \frac{\alpha}{RT} \right)_{ij} \tag{B-4}$$

$$\left(\beta - \frac{\alpha}{RT} \right)_{ij} = \frac{1}{2} \left[\left(\beta_i - \frac{\alpha_i}{RT} \right) + \left(\beta_j - \frac{\alpha_j}{RT} \right) \right] (1 - C_{ij}) \tag{B-5}$$

210

Helmholtz free energy departure function, A^E, is the difference between the molar Helmholtz free energy of pure species i and the ideal gas at the same temperature and pressure. Therefore, if we let ϑ be the specific area of the molecule on the surface, we obtain:

$$A_i(T,\pi) - A_i^{IG}(T,\pi) = \left(-\int_{\infty}^{\vartheta_i}\pi d\vartheta\right) - \left(-\int_{\infty}^{\frac{RT}{\vartheta}}\frac{RT}{\vartheta}d\vartheta\right)$$ (B-6)

For the generalized 2-D EOS, Equation B-6 becomes:

$$A_i(T,\pi) - A_i^{IG}(T,\pi) =$$

$$\left(-\int_{\infty}^{\vartheta_i}\left[\frac{RT}{\vartheta - b_{2,i}^{1/m}\vartheta^{1-1/m}} - \frac{a_2}{\vartheta^2 + Ub_{2,i}\vartheta + Wb_{2,i}^2}\right]d\vartheta\right) - \left(-\int_{\infty}^{\frac{RT}{\pi}}\frac{RT}{\vartheta}d\vartheta\right)$$

$$= -RT\ln\left(\frac{\pi\left(\vartheta^m - b_{2,i}^m\right)^{1/m}}{RT}\right) - \frac{a_{2,i}}{b_{2,i}\sqrt{U^2 - 4W}}\ln\left(\frac{\vartheta_i + b_{2,i}\left(U - \sqrt{U^2 - 4W}\right)/2}{\vartheta_i + b_{2,i}\left(U + \sqrt{U^2 - 4W}\right)/2}\right)$$ (B-7)

If U=W=0, then

$$A_i(T,\pi) - A_i^{IG}(T,\pi) = -RT\ln\left(\frac{\pi\left(\vartheta^m - b_{2,i}^m\right)^{1/m}}{RT}\right) - \frac{a_{2,i}}{\vartheta_i}$$ (B-8)

Where $a_{2,i}$ and $b_{2,i}$ are 2-D parameters for component i.

Similarly, the mixture Helmholtz free energy departure function, which is the difference between the molar Helmholtz free energy of a mixture, A_m, and that of the same mixture as an ideal gas, A_m^{IGM}, at the same temperature, pressure, and composition is:

$$A_m(T,\pi,x) - A_m^{IGM}(T,\pi,x) = -RT \ln\left(\frac{\pi\left(\vartheta_m^m - b_{2,m}^m\right)^{1/m}}{RT}\right)$$

$$- \frac{a_{2,m}}{b_{2,m}\sqrt{U^2 - 4W}} \ln\left(\frac{\vartheta_m + b_{2,m}\left(U - \sqrt{U^2 - 4W}\right)/2}{\vartheta_m + b_{2,m}\left(U + \sqrt{U^2 - 4W}\right)/2}\right) \qquad \text{(B-9)}$$

If U=W=0, then

$$A_m(T,\pi,x) - A_m^{IGM}(T,\pi,x) = -RT \ln\left(\frac{\pi\left(\vartheta_m^m - b_{2,m}^m\right)^{1/m}}{RT}\right) - \frac{a_{2,m}}{\vartheta_m} \qquad \text{(B-10)}$$

Thus, the excess Helmholtz free energy for mixing at constant spreading temperature and pressure, $A^E(T,\pi,x)$, is:

$$A^E(T,\pi,x) = A_m(T,\pi,x) - A_m^{IGM}(T,\pi,x)$$

$$= A_m(T,\pi,x) - \sum_i x_i A_i(T,\pi) - RT \sum_i x_i \ln x_i$$

$$A^E(T,\pi,x) = A_m^{IGM}(T,\pi,x) - RT \ln\left(\frac{\pi\left(\vartheta_m^m - b_{2,m}^m\right)^{1/m}}{RT}\right) - \frac{a_{2,m}}{\vartheta_m} - \sum_i x_i A_i^{IG}(T,\pi)$$

$$+ RT \sum_i x_i \ln\left(\frac{\pi\left(\vartheta_i^m - b_{2,i}^m\right)^{1/m}}{RT}\right) + \sum_i \frac{x_i a_{2,i}}{\vartheta_i} - RT \sum_i x_i \ln x_i \qquad \text{(B-11)}$$

$$A_m^{IGM}(T,\pi,x) - \sum_i x_i A_i^{IG}(T,\pi) = RT \sum_i x_i \ln x_i \qquad \text{(B-12)}$$

Thus,

$$A^E(T,\pi,x) = -RT \ln\left(\frac{\pi\left(\vartheta_m^m - b_{2,m}^m\right)^{1/m}}{RT}\right) - \frac{a_{2,m}}{\vartheta_m} + RT \sum_i x_i \ln\left(\frac{\pi\left(\vartheta_i^m - b_{2,i}^m\right)^{1/m}}{RT}\right)$$

$$+ \sum_i \frac{x_i a_{2,i}}{\vartheta_i}$$

$$A^E(T,\pi,x) = -\frac{a_{2,m}}{\vartheta_m} + \sum_i \frac{x_i a_{2,i}}{\vartheta_i} + RT \sum_i x_i \ln\left(\frac{\left(\vartheta_i^m - b_{2,i}^m\right)^{1/m}}{\left(\vartheta_m^m - b_{2,m}^m\right)^{1/m}}\right) \qquad \text{(B-13)}$$

Expressions for the excess Helmholtz free energy of liquid mixtures have usually been derived using lattice models with the assumption that there are no free sites on the lattice. This is approximately equivalent to the assumption that in a liquid solution the molecules are so closely packed that there is no free volume, this limit in an equation of state is:

$$\lim_{\pi \to \infty} \vartheta_i = b_{2,i}$$

$$\lim_{\pi \to \infty} \vartheta_m = b_{2,m}$$

From the 2-D EOS:

$$\left[\pi + \frac{a_2}{\vartheta^2 + Ub_2\vartheta + Wb_2{}^2} \right] = \frac{RT}{\vartheta - b_2{}^m \vartheta^{1-m}} \tag{B-14}$$

Thus,

$$\vartheta^m - b_2{}^m = \frac{1}{\vartheta^{1-m}} \frac{RT}{\left[\pi + \frac{a_2}{\vartheta^2 + Ub_2\vartheta + Wb_2{}^2} \right]} \tag{B-15}$$

$$\lim_{\pi \to \infty} \left(\frac{\left(\vartheta_i^m - b_{2,i}^m\right)^{1/m}}{\left(\vartheta_m^m - b_{2,m}^m\right)^{1/m}} \right) = \left(\frac{b_{2,m}}{b_{2,i}} \right)^{1/,m-1} \tag{B-16}$$

Therefore, the access Helmholtz free energy at infinite spreading pressure, A_∞^E, is:

$$A_\infty^E(x) = -\frac{a_{2,m}}{b_{2,m}} + \sum_i x_i \frac{a_{2,i}}{b_{2,i}} + (\frac{1}{m} - 1)RT\sum_i x_i \ln\frac{b_{2,m}}{b_{2,i}} \tag{B-17}$$

For 2-D, $b_{2,m} = \beta_m A$, $a_{2,m} = \alpha_m A$. To simplify, let $\beta = \beta_m$ and $\alpha = \alpha_m$, then:

$$\frac{A_\infty^E}{RT} = -\frac{\alpha}{\beta RT} + \sum_i x_i \frac{\alpha_i}{\beta_i RT} + (\frac{1}{m} - 1)\sum_i x_i \ln\frac{\beta}{\beta_i} \tag{B-18}$$

if $U \neq 0$ and/or $W \neq 0$, then:

$$\frac{A_\infty^E}{RT} = -\frac{\alpha}{F\beta RT} + \sum_i x_i \frac{\alpha_i}{F\beta_i RT} + (\frac{1}{m} - 1)\sum_i x_i \ln\frac{\beta}{\beta_i} \tag{B-19}$$

where:

213

$$F = \sqrt{U^2 - 4W} \Big/ \ln\left(\frac{1 + \left(U - \sqrt{U^2 - 4W}\right)/2}{1 + \left(U + \sqrt{U^2 - 4W}\right)/2}\right)$$ (B-20)

If U=W=0, then F=1.

B.3 Fugacity Calculation

Based on Equations B-4 and B-19, β and α, thus, can be expressed as:

$$\beta = \sum_i \sum_j x_i x_j \left(\beta - \frac{\alpha}{RT}\right)_{ij} \Big/ \left(1 - \sum_i x_i \frac{\alpha_i}{\beta_i RT} + F\frac{A_\infty^E}{RT} - F(\frac{1}{m} - 1)\sum_i x_i \ln\frac{\beta}{\beta_i}\right)$$
(B-21)

where numerical methods can be used to solve for β and

$$\frac{\alpha}{RT} = \beta - \sum_i \sum_j x_i x_j \left(\beta - \frac{\alpha}{RT}\right)_{ij}$$ (B-22)

Fugacity in the adsorbed phase for the generalized 2-D EOS can be expressed as [Zhou, 1994]:

$$\ln\widehat{\phi}_i = \int_0^\omega \left\{ \frac{1}{RT\omega}\left[\frac{\partial(A\pi)}{\partial\omega_i}\right]_{T,M_s,n_j} - \frac{1}{\omega} \right\} d\omega - \ln Z_a$$ (B-23)

where M_s is the mass of the adsorbent.

$$A\pi = \frac{\omega RT}{1 - (\beta\omega)^m} - \frac{\alpha\omega^2}{1 + U\beta\omega + W(\beta\omega)^2} = S_1 + S_2$$ (B-24)

$$\ln\widehat{\phi}_i = F_1 + F_2 - \ln Z_a$$ (B-25)

Where $F_1 = \int_0^\omega \left\{ \frac{1}{RT\omega}\left[\frac{\partial S_1}{\partial\omega_i}\right]_{T,M_s,n_j} - \frac{1}{\omega} \right\} d\omega$ (B-26)

$$F_2 = \int_0^\omega \left\{ \frac{1}{RT\omega}\left[\frac{\partial S_2}{\partial\omega_i}\right]_{T,M_s,n_j} \right\} d\omega$$ (B-27)

214

$$\left[\frac{\partial S_1}{\partial \omega_i}\right]_{T,M_s,n_j} = \frac{RT}{1-(\beta\omega)^m} + \frac{m\omega RT(\beta\omega)^{m-1}}{\left(1-(\beta\omega)^m\right)^2}\left(\frac{\partial(\beta\omega)}{\partial \omega_i}\right) \tag{B-28}$$

Where:

$$\beta\omega = \frac{\frac{1}{\omega}\sum_k\sum_j \omega_k\omega_j\left(\beta - \frac{\alpha}{RT}\right)_{kj}}{1 - \frac{1}{\omega}\sum_{ki}\omega_k\frac{\alpha_k}{\beta_k RT} + F\frac{A_\infty^E}{RT} - F(\frac{1}{m}-1)\sum_k x_k \ln\frac{\beta}{\beta_k}} = \frac{T_1}{T_2} \tag{B-29}$$

$$T_2 = 1 - Q_1 + Q_2 - Q_3 \tag{B-30}$$

$$\frac{\partial T_1}{\partial \omega_i} = 2\sum_j\left(\beta - \frac{\alpha}{RT}\right)_{ij} x_j - \sum_k\sum_j x_k x_j\left(\beta - \frac{\alpha}{RT}\right)_{kj} \tag{B-31}$$

$$\frac{\partial Q_1}{\partial \omega_i} = \frac{1}{\omega}\left(\frac{\alpha_i}{\beta_i RT} - \sum_k x_k \frac{\alpha_k}{\beta_k RT}\right) \tag{B-32}$$

The NTRL model [see, e.g., Tester, 1996] is used to account for the Excess Helmholtz free energy in the adsorbed phase:

$$Q_2 = F\frac{A_\infty^E}{RT} \approx F\frac{\Delta G^E}{RT} = F\sum_{l=1}^{NC}\left[\frac{x_l\sum_{j=1}^{NC}\tau_{jl}G_{jl}x_j}{\sum_{k=1}^{NC}G_{kl}x_k}\right] = \frac{F}{\omega}\sum_{l=1}^{NC}\left[\frac{\omega_l\sum_{j=1}^{NC}\tau_{jl}G_{jl}\omega_j}{\sum_{k=1}^{NC}G_{kl}\omega_k}\right] \tag{B-33}$$

where $\tau_{ii} = 0$, $G_{ji} = \exp(-\alpha_{ji}\tau_{ji})$, and $\alpha_{ji} = \alpha_{ij}$.

$$\frac{\partial Q_2}{\partial \omega_i} = -\frac{F}{\omega^2} \sum_{l=1}^{NC} \left[\frac{\omega_l \sum_{j=1}^{NC} \tau_{jl} \ddot{G}_{jl} \omega_j}{\sum_{k=1}^{NC} G_{kl} \omega_k} \right]$$

$$+ \frac{F}{\omega} \sum_{l=1}^{NC} \left[\frac{\frac{\partial \left(\omega_l \sum_{j=1}^{NC} \tau_{jl} G_{jl} \omega_j \right)}{\partial \omega_i} \left(\sum_{k=1}^{NC} G_{kl} \omega_k \right) - \frac{\partial \left(\sum_{k=1}^{NC} G_{kl} \omega_k \right)}{\partial \omega_i} \left(\omega_l \sum_{j=1}^{NC} \tau_{jl} G_{jl} \omega_j \right)}{\left(\sum_{k=1}^{NC} G_{kl} \omega_k \right)^2} \right]$$

$$\frac{\partial Q_2}{\partial \omega_i} = -\frac{Q_2}{\omega} + \frac{F}{\omega} \sum_{l=1}^{NC} \left[\frac{\Delta_{li} \sum_{j=1}^{NC} \tau_{ji} G_{ji} \omega_j + \omega_l \tau_{il} G_{il}}{\left(\sum_{k=1}^{NC} G_{kl} \omega_k \right)} - \frac{G_{il} \left(\omega_l \sum_{j=1}^{NC} \tau_{jl} G_{jl} \omega_j \right)}{\left(\sum_{k=1}^{NC} G_{kl} \omega_k \right)^2} \right]$$

where: $\Delta_{ij} = 0$ when $j \neq i$

$\Delta_{ij} = 1$ when $j = i$

$$\frac{\partial Q_2}{\partial \omega_i} = -\frac{F}{\omega} \left\{ \frac{Q_2}{F} - \sum_{l=1}^{NC} \left[\frac{\Delta_{li} \sum_{j=1}^{NC} \tau_{ji} G_{ji} x_j + x_l \tau_{il} G_{il}}{\left(\sum_{k=1}^{NC} G_{kl} x_k \right)} - \frac{G_{il} \left(x_l \sum_{j=1}^{NC} \tau_{jl} G_{jl} x_j \right)}{\left(\sum_{k=1}^{NC} G_{kl} x_k \right)^2} \right] \right\} = -\frac{FL_i}{\omega}$$

(B-34)

$$\frac{\partial Q_3}{\partial \omega_i} = F \frac{1/m - 1}{\omega} \left[-\sum_k x_k \ln \frac{\beta}{\beta_k} + \ln \frac{\beta}{\beta_i} + \frac{1}{\beta} \frac{\partial (\beta \omega)}{\partial \omega_i} - 1 \right]$$

(B-35)

$$\frac{\partial (\beta \omega)}{\partial \omega_i} = \frac{\partial T_1}{\partial \omega_i} \frac{1}{T_2} - \frac{T_1}{T_2^2} \frac{\partial T_2}{\partial \omega_i}$$

(B-36)

where: $\dfrac{\partial T_2}{\partial \omega_i} = -\dfrac{\partial Q_1}{\partial \omega_i} + \dfrac{\partial Q_2}{\partial \omega_i} - \dfrac{\partial Q_3}{\partial \omega_i}$

(B-37)

So:

$$\frac{\partial(\beta\omega)}{\partial\omega_i} = \frac{2\sum_j\left(\beta - \frac{\alpha}{RT}\right)_{ij}x_j - \sum_k\sum_j x_k x_j\left(\beta - \frac{\alpha}{RT}\right)_{kj}}{\left(1 - \sum_i x_i\frac{\alpha_i}{\beta RT} + F\frac{A_\infty^E}{RT} - F(\frac{1}{m}-1)\sum_i x_i\ln\frac{\beta}{\beta_i}\right)}$$

$$-\frac{\sum_k\sum_j x_k x_j\left(\beta - \frac{\alpha}{RT}\right)_{kj}}{\left(1 - \sum_k x_k\frac{\alpha_k}{\beta RT} + F\frac{A_\infty^E}{RT} - F(\frac{1}{m}-1)\sum_i x_i\ln\frac{\beta}{\beta_i}\right)^2} \times \qquad\text{(B-38)}$$

$$\left(-\frac{\alpha_i}{\beta_i RT} + \sum_k x_k\frac{\alpha_k}{\beta_{ki}RT} - FL_i - F(\frac{1}{m}-1)\left(-\sum_k x_k\ln\frac{\beta}{\beta_k} + \ln\frac{\beta}{\beta_i} + \frac{1}{\beta}\frac{\partial(\beta\omega)}{\partial\omega_i} - 1\right)\right)$$

where numerical methods can be used to solve for $\frac{\partial(\beta\omega)}{\partial\omega_i}$ and let $M_i = \frac{\partial(\beta\omega)}{\partial\omega_i}$, So:

$$F_1 = \int_0^\omega\left\{\frac{1}{RT\omega}\left[\frac{\partial S_1}{\partial\omega_i}\right]_{T,M_s,n_j} - \frac{1}{\omega}\right\}d\omega$$

$$F_1 = \int_0^\omega\left\{\frac{1}{\omega(1-(\beta\omega)^m)} + \frac{m(\beta\omega)^{m-1}}{(1-(\beta\omega)^m)^2}M - \frac{1}{\omega}\right\}d\omega$$

$$F_1 = -\frac{1}{m}\ln\left(1-(\beta\omega)^m\right) + \frac{M}{\beta}\frac{(\beta\omega)^m}{1-(\beta\omega)^m} \qquad\text{(B-39)}$$

$$\left[\frac{\partial S_2}{\partial\omega_i}\right]_{T,M_s,n_j} = \frac{-\frac{\partial(\alpha\omega^2)}{\partial\omega_i}}{1+U\beta\omega+W(\beta\omega)^2} + \frac{\alpha\omega^2(U+2W\beta\omega)\frac{\partial(\beta\omega)}{\partial\omega_i}}{(1+U\beta\omega+W(\beta\omega)^2)^2} \qquad\text{(B-40)}$$

$$-\frac{\partial(\alpha\omega^2)}{\partial\omega_i} = -\frac{\partial\left(\beta\omega^2 - \sum_k\sum_j\omega_k\omega_j\left(\beta - \frac{\alpha}{RT}\right)_{kj}\right)}{\partial\omega_i}RT \qquad\text{(B-41)}$$

$$= -\omega RT\left(M_i + \beta - 2\sum_j x_j\left(\beta - \frac{\alpha}{RT}\right)_{ij}\right)$$

217

$$F_2 = \int_0^\omega \left\{ \frac{1}{RT\omega} \left[\frac{\partial S_2}{\partial \omega_i} \right]_{T,M_s,n_j} \right\} d\omega$$

$$= \frac{1}{RT} \int_0^\omega \left\{ \frac{-\dfrac{1}{\omega} \dfrac{\partial(\alpha\omega^2)}{\partial\omega_i}}{1 + U\beta\omega + W(\beta\omega)^2} + \frac{\alpha\omega(U + 2W\beta\omega)\dfrac{\partial(\beta\omega)}{\partial\omega_i}}{\left(1 + U\beta\omega + W(\beta\omega)^2\right)^2} \right\} d\omega$$

$$F_2 = R_1 + R_2 \tag{B-42}$$

$$R_1 = \frac{1}{RT} \int_0^\omega \left\{ \frac{-\dfrac{1}{\omega}\dfrac{\partial(\alpha\omega^2)}{\partial\omega_i}}{1 + U\beta\omega + W(\beta\omega)^2} \right\} d\omega = \frac{-\dfrac{1}{\omega}\dfrac{\partial(\alpha\omega^2)}{\partial\omega_i}}{RT} \int_0^\omega \left\{ \frac{1}{1 + U\beta\omega + W(\beta\omega)^2} \right\} d\omega$$

$$= \frac{-\dfrac{1}{\omega}\dfrac{\partial(\alpha\omega^2)}{\partial\omega_i}}{RT\beta\sqrt{U^2 - 4W}} \ln\left(\frac{2W\beta\omega + U - \sqrt{U^2 - 4W}}{2W\beta\omega + U + \sqrt{U^2 - 4W}} \right)\Bigg|_0^\omega$$

$$= \frac{-\dfrac{1}{\omega}\dfrac{\partial(\alpha\omega^2)}{\partial\omega_i}}{RT\beta\sqrt{U^2 - 4W}} \ln\left(\frac{2 + \omega\beta\left(U + \sqrt{U^2 - 4W}\right)}{2 + \omega\beta\left(U - \sqrt{U^2 - 4W}\right)} \right)$$

$$\tag{B-43}$$

$$R_1 = \frac{-\left(M_i + \beta - 2\sum_j x_j \left(\beta_{ij} - \dfrac{\alpha_{ij}}{RT} \right) \right)}{\beta\sqrt{U^2 - 4W}} \ln\left(\frac{2 + \omega\beta\left(U + \sqrt{U^2 - 4W}\right)}{2 + \omega\beta\left(U - \sqrt{U^2 - 4W}\right)} \right) \tag{B-44}$$

218

$$R_2 = \frac{1}{RT} \int_0^\infty \left\{ \frac{\alpha\omega(U+2W\beta\omega)\frac{\partial(\beta\omega)}{\partial\omega_i}}{\left(1+U\beta\omega+W(\beta\omega)^2\right)^2} \right\} d\omega$$

$$= \frac{\alpha M_i}{RT} \int_0^\infty \left\{ \frac{\omega(U+2W\beta\omega)}{\left(1+U\beta\omega+W(\beta\omega)^2\right)^2} \right\} d\omega$$

$$= \frac{\alpha M_i}{\beta RT} \int_0^\infty \left\{ \frac{\omega(U\beta+2W\beta^2\omega)}{\left(1+U\beta\omega+W(\beta\omega)^2\right)^2} \right\} d\omega$$

$$= \frac{\alpha M_i}{\beta RT} \int_0^\infty \left\{ \frac{\omega}{\left(1+U\beta\omega+W(\beta\omega)^2\right)^2} \right\} d\left(1+U\beta\omega+W(\beta\omega)^2\right)$$

$$= \frac{-\alpha M_i}{\beta RT} \int_0^\infty \omega d\left(\frac{1}{1+U\beta\omega+W(\beta\omega)^2} \right)$$

$$= \frac{-\alpha M_i}{\beta RT} \left(\frac{\omega}{1+U\beta\omega+W(\beta\omega)^2} \right)\Big|_0^\infty + \frac{\alpha M_i}{\beta RT} \int_0^\infty \left(\frac{1}{1+U\beta\omega+W(\beta\omega)^2} \right) d\omega$$

$$= \frac{-\alpha M_i}{\beta RT} \frac{\omega}{1+U\beta\omega+W(\beta\omega)^2} + \frac{\alpha M_i}{RT\beta^2 \sqrt{U^2-4W}} \ln\left(\frac{2+\omega\beta\left(U+\sqrt{U^2-4W}\right)}{2+\omega\beta\left(U-\sqrt{U^2-4W}\right)} \right)$$

$$\text{(B-45)}$$

So:

$$\ln\hat{\phi}_i = -\frac{1}{m}\ln\left(1-(\beta\omega)^m\right) + \frac{M_i}{\beta}\frac{(\beta\omega)^m}{1-(\beta\omega)^m} - \ln Z_a + R_1 + R_2 \qquad \text{(B-46)}$$

The values of U and W must satisfy the following constraints in the above fugacity expressions:

$$U^2 - 4W > 0$$

If W=U=0:

$$\ln\hat{\phi}_i = -\frac{1}{m}\ln\left(1-(\beta\omega)^m\right) + \frac{M_i}{\beta}\frac{(\beta\omega)^m}{1-(\beta\omega)^m} - \left(M_i + \beta - 2\sum_j x_j\left(\beta - \frac{\alpha}{RT}\right)_{ij} \right)\omega - \ln Z_a$$

$$\text{(B-47)}$$

219

VITA (2)

Zhejun Pan

Candidate for the Degree of

Doctor of Philosophy

Thesis: MODELING OF GAS ADSORPTION USING TWO-DIMENSIONAL EQUATIONS OF STATE

Major Field: Chemical Engineering

Biographical:

Education: Received Bachelor of Science degree in Chemical Engineering and Master of Science degree in Control Science and Engineering from Zhejiang University, China in June 1996 and February 1999, respectively. Completed the requirements for the Doctor of Philosophy degree with a major in Chemical Engineering at Oklahoma State University in May 2004.

Experience: Employed as a graduate assistant in Zhejiang University from 1996 to 1999. Employed as a graduate assistant in Oklahoma State University from 2000 to present.

Professional Organization: Member of the American Institute of Chemical Engineers